APPLICATION OF SPECTROSCOPY TO PROTEIN CHARACTERIZATION

A Dissertation
Presented to
The Academic Faculty

By

Laurie Shireen Sanii

In Partial Fulfillment
Of the Requirements for the Degree
Doctor of Philosophy in Chemistry

Georgia Institute of Technology

December, 2005

APPLICATION OF SPECTROSCOPY TO PROTEIN CHARACTERIZATION

Approved by:

Dr. Mostafa A. El-Sayed, Chairman
School of Chemistry and Biochemistry
Laser Dynamics Laboratory
Georgia Institute of Technology

Dr. Charles Liotta
School of Chemistry and Biochemistry
Georgia Institute of Technology

Dr. Laren Tolbert
School of Chemistry and Biochemistry
Georgia Institute of Technology

Dr. John Zhang
School of Chemistry and Biochemistry
Georgia Institute of Technology

Dr. Mohan Srinivasarao
School of Polymer, Textile and Fiber Engineering and School of Chemistry and Biochemistry
Georgia Institute of Technology

Date Approved: August 2005

This thesis is dedicated to my husband Dr. Robert Kriegel, has been there for me for the past seven years. Without his love and support, completion of this work would have been impossible. I would also like to thank my parents, Mike and Linda Sanii. They installed in me both a love of learning and also a work ethic that gave me the drive to keep going.

ACKNOWLEDGEMENTS

I would like to express my sincerest gratitude to my advisor, Dr. Mostafa A. El-Sayed. He taught me the value of perseverance, and his patience and wisdom have been invaluable to me during my time as a student. I would like to thank the Chemical Sciences, Geosciences, and Biosciences Division, Office of Basic Energy Science, Office of Sciences, U.S. Department of Energy (under grant DE-FG02-97ER14799) for the funding to carry out this work. I would like to thank the members of my thesis committee for taking the time to read this thesis and provide guidance: Dr. Charles Liotta, Dr. Laren Tolbert, Dr. Mohan Srinivasarao, and Dr. John Zhang. Outside my thesis committee, I could like to thank Dr. Steve Michielsen of Textiles for his guidance and support during the course of the Raman experiments. Thanks to Dr. Bart Kahr at the University of Seattle for his attempts at CD microscopy with my crystals. Thanks also to Dr. Bridgette Barry, who advised me with the FTIR spectroscopy and was so nice to give me a tour of her labs. I would like to thank Dr. Rod Donlan at the Centers for Disease Control (CDC) here in Atlanta for his support and was happy to have the opportunity to collaborate with him on a paper. Thanks so to Dr. Jianping (Jack) Wang for taking the time to teach me with time-resolved FTIR spectroscopy, and Dr. Colin Heyes in the initial efforts in synthesis of these crystals. Thanks to Ms. Carol Dawkins for helping me de-stress and feel less alone.

I would also like to thank my best friend, Dr. Cristin Moran, for both lifting my spirits many times during the course of graduate school and for her help with some of the Raman microscopy experiments presented in this thesis. I was excited to be able to

collaborate with her on a manuscript and will treasure her friendship always. I would also like to acknowledge some of the friends I've made during the course of my time at Georgia Tech that have made the journey more enjoyable: Dr. Rick Redic, Matija Crne, Xiaohua Huang, Rebecca Johnson, Marian Vargas, and of course my husband, Dr. Robert Kriegel. Thanks to Dr. Marcus Weck's research group for the cheap sodas.

In addition, I would like to thank my parents, Mike and Linda Sanii, and my 'surrogate' parents, Habib and Pauline Jafarzadeh. Their love and support at many times helped me keep moving forward. Finally, I would also like to thank my grandmother, Mrs. Lenore Wright, for listening to me during the many times I felt overwhelmed. If I am half as cool as she is when I am her age, I will consider my life a success.

TABLE OF CONTENTS

	PAGE
DEDICATION	iii
ACKNOWLEDGEMENTS	iv
LIST OF TABLES	xiii
LIST OF FIGURES	xiv
SYMBOLS AND ABBREVIATIONS	xxiii
SUMMARY	xxv
-REFERENCES	xxx
CHAPTER 1 - THESIS INTRODUCTION: SUMMARY OF THE STUDIES OF THE STRUCTURE AND FUNCTION OF THE TRANSMEMBRANE PROTEIN BACTERIORHODOPSIN OF THE ORGANISM HALOBACTERIUM SALINARIUM AND ITS BICELLE CRYSTALLIZATION METHOD	1
ABSTRACT	1
1.1 - BACTERIORHODOPSIN – STRUCTURE AND FUNCTION	1
1.2 - PHOTOCYCLE AS A MEANS OF ATP PRODUCTION	8
1.3 - THE INTERMEDIATES OF THE BR PHOTOCYCLE	10
1.4 - CRYSTALLOGRAPHY OF BR	21
-REFERENCES	30
CHAPTER 2 – EXPERIMENTAL DETAILS OF ALL WORK ATTEMPTED	37
ABSTRACT	37

2.1.- THE BICELLE CRYSTALLIZATION USING THE BOWIE AND FARHAM METHOD 37

2.2 – REPLICATION OF THE IMPROVED BICELLE METHOD OF BOWIE AND FARHAM IN OUR LABS 41

2.3 - SAMPLE PREPARATION AND DATA ACQUISITION FOR LIGHT/DARK ADAPTATION EXPERIMENTS 43

2.4 – SAMPLE PREPARATION AND DATA ACQUISITION FOR SINGLE-CRYSTAL VISIBLE SPECTROSCOPY 45

2.5 – SAMPLE PREPARATION AND DATA ACQUISITION FOR SINGLE-CRYSTAL RAMAN SPECTROSCOPY 46

2.6 – SAMPLE PREPARATION AND DATA ACQUISITION FOR VISIBLE SPECTROSCOPY OF A MASS OF BCBR CRYSTALS DRIED IN THE DARK 50

2.7 – SAMPLE PREPARATION AND DATA ACQUISITION CIRCULAR DICHROISM EXPERIMENTS 51

2.8 – SAMPLE PREPARATION AND DATA ACQUISITION FOR SINGLE-CRYSTAL FTIR EXPERIMENTS 56

2.9 – SAMPLE PREPARATION AND DATA ACQUISITION FOR SINGLE-CRYSTAL POLARIZED RAMAN EXPERIMENTS 61

2.10 – TRANSMISSION MICROSCOPY OF BCBR CRYSTALS TO LOCATE UNTWINNED SINGLE CRYSTALS 65

2.11 – SAMPLE PREPARATION AND DATA ACQUISITION FOR NANOSECOND TRANSIENT ABSORPTION (FLASH PHOTOLYSIS) EXPERIMENTS 66

2.12 – SAMPLE PREPARATION AND DATA ACQUISITION FTIR DIFFERENCE SPECTROSCOPY ON BCBR CRYSTALS. 72

2.13 – SAMPLE PREPARATION AND DATA ACQUISITION FOR FTIR DIFFERENCE EXPERIMENTS AFTER DESICANT COLUMN ADDED 80

-REFERENCES 82

CHAPTER 3 – LIGHT-DARK ADAPTATION AND TRAPPING OF THE DEPROTONATED SCHIFF BASE IN BICELLE BACTERIORHODOPSIN CRYSTALS STUDIED BY VISIBLE AND RAMAN SPECTROSCOPY 83

ABSTRACT 83

3.1 - UV-VISIBLE SPECTROSCOPY OF THE NATIVE MEMBRANE AND THE STRUCTURE OF RETINAL 83

3.2 - CONVERSION BETWEEN TWO RETINAL ISOMERS IN NATIVE FORM OF BACTERIORHODOPSIN DURING LIGHT/DARK ADAPTATION 85

3.3 - DOES RETINAL ISOMERIZE IN BICELLE BACTERIORHODOPSIN CRYSTALS? 87

EXPERIMENTAL METHODS 88

3.4 - LIGHT ADAPTATION EXPERIMENTS ON A MASS OF DETERGENT-EMBEDDED BCBR CRYSTALS 88

3.5 –SINGLE-CRYSTAL VISIBLE SPECTROSCOPY 90

3.6 –SINGLE-CRYSTAL RAMAN SPECTROSCOPY 92

3.7 –VISIBLE SPECTROSCOPY OF A MASS OF BCBR CRYSTALS DRIED IN THE DARK 94

RESULTS AND DISCUSSION 95

3.8 – LIGHT AND DARK ADAPTATION OF THE RETINAL WITHIN THE BICELLE CRYSTALS 95

3.9 – COMPARISON OF SINGLE-CRYSTAL VISIBLE ABSORPTION TO NATIVE 96

3.10 – EFFECT OF BCBR CRYSTAL DEHYDRATION IN THE DARK 99

3.11- EFFECT OF DEHYDRATION OF SINGLE BCBR CRYSTAL 100

-REFERENCES 104

CHAPTER 4 – EVIDENCE FOR THE CREATION OF THE M_{412} INTERMEDIATE BY RAMAN SPECTROSCOPY 108

ABSTRACT 108

4.1 – RAMAN SPECTROSCOPY 108

4.2 - RESONANCE RAMAN SPECTROSCOPY 109

4.3 – RAMAN SPECTROSCOPY OF BACTERIORHODOPSIN 113

4.4 – RAMAN MICRO-SPECTROSCOPY OF BCBR CRYSTALS 119

EXPERIMENTAL METHODS 120

4.5 - GROWTH OF BCBR CRYSTALS AND WASHING FROM THEIR DETERGENT MATRIX 120

4.6 - SINGLE-CRYSTAL RAMAN SPECTROSCOPY 122

RESULTS AND DISCUSSION 122

4.7 – SINGLE-CRYSTAL RAMAN SPECTROSCOPY OF HYDRATED NATIVE BR FILM AT 514 NM AND 830 NM 123

4.8 – SINGLE-CRYSTAL RAMAN SPECTROSCOPY OF SINGLE HYDRATED BCBR CRYSTAL AT 514 NM AND 830 NM 126

4.9 – EFFECT OF INCREASING THE 514 NM LASER POWER ON THE RAMAN SPECTRUM OF A SINGLE HYDRATED BCBR CRYSTAL 129

-REFERENCES 131

CHAPTER 5 – STUDY OF THE PROTON PUMP PROCESS USING FLASH PHOTOLYSIS SPECTROSCOPY 135

ABSTRACT 135

5.1 - DETECTING PHOTOCYCLE INTERMEDIATES BY PUMP-PROBE NANOSECOND SPECTROSCOPY 135

5.2 - CHARACTERIZATION OF THE M INTERMEDIATE OF THE PHOTOCYCLE 138

5.3 - EFFECTS OF LIPID REMOVAL ON PHOTOCYCLE KINETICS 140

5.4 – THE M RISE PROCESS 143

5.5 – THE M DECAY PROCESS 143

5.6 - KINETIC STUDIES ON CBR CRYSTALS 144

5.7 - KINETIC STUDIES ON BCBR CRYSTALS 146

EXPERIMENTAL METHODS 146

5.8 - DETECTING PHOTOCYCLE INTERMEDIATES BY PUMP-PROBE NANOSECOND SPECTROSCOPY 146

5.9 – SAMPLE PREPARATION 147

5.10 - INSTRUMENTATION 148

RESULTS AND DISCUSSION 151

5.11 – FLASH PHOTOLYSIS OF BCBR CRYSTALS 151

5.12 - M RISE OF BCBR CRYSTALS IN H_2O 151

5.13 - M RISE OF BCBR CRYSTALS IN D_2O 156

5.14 - M DECAY OF BCBR CRYSTALS IN H_2O 158

5.15 - M DECAY OF BCBR CRYSTALS IN D_2O 162

5.16 - KINETIC ISOTOPE EFFECT IN M RISE AND DECAY IN BCBR CRYSTALS 164

-REFERENCES 167

CHAPTER 6 - DETERMINATION OF THE ROLE OF ASPARTATE RESIDUE IN THE FUNCTION OF BCBR CRYSTALS BY FTIR DIFFERENCE SPECTROSCOPY 171

ABSTRACT 171

6.1 - DETECTING CHANGES IN AMINO ACID PROTONATION STATES IN BR CRYSTALS BY FTIR DIFFERENCE SPECTROSCOPY 172

EXPERIMENTAL 173

6.2 – FTIR DIFFERENCE EXPERIMENTS 173

RESULTS AND DISCUSSION 183

-REFERENCES 187

CHAPTER 7- MODEL SYSTEM FOR GROWING AND QUANTIFYING *STREPTOCOCCUS PNEUMONIAE* BIOFILMS IN SITU AND IN REAL TIME 188

ABSTRACT 188

7.1 - BIOFILMS: THEIR INFRASTRUCTURE AND EFFECTS ON SURFACES 189

7.2 - PROBLEMS BIOFILMS PRESENT TO THE MEDICAL FIELD 189

7.3 - BIOFILM STUDIES: BACKGROUND 190

7.4 - NONDESTRUCTIVE BIOFILM ANALYSIS: USE OF ATR/FTIR 191

7.5 - FTIR SPECTRA BAND ASSIGNMENTS IN BIOFILMS 194

7.6 - USE OF ATR/FTIR IN STUDY OF *STREPTOCOCCUS PNEUMONIAE* BIOFILMS 195

EXPERIMENTAL METHODS 196

7.7 - BENCH SETUP FOR ATR/FTIR EXPERIMENTS 196

7.8 - PREPARATION OF ATR FLOW CELL 197

7.9 - PREPARATION OF *S. PNEUMONIAE* AND REACTOR INOCULATION 200

7.10 - GERMANIUM COUPON PROCESSING AND ANALYSIS 200

7.11 - IRE PROCESSING AND ANALYSIS 201

7.12 - FTIR SPECTRA ANALYSIS 202

RESULTS AND DISCUSSION 202

-REFERENCES 212

LIST OF TABLES

CHAPTER 5

TABLE 5.1: SUMMARY OF THE M RISE AND DECAY TIMES COMPARING THE PHOTOCYCLE KINETICS OF THE BCBR CRYSTAL CRYSTALS IN DEIONIZED, DISTILLED WATER (H_2O) TO THAT OF THE NATIVE UNDER THE SAME CONDITIONS. 154

TABLE 5.2: COMPARISON IS ISOTOPE EFFECTS FOR BOTH THE M RISE AND M DECAY PROCESSES BETWEEN NATIVE AND CRYSTALS. 157

CHAPTER 7

TABLE 7.1: TOTAL AND VIABLE COUNTS OF BIOFILM–ASSOCIATED *S. PNEUMONIAE* COLLECTED FROM GERMANIUM COUPONS EXPOSED IN THE BIOFILM REACTOR.[32]
[A] DATA ARE MEANS +/- STANDARD DEVIATIONS (*N*-3)
[B] η=2 210

LIST OF FIGURES

CHAPTER 1 PAGE

FIGURE 1.1: A SINGLE MONOMER OF BR. 2

FIGURE 1.2: THE CONVERSIONS OF RETINAL ISOMER CONVERSIONS IN NATIVE BR. 3

FIGURE 1.3: ARRANGEMENT OF THE THREE MONOMERS WITHIN UNIT CELL AND WITHIN THE LATTICE. 4

FIGURE 1.4: A SIDE-VIEW ARRANGEMENT OF A SINGLE BR MONOMER IN THE PHOSPHOLIPID BILAYER. 5

FIGURE 1.5: THE PHOTOCYCLE OF BR, SHOWING THE PROTON RELEASE AND PROTON UPTAKE STEPS. 7

FIGURE 1.6: THE FUNCTION OF BR IN RELATION TO ATP SYNTHESIS. 8

FIGURE 1.7: COORDINATION OF THE RETINAL OF THE ALL-*TRANS*, BR_{568} SPECIES WITH SURROUNDING WATER MOLECULES AND AMINO ACIDS. 11

FIGURE 1.8: REGION OF THE HYDROGEN-BONDED NETWORK NEAR THE RETINAL SCHIFF BASE AND WATER 402 IN THE K_{610} INTERMEDIATE. 12

FIGURE 1.9: COORDINATION OF THE RETINAL OF THE 13-CIS, K_{610} SPECIES WITH SURROUNDING WATER MOLECULES AND AMINO ACIDS. 13

FIGURE 1.10: COORDINATION OF THE RETINAL OF THE L_{550} SPECIES WITH SURROUNDING WATER MOLECULES AND AMINO ACIDS. 14

FIGURE 1.11: THREE M STATES. 16

FIGURE 1.12: COMPARISON OF THE CYTOPLASMIC REGIONS OF THE PARENT BR_{568} SPECIES AND THE M2' STATE 18

FIGURE 1.13: COMPARISON OF THE CYTOPLASMIC REGIONS OF THE PARENT BR_{568} SPECIES (GREEN) AND THE N' STATE. 19

FIGURE 1.14: STRUCTURAL DIFFERENCES BETWEEN BR_{568} AND THE D85S MUTANT, WHICH IS USED AS A MODEL FOR THE STRUCTURE OF THE O INTERMEDIATE. 21

FIGURE 1.15: A HYPOTHESIS OF THE STEPS LEADING TO THE FORMATION OF THREE-DIMENSIONAL CBR CRYSTALS. 23

FIGURE 1.16: MORPHOLOGY OF CBR CRYSTALS THAT CAN BE GROWN BY THE *IN-CUBO* METHOD. 25

FIGURE 1.17: STRUCTURES OF THE TWO DETERGENTS USED IN BICELLE CRYSTALLIZATION OF BR. 26

FIGURE 1.18: TYPICAL DIAMOND-SHAPED BR CRYSTALS FORMED BY THE BICELLE METHOD. 27

FIGURE 1.19: COMPARISON OF THE PROTEIN PACKING STRUCTURE OF BOWIE AND FARHAM'S BICELLE BR CRYSTALS WITH THAT OF ROSENBUSCH AND LANDAU'S CBR CRYSTALS. 28

CHAPTER 2

FIGURE 2.1: COMPARISON OF BICELLE CRYSTALS MADE IN THIS LAB (LEFT) TO THOSE PRODUCED BY BOWIE AND FARHAM IN THE LITERATURE[1] (RIGHT). 40

FIGURE 2.2: LARGER BICELLE CRYSTALS MADE BY THE IMPROVED BICELLE METHOD (LEFT) AND RESULTING X-RAY DIFFRACTION PATTERN ACQUIRED FROM THE LARGER BICELLE CRYSTALS (RIGHT). 42

FIGURE 2.3: ASSEMBLY OF THE BICELLE CRYSTAL SANDWICH USED TO TAKE VISIBLE SPECTRA OF A SAMPLE OF MULTIPLE CRYSTALS EMBEDDED WITHIN THE DETERGENT MATRIX. 43

FIGURE 2.4: TOP-DOWN VIEW OF THE OPTICAL SETUP FOR PHOTO EXCITATION EXPERIMENTS ATTEMPTED USING THE 488 NM ARGON LASER. 48

FIGURE 2.5: CD SPECTRUM OF NATIVE BR IN WATER AS DESCRIBED BY WANG *ET AL.*[10] (LEFT) AND THE CD SPECTRA OF A SOLUTION OF NATIVE BR IN WATER AT THREE DIFFERENT CONCENTRATIONS (RIGHT). 52

FIGURE 2.6: EXAMINATION OF CRYSTALS BY CD SPECTROSCOPY. 54

FIGURE 2.7: EXAMPLE OF HOW ONE SAMPLE OF CRYSTALS WITHIN THEIR MATRIX WAS ROTATED INTO THREE DIFFERENT ORIENTATIONS. 54

FIGURE 2.8: THE INCONSISTENT CD SPECTRA OBTAINED FROM THREE DIFFERENT MULTIPLE-CRYSTAL SAMPLES. 55

FIGURE 2.9: COMPARISON OF THE FTIR SPECTRUM OF A SINGLE BICELLE CRYSTAL IN D_2O (LEFT) TO THAT OF A CONCENTRATED PELLET OF NATIVE BR IN D_2O. 58

FIGURE 2.10: FTIR SPECTRUM OF THE 3:1 DMPC: CHAPSO MATRIX. 59

FIGURE 2.11: DESCRIPTION OF THE LIMITATIONS OF USING A LASER POINTER AS EXCITATION SOURCE FOR SINGLE-CRYSTAL FTIR SPECTROSCOPY. 60

FIGURE 2.12: THE THREE ORIENTATIONS OF THE LONG AXIS OF A SINGLE BICELLE CRYSTAL RELATIVE TO PLANE-POLARIZED LIGHT. 63

FIGURE 2.13: THE RAMAN SPECTRA RESULTING FROM THE THREE DIFFERENT CRYSTAL ORIENTATIONS SHOW NO ORIENTATION-DEPENDENT INTENSITY DIFFERENCES. 64

FIGURE 2.14: CHANGES IN THE TRANSMISSION OF POLARIZED LIGHT IN MULTIPLE CRYSTALS VIEWED UNDER A ROTATING STAGE. 65

FIGURE 2.15: TOP-DOWN VIEW OF THE BENCH SETUP FOR THE FIRST ATTEMPT AT FLASH PHOTOLYSIS EXPERIMENTS WITH SEVERAL BICELLE CRYSTALS STIRRED IN DDW. 68

FIGURE 2.16: THE FILTER TRANSMISSION PROFILE FOR THE FLASH PHOTOLYSIS EXPERIMENTS. 68

FIGURE 2.17: SIDE (LEFT) AND TOP-DOWN VIEWS OF THE DESIGN OF THE MULTI-WELL SAMPLE HOLDER FOR TRANSIENT ABSORPTION EXPERIMENTS ON MULTIPLE CRYSTALS. 70

FIGURE 2.18: BENCH DIAGRAM FOR USING THE 532 NM INCIDENT PULSED LASER AS EXCITATION SOURCE FOR M_{412} DECAY EXPERIMENTS ON A CRYSTAL SAMPLE. 71

FIGURE 2.19: PHOTOGRAPH OF THE SIDE-VIEW OF THE SAME BENCH SETUP. 72

FIGURE 2.20: TYPICAL FTIR ABSORPTION SPECTRUM FOR A MASS OF BCBR CRYSTALS SOAKED IN D_2O ON A SINGLE CAF_2 WINDOW. 73

FIGURE 2:21: INSET OF THE PROTEIN REGION FROM ABOVE. 74

FIGURE 2.22: OVERHEAD BENCH SETUP FOR FTIR DIFFERENCE SPECTROSCOPY EXPERIMENTS. 75

FIGURE 2.23: THREE DIFFERENT ATTEMPTS TO REPLICATE THE IR DIFFERENCE SPECTRUM OF NATIVE BR AT 5ºC. 76

FIGURE 2.24: FOUR DIFFERENT 'BACKGROUND' SPECTRA OF THE EMPTY FTIR SAMPLE CHAMBER. 77

FIGURE 2.25: DIFFERENCES BETWEEN THESE BACKGROUND SPECTRA. 78

FIGURE 2.26: ADDITION OF DESICCANT COLUMN TO REMOVE RESIDUAL WATER VAPOR IN PURGE AIR BEFORE IT ENTERS FTIR SAMPLE CHAMBER. 79

CHAPTER 3

FIGURE 3.1: ABSORPTION SPECTRUM OF THE LIGHT-ADAPTED PURPLE MEMBRANE. 84

FIGURE 3.2: MICROSCOPE IMAGES OF A RANDOM ASSEMBLY OF MULTIPLE BICELLE CRYSTALS EMBEDDED WITHIN THEIR DETERGENT MATRIX (LEFT) AND OF A HYDRATED FILM OF NATIVE BR (RIGHT). 89

FIGURE 3.3: ASSEMBLY OF THE BICELLE CRYSTAL SANDWICH USED TO TAKE VISIBLE SPECTRA OF A SAMPLE OF MULTIPLE CRYSTALS EMBEDDED WITHIN THE DETERGENT MATRIX. 90

FIGURE 3.4: EFFECT OF LIGHT ADAPTATION ON THE VISIBLE ABSORPTION SPECTRUM OF SEVERAL BICELLE BR CRYSTALS SUSPENDED IN THE DETERGENT MATRIX. 96

FIGURE 3.5: COMPARISON OF BAND WIDTHS AT HALF-HEIGHT BETWEEN THE AVERAGE LIGHT-ADAPTED STATE OF A HYDRATED NATIVE FILM OF BR (SOLID LINE) AND THE AVERAGE LIGHT-ADAPTED STATE OF A SINGLE BCBR CRYSTAL (CIRCLES). 97

FIGURE 3.6: SPECTRUM OF A SINGLE HYDRATED BCBR CRYSTAL BEFORE (SOLID LINE) AND AFTER (CIRCLES) DRYING WITH STREAM OF NITROGEN UNDER BROAD BAND LIGHT. 98

FIGURE 3.7: SPECTRUM OF A MASS OF BCBR CRYSTALS AFTER DRYING IN THE DARK FOR A PERIOD OF 3-4 DAYS UNDER AMBIENT TEMPERATURE AND PRESSURE. 100

FIGURE 3.8: CHANGES IN THE RAMAN SPECTRUM OF A SINGLE AIR-EXPOSED BCBR CRYSTAL DURING INCREASE OF THE POWER OF THE 488 NM LINE OF AN ARGON LASER. 101

FIGURE 3.9: THE RAMAN SPECTRUM OF A SINGLE AIR-EXPOSED BCBR CRYSTAL LEFT IN THE DARK FOR A PERIOD OF 3-4 DAYS. 102

CHAPTER 4

FIGURE 4.1: DESCRIPTION OF THE PROCESSES INVOLVED IN OF NORMAL RAMAN SCATTERING SPECTROSCOPY. 110

FIGURE 4.2: SKETCH OF THE RESONANCE RAYLEIGH AND RAMAN SCATTERING PROCESSES. 112

FIGURE 4.3: RAMAN SPECTRUM OF $BR_{568.}$ 116

FIGURE 4.4: RAMAN SPECTRUM OF THE M_{412} INTERMEDIATE IN THE NATIVE PARENT BR_{568}. 118

FIGURE 4.5: COMPARISON OF THE FINGERPRINT REGIONS BETWEEN (LEFT) THE LIGHT-ADAPTED, ALL-*TRANS* BR_{568} AND (RIGHT) THE M_{412} INTERMEDIATES. 118

FIGURE 4.6: THE GROUND STATE (BLACK) AND EXCITED STATE (RED) RAMAN SPECTRUM ON A HYDRATED NATIVE BR_{568} FILM. 124

FIGURE 4.7: THE UNPHOTOLYZED NATIVE BR (BLACK) AND PHOTOLYZED (RED) RAMAN SPECTRUM ON A SINGLE HYDRATED BICELLE CRYSTAL. 127

FIGURE 4.8: INTENSITY CHANGES IN THE RAMAN SPECTRUM OF A SINGLE HYDRATED BICELLE CRYSTAL UNDER INCREASING POWER OF THE INCIDENT 514 NM LASER. 130

CHAPTER 5

FIGURE 5.1: SIDE-VIEW OF RETINAL (SHOWN HERE AS “SB” FOR SCHIFF BASE”) WITHIN ITS BINDING POCKET, LOCATED AT THE CENTER OF THE SEVEN-ALPHA HELICES OF THE PROTEIN. 137

FIGURE 5.2: STRUCTURES OF THE LIPID MOLECULES PRESENT IN THE NATIVE PM. 141

FIGURE 5.3: EFFECT OF THE STRUCTURE AND TYPE OF ENVIRONMENT OF THE PROTEIN IN BACTERIORHODOPSIN. 142

FIGURE 5.4: COMPARISON OF THE PHOTOCYCLE KINETICS OF CBR CRYSTALS TO NATIVE MEMBRANE. 145

FIGURE 5.5: THE MULTI-WELL SAMPLE HOLDER USED FOR FLASH PHOTOLYSIS EXPERIMENTS ON SOLUTIONS OF CRYSTALS SHOWS FROM THE SIDE (LEFT) AND FROM THE TOP-DOWN (RIGHT). 148

.

FIGURE 5.6: TRANSMISSION SPECTRUM FOR THE FILTER USED IN THESE EXPERIMENTS. 150

FIGURE 5.7: BENCH DIAGRAM FOR USING THE 532 NM INCIDENT PULSED LASER AS EXCITATION SOURCE FOR M_{412} DECAY EXPERIMENTS ON A CRYSTAL SAMPLE. 150

FIGURE 5.8: COMPARISON OF M RISE KINETICS IN DEIONIZED DISTILLED WATER (DDW), EXPRESSED AS THE INTENSITY OF THE 412 NM ABSORPTION. 153

FIGURE 5.9: COMPARISON OF M RISE KINETICS IN H_2O AND D_2O OF BCBR CRYSTALS, EXPRESSED AS THE CHANGE IN THE 412 NM ABSORPTION INTENSITY. 153

FIGURE 5.10: COMPARISON OF M RISE KINETICS IN H_2O AND D_2O OF NATIVE BR, EXPRESSED AS THE CHANGE IN THE 412 NM ABSORPTION INTENSITY. 157

.

FIGURE 5.11: COMPARISON OF M DECAY KINETICS IN DEIONIZED DISTILLED WATER (DDW), EXPRESSED AS THE INTENSITY OF THE 412 NM ABSORPTION. 158

FIGURE 5.12: COMPARISON OF M DECAY KINETICS IN H_2O AND D_2O OF BCBR, EXPRESSED AS THE CHANGE IN THE 412 NM ABSORPTION INTENSITY. 163

FIGURE 5.13: COMPARISON OF M DECAY KINETICS IN H_2O AND D_2O OF NATIVE BR, EXPRESSED AS THE CHANGE IN THE 412 NM ABSORPTION INTENSITY. 163

CHAPTER 6

FIGURE 6.1: CHANGES IN THE FTIR SPECTRUM UPON EXCITATION WITH 514 NM LASER FOR SEVERAL CBR CRYSTALS WITHIN THEIR DETERGENT MATRIX (ABOVE) AND FOR A NATIVE HYDRATED MEMBRANE (BELOW) AS DETAILED BY HEBERLE *ET AL*.[1] 173

FIGURE 6.2: TYPICAL FTIR ABSORPTION SPECTRUM FOR A MASS OF BCBR CRYSTALS SOAKED IN D_2O ON A SINGLE CAF_2 WINDOW. 174

FIGURE 6.3: INSET OF THE PROTEIN REGION FROM ABOVE. 175

FIGURE 6.4: OVERHEAD BENCH SETUP FOR FTIR DIFFERENCE SPECTROSCOPY EXPERIMENTS. 176

FIGURE 6.5: THREE DIFFERENT ATTEMPTS TO REPLICATE THE IR DIFFERENCE SPECTRUM OF NATIVE BR AT 5ºC. 177

FIGURE 6.6: FOUR DIFFERENT ‘BACKGROUND’ SPECTRA OF THE EMPTY FTIR SAMPLE CHAMBER. 179

FIGURE 6.7: DIFFERENCES BETWEEN THE BACKGROUND SPECTRA OF FIGURE 6.6. 179

FIGURE 6.8: CHANGES IN THE DIFFERENCE SPECTRUM OF THE EMPTY SAMPLE CHAMBER BEFORE THE COLUMN IS ADDED, TAKEN AT 30-MINUTE INTERVALS APART. 182

FIGURE 6.9: CHANGES IN THE DIFFERENCE SPECTRUM OF THE EMPTY SAMPLE CHAMBER AFTER THE COLUMN IS ADDED, TAKEN AT 30-MINUTE INTERVALS APART. 182

FIGURE 6.10: DIFFERENCE SPECTRUM OF A MASS OF BCBR CRYSTALS IN H_2O (A) AND OF NATIVE BR IN H_2O (B). 184

FIGURE 6.11: DIFFERENCE SPECTRUM OF A MASS OF BCBR CRYSTALS IN D_2O (A) AND OF NATIVE BR IN D_2O (B). 185

CHAPTER 7

FIGURE 7.1: TOP-DOWN VIEW OF ATR/FTIR FLOW CELL. 192

FIGURE 7.2: GENERATION OF THE EVANESCENT FIELD, WITH AN EFFECTIVE PENETRATION DEPTH OF 1µM FROM THE SURFACE OF THE IRE. 194

FIGURE 7.3: EXPERIMENTAL SETUP FOR THE ATR/FTIR FLOW CELL EXPERIMENT. 197

FIGURE 7.4: THE UN-ASSEMBLED (LEFT) AND ASSEMBLED (RIGHT) ATR FLOW CELL, MANUFACTURED BY HARRICK SCIENTIFIC. 199

FIGURE 7.5: THE BIOFILM REACTOR. 199

FIGURE 7.6: FTIR SPECTRA OF *S. PNEUMONIAE* BIOFILMS OVER THE COURSE OF 189 HOURS FOLLOWING INOCULATION. 204

FIGURE 7.7: THE CHANGING FTIR SPECTRUM OF CP-1 BIOFILM OVER THE COURSE OF 188 HOURS FOLLOWING INOCULATION AS REPORTED BY BREMER AND GEESEY. 205

FIGURE 7.8: THE CHANGING FTIR SPECTRUM OF *PSEUDOMONAS CEPACIA* BIOFILM OVER THE COURSE OF 76 HOURS FOLLOWING INOCULATION. 206

FIGURE 7.9: *S. PNEUMONIAE* BIOFILM ON IRE SURFACE[32] AFTER STAINING WITH WGA-AF AND DAPI AND IMAGING WITH DAPI FILTER SET. 208

FIGURE 7.10: *S. PNEUMONIAE* BIOFILM ON IRE SURFACE[32] AFTER STAINING WITH WGA-AF AND DAPI AND IMAGING WITH A FITC FILTER SET. 208

FIGURE 7.11: *S. PNEUMONIAE* BIOFILM ON IRE SURFACE[32] AFTER STAINING WITH WGA-AF AND DAPI AND IMAGING WITH DAPI FILTER SET. 209

FIGURE 7.12: FIGURE 10: *S. PNEUMONIAE* BIOFILM ON IRE SURFACE[32] AFTER STAINING WITH WGA-AF AND DAPI AND IMAGING WITH A FITC FILTER SET. 209

SYMBOLS AND ABBREVIATIONS

ATR/FTIR	Total Attenuated Reflectance/ Fourier Transform Infrared Spectroscopy
°C	Degrees Celcius
μm^2	Square micrometer
α	Alpha
Å	Angstrom
ADP	Adenosine diphosphate
Ala_{215}	Alanine 215
AS	Anti-Stokes
Asp_{212}	Aspartate 212
Asp_{85}	Aspartate 85
Asp_{96}	Aspartate 96
ATP	Adenosine triphosphate
bcbR	Bicelle bR
BHI	Brain Heart Infusion
bR	Bacteriorhodopsin
cbR	*In-cubo* bacteriorhodopsin crystals
CDC	Centers for Disease Control
CFU	Colony-forming unit
CHAPS	3-[(3-Cholamidopropyl) dimethylammonio]-1-propanesulfonate
CHAPSO	3-[(3-Cholamidopropyl) dimethylammonio]-2-hydroxy-1-propanesulfonate
cm^{-1}	wavenumbers
cm^{-2}	Square centimeter
CO_2	Carbon dioxide
DAPI	4’6-diamidino-2-phenyl indole
DDW	Deionized distilled water
DIC	Differential interference contrast
DMPC	1,2-Dimyristoyl-*sn*-Glycero-3-Phosphocholine
DNA	Deoxyribonucleic acid
EPS	Extracellular Polymeric Substances
GLS	Glycolipid sulfate
h	hour
H. salinarium	*Halobacterium salinarium*
H^+	Proton
H_2O	water
Hz	Hertz
IR	Infrared
IRE	Internal Reflection Element
kDa	Kilodalton

kHz	Kilohertz
KIE	Kinetic Isotope Effect
$\lambda_{\mu\alpha\xi}$	Absorption maximum
Lys_{216}	Lysine 216
M	Molar
$\gamma\mu$	Microgram
mg	Milligram
MHz	Mega Hertz
mJ	Millijoule
mL	Milliliter
$\mu\mu$	Micrometer
mm	Millimeter
mM	Millimolar
MO	Monoolein
MP	Monopalmitoyl
ms	Microsecond
$\mu\sigma$	Microsecond
$NADP^+$	Nicotinamide adenine dinucleotide phosphate
NADPH	Reduced nicotinamide adenine dinucleotide phosphate
NaH_2PO_4	Sodium phosphate monobasic
Nd:YAG	Neodymium:Yttrium Aluminum Garnet
N-H	Nitrogen-hydrogen
nm	nanometer
ν_o	Incident wavelength
O_2	Molecular oxygen
OG	ß-octylglucoside
PBS	Phosphate-buffered saline
PG	Phosphatidyl glycerol
PGP-Me	5-phosphatidyl glycerophosphate
PGS	Phosphatidyl glycerosulfate
P_i	Inorganic phosphate
pKA	Negative log of the acid dissociation constant, Ka.
PM	Purple membrane
PMT	Photomultiplier tube
ps	Picoseconds
PSB	Protonated Schiff base
R	Rayleigh
RNA	Ribonucleic acid
Rpm	Revolutions per minute
S	Stokes
S. pneumoniae	*Streptococcus pneumoniae*
SQ	Squaline

Thr_{178}	Threonine 178
Trp_{182}	Tryptophan 182
W	Watt
Xe	Xenon

SUMMARY

There are two contributions of this thesis. In the first part and bulk of the thesis (the first six chapters) our studies are aimed at the relationship between the protein packing structure of bacteriorhodopsin (bR) and its function as a proton pump. In 2002, a novel crystallization method published by Bowie and Farham[1] resulted in an unusual antiparallel monomeric packing structure of bicelle bacteriorhodopsin (bcbR) crystals, the spectroscopic properties of which had not been studied. In this thesis, these 'bicelle bR crystals' are investigated to better understand how the changes in the protein tertiary structure affect the function. Specifically: Does the retinal Schiff base retain its ability to isomerize in this unusual protein packing structure of bR? How is the hydration of its binding pocket affected? Does the protein retain the ability to undergo the photocycle and pump protons? If so, how are the rates of the deprotonation/reprotonation of the Schiff base affected by the antiparallel monomer packing structure of the protein? Is Asp_{85} still the proton acceptor during the deprotonation process of the photocycle? In this work, visible, Raman, FTIR, and single-wavelength transient absorption spectroscopy (flash photolysis) have been used to answer these questions.

The first chapter of this thesis provides an introduction to the structure and function of the purple transmembrane protein bacteriorhodopsin (bR) of the organism *Halobacterium salinarium*, detailing the spectroscopic characterization of the photocycle. The protein was first characterized by Oesterhelt and Stoeckenius[2] in 1971 and has been studied for over thirty years. The bR packing structure resulting from the *in-cubo* crystallization method for bR, first published by Rosenbusch and Landau in 1996, is

introduced later in this chapter. In their crystals, the parallel trimer protein packing motif of native bR is preserved, and the photocycle kinetics is practically unchanged from that of native.[3] In contrast, the bcbR crystals studied in this thesis have an antiparallel monomer packing structure. How will this affect the function of bR crystallized in this way?

The second chapter of the thesis details *all* experiments attempted during the course of this work. It begins with discussing the details of the synthetic method to duplicate the bcbR crystallization method in our labs, as well as the modified synthesis method which gave us the larger bcbR crystals that were used for further spectroscopy. The experimental details of each successful experiment are provided again in the following chapters that address the questions at hand.

Chapter three discusses the ability of the retinal Schiff base of the bcbR crystals to isomerize upon exposure to light. It is observed that the retinal Schiff base within the bcbR crystals is still photo-responsive; reversible changes in the absorption maximum upon exposure to light illustrates that the light-dark adaptation processes are still taking place. The visible absorption spectrum of hydrated, light-adapted single bcbR crystals is compared to that of hydrated, light-adapted native bR to better understand the hydration environment of the retinal Schiff base binding pocket within the bcbR crystals. From these studies, it is concluded that the band broadening in single bcbR crystals relative to native bR is due to a difference in hydration environments among the various retinal binding pockets within the bcbR crystals, a characteristic shared in the cbR crystals. Finally, experiments are described that show that the deprotonated retinal Schiff base of the bcbR crystals can be formed photochemically (not thermally) and is ‘trapped’ by

dehydration. In these visible and Raman spectroscopy experiments, it was shown that it is possible to 'trap' the deprotonated retinal Schiff base if the bcbR crystals are dried under exposure to either broad band light, or 514 nm laser excitation. Raman and visible spectroscopy performed on bcbR crystals that are dehydrated in the dark do not result in the previously-observed deprotonated Schiff base, thereby confirming that retinal Schiff base deprotonation is a photochemical process, not simply the product of a thermal deprotonation of the parent species. A manuscript based on the work described in this chapter has been accepted for publication by Photochemistry and Photobiology.

Chapter four discusses the use of Raman microspectroscopy on single hydrated bcbR crystals using the 514 nm incident wavelength in an attempt to detect bands belonging to the M intermediate. In Chapter three, dehydration under broadband light was used as a means to both create and trap the M intermediate in the bcbR crystals. In this chapter, the focus is on the formation of the M intermediate in hydrated single bcbR crystals. From these studies, Raman bands belonging to both the parent and the M intermediate are observed in the hydrated bcbR crystals. To demonstrate that the new bands appearing are actually due to the photochemical formation of the M intermediate and not simply due to resonance enhancement of a thermally formed M analogue, Raman band intensities were monitored as a function of 514 nm laser power. In these studies the intensities of the Raman bands increased nonlinearly with the increasing laser power, confirming that in the hydrated bcbR crystals the M intermediate is being formed photochemically.

Chapter five discusses the use of single-wavelength transient absorption spectroscopy (flash photolysis) to monitor the rise and decay kinetics of the M intermediate in bcbR crystals in both H_2O and D_2O. In these studies, the M intermediate rise time in bcbR

crystals is found to be faster compared to that of native bR and cbR crystals, with a decay time that is much slower than in these other two forms of bR. Possible explanations for these observations are given. Data contained within chapters four and five have been written in a manuscript that was published Biophysical Journal.[4]

In Chapter six, FTIR difference spectroscopy is used to monitor both the changes in the protein *and* the surrounding amino acids during the proton transfer time scale. All work up to this chapter had solely monitored the changes in the retinal Schiff base in the bcbR crystals. FTIR difference spectroscopy permits the observation of changes not only in the retinal, but also in the surrounding amino acids. Model experiments performed by Heberle *et al*.[3] on cbR crystals are discussed as guide for these experiments on bcbR crystals. In chapter five, it was determined that the M rise process in the hydrated bcbR crystals was much faster than it is in either native bR or cbR crystals; the goal of the experiments in Chapter six is to probe whether the faster M rise process is facilitated by a different amino acid residue serving as the proton acceptor in the reaction. It is found that, as in the case for native bR and cbR crystals, Asp_{85} is the proton acceptor during the formation of the M intermediate in bcbR crystals. In addition, the C=C stretch region of the deprotonated retinal Schiff base in the bcbR crystals in either H_2O or D_2O is found to be more broad than in native and in the previously-observed cbR crystals. The possibility of our ability to resolved the C=C stretch in the two M states in bcbR crystals is discussed.

The second contribution of the thesis, described in Chapter seven, describes the surface attachment and growth of the biofilm formed by the pathogenic bacterium *Streptococcus pneumoniae* using attenuated total reflection/Fourier transform infrared

spectroscopy (ATR/FTIR). This organism was chosen for its clinical significance; it is one of the organisms suspected in forming biofilms in individuals who develop otitis media, one of the most common causes of ear infections of childhood.[5] In contrast to previous ATR/FTIR experiments examining the formation of biofilms on surfaces, this method is unique in that it combines two techniques - ATR/FTIR and Epifluorescence microscopy – which when used together allow for the simultaneous monitoring of the IR spectrum of the *S. pneumoniae* biofilm as it develops and as provides a method for quantifying total and viable cell counts at various stages during the development. The formation of both the protein and the polysaccharide were followed in time by monitoring their absorbance bands in the IR spectrum and were correlated with the total and viable biofilm cell counts to quantify the biofilm-associated cells. Previous work by Bremer and Geesey on biofilm formation of an unidentified environmental organism ("CP-1") and work by Nivens *et al*.[7] on *Burkholderia (Pseudomonas) cepacia* both demonstrated that the protein component develops at a faster rate than the polysaccharide component. In contrast, in these studies it was found that *S. pneumoniae* biofilm development has a faster rate of polysaccharide development relative to protein. This increase in the ratio of polysaccharide to protein with *S. pneumoniae* indicates that there are distinct differences in biofilm structure that may be exhibited by different organisms.[8] Furthermore, the staining results provide evidence that the EPS of *S. pneumoniae* is at least partially comprised of the capsular polysaccharide *N*-acetylglucosamine.[8] Data contained within this chapter were published in 2004 in Applied and Environmental Microbiology.[9]

References

(1) Bowie, J.; Farham, S. *Journal of Molecular Biology* **2002**, *316*, 1.

(2) Oesterhelt, D.; Stoeckenius, W. *Nature (London), New Biology* **1971**, *233*, 149.

(3) Heberle, J.; Buldt, G.; Koglin, E.; Rosenbusch, J. P.; Landau, E. M. *Journal of molecular biology* **1998**, *281*, 587.

(4) Sanii, L. S.; Schill, A. W.; Moran, C. E.; El-Sayed, M. A. *Biophysical Journal* **2005**, *89*, 444.

(5) Werkhaven, J. A.; Reinisch, L.; Sorrell, M.; Tribble, J.; Ossoff, R. H. *Laryngoscope* **1994**, *104*, 264.

(6) Bremer, P. J.; Geesey, G. G. *Biofouling* **1991**, *3*, 89.

(7) Nivens, D. E.; Palmer, R. J., Jr.; White, D. C. *Journal of Industrial Microbiology* **1995**, *15*, 263.

(8) Donlan, R. M.; Piede, J. A.; Heyes, C. D.; Sanii, L.; Murga, R.; Edmonds, P.; El-Sayed, I.; El-Sayed, M. A. *Applied and Environmental Microbiology* **2004**, *70*, 4980.

(9) Donlan, R. M.; Piede, J. A.; Heyes, C. D.; Sanii, L. S.; Murga, R.; Edmonds, P.; El-Sayed, I.; El-Sayed, M. A. *Applied and Environmental Microbiology* **2004**, *70*, 4980.

CHAPTER 1

THESIS INTRODUCTION: SUMMARY OF THE STUDIES OF THE STRUCTURE AND FUNCTION OF THE TRANSMEMBRANE PROTEIN BACTERIORHODOPSIN OF THE ORGANISM HALOBACTERIUM SALINARIUM AND ITS BICELLE CRYSTALLIZATION METHOD

Abstract

In this chapter, previous studies on the structure and function of wild type bacteriorhodopsin membranes are reviewed.

1.1. Bacteriorhodopsin - Structure and Function

Bacteriorhodopsin ("bR") is a 248-amino acid, 26 kDa transmembrane protein first discovered in the purple membrane (cell membrane) of the salt-marsh bacterium *Halobacterium salinarium* by Oesterhelt and Stoeckenius in 1971.[1] The *H. salinarium* cell's membrane contains lipids, which maintain the structural integrity of the cell. A single monomer of bR consists of seven α-helices labeled A→G, looped across the lipid bilayer, named from its N terminus to its C terminus, which surround a single molecule of the chromophore retinal[2] Figure 1.1 shows a single monomer of bR with the seven alpha helices surrounding the retinal chromphore, shown here in green. This image was made with VMD and is owned by the Theoretical and Computational Biophysics Group, an NIH Resource for Macromolecular Modeling and Bioinformatics, at the Beckman Institute, University of Illinois at Urbana-Champaign, URL http://www.ks.uiuc.edu/.

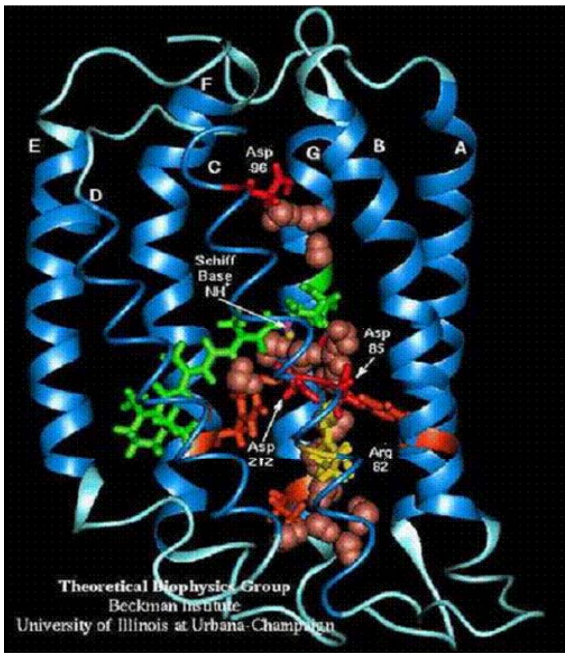

Figure 1.1: A single monomer of bR.

Retinal is bound to the Lys_{216} residue via a positively-charged, protonated Schiff base (PSB). Bound to the protein in this way the protein's absorption maximum (λ_{max}) is red-shifted to 570 nm, giving it its characteristic purple color. This is in contrast to retinal's 380 nm λ_{max} in solution.[1] Retinal contained within this binding pocket has the ability to photo-isomerize about its C_{13}-C_{14} bond. This photo-isomerization makes it possible for retinal to be found in either the all-*trans*,15-*anti* or the 13-*cis*,15-*syn* conformation.[3-6] When the protein is kept in the dark for several hours, the retinal isomer composition is a mix of these two isomers; under these conditions the protein is said to be "dark-adapted" and has a visible absorption spectrum centered at about 560 nm[7-10] Under illumination, this ratio shifts to nearly 98% all-*trans*,*15-anti*; the absorption shifts to about 568 nm, and the protein is said to be "light-adapted".[11] In Figure 2.2a, dark adapted bR consists of a mixture of the 13-*cis*,15-*syn* and all-*trans*,15-*anti* retinal isomers. Light adaptation shifts

this population to over 98% of the all-*trans*, 15-*anti* isomer. In Figure 2.2b, the all-*trans*,15-*anti* retinal isomer is converted to the high energy 13-*cis*,15-*anti* conformation via the absorption of a photon in the first step of the photocycle to form the K_{610} intermediate.

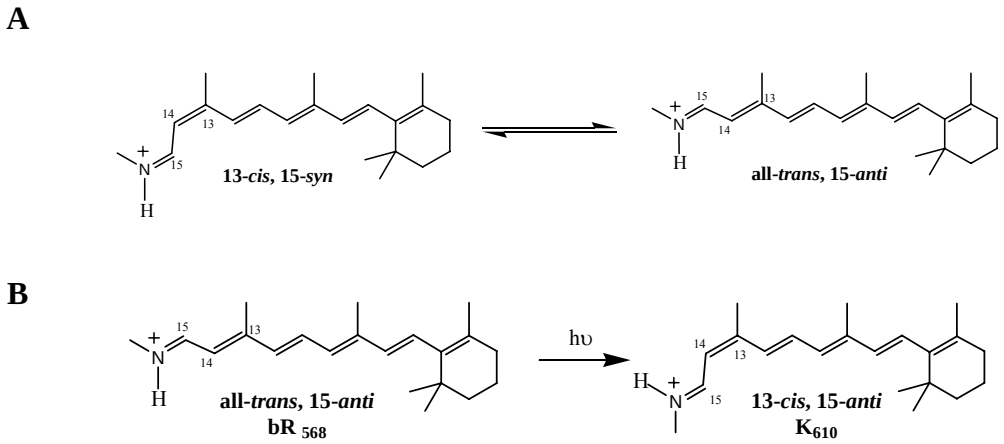

Figure 1.2: The conversions of retinal isomer conversions in native bR.

The thermal relaxation of the 13-*cis*,15-*anti* isomer will drive the photocycle that results in the movement of protons from the cytoplasmic to extracellular side of the cell. Photoexcitation of the all-*trans*,15-*anti* retinal yields the K_{610} intermediate of the photocycle, the 13-*cis*,15-*anti* isomer with a quantum efficiency[12-14] of approximately 0.6. This 13-*cis*,15-*anti* form stores enough potential energy in the protein to allow it to pump a proton across the membrane and revert back thermally to the all-*trans*,15-*anti* form via a series of intermediate whose absorption spectra have been well characterized.[15-20] Three bR monomers together make up the trimer unit cell. These

trimer unit cells are arranged in a hexagonal lattice within the purple membrane.[2] Figure 1.3 shows the three bR monomers making up the trimer unit cell (left) and the hexagonal lattice made up of the trimer units cells (right). Lipids are shown in white. These images was made with VMD and is owned by the Theoretical and Computational Biophysics Group, an NIH Resource for Macromolecular Modeling and Bioinformatics, at the Beckman Institute, University of Illinois at Urbana-Champaign, URL http://www.ks.uiuc.edu/.

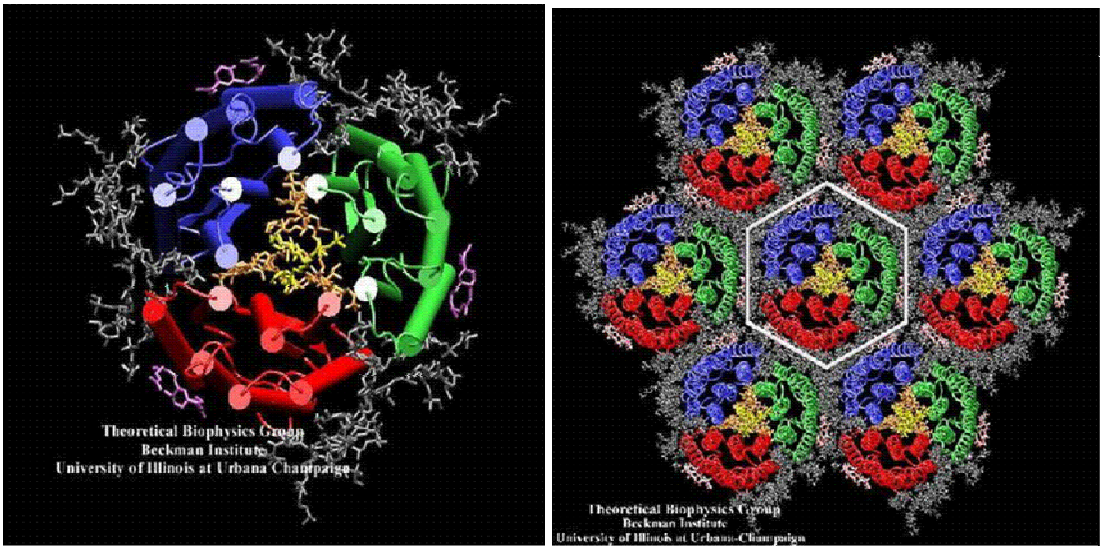

Figure 1.3: Arrangement of the three monomers within unit cell and within the lattice.

Lipids (about 10 lipid molecules per bR) hold this hexagonal lattice together and account for about 20% of the membrane weight (80% by the bR).[21,22] Figure 1.4 shows a side-view arrangement of a single bR monomer inserted in the phospholipid bilayer as described by Nelson and Cox.[23]

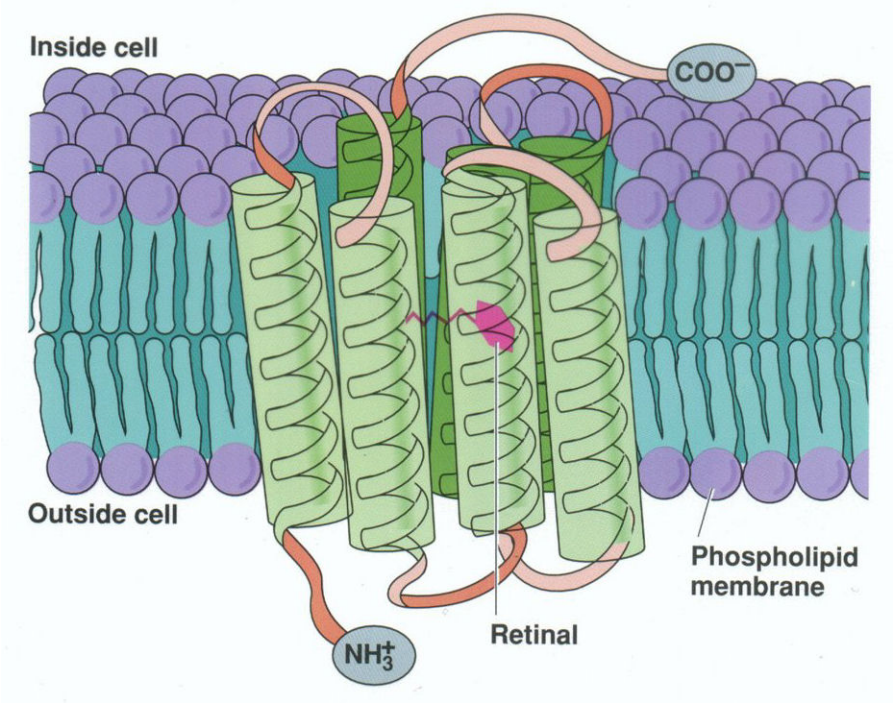

Figure 1.4: A side-view arrangement of a single bR monomer in the phospholipid bilayer.

The photocycle of bR has been studied extensively for over thirty years. It involves motions of the retinal chromophore and the surrounding protein that affect the charge density surrounding retinal. This changing charge density around retinal during the photocycle results in changes in retinal's absorption maxima during the course of the cycle. The proton translocation mechanism has been characterized by a series of steps, each involving the rise and decay of intermediates with characteristic visible absorption spectra. The intermediates of the cycle are given below with their rise times and absorption maxima in subscripts:[11,18,24-39]

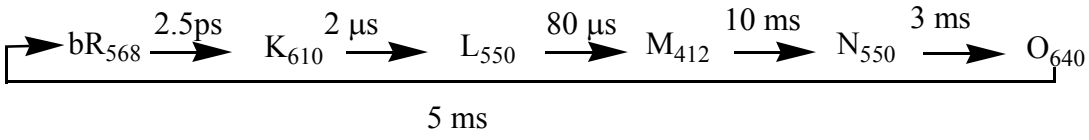

The net effect of this photocycle is the pumping of a proton from the cytoplasmic to the extracellular side of the cell membrane. The origin of this proton is the protonated Schiff base region of the retinal chromophore. Figure 1.5 shows the photocycle of bR, showing the proton release and proton uptake steps. The photocycle of bR (top) and the visible absorption spectra for the intermediates in the cycle, adapted from the work of Cartailler and Luecke.[40] Note the spectrally distinct M intermediate, the longest-lived intermediate in the photocycle. Figure 1.5a demonstrates the proton translocation steps of the bR photocycle, and Figure 1.5b shows the absorption spectrum for each of the intermediates. Note that the absorption spectrum of the M_{412} intermediate is blue-shifted and thus spectrally well-resolved from the other intermediates.

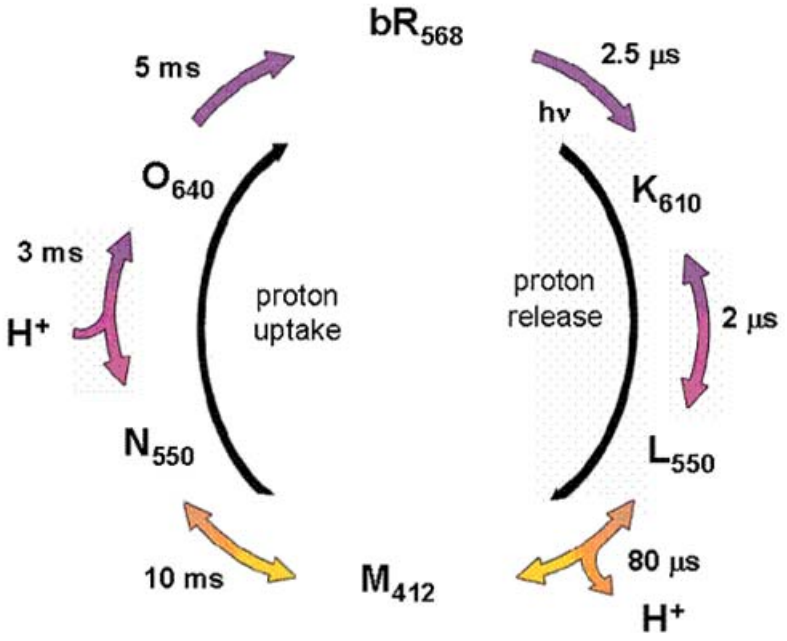

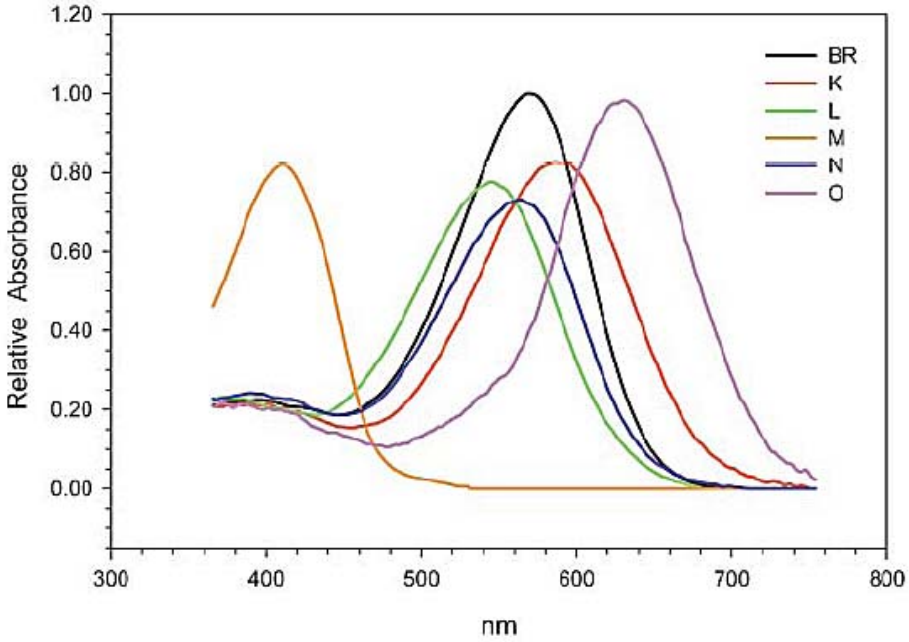

Figure 1.5: The photocycle of bR, showing the proton release and proton uptake steps.

1.2. Photocycle as a means of ATP production

During the photocycle, protons are moved from the cytoplasmic to extracellular side of the cell, which establishes a proton gradient. This proton gradient is important because it drives the reaction of adenosine diphosphate (ADP) plus inorganic phosphate (P_i) via the enzyme ATP synthase to create adenosine triphosphate (ATP). This process is shown in Figure 1.6.

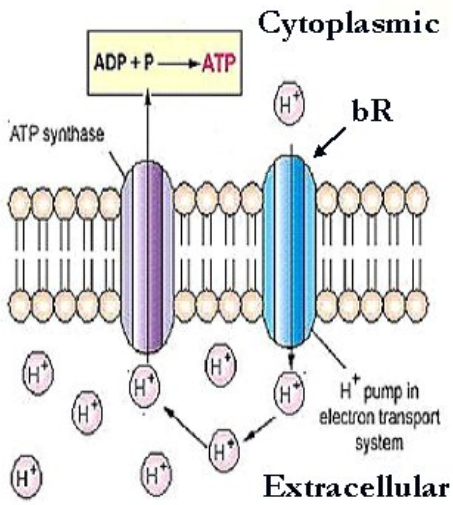

Figure 1.6: The function of bR in relation to ATP synthesis.

The bR protein moves protons from the cytoplasmic to the extracellular side of the phospholipids bilayer, in the process creating a high proton concentration on the extracellular side relative to the cytoplasmic side (creation of a proton gradient). This proton gradient results in the movement of the protons through the enzyme ATP

synthase, which uses the proton movement to add adenosine diphosphate (ADP) and inorganic phosphate (P_i) to create adenosine triphosphate (ATP).[41]

The creation of ATP is important because this molecule is the energy currency for the cell; its arrangement of three negatively-charged phosphate groups is an unstable energy-storing spring that relaxes upon the enzymatic transfer of the terminal phosphate group to other compounds.[42] The phosphorylation of compounds then primes them to undergo some kind of change that performs work for the cell. In summary then, the price of most cellular work is the breakdown of ATP to ADP and P_i (inorganic phosphate) and the cell must constantly regenerate its ATP supply.

There are two means for energy (ATP) production within the cell: oxidative phosphorylation and photosynthesis. [42,43] Which process takes place is dictated by the amount of oxygen available to the cell. Under conditions of sufficient oxygen tension, aerobic cellular respiration takes place, with oxidative phosphorylation being the last step of this process. During cellular respiration, the cell breaks down glucose through a series of energy-releasing reactions that have the net effect of transferring electrons to hydrogen ions and molecular oxygen to form water in the last step of the process, oxidative phosphorylation.[42] The energy released in these reactions is stored in a form that the mitochondrion (the cell's energy-producing factories) can use to make ATP. It is important to note that for oxidative phosphorylation to take place there must be a sufficient O_2 tension in the cell's environment.

In photosynthesis, on the other hand, ATP synthesis occurs by the light energy-induced breakdown of carbon dioxide and water to produce organic material and oxygen in the "light reaction" stage of photosynthesis.[43] In this stage, absorbed light drives both

electron transfer and hydrogen transfer reactions from water to the acceptor $NADP^+$ (nicotinamide adenine dinucleotide phosphate) to create NADPH. NADPH is now a source of energized electrons. In addition, the light reactions also generate ATP by providing enough energy for phosphorylation of ADP, the addition of a phosphate group to ADP to produce ATP. A key difference between these two processes of ATP generation: for oxidative phosphorylation to occur there must be a sufficient level of oxygen present to act as acceptor for the electrons and hydrogen ions in the energy-releasing reactions that drive ATP synthesis. On the other hand, for photosynthesis to occur there must be sufficient light energy to provide enough solar power to start the breakdown of CO_2 and water to ultimately produce organic material and oxygen.

Under conditions of low oxygen tension, the bacterium produces more purple membrane, which allows the organism to switch from oxidative phosphorylation to photosynthesis as a means of energy production.[44]

1.3. The Intermediates of the bR Photocycle

As mentioned before, in the dark, bR contains a 1:1 ratio of 13-*cis,*15-*syn* and the all-*trans,*15-*anti* retinal isomers and has an absorption maximum in the visible of 560 nm. Upon exposure to light (light adaptation), this isomeric ratio changes to nearly 98% all-*trans,*15-*anti* and the absorption maxima shifts to 568 nm. It is the all-*trans,*15-*anti* retinal that is capable of undergoing the photocycle upon photon absorption. The motions of retinal within its binding pocket and surrounding water molecules have been studied by a number of groups. In 2003 Lanyi and Schobert[45] published structural

models describing the motions of retinal and its interaction with water molecules and surrounding charged amino acids that participate in the proton translocation mechanism. In the parent, all-*trans* bR_{568} state, retinal is in its all-*trans* form. The N—H bond is pointing toward the oxygen atom of water 402, and a hydrogen-bonded network exists between the protonated Schiff base of retinal, water 402, Asp_{85}, Asp_{212}, and water 401 Figure 1.7 shows the coordination of the retinal of the all-*trans*, bR_{568} species with surrounding water molecules and amino acids, adapted from Lanyi and Schobert.[45] Carbon atoms are shown in grey, nitrogen in blue, oxygen in white, and hydrogen in red.

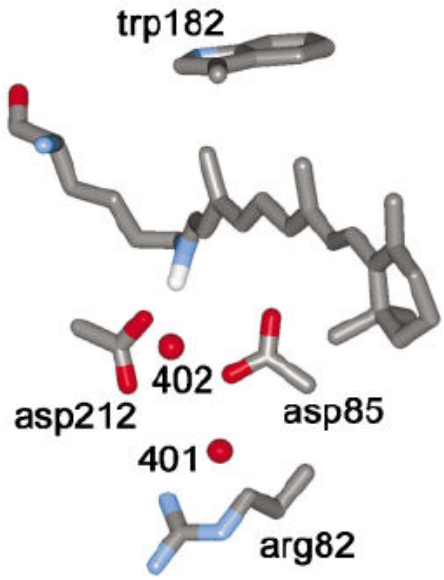

Figure 1.7: Coordination of the retinal of the all-*trans*, bR_{568} species with surrounding water molecules and amino acids.

The K intermediate was first characterized in 1974 by Stoekenius and Lozier using flash spectroscopy [26] as a 610-nm-absorbing species. In native bR under ambient

temperature the rise time of K is 3-5 ps[46,47] and it decays in 1 ms.[48] In 1982 Rothschild and Marrero used Fourier-transform infrared (FTIR) difference spectroscopy[49] to compare the structural changes occurring between bR_{568} and K_{610}. While the bR_{568} species has a protonated Schiff base, the K intermediate has a Schiff base that is altered but still is associated to some degree with a proton. The most recent crystallographic evidence of the structure of K was provided by Schobert *et al.*[50] in 2002 and demonstrates that the retinal is in 13-*cis*, 15-*anti* form, with the C_{13}=C_{14} bond rotated nearly fully *cis* from its initial *trans* configuration. However, the C_{14}-C_{15} and the C_{15}=NZ bonds are partially counter-rotated. In this form the N-H bond vector is roughly in the extracellular direction, but the angle of the hydrogen bond with water 402, which connects it to the anionic Asp85 and Asp96, is not optimal. Figure 1.8 shows the region of the hydrogen-bonded network near the retinal Schiff base and water 402 in the K_{610} intermediate, adapted from Schobert *et al*.[50] Hydrogen bonds are shown in green.

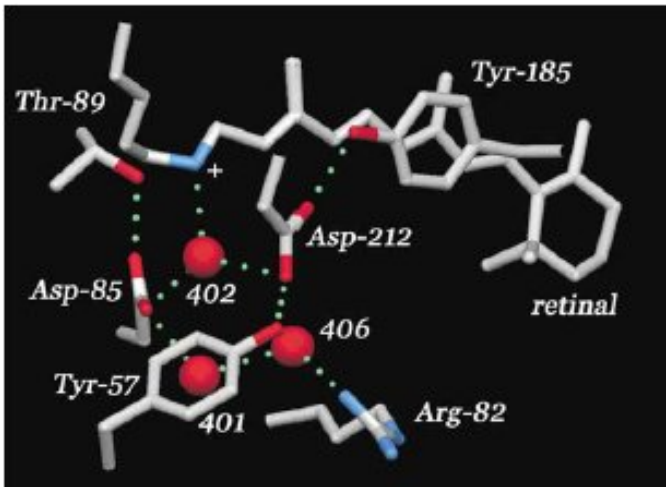

Figure 1.8: Region of the hydrogen-bonded network near the retinal Schiff base and water 402 in the K_{610} intermediate.

This weakening of the hydrogen bond may account for the deprotonation step that occurs later in the cycle. Figure 1.9 shows another illustration of the K_{610} intermediate as characterized by Lanyi and Schobert.[45]

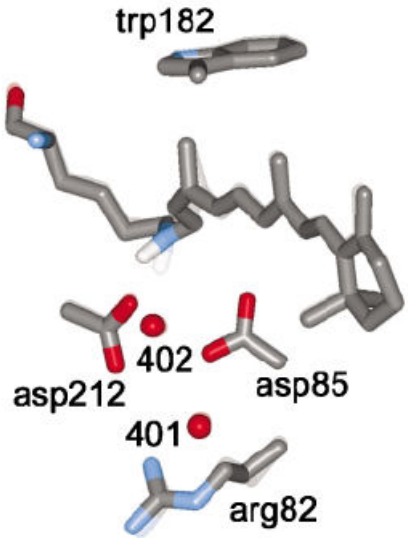

Figure 1.9: Coordination of the retinal of the 13-cis, K_{610} species with surrounding water molecules and amino acids.

The bR_{568} parent is shown in shadow overlay to describe the atomic changes between these two intermediates, and again shows how the N-H trajectory of the retinal changes in relation to water 402, moving away from the oxygen atom. The K_{610} intermediate is a high-energy state,[45] with about half of the excess energy gained residing in the distorted bond angle at C_{13}, and the rest of the excess energy most likely residing in the bond torsions along the retinal between C_{14} and the nitrogen atom, and also the increased charge separation between water 402 and NHZ^+ from the weakening of the hydrogen bond between the Schiff base and water 402. The retinal is distorted because the

surrounding protein matrix resists accommodation of the changed geometry upon its photo-isomerization.[45] Proton transfer to water 402, and then from water 402 to Asp_{85} that would break the electrostatic interaction of the Schiff base with its counter-ion is hindered by the acute angle of the NZ-H···O atoms.[45,51]

Stoekenius and Lozier were also the first to characterize the L intermediate in 1974 by using flash spectroscopy as a 550 nm-absorbing species.[26] In native bR, the K→ L transition is approximately 1 μs and it decays in 40 μs.[27,52-54] Lanyi and Schobert[45] have also characterized the L_{550} intermediate, the retinal takes on a less distorted 13-*cis*, 15-*anti* configuration than its K_{610} precursor.[55-57] Figure 1.10 details the structures of L_{550}.

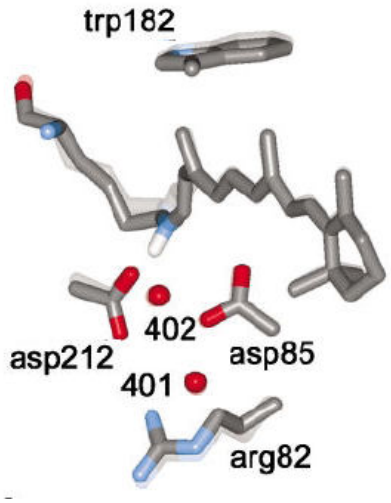

Figure 1.10: Coordination of the retinal of the L_{550} species with surrounding water molecules and amino acids.

In the L_{550} species, rotation of the C_{13}=C_{14} and the C=NZ bonds return the NZ-H···O hydrogen bond closer to linearity, and perhaps shorten the proton transfer path to Asp_{85}

via water 402.[45] Carbon atoms are shown in grey, nitrogen in blue, oxygen in white, and hydrogen in red. The arrangement of atoms in the previous bR_{568} structure is shown in shadow overlay for comparison. In the L_{550} species, rotation of the C13=C14 and the C=NZ bonds return the NZ-H···O hydrogen bond closer to linearity, and perhaps shorten the proton transfer path to Asp_{85} via water 402.[45]

The M intermediate was first characterized in 1974 by Stoekenius and Lozier using flash spectroscopy as a 412 nm-absorbing species.[26] The M_{412} intermediate is distinct for several reasons. One, it is the only intermediate of the cycle in which the Schiff base is deprotonated; as a result, its visible absorption is blue-shifted relative to all other intermediates in the cycle.[32,58-61] Two, it is the longest-lived intermediate of the cycle.[18] The rise time is often characterized in the tens of microseconds[62,63] with a decay time in the tens of milliseconds.[64,65] Three, the M_{412} state is often called the 'molecular switch' in the cycle; during the lifetime of this intermediate the retinal rotates its orientation from the hydrophilic extracellular channel to the more hydrophobic cytoplasmic channel.[66-71] The M_{412} intermediate has often been characterized as not a single intermediate but a series of intermediates in which the Schiff base is deprotonated. In 1975 Slifkin and Caplan demonstrated that there were at least two species of M_{412} intermediate present with different lifetimes,[72] a finding that has been repeatedly confirmed.[73] The rise time of this intermediate has often been characterized as a biexponential process.[62,74] Two primary models have been presented to account for the biexponential rise of M_{412}. The first model is of that of parallel photocycles; that there are two different ground state bR species, each going through their own photocycle with the same spectral intermediates.[75-77] The other model assumes that there is only one

photocycle but that there is a transition between two M states, M_1 and M_2, that is spectrally silent in the visible region.[20,65,78,79] The idea is that during the $M_1 \rightarrow M_2$ transition the Schiff base redirects its orientation from the extracellular to the cytoplasmic half-channel [80] when it accepts the proton from Asp_{96}, the only ionizable residue in the cytoplasmic half-channel.[38]

Exploring this later idea of a single pathway involving multiple M states, in 2003 Lanyi and Schobert described three distinct M states, dubbed M1, M2, and M2' (Figure 1.11).

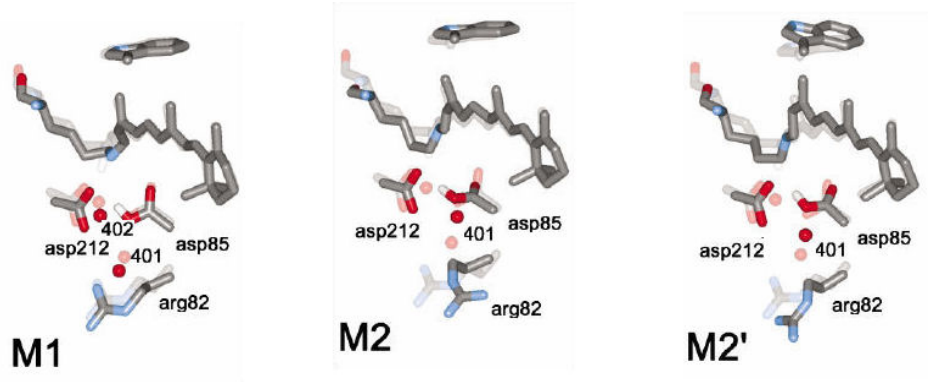

Figure 1.11: Three M states.

Carbon atoms are shown in grey, nitrogen in blue, oxygen in white, and hydrogen in red. The parent bR_{568} structures are shown in shadow behind each M state to emphasize the changes. The switching of the retinal nitrogen atom's orientation from the extracellular to the cytoplasmic side occurs going from M1 to M2; this rotational freedom is allowed by the loss of the electrostatic interaction between the nitrogen and its counter-ions and hydrogen bond present in M1. In M2' small changes in the cytoplasmic region

take place, due to F-G helix repacking and the pushing of retinal's 13-methyl group against the Trp_{182} indole ring.[45]

In the M1 state, the retinal resembles K but contains a deprotonated Schiff base and a less distorted C_{13} bond angle.[45] Water 402 moves away from the unprotonated Schiff base, which breaks the connection between NZ, Asp_{85} and Asp_{212}.[45] In the M1 state the L↔M1 equilibrium still favors the protonated Schiff base[39,45,81] but further relaxation in M2 will shift the equilibrium toward more extensive deprotonation.[45] During the M1 to M2 reaction, the nitrogen of the Schiff base switches from facing the extracellular channel to the cytoplasmic channel. This can occur since the Schiff base nitrogen at this point has lost its electrostatic interaction with its counter-ion[51,82] as well as its hydrogen bond[70] that were present in M1.[45] The M1 to M2 reaction has been deduced mainly from the kinetics[39,45,81] and a small absorbance shift in the maximum of the M state[45,83,84] In the M2 state water 402 is no longer detected.[45] In M2', small changes in the cytoplasmic region take place, initiated by both repacking of side-chains between helices F and G,[45,85] and the pushing of the 13-methyl group of retinal against the Trp_{182} indole ring of the F helix.[45] When the Trp_{182} indole ring tilts, it breaks its connection with the carbonyl group of Ala_{215} via water 501, which up to this point served as the link between helices F and G near the retinal.[45,85] A comparison between the bR_{568} and M2' state is shown in Figure 1.12.[85]

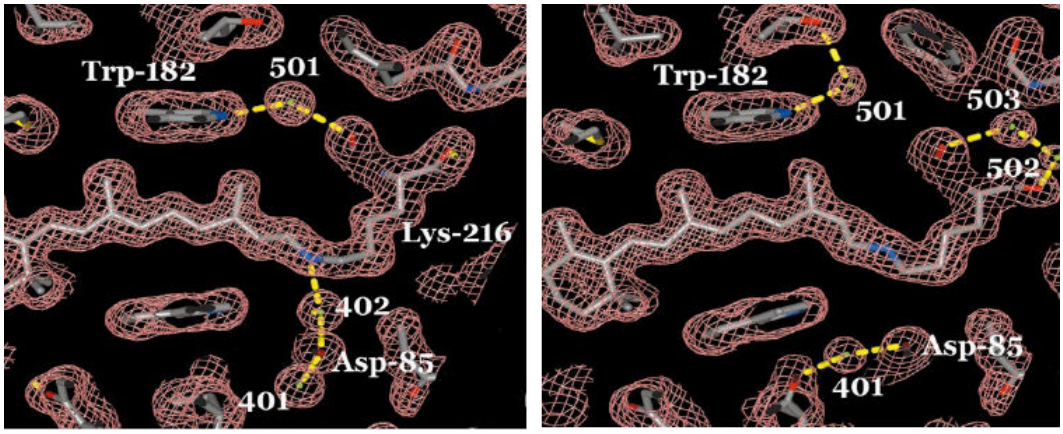

Figure 1.12: Comparison of the cytoplasmic regions of the parent bR_{568} species and the M2' state

In the parent species, water 501 in the cytoplasmic region connects the Trp_{182} residue on the F helix to the Ala_{215} residue on the G helix. In the M2' state the hydrogen bridge connecting Trp_{182}, water 501, and Ala_{215} no longer exists, and a new hydrogen bond forms between water 502 and water 503.

After this happens, water 501 no longer connects helices F and G, and instead forms a hydrogen bond between Thr_{178} and Trp_{182}, which both reside on helix F. Water 502 remains hydrogen-bonded to Lys_{216}, but it has moved 1.3 Å and acquired a new hydrogen bond to a new water molecule 503, which had not been evident in the bR_{568} state.[85] These steps, followed by a cascade of detailed events as described in detail by both Luecke *et al.*[85] and Schobert *et al.*[71] result in the eventual movement of a proton from the Asp_{96} residue to the deprotonated Schiff base. Reprotonation of the Schiff base of retinal results in the generation of the next intermediate of the cycle, the N intermediate.

The N intermediate was first characterized by transient absorption experiments in 1975 by Lozier *et al.* as a 520 nm-absorbing species.[27] The rise time of N_{520} is

approximately 1 ms and it decays in approximately 3 ms.[18,86] The origin of the proton used to reprotonate the retinal Schiff base is Asp_{96}.[71,87-92] During the protonation step, the pK_a of Asp_{96} drops[71,93] from above 11 to nearly 7,[71,94-96] and pathways are created for first transferring a proton from Asp_{96} to retinal, and then for reprotonating Asp_{96} from the cytoplasmic side.[71] In 2003 Schobert *et al*.[71] described the crystal structures of actually two N species to 1.62 Å resolution, N and N'. In the N structure, the retinal is reprotonated but the Asp_{96} residue is not; in the N' species, the Asp_{96} residue is reprotonated. In both cases, the retinal is in the 13-*cis*, 15-*anti* conformation.[71] Figure 1.13 compares the bR_{568} to the N' state.

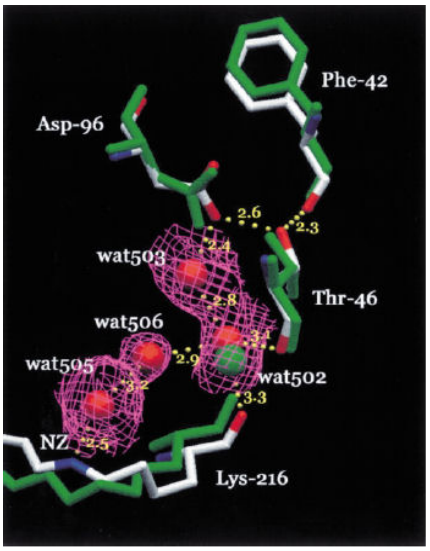

Figure 1.13: Comparison of the cytoplasmic regions of the parent bR_{568} species (green) and the N' state.

In N', a chain of hydrogen-bonded water molecules exists between Asp_{96} and retinal. Hydrogen bonds are shown in gold, with the reported distances in angstroms. Note how in the bR_{568} species the nitrogen atom is facing downward (extracellular side)

and a lone water 502 molecule (shown in green) exists in the channel. In N', the nitrogen atom faces upward (cytoplasmic side) and is connected to Asp_{96} on the cytoplasmic side via a hydrogen-bonded network of water molecules (shown in red).[71] The conformation of retinal in N is 13-*cis*, 15-*anti.*[24]

The O intermediate was first characterized in 1975 by Lozier *et al*. using low temperature and flash spectroscopy as a 640 nm-absorbing species.[27] The rise time of O_{640} is approximately 3 ms and it decays in approximately[27] 5 ms back to bR_{568}. The most recent crystallographic evidence of the structure of O_{640} was provided by Rouhani *et al*.[97] In this intermediate the retinal has isomerized back to its all-*trans* form from the 13-*cis*, 15-*anti* form of N_{550}, the retinal is protonated, Asp_{96} is deprotonated, and Asp_{85} is still protonated. Large-scale changes are confined to the extracellular side, in contrast to the M and N intermediates, where changes occur mainly on the cytoplasmic side.[97] There is increased hydration on the cytoplasmic side, suggesting how Asp_{96} might communicate with the bulk.[97] Only during the decay of O does the Asp_{85} deprotonate, returning everything for another turn of the cycle. Figure 1.14 illustrates the differences between bR_{568} and the O intermediate as described by Rouhani *et al*.[97]

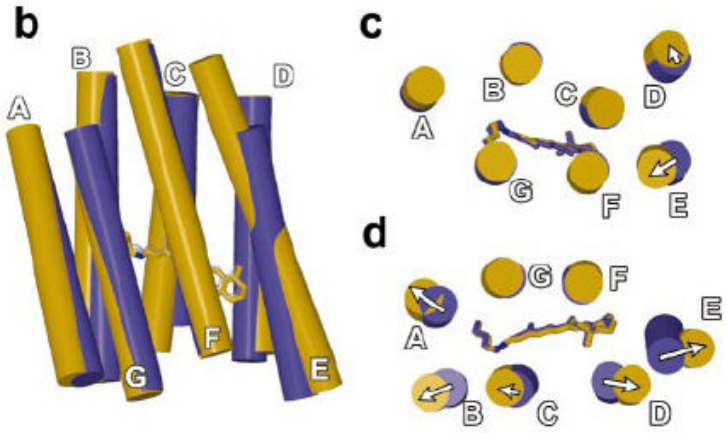

Figure 1.14: Structural differences between bR_{568} and the D85S mutant, which is used as a model for the structure of the O intermediate

In (1.14b), the side view of a representative monomer comparing bR_{568} (purple) to O (gold) demonstrates that deviations occur mostly in the extracellular region (bottom). The minimal deviation on the cytoplasmic side between these two forms is shown again in (1.14c), and the larger deviation on the extracellular side is shown in (1.14d). The arrows indicate the displacement direction of each helix in the O state relative to the bR_{568} parent. The outward tilts of the helices result in increasing the size of the extracellular cavity.

In the O intermediate, there is an opening of the extracellular side of the channel caused by greater outward tilting of the helices on that end than on the cytoplasmic end.

1.4 Crystallography of bR

Most of the atomic details of bR structure from 1975-1996 have come from cryo-electron diffraction studies. [98-100] In 1990 the atomic resolution breakthrough occurred, allowing

resolution[100] to 3.5 Å, later refined[98] to 2.5 Å. At the time, electron diffraction had been the method of choice because it can be performed on bR's native two-dimensional crystal lattice at various tilting angles, a process whereby projection maps help build up atomic structure.

In contrast to electron diffraction, X-ray diffraction gives better-resolved structural information. However, the main disadvantage to this technique at deciphering atomic detail of bR was that it requires three-dimensional crystals, which had until recently been very hard to obtain for membrane proteins. Crystallization of proteins in general requires a homogenous and monodisperse solution of the protein at relatively high concentration.[101] Unfortunately for crystallographers studying *transmembrane* proteins in general and bR in particular, the dual nature of transmembrane proteins (hydrophilic surface, hydrophobic interior) makes it difficult to crystallize. Conditions must be found where both extremes will be stably solubilized. If both extremes are no solubilized well, the protein tends to aggregate to amorphous (non-ordered) species that prevents ordered crystal growth.[101]

In the early 1970's the first reports surfaced of using detergents as efficient agents in solubilizing membrane proteins.[102,103] However, these crystals were of low quality, taking five years to accomplish the first high resolution structure of the membrane protein, a bacterial photosynthetic reaction center.[104] It was clear that solubilization of transmembrane proteins was possible but didn't quickly produce the best crystals for high-resolution work.

It was at this point that Landau and co-workers looked toward the use of lipid bilayers to solubilized transmembrane proteins, publishing their novel *in-cubo* method for

making 3-D 'cbR' crystals in 1996, with the X-ray structure refined to 3.7 Å.[105] In 1997 this structure was refined[106] to 2.5 Å, then in 1999 to 1.9 Å.[107] In their *in-cubo* method, Monoolein or Monopalmitoyl (MO or MP) created aqueous and hydrophobic compartments into which either the protein monomers of bR or lattice fragments could partition. Sϕrensen salt precipitant added to this reduces the cubic cell's unit size, making the cubic phase less stable by increasing the curvature of the hydrophobic bilayer. Planar domains are formed as the protein molecules move through the bilayer network laterally. Over time, this nucleation stage leads to protein crystallization of the protein into lamellar, planar domains in a hexagonal arrangement of unit cells in a period of several months. Addition of water demonstrates that the process is reversible, causing the protein to diffuse back into the curved bilayers.[108] This crystallization method hypothesis was detailed by Nollert *et al.*[108] and is shown in Figure 1.15. This removes the native lipids and puts detergent molecules in their place.[105]

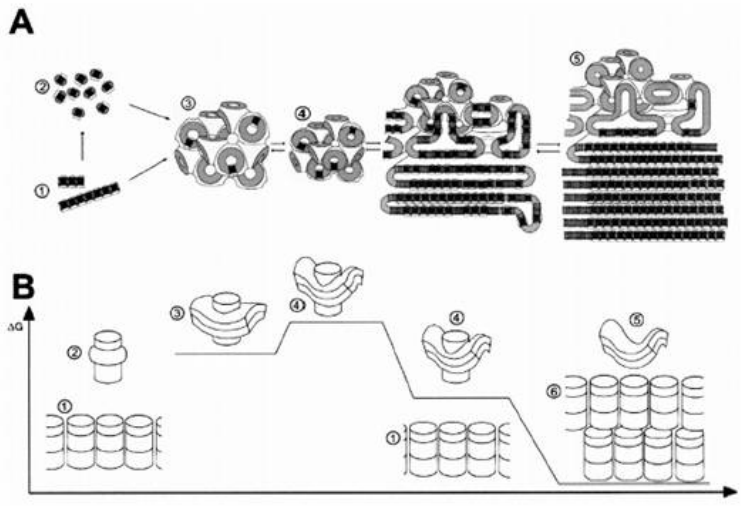

Figure 1.15: A hypothesis of the steps leading to the formation of three-dimensional cbR crystals.

Figure 1.15 gives a hypothesis of the steps leading to the formation of three-dimensional cbR crystals by the incorporation of bR into curved lipid bilayers and subsequent phase separation into lamellar structures as detailed by Nollert *et al*.[108] Purple patches (1) or detergent-solubilized monomers (2) insert into the curved bilayer of the bicontinuous cubic phase (3). The unit cell size is reduced and the membrane curvature is enhanced by addition of Sørensen salt (4). Separation of protein and purple membrane lipid from the highly curved cubic phase bilayer into growing planar domains (5) favors crystal nucleation. Figure 1.15b shows the various states of the protein-membrane interactions during crystallization and the changes in free energy (ΔG).

Crystallographers took advantage of this new 3-D crystallization method, increasing the atomic resolution of bR's ground state structure to 1.43 Å.[50] Typical cbR crystals produced by this method[105] are shown in Figure 1.16.

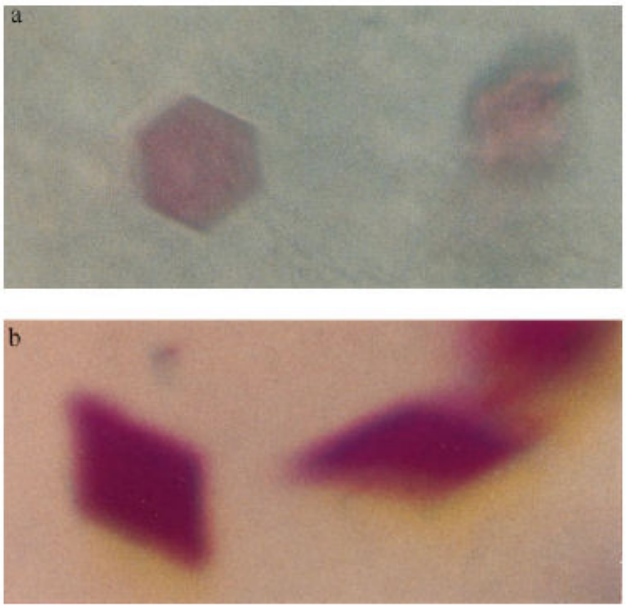

Figure 1.16: Morphology of cbR crystals that can be grown by the *in-cubo* method.

Morphology of cbR crystals that can be grown by the *in-cubo* method by using either the detergent monoolein (which produces the hexagonal crystals in (a) or monopalmitolein (which produces the rhomboid crystals in (b)), adapted from Landau and Rosenbusch.[105]

After the creation of this 3-D crystallization method for bR, the cbR crystals were shown to be functional using Raman and FTIR,[109] and the X-ray structures of photocycle intermediates were determined at ever higher resolution.[101] Unfortunately, this crystallization method was not the best one to use to address these questions, primarily because the crystallization process itself is labor- and time-intensive, the crystals are small in size and number, and the resulting gel-like phase is difficult to manipulate for spectroscopic measurements.[110]

In 2002, Bowie and co-workers came up with an alternative 3-D crystallography method for bR, the bicelle method, which results in the creation of bicelle bR (bcbR) crystals.[110] This bicelle name arises from partial bilayer/partial micelle nature of the bilayer disks formed by the combination of the two detergents used in the crystallization, 1,2-Dimyristoyl-*sn*-Glycero-3-Phosphocholine (DMPC) and 3-[(3-Cholamidopropyl) dimethylammonio]-2-hydroxy-1-propanesulfonate (CHAPSO). The structures of these two detergents, along with their arrangement around the protein, are shown in Figure 1.17 as adapted from Bowie and Farham.[110]

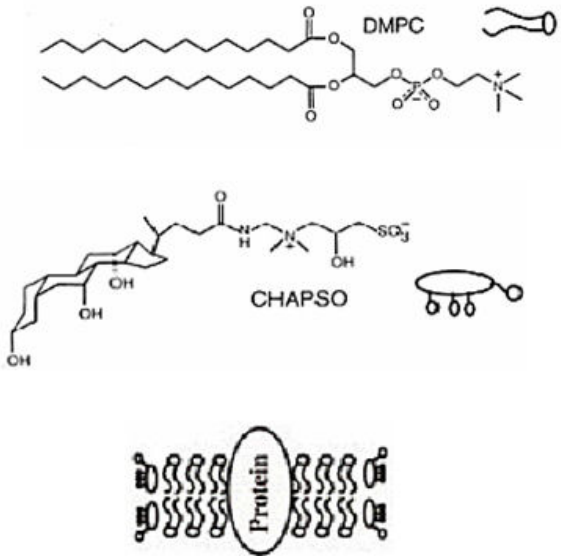

Figure 1.17: Structures of the two detergents used in bicelle crystallization of bR.

Typical diamond-shaped bcbR crystals grown by Bowie and Farham are shown in Figure 1.18. The average short-axis length is 50 μm and long axis is 100 μm.[110]

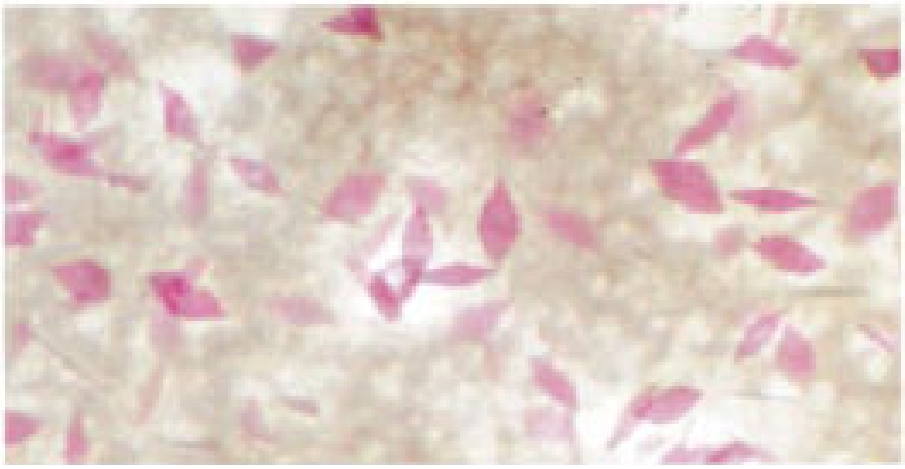

Figure 1.18: Typical diamond-shaped bR crystals formed by the bicelle method.

Figure 1.19 shows the antiparallel arrangement of the monomers of the bicelle crystal, which diffracted to 2.0 Å.[110] In (A), the top-down view of bicelle crystals reveal that the protein packs as antiparallel monomers (antiparallel monomers shaded differently). In (B), the side view of the bicelle packing structure is shown. In contrast, in (C) the packing structure of cbR crystals reveals that the protein trimers are intact in this form. The trimer arrangement of the protein helices of the cbR crystals resemble the trimer packing structure of bR in the native form, and as mentioned earlier, FTIR and Raman studies have shown that cbR crystals are functional and have similar kinetics to that of native bR.[109] However, within the bcbR crystals the protein packing is very different than anything that has been observed before in bR crystals. To date, only the bcbR crystal structure has been published. No functional studies have been done on these bcbR crystals. In this novel crystalline form, is the protein is still functionally relevant? Can the retinal inside isomerize to produce the all-*trans* and 13-*cis* retinal isomers? How does the hydration environment surrounding the retinal in the bicelle crystal packing

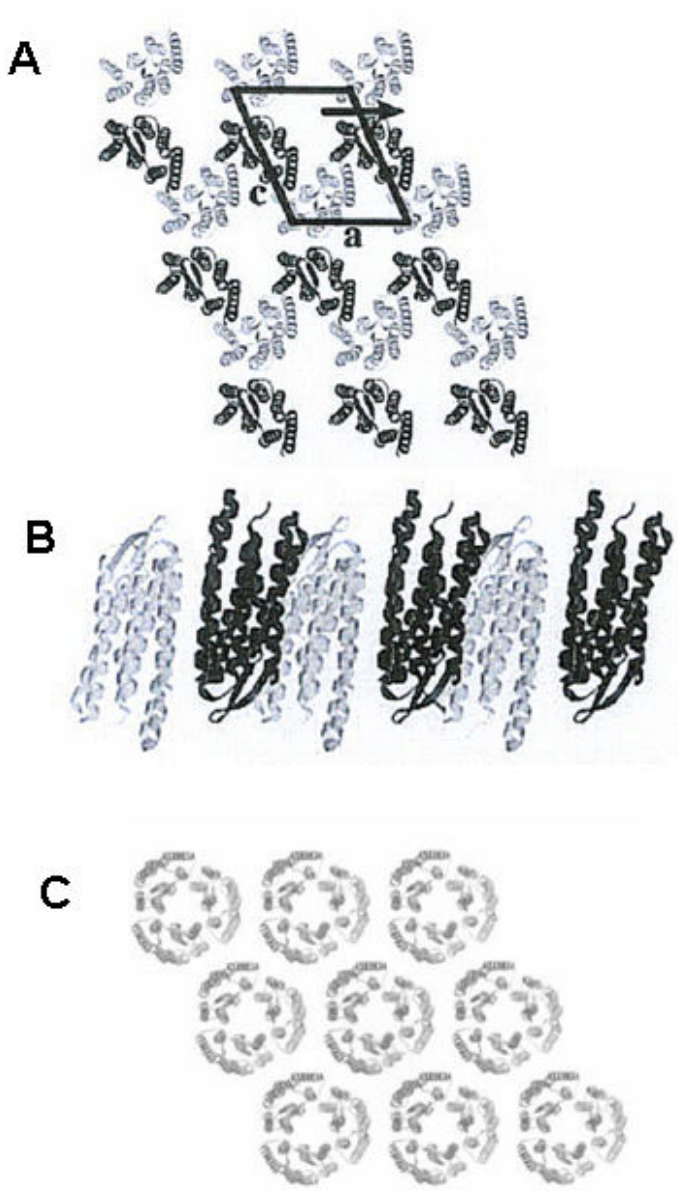

Figure 1.19: Comparison of the protein packing structure of Bowie and Farham's bicelle bR crystals with that of Rosenbusch and Landau's cbR crystals.

differ from that of the cbR crystals or from the native? Does bR still undergo a photocycle? If so, what are the lifetimes of the intermediates as compared to bR in its native form? Is Asp_{85} the proton acceptor during M rise, or is nearly Asp_{212}? This thesis will address these questions by using a variety of spectroscopic techniques.

In the course of this work, several experiments were attempted. Some of these were successful, and some were not. The following chapter will address the experimental details for all work attempted, starting with the initial bicelle synthesis attempts made in this lab.

References

(1) Oesterhelt, D.; Stoeckenius, W. *Nature (London), New Biology* **1971**, *233*, 149.

(2) Blaurock, A. E.; Stoeckenius, W. *Nature (London), New Biology* **1971**, *233*, 152.

(3) Lanyi, J. K. *FEBS letters* **1984**, *175*, 337.

(4) Tsuda, M.; Glaccum, M.; Nelson, B.; Ebrey, T. G. *Nature* **1980**, *287*, 351.

(5) Maeda, A.; Iwasa, T.; Yoshizawa, T. *Journal of biochemistry* **1977**, *82*, 1599.

(6) Ahl, P. L.; Cone, R. A. *Biophysical journal* **1984**, *45*, 1039.

(7) Tanford, C. *Annual review of biochemistry* **1983**, *52*, 379.

(8) Harbison, G. S.; Smith, S. O.; Pardoen, J. A.; Winkel, C.; Lugtenburg, J.; Herzfeld, J.; Mathies, R.; Griffin, R. *Proceedings of the National Academy of Sciences* **1984**, *81*, 1706.

(9) Sperling, W.; Carl, P.; Rafferty, C. N.; Dencher, N. A. *Biophysics of Structure and Mechanism* **1977**, *3*, 79.

(10) Aton, B.; Doukas, A. G.; Callender, R. H.; Becher, B.; Ebrey, T. G. *Biochimica et Biophysica Acta* **1979**, *576*, 424.

(11) Jan, L. Y. *Vision Research* **1975**, *15*, 1081.

(12) Govindjee, R.; Balashov, S. P.; Ebrey, T. G. *Biophysical Journal* **1990**, *58*, 597.

(13) Rohr, M.; Gaertner, W.; Schweitzer, G.; Holzwarth, A. R.; Braslavsky, S. E. *Journal of Physical Chemistry* **1992**, *96*, 6055.

(14) Logunov, S. L.; El-Sayed, M. A.; Song, L.; Lanyi, J. K. *Journal of Physical Chemistry* **1996**, *100*, 2391.

(15) Birge, R. R.; Gillespie, N. B.; Izaguirre, E. W.; Kusnetzow, A.; Lawrence, A. F.; Singh, D.; Song, Q. W.; Schmidt, E.; Stuart, J. A.; Seetharaman, S.; Wise, K. J. *Journal of Physical Chemistry B* **1999**, *103*, 10746.

(16) Becher, B.; Tokunaga, F.; Ebrey, T. G. *Biochemistry* **1978**, *17*, 2293.

(17) Gillbro, T. *Biochimica et Biophysica Acta* **1978**, *504*, 175.

(18) Stoeckenius, W.; Lozier, R. H.; Bogomolni, R. A. *Biochimica et Biophysica Acta* **1979**, *505*, 215.

(19) Krebs, M. P.; Khorana, H. G. *Journal of Bacteriology* **1993**, *175*, 1555.

(20) Lanyi, J. K. *Acta physiologica Scandinavica. Supplementum* **1992**, *607*, 245.

(21) Kates, M. *Techniques of Lipidology: Isolation, Analysis, and Identification of Lipids*; American Elsevier Publishing Company, Inc.: New York, NY, 1973.

(22) Dracheva, S.; Bose, S.; Hendler, R. W. *FEBS letters* **1996**, *382*, 209.

(23) Nelson, D. L.; Cox, M. M. *Lehninger: Principles of Biochemistry – 4th edition" by Nelson and Cox*, 4th ed., 2004.

(24) Fodor, S. P.; Ames, J. B.; Gebhard, R.; van den Berg, E. M.; Stoeckenius, W.; Lugtenburg, J.; Mathies, R. A. *Biochemistry* **1988**, *27*, 7097.

(25) Oesterhelt, D.; Hess, B. *European Journal of Biochemistry* **1973**, *37*, 316.

(26) Stoeckenius, W.; Lozier, R. H. *Journal of Supramolecular Structure* **1974**, *2*, 769.

(27) Lozier, R. H.; Bogomolni, R. A.; Stoeckenius, W. *Biophysical Journal* **1975**, *15*, 955.

(28) Henderson, R. *Annual Review of Biophysics and Bioengineering* **1977**, *6*, 87.

(29) Michel, H.; Oesterhelt, D. *FEBS Letters* **1976**, *65*, 175.

(30) Bakker, E. P.; Rottenberg, H.; Caplan, S. R. *Biochimica et biophysica acta* **1976**, *440*, 557.

(31) Belyakova, T. N.; Kadziauskas, J.; Skulachev, V. P.; Smirnova, I. A.; Chekulaeva, L. N.; Jasaitis, A. *Doklady Akademii Nauk SSSR* **1975**, *223*, 483.

(32) Lewis, A.; Spoonhower, J.; Bogomolni, R. A.; Lozier, R. H.; Stoeckenius, W. *Proc. Natl. Acad. Sci. U.S.* **1974**, *71*, 4462.

(33) Braiman, M.; Mathies, R. *Proceedings of the National Academy of Sciences of the United States of America* **1982**, *79*, 403.

(34) Mathies, R. A.; Brito Cruz, C. H.; Pollard, W. T.; Shank, C. V. *Science* **1988**, *240*, 777.

(35) Pollard, W. T.; Cruz, C. H.; Shank, C. V.; Mathies, R. A. *Journal of Chemical Physics* **1989**, *90*, 199.

(36) Ames, J. B.; Mathies, R. A. *Biochemistry* **1990**, *29*, 7181.

(37) Braiman, M. S.; Mogi, T.; Marti, T.; Stern, L. J.; Khorana, H. G.; Rothschild, K. J. *Biochemistry* **1988**, *27*, 8516.

(38) Gerwert, K.; Hess, B.; Soppa, J.; Oesterhelt, D. *Proceedings of the National Academy of Sciences of the United States of America* **1989**, *86*, 4943.

(39) Varo, G.; Lanyi, J. K. *Biochemistry* **1991**, *30*, 5016.

(40) Cartailler, J.-P.; Luecke, H. *Annual Review of Biophysics and Biomolecular Structure* **2003**, *32*, 285.

(41) Mitchell, P. *Chemiosmotic coupling in oxidative and photosynthetic phosphorylation*; Glynn Research Ltd, 1966.

(42) Campbell, N. A. Cellular Respiration: Harvesting Chemical Energy. In *Biology*; 3rd ed.; Brady, E. B., Ed.; The Benjamin/Cummings Publishing Company, Inc.: Redwood City, 1993.

(43) Campbell, N. A. Photosynthesis. In *Biology*; 3rd ed.; Brady, E. B., Ed.; The Benjamin/Cummings Publishing Company, Inc.: Redwood City, 1993.

(44) Oesterhelt, D.; Stoeckenius, W. *Proceedings of the National Academy of Sciences of the United States of America* **1973**, *70*, 2853.

(45) Lanyi, J. K.; Schobert, B. *Journal of Molecular Biology* **2003**, *328*, 439.

(46) Doig, S. J.; Reid, P. J.; Mathies, R. A. *Springer Proceedings in Physics* **1992**, *68*, 45.

(47) Polland, H. J.; Franz, M. A.; Zinth, W.; Kaiser, W.; Koelling, E.; Oesterhelt, D. *Biophysical Journal* **1986**, *49*, 651.

(48) Maeda, A.; Tomson, F. L.; Gennis, R. B.; Balashov, S. P.; Ebrey, T. G. *Biochemistry* **2003**, *42*, 2535.

(49) Rothschild, K. J.; Marrero, H. *Proceedings of the National Academy of Sciences of the United States of America* **1982**, *79*, 4045.

(50) Schobert, B.; Cupp-Vickery, J.; Hornak, V.; Smith, S. O.; Lanyi, J. K. *Journal of Molecular Biology* **2002**, *321*, 715.

(51) Herzfeld, J.; Tounge, B. *Biochemica et Biophysica Acta* **2000**, *1460*, 95.

(52) Milder, S. J.; Kliger, D. S. *Biophysical Journal* **1988**, *53*, 465.

(53) Hofrichter, J.; Henry, E. R.; Lozier, R. H. *Biophysical Journal* **1989**, *56*, 693.

(54) Wan, C. Z.; Qian, J.; Johnson, C. K. *Biochemistry* **1991**, *30*, 394.

(55) Smith, S. O.; Mathies, R. A. *Biophysical Journal* **1985**, *47*, 251.

(56) Maeda, A.; Sasaki, J.; Pfefferle, J. M.; Shichida, Y.; Yoshizawa, T. *Photobiochemistry and Photobioology* **1991**, *54*, 911.

(57) Lanyi, J. K. *Molecular membrane biology* **2004**, *21*, 143.

(58) Kalisky, O.; Ottolenghi, M.; Honig, B.; Korenstein, R. *Biochemistry* **1981**, *20*, 649.

(59) Aton, B.; Doukas, A. G.; Callender, R. H.; Becher, B.; Ebrey, T. G. *Biochemistry* **1977**, *16*, 2995.

(60) Marcus, M. A.; Lewis, A. *Science* **1977**, *195*, 1328.

(61) Campion, A.; Terner, J.; El-Sayed, M. A. *Nature* **1977**, *265*, 659.

(62) Jang, D. J.; El-Sayed, M. A. *Proceedings of the National Academy of Sciences of the United States of America* **1988**, *85*, 5918.

(63) Heyes, C. D.; El-Sayed, M. A. *Biophysical Journal* **2003**, *85*, 426.

(64) Hanamoto, J. H.; Dupuis, P.; El-Sayed, M. A. *Proceedings of the National Academy of Sciences of the United States of America* **1984**, *81*, 7083.

(65) Varo, G.; Lanyi, J. K. *Biochemistry* **1990**, *29*, 2241.

(66) Kataoka, M.; Kamikubo, H.; Tokunaga, F.; Brown, L. S.; Yamazaki, Y.; Maeda, A.; Sheves, M.; Needleman, R.; Lanyi, J. K. *Journal of molecular biology* **1994**, *243*, 621.

(67) Lanyi, J. K. *Advances in Chemistry Series* **1994**, *240*, 491.

(68) Subramaniam, S.; Lindahl, M.; Bullough, P.; Faruqi, A. R.; Tittor, J.; Oesterhelt, D.; Brown, L.; Lanyi, J.; Henderson, R. *Journal of Molecular Biology* **1999**, *287*, 145.

(69) Subramaniam, S.; Henderson, R. *Nature* **2000**, *406*, 653.

(70) Lanyi, J.; Schobert, B. *Journal of molecular biology* **2002**, *321*, 727.

(71) Schobert, B.; Brown, L. S.; Lanyi, J. K. *Journal of Molecular Biology* **2003**, *330*, 553.

(72) Slifkin, M. A.; Caplan, S. R. *Nature* **1975**, *253*, 56.

(73) Hendler, R. W.; Dancshazy, Z.; Bose, S.; Shrager, R. I.; Tokaji, Z. *Biochemistry* **1994**, *33*, 4604.

(74) Takeuchi, Y.; Ohno, K.; Yoshida, M.; Nagano, K. *Photochemistry and Photobiology* **1981**, *33*, 587.

(75) Balashov, S. P.; Govindjee, R.; Ebrey, T. G. *Biophysical Journal* **1991**, *60*, 475.

(76) Eisfeld, W.; Althaus, T.; Stockburger, M. *Biophysical Chemistry* **1995**, *56*, 105.

(77) Hendler, R. W.; Shrager, R. I.; Bose, S. *Journal of Physical Chemistry B* **2001**, *105*, 3319.

(78) Oka, T.; Yagi, N.; Tokunaga, F.; Kataoka, M. *Biophysical journal* **2002**, *82*, 2610.

(79) Perkins, G. A.; Liu, E.; Burkard, F.; Berry, E. A.; Glaeser, R. M. *Journal of structural biology* **1992**, *109*, 142.

(80) Schatzler, B.; Dencher, N. A.; Tittor, J.; Oesterhelt, D.; Yaniv-Checover, S.; Nachliel, E.; Gutman, M. *Biophysical Journal* **2003**, *84*, 671.

(81) Zimanyi, L.; Varo, G.; Chang, M.; Ni, B.; Needleman, R.; Lanyi, J. K. *Biochemistry* **1992**, *31*, 8535.

(82) Herzfeld, J.; Lansing, J. C. *Annual Review of Biophysics and Biomolecular Structure* **2002**, *31*, 73.

(83) Varo, G.; Lanyi, J. K. *Biochemistry* **1991**, *30*, 5008.

(84) Drachev, L. A.; Kaulen, A. D.; Komrakov, A. Y. *FEBS Letters* **1992**, *313*, 248.

(85) Luecke, H.; Schobert, B.; Cartailler, J.-P.; Richter, H.-T.; Rosengarth, A.; Needleman, R.; Lanyi, J. K. *Journal of Molecular Biology* **2000**, *300*, 1237.

(86) Schreckenback, T.; Wilckhoff, B.; Oesterhelt, D. *European Journal of Biochemistry* **1977**, *76*, 499.

(87) Sasaki, J.; Shichida, Y.; Lanyi, J. K.; Maeda, A. *Journal of Biological Chemistry* **1992**, *267*, 20782.

(88) Rothschild, K. J.; Marti, T.; Sonar, S.; He, Y. W.; Rath, P.; Fischer, W.; Khorana, H. G. *Journal of Biological Chemistry* **1993**, *268*, 27046.

(89) Brown, L. S.; Dioumaev, A. K.; Needleman, R.; Lanyi, J. K. *Biophysical journal* **1998**, *75*, 1455.

(90) Lanyi, J. K. *Abstracts of Papers, 223rd ACS National Meeting, Orlando, FL, United States, April 7-11, 2002* **2002**, PHYS.

(91) Tanimoto, T.; Furutani, Y.; Kandori, H. *Biochemistry* **2003**, *42*, 2300.

(92) Borucki, B.; Otto, H.; Heyn, M. P. *Journal of Physical Chemistry B* **2004**, *108*, 2076.

(93) Szaraz, S.; Oesterhelt, D.; Ormos, P. *Biophysical Journal* **1994**, *67*, 1706.

(94) Zscherp, C.; Schlesinger, R.; Tittor, J.; Oesterhel, D.; Heberle, J. *Proc. Natl. Acad. Sci. U.S.* **1999**, *96*, 5498.

(95) Li, Q.; Bressler, S.; Ovrutsky, D.; Ottolenghi, M.; Friedman, N.; Sheves, M. *Biophysical Journal* **2000**, *78*, 354.

(96) Dioumaev, A. K.; Brown, L. S.; Needleman, R.; Lanyi, J. K. *Biochemistry* **2001**, *40*, 11308.

(97) Rouhani, S.; Cartailler, J. P.; Facciotti, M. T.; Walian, P.; Needleman, R.; Lanyi, J. K.; Glaeser, R. M.; Luecke, H. *Journal of molecular biology* **2001**, *313*, 615.

(98) Grigorieff, N.; Ceska, T. A.; Downing, K. H.; Baldwin, J. M.; Henderson, R. *Journal of Molecular Biology* **1996**, *259*, 393.

(99) Henderson, R.; Unwin, P. N. T. *Nature (London, United Kingdom)* **1975**, *257*, 28.

(100) Henderson, R.; Baldwin, J. M.; Ceska, T. A.; Zemlin, F.; Beckmann, E.; Downing, K. H. *Journal of Molecular Biology* **1990**, *213*, 899.

(101) Pebay-Peyroula, E.; Neutze, R.; Landau, E. M. *Biochemica et Biophysica Acta* **2000**, *1460*, 119.

(102) Helenius, A.; Simons, K. *Biochimica et biophysica acta* **1975**, *415*, 29.

(103) Tanford, C.; Reynolds, J. A. *Biochimica et biophysica acta* **1976**, *457*, 133.

(104) Deisenhofer, J.; Epp, O.; Miki, K.; Huber, R.; Michel, H. *Nature (London, United Kingdom)* **1986**, *318*, 618.

(105) Landau, E. M.; Rosenbusch, J. P. *Proceedings of the National Academy of Sciences of the United States of America* **1996**, *93*, 14532.

(106) Pebay-Peyroula, E.; Rummel, G.; Rosenbusch, J. P.; Landau, E. M. *Science (Washington, D. C.)* **1997**, *277*, 1676.

(107) Belrhali, H.; Nollert, P.; Royant, A.; Menzel, C.; Rosenbusch, J. P.; Landau, E. M.; Pebay-Peyroula, E. *Structure (London)* **1999**, *7*, 909.

(108) Nollert, P.; Qiu, H.; Caffrey, M.; Rosenbusch, J. P.; Landau, E. M. *FEBS Letters* **2001**, *504*, 179.

(109) Heberle, J.; Buldt, G.; Koglin, E.; Rosenbusch, J. P.; Landau, E. M. *Journal of molecular biology* **1998**, *281*, 587.

(110) Bowie, J.; Farham, S. *Journal of Molecular Biology* **2002**, *316*, 1.

CHAPTER 2

EXPERIMENTAL DETAILS

Abstract

In this chapter, the steps involved in developing each experimental design are described for all work attempted during the course of this thesis work. In some cases, unforeseen issues arose, ultimately resulting in a change of course or a discontinuation of the experiment. Throughout the chapter, the reader is referred to the location in this thesis of the data acquired from successful experimental designs.

2.1. The Bicelle Crystallization Using the Bowie and Farham Method

Initial attempts are described for the bicelle crystallization of bR by the 'hanging drop' method, detailed by Bowie and Farham.[1] This produced diamond-shaped crystals with average short axis: long axis dimensions of 50 μm x 100 μm. The experimental details for this 'hanging drop method' crystallization replicated in our labs are given in this section. The specific supplies and chemicals are also detailed below.

In order to carry out crystallization of bR by the hanging-drop method, three crystallization supply components were ordered from Hampton Research (Aliso Viejo, CA): crystallization plates, glass circular cover slips, and vacuum grease. The specific plates were the Linbro® plates, which each contain 24 removable, ungreased reservoirs, along with a tray cover. The Linbro® plate with cover is made of clear, rigid polystyrene. These stackable plates have distortion-free flat bottom wells of fine clarity. Approximate plate size is 15.0 x 10.8 x 2.2 cm, and approximate well size is 1.7 x 1.6 cm (with a

typical fill volume of 700 to 1000 μL). Raised, wide rings around the reservoirs minimize cross contamination and allow one to seal each well with 22 mm circle or square cover slides. A 50-plate case of these plates is catalog number HR3-110. In these experiments the 22 mm thick plain (non-siliconized) glass circle slides were used. The thick slides were chosen to avoid breakage. A 3.0 oz. pack of approximately 75 slides is catalog number HR3-243. The cover slips were sealed over the reservoirs using Dow Corning vacuum grease, Hampton catalog number HR3-510 for a 150 g tube.

Initial crystallization attempts done according to the literature[1] involved the use of three chemicals, DMPC (1,2-Dimyristoyl-*sn*-Glycero-3-Phosphocholine), Chapso (3-[(3-Cholamidopropyl)dimethylammonio]-2-hydroxy-1-propanesulfonate) and OG (β-octylglucoside), and one salt, $NaH_2PO_4 \cdot 2\ H_20$ (Sodium phosphate monobasic, dihydrate). DMPC was purchased as a white solid from Avanti Polar Lipids (Alabaster, AL), catalog number 770345. Chapso was also purchased as a white solid from Sigma-Aldrich (St. Louis, MO), catalog number C3649. OG was purchased as a white solid from $NaH_2PO_4 \cdot 2\ H_20$ was also purchased from Fisher Scientific, catalog number AC27175-0010. In preparing the detergent solution, the DMPC and Chapso were added together in a 3:1 molar ratio, and water was added to make a 40% (3:1) DMPC:Chapso solution. Because the viscosity of this mixture was relatively high at room temperature, this solution was kept in a vial on ice to keep the viscosity low enough to allow pipetting. A 1% solution of β-octylglucoside in water was made and kept in a separate vial.

The bR samples were obtained from a cell line of *Halobacterium salinarium* and were purified by established procedures.[2] The concentration of bR in water was adjusted to approximately 10 mg/mL by monitoring the absorbance of the light-adapted (20

minutes light exposure using a 40 W bulb) bR sample at 570 nm until the absorbance spectrum was constant. This 10 mg/mL bR solution was mixed in a 4:1 molar ratio with the 40% (3:1) DMPC:Chapso solution, making the bR/detergent solution used is subsequent steps.

The following details the 'hanging drop method' used for the bicelle crystallization used here. A solution of 3.2 M $NaH_2PO_4 \cdot 2\ H_20$ in H_2O was made, pH 3.5, and a few drops of this saturated salt "well solution" were added to each of the 24 reservoirs in the plate. A small amount of vacuum grease was smeared on the surface of each cover slip, making it surface more hydrophobic and thus preventing the spreading out of the bR/detergent solution to be applied. To each cover slip was added 6 μL of the cold bR/detergent solution, 2.5 μL of the saturated salt solution, and 1 μL of OG. These components were mixed by pipetting up and down several times. Vacuum grease was applied to the rim of each reservoir, and the cover slips were sealed over the reservoirs so that the 9.5 μL drop of mixed components was hanging over the saturated salt solution. Plates were placed in a Sheldon Manufacturing Inc. general purpose 37°C model # 1535 convection oven (Cornelius, OR) for a period of 4-8 weeks, at which point diamond-shaped crystals of size 50 x 100 μm were observed under 500x total magnification with an Olympus IX microscope (Tokyo, Japan). Images were taken with the attached Olympus model DP11 CCD camera. Crystallization was considered complete after all of the purple protein had been taken up from the matrix. Figure 2.1 shows typical crystals grown in this lab (left) compared to those of Bowie and Farham[1] (right). The color difference is due to a difference in illumination intensity between the two microscopes used to take these images.

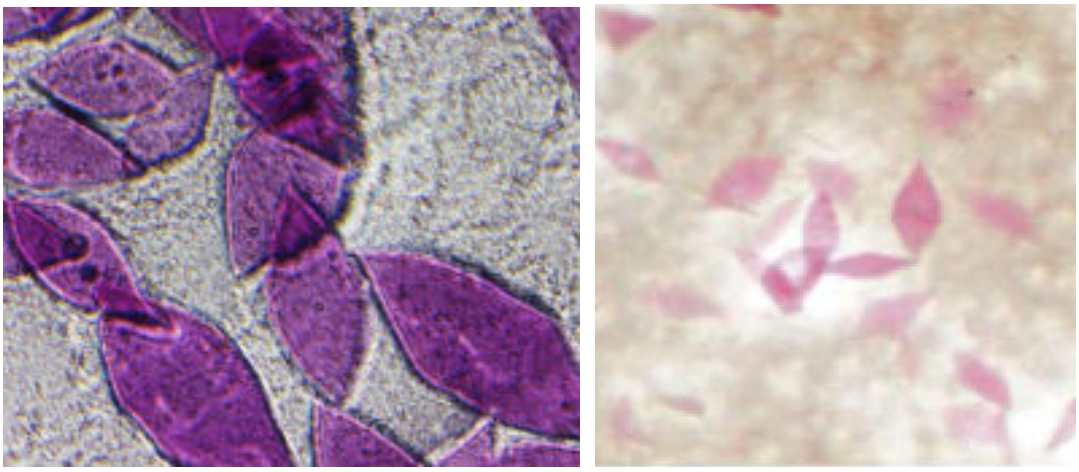

Figure 2.1: Comparison of bicelle crystals made in this lab (left) to those produced by Bowie and Farham in the literature[1] (right).

After these initial synthesis efforts were successful, it was important to establish that the packing structure of these crystals were a match to those of Bowie and Farham's by X-ray diffraction. The plates of crystals were transported to the laboratory of Dr. Allan Orville at Georgia Tech, where graduate student George Lountos attempted to get a diffraction pattern from the crystals. The instrument was a RU-H3R rotating copper anode x-ray source with a Rigaku R-Axis IV++ detector from Molecular Structure Corporation (The Woodlands, TX). The Crystal Clear software program (Rigaku/MSC, The Woodlands, TX) was used to operate the instrument. The MOSFLM software package (MRC Laboratory of Molecular Biology, Cambridge, UK) was used to analyze the image. The rotation angle was 0.5 degrees with 2 minute exposure time. The lambda value (x-rays wavelength) was 1.54 Å. The crystal was placed in a -170°C nitrogen cold stream.

In these initial X-ray diffraction attempts, no data could be acquired using the Georgia Tech instrument due to the small dimensions of the crystal. Sending these

crystals to be analyzed by members of the Orville group during their next trip to National Synchrotron Light Source at the Brookhaven National Laboratory (Brookhaven, NY) was discussed. Unfortunately, they did not have time to do this during their trip.

At about this point Dr. Farham of the Bowie group passed along a method to create bicelle crystals of approximately twice the size of the originals, a method which was recently published in the literature.[3] The solutions of the so-called 'improved bicelle method' used to produce larger bicelle crystallization are presented here.

2.2. Replication of the Improved Bicelle Method of Bowie and Farham in our labs

In this improved method, both the components of the well solution and the ratio of detergents were changed to produce bicelle crystals that were roughly twice the original size. This method produced bicelle bR crystals with average dimentions of 100 x 200 μm. The specific changes are described in this section.

The well solution was changed from the 3.2 M $NaH_2PO_4 \cdot 2\ H_20$ to a mixture of 4.0 M $NaH_2PO_4 \cdot 2\ H_20$ and 6 M hexanediol in H_2O. Specifically, each well consisted of a mixture of 285 μL 4.0 M $NaH_2PO_4 \cdot 2\ H_20$, 10 μL 6 M hexanediol, and 205 μL of H_2O. The molar ratio of the DMPC:Chapso detergents was changed from 3:1 to 2.8:1. These two detergents were still diluted to a 40% solution in water to make a 40% (2.8:1) DMPC:Chapso solution. The 10 mg/mL bR solution was mixed in a 4:1 ratio with the

40% (2.8:1) DMPC:Chapso solution, making the bR/detergent solution used is subsequent steps.

As mentioned above, to each cover slip was added 6 μL of the bR/detergent solution, 2.5 μL of the new well solution, and 1 μL of OG. These components were mixed and the samples incubated at 37°C for a period of 4-8 weeks, at which point diamond-shaped crystals of size 100 x 200 μm were observed under microscope. Crystallization was considered complete after all of the purple protein had been taken up from the matrix. These larger crystals are shown in Figure 2.2.

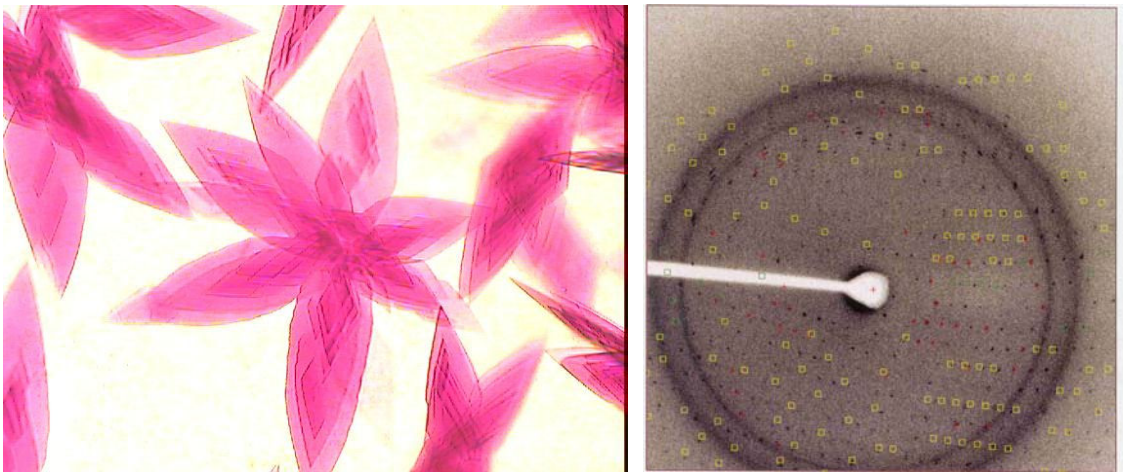

Figure 2.2: Larger bicelle crystals made by the improved bicelle method (left) and resulting X-ray diffraction pattern acquired from the larger bicelle crystals (right).

These larger crystals were again taken to the Orville labs and this time a diffraction pattern was successfully acquired (Figure 2.2) using the same instrumentation and parameters above. The data was sent to the laboratory of Dr. James Bowie and Salem Farham at UCLA and confirmed as a match to theirs.

2.3. Sample Preparation and Data Acquisition for Light/Dark Adaptation Experiments

The bicelle bR crystals within their detergent matrix were examined by visible spectroscopy to determine if the bR crystallized by this method was still capable of photoisomerization. Because exposure to air dries out the matrix and embedded crystals, the glass cover slip of matrix-embedded bicelle bR crystals to be examined was removed from its crystallization well, a 2 mm thick circular rubber o-ring spacer was placed around the matrix spot, and a second slide was placed above it (Figure 2.3).

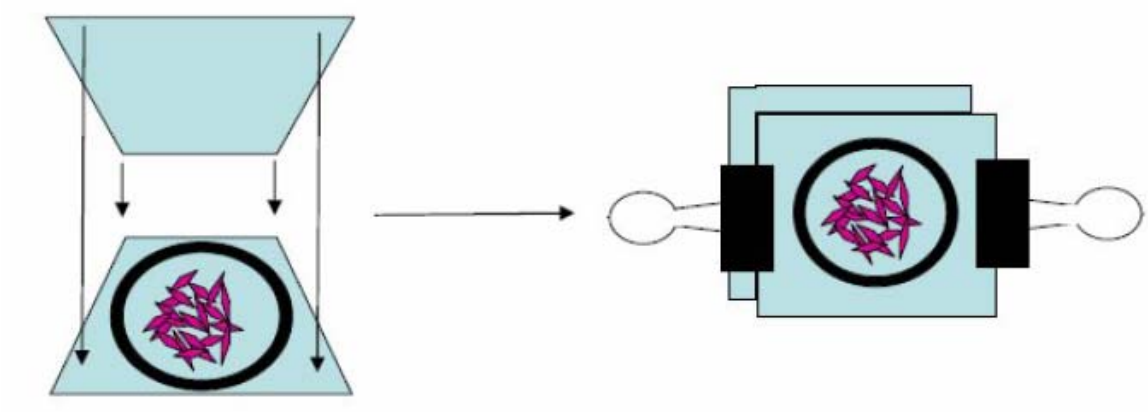

Figure 2.3: Assembly of the bicelle crystal sandwich used to take visible spectra of a sample of multiple crystals embedded within the detergent matrix

The o-ring spacer provided a sealed compartment to prevent sample desiccation during the experiment, eliminating spectral changes due to fluctuations in the hydration level of the sample during the experiment. Paper clips placed on either side of the assembly kept the two glass slides in place.

A Shimadzu 3101 PC UV/VIS/NIR double-beam spectrophotometer (Shimadzu Corp., Kyoto, Japan) was used to examine the matrix-embedded crystals in the range from 400-800 nm. An ISR-260 integration sphere attachment (Shimadzu Corp.) replaced the solution-phase sample holder in order to increase signal intensity. The sample sandwich of either the hydrated native bR film or of several crystals within their detergent matrix was placed in the integration sphere, scanned, and adjusted in the beam path until maximum signal was found. Once this position was found, the chamber door closed, and the sample kept in the dark overnight. After scanning this dark-adapted sample from 400-800 nm, the chamber door was opened and a white light source (desk lamp with 40W incandescent bulb) was used to focus a spot of light on the sample. Care was taken to distance the light source from the sample to prevent denaturation by the lamp's radiant heat. The sample was scanned periodically until the visible spectrum remained constant. At this point, the chamber door was closed and the spectrum was monitored periodically to see if the light-dark adaptation process was reversible. The X-Y absorption data were plotted using the OriginPro software package version 7.5 (OriginLab, Northampton, MA). The data acquired from this experiment are discussed in Chapter 3.

2.4. Sample Preparation and Data Acquisition for Single-Crystal Visible Spectroscopy

For the single-crystal visible spectroscopy experiments studying the effect of dehydration under bright field exposure on a single bcbR crystal, the bcbR crystals were removed from their detergent matrix and fixed to a glass slide by the following procedure: crystals were first removed from their detergent matrix by adding a few drops of deionized, distilled water (DDW) to the matrix, gently mixing the matrix gel to loosen the components, and then transferring to a micro-centrifuge tube containing DDW. After vortexing the tube to dislodge the crystals from the matrix, the crystals would settle to the bottom of the tube within a matter of minutes, leaving the matrix components on top, in the supernatant. The supernatant was then removed by pipette, more DDW added, and the process repeated until the milky matrix components were no longer detected by eye. A 5-10 µL drop of crystals in DDW were then removed by pipette and placed on a glass slide. The crystals settled to the bottom of this drop, close to the surface of the glass slide, and the excess DDW was removed by a combination of pipetting and evaporation as the crystals were exposed to ambient lighting and temperature. Once the excess DDW had been removed, the crystals became immobilized on the glass slide and were easily transported to the microscope for single-crystal visible spectroscopy. A S.E.E. 1000 MSP visible microspectrometer running the SEEScope version 4.0.0 software package (S.E.E. Inc, Middleboro, MA) was used for single-crystal visible absorption experiments to compare the light-adapted spectrum of hydrated single crystals to hydrated native films. The microspectrometer had a wavelength range from 400-800 nm that allows for the examination of the retinal absorption within the protein. The 20X objective used in these

experiments has a sampling area of 8 μm squared. Since on average these crystals are 100 x 200 μm in size, several different areas on a single crystal could be examined individually. Spectra were collected from multiple areas of the same crystal, and also from different crystals. The same process was repeated for several locations on a hydrated native film as well. In all cases, spectra were collected after the sample was exposed to a drop of DDW for a period of one hour under the same intensity bright field of the microscope. All data taken was saved as .spc files and opened again in the ONMIC v 5.2 software package (Nicolet Instrument Corp, Madison WI), where the baseline could be smoothed. After smoothing, the data were saved as .csv files and opened in the OriginPro software package v7.5 for plotting. All the crystal spectra were averaged, and all the native film spectra were averaged. The same microspectrometer was also used for the single crystal visible absorption experiments examining the effect of dehydration of a single crystal by dry nitrogen stream under constant bright field exposure of the microscope. Data for these experiments are presented in Chapter 3.

2.5. Sample Preparation and Data Acquisition for Single-Crystal Raman Spectroscopy

All microscale Raman experiments were carried out a Holoprobe Research 785 Raman microscope running the Kaiser Optical systems' "Holoprobe" software package (both Kaiser Optical, Ann Arbor, MI). For the single-crystal Raman experiments studying the effect of dehydration on a single bcbR crystal under increasing 514 nm laser irradiation from an external Argon laser, the crystals were removed from their detergent matrix as described above and fixed to a glass slide that was covered by a piece of aluminum foil.

The aluminum foil was used to prevent the appearance of interfering phonon Raman bands caused by interaction of the 785 nm Raman incident laser with the glass surface. For the experiments studying the effect of dehydration on a single bcbR crystal dried in the dark, the crystals were removed from their detergent matrix and fixed to an aluminum foil-covered glass slide by the procedure above. The focus was set on a single crystal was set under bright field exposure of the microscope using the 20X objective and a 5-10 µL drop of DDW was added to the crystal surface to re-hydrate it. The bright field turned off and the crystal was kept on the stage of the Raman microscope in the dark for a period of 4 days at ambient temperature and pressure and allowed to dry. After this period of time, the excess DDW on the surface evaporates, bringing the crystal into focus again without the need for exposing the crystal to the bright field of the microscope to check the focus before acquisition of the dehydrated crystal Raman spectrum. A Holoprobe Research 785 Raman microscope running the Kaiser Optical Systems' "Holograms" software package was used for single-crystal Raman experiments to examine the effect of dehydration on the Raman spectrum of single crystals. The Raman microscope had a spatial (microscope) resolution of approximately 1 µm, a 3 mW 785 nm incident laser with a spot size of approximately 15 µm diameter, and spectrometer spectral resolution of approximately 3 cm^{-1}. The crystals were examined under 10x objective. The Raman microscope was housed in a black felt-lined Plexiglass box to prevent the entrance of stray light.

For the experiments studying the effect of dehydration under increasing 514 nm laser power, laser excitation was provided by the 514 nm line of an Innova 300 Argon laser (Coherent, Santa Clara, CA). To allow the passage of laser light onto the stage, a

hole was drilled into the left side of the box and a series of mirrors and lenses focused the Argon line toward the sample on the stage. Figure 2.4 gives the top-down view of the optical setup for photo excitation experiments attempted using the 488 nm Argon laser.

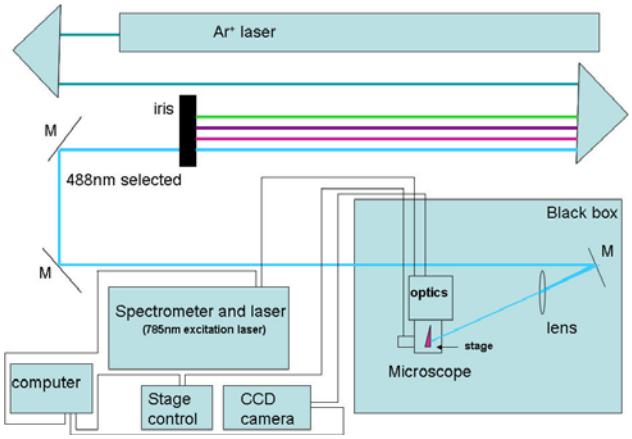

Figure 2.4: Top-down view of the optical setup for photo excitation experiments attempted using the 488 nm Argon laser.

The 488 nm line is selected, passed into the Plexiglas box, and focused by a lens onto the sample. The Raman spectrum of the same area of a single crystal was taken in the range from 2000-1000 cm-1, under increasing 514 nm laser power from 0.01W to 0.3 W.

For the experiments studying the effect of dehydration on a single bcbR crystal dried in the dark, the crystals were removed from their detergent matrix and fixed to an aluminum foil-covered glass slide by the procedure above. The focus was set on a single crystal was set under bright field exposure of the microscope using the 20X objective and a 5-10 µL drop of DDW was added to the crystal surface to re-hydrate it. The bright field turned off and the crystal was kept on the stage of the Raman microscope in the dark for a period of 4 days at ambient temperature and pressure and allowed to dry. After this period of time, the excess DDW on the surface evaporates, bringing the crystal into focus

again without the need for exposing the crystal to the bright field of the microscope to check the focus before acquisition of the dehydrated crystal Raman spectrum. In both experiments, the data was saved as a series of .spc files and opened again using the ONMIC v 5.2 software package, where the baseline could be smoothed. After smoothing, the data were saved as .csv files and opened in the OriginPro software package v7.5 for plotting. The data collected from these experiments are discussed in Chapter 3.

For the single-crystal Raman experiments studying the effect of increasing the incident 514 nm laser power on a single *hydrated* bcbR crystal, the crystals were removed from their detergent matrix as described above and fixed to a glass slide that was covered by a piece of aluminum foil. While the 514 nm line of the external Argon laser that had been used with the Holoprobe 785 was fine for working with dried crystals, working with hydrated crystals posed a significant problem: the drop of water on the sample needed to maintain its hydration through the course of this experiment would distort the path of a 514 nm laser being directed externally to the sample. Needed was an instrument with a built-in 514 nm laser so the laser could be directly put onto the sample, directly downward from the objective. For this reason, a different micro Raman spectrometer was necessary, one capable of an incident 514 nm wavelength. Since at the time such an instrument was not located on the Georgia Tech campus, Raman spectra of single hydrated crystals were acquired by Dr. Cristin Moran at Wright-Pattern Air Force Research Lab (AFRL) in Dayton, OH using a Renishaw in Via Raman spectrometer running the WiRE 2.0 software package (Renishaw, Gloucestershire, UK). This spectrometer had a tuneable incident laser wavelength, and the crystals were examined

under both 830 nm and 514 nm wavelengths. The sampling area was approximately 1 μm^2. In order to ensure that the hydration level of all samples remained uniform, all Raman spectra were taken by submerging the objective underwater to obtain the spectrum of the native film or the single crystal. The intense Raman band at 520 cm^{-1} of a silicon wafer was used for automatic wavelength calibration by the software. All data presented were imported as x-y data first to OMNIC E.S.P. 5.2 (Nicolet Instrument Corp, Waltham, MA) for baseline correction, and then transferred to Microcal Origin 7.5 software package. The data from these experiments resulted in a publication in Biophysical Journal[4] and is presented in Chapter 4.

2.6. Sample Preparation and Data Acquisition for Visible Spectroscopy of a Mass of bcbR Crystals Dried in the Dark

The bcbR crystals were removed from their detergent matrix by the washing procedure in Section 2.4. A mass of crystals in DDW was concentrated to a rectangular sample size of approximately 3 x 7 mm and allowed to dry for a period of 4 days in the dark until the excess DDW had been removed by evaporation. The glass slide with its mass of crystals immobilized to the surface was transferred under red light to the sample chamber of the spectrometer. A Beckman DU 650 UV-Vis spectrometer (Beckman Instruments, Inc, Arlington Heights, IL) was used for visible spectroscopy experiments studying the effect of dehydration of a mass of bcbR crystals dried in the dark. Unlike the visible microspectrometer, which acquires spectra under bright field illumination and CCD camera, this spectrometer has a scanning monochromator, which allows for the acquisition of a dark-adapted spectrum of the crystals without their exposure to broad

band white light. The wavelength range from 300-800 nm was scanned on the 3 x 7 mm rectangular spot of crystals. The X-Y data was saved in ASCII format and opened again in the OriginPro software package v7.5 for plotting. Scanning within this wavelength range involved the changing of grating that resulted in spikes in the spectrum. These spikes were subtracted out using the OriginPro software package. The data collected in these experiments is presented in Chapter 3.

2.7. Sample Preparation and Data Acquisition for Circular Dichroism Experiments

The bicelle bR crystals within their detergent matrix were examined by circular dichroism (CD) spectroscopy to determine the effect of crystallization on the CD spectrum of bR. The samples were prepared in the same way as described above for the visible spectroscopy experiments presented in Section 2.3: a sample of matrix-embedded crystals were sandwiched between two circular glass cover slips separated by a rubber o-ring. At the time of these experiments, Georgia Tech did not yet own a working CD spectrometer, so the experiments were carried out in laboratory of Dr. Jenny Yang at Georgia State University. Her research scientist Dr. Yiming Ye provided training on the CD spectrometer, the details of which are described in the next paragraph. A sample of native bR in water, which has a well-characterized bilobic CD spectrum in the literature[5-9] (Figure 2.5) was also taken as a standard to make sure the instrument was functioning properly.

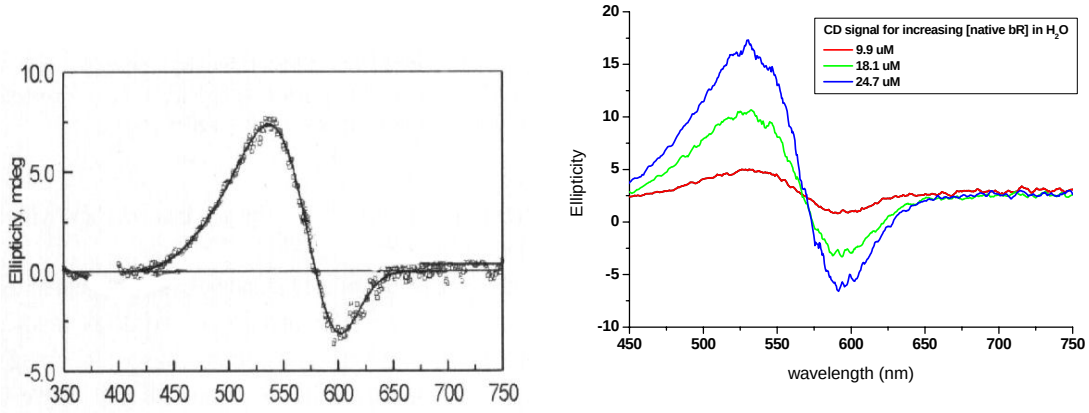

Figure 2.5: CD spectrum of native bR in water as described by Wang *et al*.[10] (left) and the CD spectra of a solution of native bR in water at three different concentrations (right).

The CD spectrometer was a JASCO 710 (Jasco, Great Dunmow, UK). The rectangular solution cell sample holder was placed in the chamber. The wavelength region between 350-750 nm was scanned. Three different concentrations of the native bR solution described above was scanned to determine the approximate optical density (OD) to get reasonable signal. These three concentrations were 6 μM with an OD of 0.4, 9.9 μM with an OD of 0.8, and 6 μM with an OD of 1.35. The resulting CD spectra of these three solutions are shown in Figure 2.5, and demonstrate that the CD spectra of the native solutions is in agreement with the literature.[10]

Next were the experiments on the crystals within their detergent matrix. Since the crystals were contained between two circular glass cover slips, (crystal sandwich) the sample holder in the chamber had to be changed from the solution-cell sample holder to the cylindrical sample holder. Figure 2.6 illustrates this sample holder and the way that the crystals were examined. Several "sandwiches" like this were made and each sample

was rotated in three different orientations. All this was done to make sure that any signal resulting was constant. Figure 2.7 illustrates how a sample was rotated in this way.

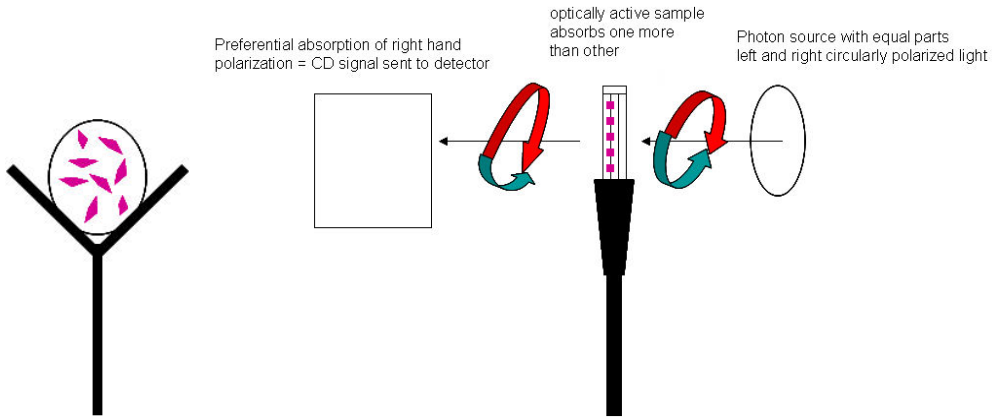

Figure 2.6: Examination of crystals by CD Spectroscopy.

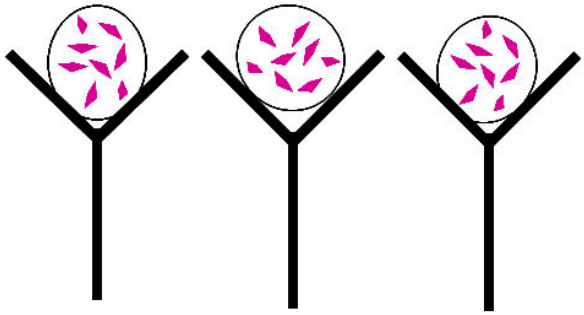

Figure 2.7: Example of how one sample of crystals within their matrix was rotated into three different orientations

Each sample's average CD signal was derived from the different orientations and the three different sample spectrum averages are compared on one scale in Figure 2.8.

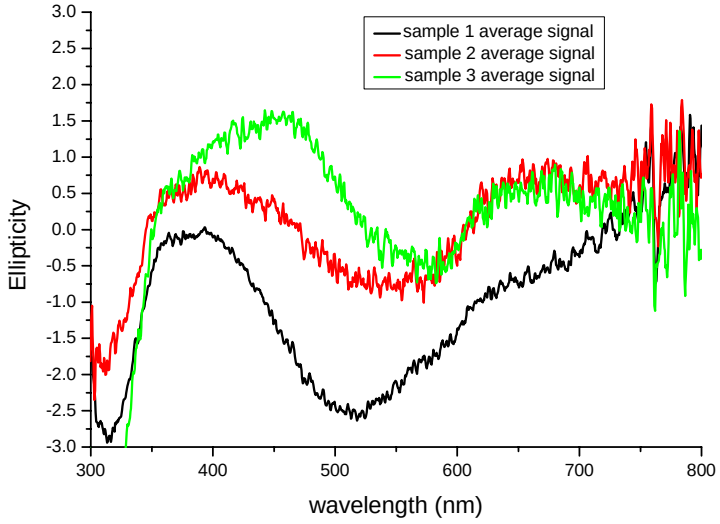

Figure 2.8: The inconsistent CD spectra obtained from three different multiple-crystal samples.

The data derived from these experiments were inconsistent, likely due to scattering of the incident light by the crystal surfaces. What was really needed was a CD microscope that would permit the examination of single crystals. At the time, no such instrument existed commercially.

At about this time, Dr. Mohan Srinivasarao of the School of Textile & Fiber Engineering at Georgia Tech suggested that Dr. Bart Kahr at the University of Washington might be able to obtain a single-crystal CD spectrum, based on a recent publication of his in the Journal of the American Chemical Society[11] describing the design of a CD microscope by their group. After communication with him, a sample of

several crystals were sent to his lab for analysis. He was unable to get good signal from the crystals on his CD microscope and suggested that expensive modifications to his system would have to be made in order to continue. At this point pursuing further CD spectroscopy on the bicelle crystals was discontinued.

2.8. Sample Preparation and Data Acquisition for Single-Crystal FTIR Experiments

This section describes the details of preparing and examining single bicelle crystals by FTIR microscopy. One of the concerns in doing FTIR work on the crystals was that the detergents used in the crystallization would give rise to interfering IR absorption bands that would obscure the C=O and N-H protein absorption bands. In order to circumvent this problem, the crystals were washed from their detergent matrix as described in Section 2.4 and individual crystals were examined by FTIR microscopy. All microscopy was performed in the laboratory of Dr. Kumar of the School of Textile & Fiber Engineering at Georgia Tech on a Perkins-Elmer Spectrum One FTIR Spectrometer AutoImage Microscope (Perkin-Elmer, Boston, MA) under the guidance of graduate student Hongming Ma.

In order to avoid IR signals from both the detergent matrix and H_2O, both had to be removed from the crystals before FTIR data acquired. Crystals were first removed from their matrix by adding a few drops of deionized, distilled water (DDW) to the matrix, gently mixing the matrix gel to loosen the components, and then transferring to a micro-centrifuge tube containing DDW. After vortexing the tube to dislodge the crystals from the matrix, the crystals would settle to the bottom of the tube within a matter of a few

minutes, leaving the matrix components on top, in the supernatant. The supernatant was then removed by pipette, more DDW added, and the process repeated until the matrix components were no longer detected by eye. After this final wash, the bulk DDW was removed by pipette, and an approximately 1 mL volume of 99% purity D_2O (Sigma Aldrich, St. Louis, MO) was added to the tube of crystals, vortexed, and allowed to sit overnight on the bench top to allow solvent exchange. The following day the D_2O supernatant was removed by pipette, another 1 mL volume was added, the sample was vortexed, and the crystals allowed to settle to the bottom before the supernatant removed. Once the crystals had been rinsed 4-5 times in this manner a volume of D_2O-soaked crystals was moved to a single 25 x 2 mm CaF_2 window (Harrick Scientific, Ossining, NY) and placed on the stage of the FTIR spectrometer microscope. Once the crystal/D_2O solution was placed on the window, the excess D_2O was removed via pipette to allow the crystals to adhere to the window. A drop of D_2O was added on top of the immobilized crystals to prevent desiccation. This window was then placed on the microscope stage for examination under 60x total magnification. A single crystal was brought into focus, and then the stage moved slightly so that a sampling area just outside the crystal was within the sampling area. An average spectrum of this area was taken (16 scans) and used as a 'background' spectrum. After the background spectrum was obtained, the stage was moved back so that the crystal was inside the sampling area and another average spectrum was obtained (16 scans) of the crystal. Figure 2.9 compares the FTIR spectrum of a single bicelle crystal in D_2O taken with the Kumar group's FTIR microscope to the FTIR spectrum of a concentrated pellet of native bR in D_2O taken with the Nicolet 860

FTIR spectrometer (Thermo Nicolet, Waltham, MA) housed in our Laser Dynamics Laboratory.

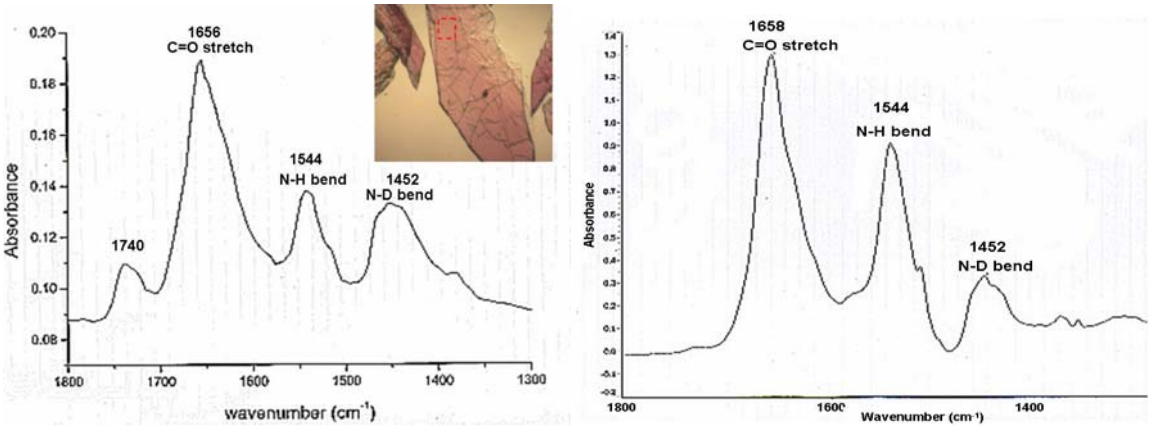

Figure 2.9: Comparison of the FTIR spectrum of a single bicelle crystal in D_2O (left) to that of a concentrated pellet of native bR in D_2O.

Comparing the two spectra, it is observed that in the single crystal spectrum the three main vibrational bands are clearly seen: carbonyl stretch, the N-H bend, and the N-D bend. The additional band at 1740 cm^{-1} observed in the crystal spectrum but not in the native is due to the C=O stretch of the ester group of residual DMPC detergent.[12] The prominent 1740 cm^{-1} absorption band in the FTIR spectrum of the 3:1 DMPC: Chapso detergent matrix alone, shown in Figure 2.10, confirms this assignment.

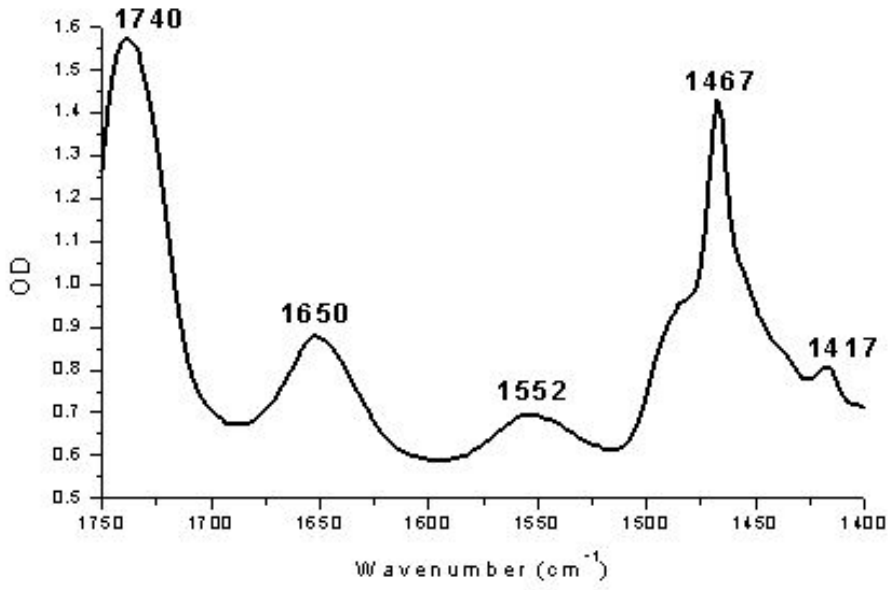

Figure 2.10: FTIR spectrum of the 3:1 DMPC: Chapso matrix

Once the ability to obtain a clear FTIR spectrum of a single bicelle crystal was confirmed, several experiments were considered. First was a thermal stability experiment in which changes in the FITR spectrum of a single crystal were monitored with increasing sample temperature. The temperature control cell used in previous FTIR thermal stability studies in this lab by bR by Heyes *et al.*[13,14] using the Nicolet Magna 860 was too large (too tall) to fit under the microscope stage of the Perkin Elmer instrument. A shorter-profile temperature control sample holder was located in the laboratory of Dr. Gary Schuster. However, this temperature control cell was still too thick to fit under the microscope objective.

Once it became obvious that a temperature study was not going to be easy to do, attention turned toward trying to capture a single-crystal FTIR spectrum upon

photoexcitation. Unfortunately the Perkin Elmer bench in the Kumar group lab was not interfaced to any laser source as was the Nicolet bench in our lab. To be able to accomplish these experiments, a portable green laser source was necessary. Research into the purchase of a portable green laser source proved cost-prohibitive, so a green (532 nm, 5 mW) Z-bolt laser pointer (Z-bolt, Portland, OR) was used instead. A spectrum was taken before, then during, illumination with the green laser pointer. Unfortunately, no change in the spectrum was observed upon illumination. Since the power output of the laser pointer could not be adjusted, increasing the exposure time was attempted. Keeping the laser on the crystal for longer periods of time still resulted in no spectral changes and eventually caused the laser to overheat and turn off. Another limitation to this these experiments is the inability to bring the laser source close enough to the crystal. Due to the close working distance between the microscope objective and the sample, the laser beam had to be brought in from the side, resulting in a less-focused spot. Figure 2.11 describes this limitation and the resulting beam diameter hitting the sample.

Figure 2.11: Description of the limitations of using a laser pointer as excitation source for single-crystal FTIR spectroscopy.

If the green laser source were in line with the objective, the laser beam would result in a more focused beam spot on the sample, with a shower distance between the laser and the sample (left). However, in these experiments the laser beam had to be brought in from the side, (right) resulting in both a longer distance between beam and sample and also a more diffuse laser spot on the sample. Lacking the ability to either do a temperature study or a photo excitation study using this single-crystal FTIR bench, further single-crystal FTIR work was not pursued.

2.9. Sample Preparation and Data Acquisition for Single-Crystal Polarized Raman Experiments

Polarized Raman experiments using the Holoprobe Research 785 nm Raman microscope were also attempted under the direction of Dr. Michielsen. In these experiments, it was necessary to keep the degree of hydration constant and avoid photoexcitation of the sample so that spectral changes arising from different crystal orientations were due only to changing the crystal orientation, not dehydration nor photoexcitation of the crystal. To keep the hydration constant, the crystal was always kept under a drop of water during data acquisition. To avoid photoexcitation of the sample, the white light of the microscope bright field was passed through a red filter before passing through the sample, and each time the crystal orientation was adjusted, the bright field was passed through the red filter.

The crystals were removed from their detergent matrix as described in Section 2.5. A solution of crystals in DDW was placed on a foil-covered glass cover slide and allowed to dry overnight in the dark. All work done from this point on was carried out

under bright field passed through a red filter to avoid photoexcitation of the crystal. Once the crystal was fixed to the slide by drying, a drop of water was added to the top of the crystal. Under red illumination, the slide was rotated until the long axis of a crystal was aligned along the y-axis of the viewing field of the monitor. The design of the microscope was such that the 785 nm laser was plane-polarized along the y-axis of the viewing field. Thus, when the long axis of the crystal was along the y-axis of the viewing field, this long axis was also aligned with the plane of polarized laser light, and the angle between the crystal's long axis and the plane of polarized light was 0° Sample adjustment was done under bright field exposure with a red filter to avoid photoexcitation of the sample. After the sample was in position, the microscope was switched to dark field, the box chamber door closed off with black fabric, and a Raman spectrum taken at this 0° position. Following this initial spectrum acquisition, red-filtered bright field was switched back on and clockwise rotation of the sample stage relative to the plane of polarized light resulted in the changing of this angle from 0° to 45°, where the 45°spectrum was taken under dark field. The red-filtered bright field was turned on once again, the sample adjusted to 90°, the switch to dark field was made, and the 90°spectrum was taken under dark field. Figure 2.12 demonstrates how the long axis of the crystal was oriented relative to the plane-polarized incident 785 nm laser. In all cases the plane of polarized light was along the y-axis of the viewing field.

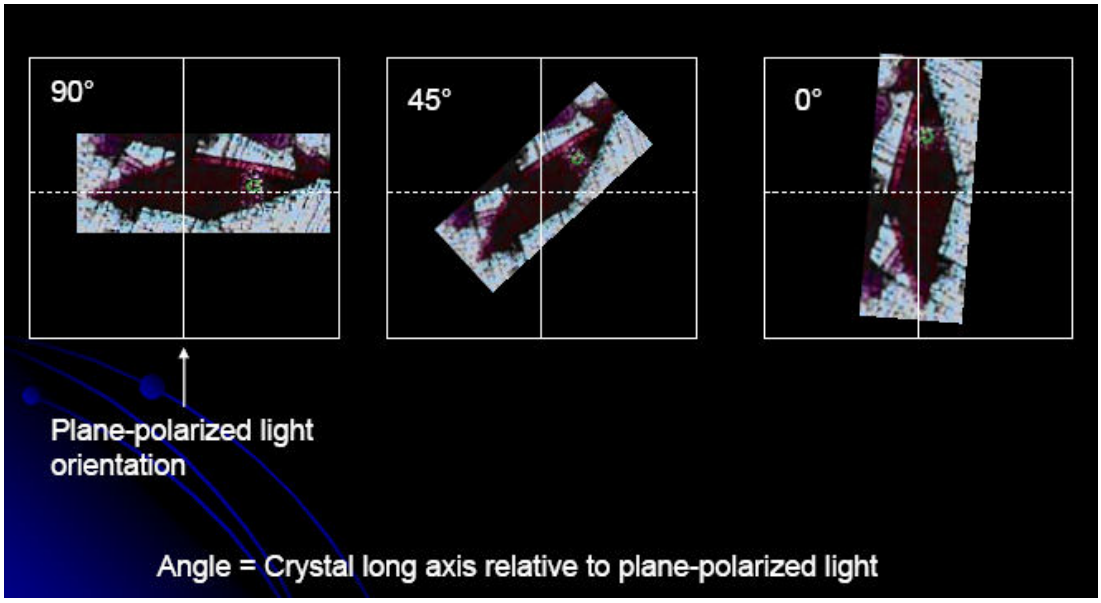

Figure 2.12: The three orientations of the long axis of a single bicelle crystal relative to plane-polarized light

Figure 2.13 shows the three Raman spectra resulting from these three different orientations. The data have been normalized to the 1008 cm^{-1} absorption (C-CH_3 rocking), which should have an intensity independent of orientation. The normalized data show no signal intensity dependence. At the time, two possibilities for this observation were considered. The first was the possibility that within the retinal binding pocket of each monomer, the retinal was not oriented. From the crystal structure of Bowie and Farham, the arrangement of protein monomers was known, but the retinal orientation within each monomer was not. The second possibility considered was that perhaps the crystal was twinned. If this were the case, then the polarized data was obtained on more than just a single layer of monomers, but on multiple layers that were rotated in relation to one another. In discussing these findings with Bowie and Farham, the latter was found to be true. It was not clear, however, if all crystals made by this

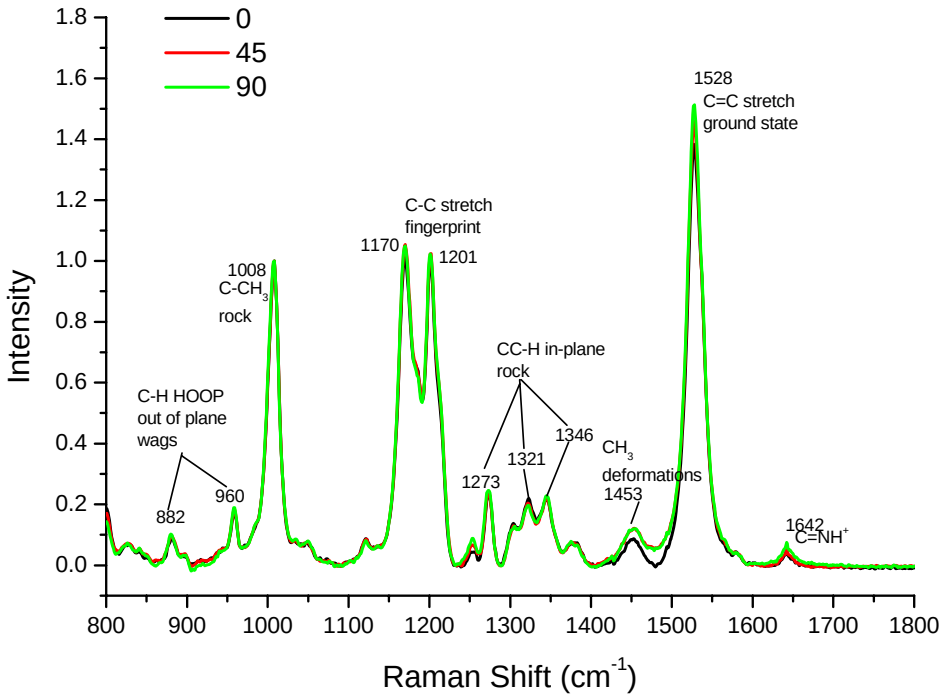

Figure 2.13 : The Raman spectra resulting from the three different crystal orientations shows no orientation-dependent intensity differences

method were twinned. If single un-twinned crystals could be located, polarized Raman spectroscopy might allow us to determine the optic axis of the crystal relative to the long axis of the crystal, which would allow us to better understand how the retinal is oriented within these crystals. Transmission microscopy of crystals viewed on a rotating stage under cross polarizers would allow us to determine which crystals, if any, were untwined by changes in their transmission of polarized light.

2.10. Transmission Microscopy of bcbR Crystals to Locate Untwinned Single Crystals

A large sample of crystals was viewed under cross polarizers using the 4x objective of a Leica DMRX transmission microscope (Leica MicroSystems, Wetzlar, Germany). The stage was rotated through a few different positions and images were taken at these positions. Figure 2.14 demonstrates the changes in the transmission of polarized light in multiple crystals viewed under a rotating stage. Top left: crystals observed with no polarizing filters in place. The rest of the images are the same crystals viewed under cross polarizers in multiple stage positions. Only small sections of some crystals are found to have an optic axis. The lack of single untwined crystals on which polarized Raman spectroscopy could be performed resulted in an end to any further polarized spectroscopy experiments.

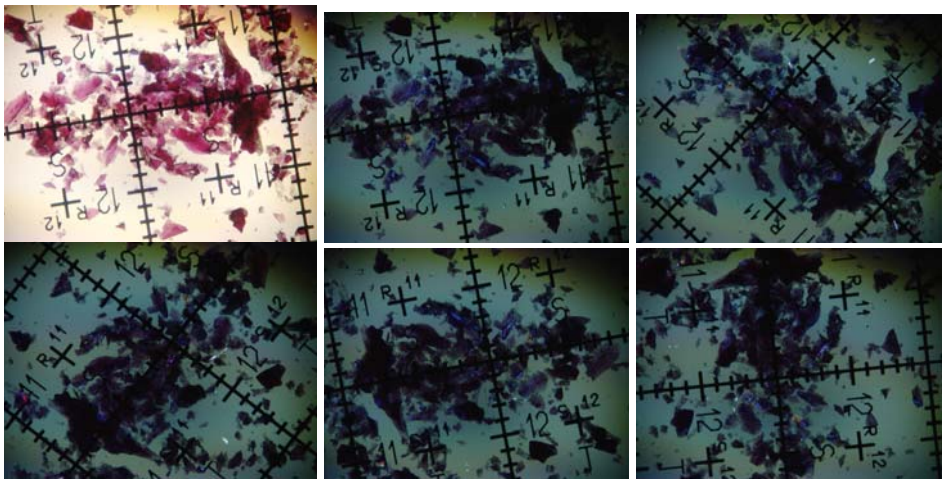

Figure 2.14: Changes in the transmission of polarized light in multiple crystals viewed under a rotating stage.

2.11. Sample Preparation and Data Acquisition for Transient Absorption (Flash Photolysis) Experiments

In the initial attempts to carry out these experiments, the previously-used solution phase bench setup was used, in which the pulsed YAG laser and probe beams are both directed through a homogenous solution of native membrane. However, the higher density of the crystals relative to water resulted in their settling to the bottom (and out of the sampling beam) faster than data could be acquired. The modifications to the solution phase sampling setup that led up to the final sampling bench setup described in Chapter 5 in this thesis, are described.

Crystals were removed from their matrix by the rinsing method described in section 2.4. A concentrated mixture of multiple crystals in deionized, distilled water (DDW) was placed in a regular plastic 3 mL volume cuvette, which contained at the bottom a small stir bar a few mm in length. This cuvette was set atop a stir plate and the plate turned on to keep the crystals circulating and within the beam path. Transient absorption experiments were carried out using the frequency doubled output of a Q-switched nanosecond pulsed Spectra Physics Quanta-Ray Series Nd:YAG laser (Spectra Physics, Mountain View, CA). Monitoring light was provided by a PTI Corporation Xenon arc lamp (PTI, San Jose, CA) running in CW mode. The monochromator was adjusted to 412 nm. A filter was placed in front of the entrance slit of a SpectraPro-300i 0.300 meter triple grating monochromator (Acton Research Corp., Acton, MA) to remove any 532 nm excitation light while allowing passage of the 412 nm light. This bench setup is described in figure 2.15. The filter's transmission profile in Figure 2.16

demonstrates that the 532 nm light is blocked while the 412 nm light passes through to the monochromator.

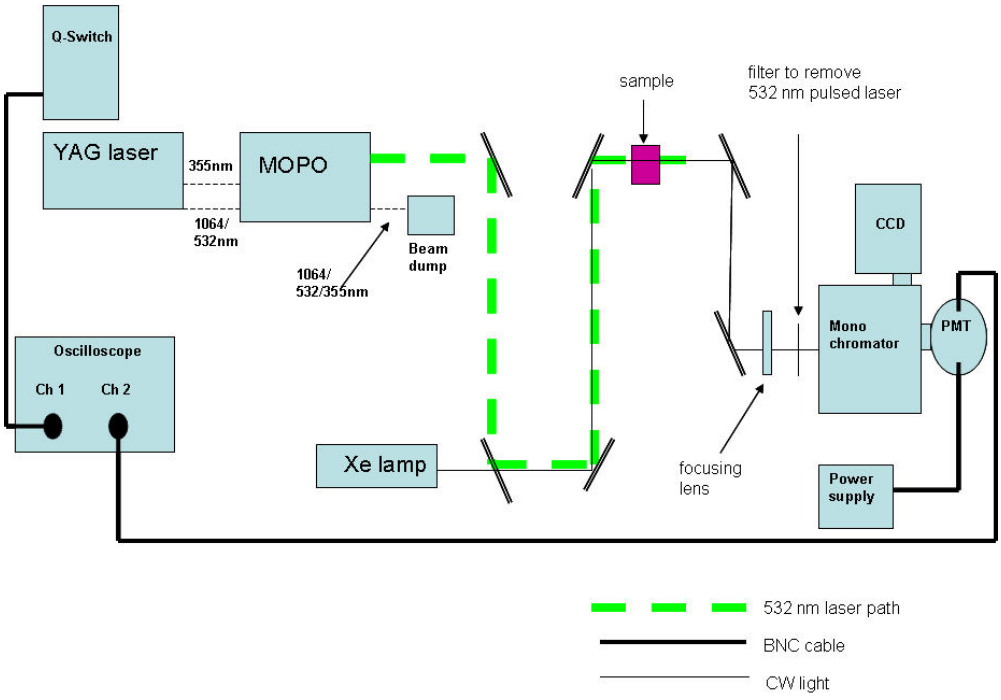

Figure 2.15: Top-down view of the bench setup for the first attempt at flash photolysis experiments with several bicelle crystals stirred in DDW.

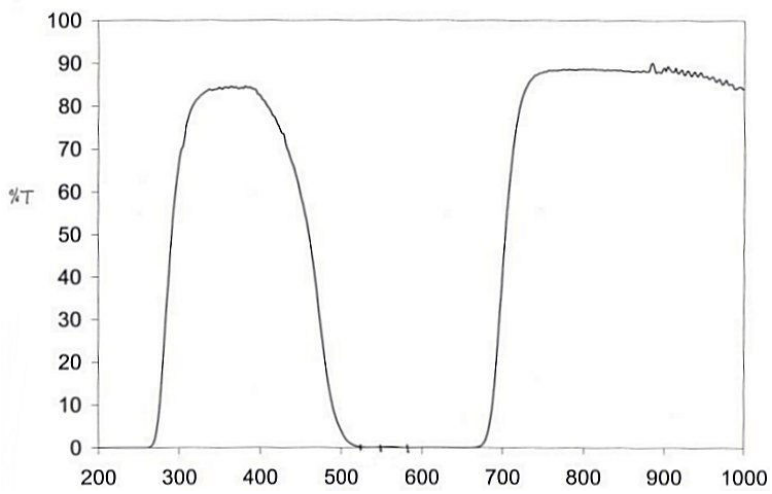

Figure 2.16: The filter transmission profile for the flash photolysis experiments.

Single wavelength kinetics monitored at 412 nm were recorded using a Hamamatsu photomultiplier tube (Hamamatsu, Hamamatsu City, Japan) whose response was digitized using a LeCroy 9350 500 MHz oscilloscope (LeCroy, Chestnut Ridge, NY). The excitation at 532 nm had a pulse energy of 1 mJ and was overlapped with the monitoring beam at the ~2 mm focal spot within the sample. The laser Q-switch triggers data acquisition by the Leroy 9350 oscilloscope at a frequency of 10 Hz. A floppy disk inserted at into the top of the oscilloscope is used to store the kinetic traces. After each experiment, the Winspec 32 software program converts this waveform data into an XY form that can be plotted using the OriginPro 7.5 software package with time on the X axis and intensity at 412 nm on the Y axis.

Initial attempts to acquire data while stirring the sample resulted in very little to no signal. Since the crystals in DDW would settle to the bottom of the cuvette, a sample holder had to be designed which would allow the passage of both. The details of this sample holder and the modified bench setup are presented here and again in Chapter 5, along with the data acquired in these experiments.

In order to run multiple samples one right after another, a multi-well sample holder was with an optically clear and flat surface was designed. Such a multi-well sampling system was designed by taking a rectangular microscope slide and using spray adhesive to attach a piece of rubber matting approximately 2 mm thick. This rubber matting contained holes punched through it (prior to its attachment to the glass) that were each approximately 3-4 mm in diameter. Figure 2.17 shows both a top-down and a side-view diagram of such a sampling tray.

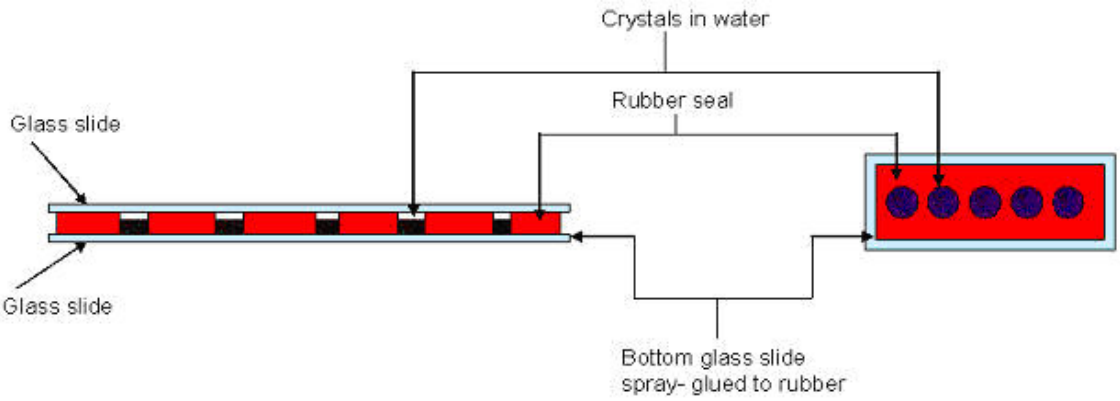

Figure 2.17: Side (left) and top-down views of the design of the multi-well sample holder for transient absorption experiments on multiple crystals.

Fellow student Alex Schill designed the modified bench setup in which both the 532 nm laser beam and the probe beam were directed downward through the new sample trays. This was accomplished by directing the 532 nm laser beam downward on the sample via the use of two mirrors and a focusing lens. The CW probe light was also directed downward and focused on the sample using the same focusing lens. After both beams passed through the bottom of the sample tray containing the crystals, a receiving fiber optics picked up both beams and delivered them to the monochromator. The filter was placed just before the monochromator entrance to block unwanted 532 nm light and only allow the passage of 412 nm light. Figure 2.18 shows a top-down bench diagram for using the 532 nm incident pulsed laser as excitation source for M_{412} decay experiments on a crystal sample.

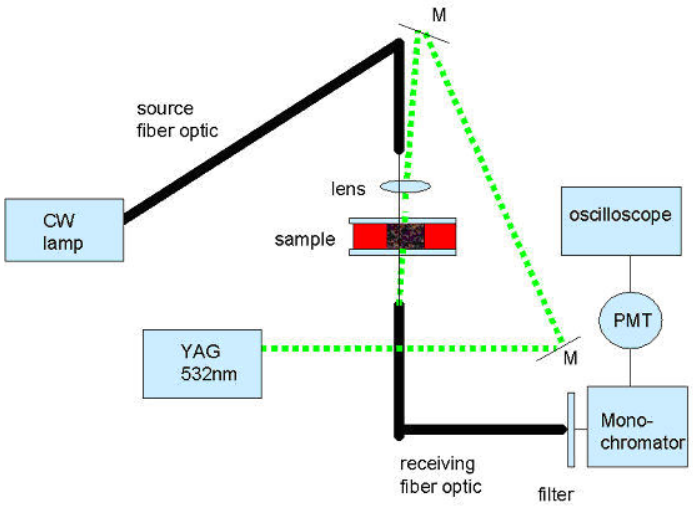

Figure 2.18: bench diagram for using the 532 nm incident pulsed laser as excitation source for M_{412} decay experiments on a crystal sample.

Notice the use of fiber optics to concentrate the CW beam and the use of a filter to remove the pulsed 532 nm laser right before it can enter the monochromator. "M" indicates the placement of mirrors used to direct the pulsed laser to the sample. Figure 2.19 is a photograph of a side-view of the same bench setup. The pulsed 532 nm laser path is shown as a broken green line from the source (not pictured) to mirror 1, upward to mirror 2, then downward from mirror 2 toward the focusing lens, then through the sample, after which point it enters the fiber optic below it. The CW probe beam is pictured as an unbroken white line that is directed from the upper fiber optic, through the lens, sample, and back into a second fiber optic beneath the sample, from which point it is directed toward the monochromator. The data collected in this manner resulted in data published in Biophysical Journal[4] and also presented in Chapter 5 of this thesis.

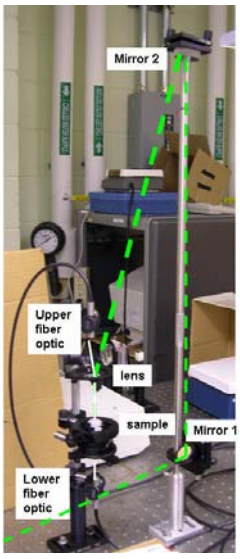

Figure 2.19: Photograph of the side-view of the same bench setup.

2.12. Sample Preparation and Data Acquisition for FTIR Difference Spectroscopy on bcbR Crystals.

Bicelle bR (bcbR) crystals were removed from their detergent matrix by the washing method described in Chapter 3. Because the technique is not a micro-scale experiment, a large volume of crystals needed to be used to achieve maximum signal. A large volume of crystals in DDW was concentrated on a single 25 mm x 2 mm CaF_2 window (Harrick Scientific Products, Pleasantville, NY) by allowing the water to evaporate under ambient temperature, light, and pressure. During this process, a small pipette was used to blow the edges of the drop toward the center, to prevent the spreading out of crystals over a large area of the window. Once a sample spot of approximately 10 mm was formed and the crystals were fixed to the window, the single window was placed in the sample chamber of a Nicolet Magna 860 FTIR Spectrometer (Thermo Nicolet Instruments, Madison, WI) and the spectrum was checked in the 4000-1000 cm^{-1} range to make sure

that water was present but not saturating. A typical spectrum for a mass of bcbR crystals that were soaked in D_2O instead of DDW was taken at this stage is shown in Figure 2.20.

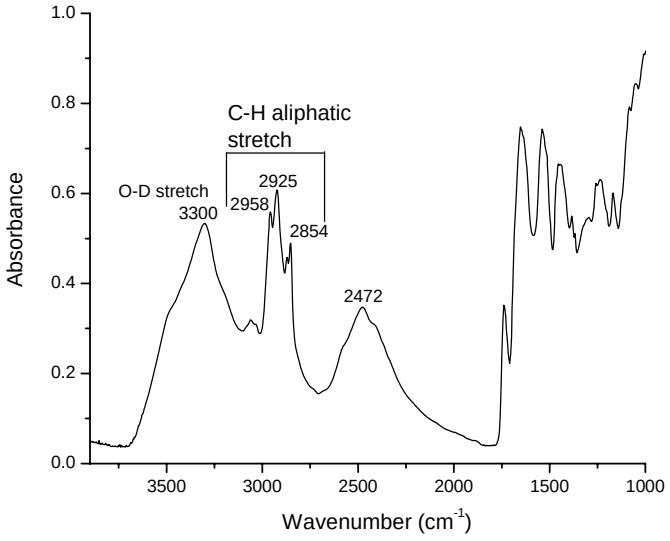

Figure 2.20: Typical FTIR absorption spectrum for a mass of bcbR crystals soaked in D_2O on a single CaF_2 window.

This spectrum clearly shows that bulk D_2O is present but not saturating in the 3300 cm^{-1} region. An inset of the protein absorption bands in Figure 2.21 shows that the C=O stretch, N-H bend, and N-D bends of the protein are all clearly observed. The 1741 cm^{-1} band is due to the C=O stretch of the ester group in the DMPC detergent. Here the amide I C=O stretching of the protein is observed at 1660 cm^{-1}, the amide II N-H bending of the protein is observed at 1537 cm^{-1}, and the N-D bending is observed at 1442 cm^{-1}.

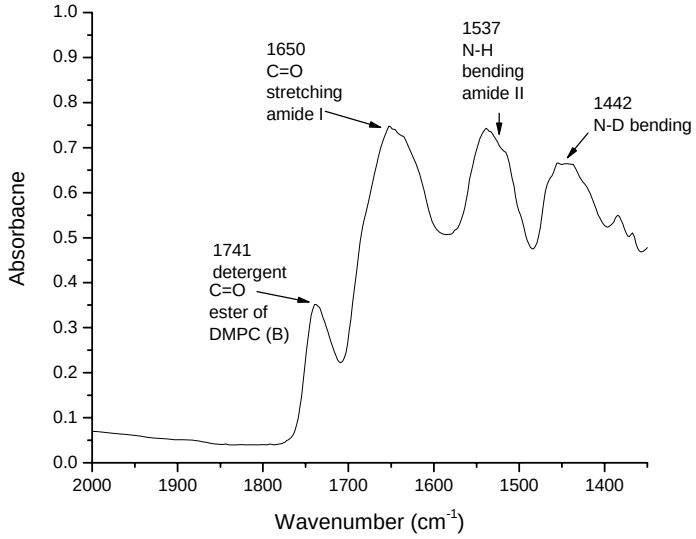

Figure 2.21: Inset of the protein region from above

Regardless of whether D_2O or DDW was used, the spectrum was checked in this way to determine if the protein hydration levels were acceptable. Vacuum grease was added to the perimeter of this CaF_2 window, with a second window added. The two windows were held together by parafilm. The vacuum grease served as an additional barrier to seal in the hydration level of the sample between the windows. The sealed CaF_2 windows were placed in a Harrick temperature control cell and then placed in the sample chamber of the FTIR spectrometer. The temperature was adjusted to 5.0ºC.

A series of optics directed the 514 nm line of an Innova 300 Argon laser (Coherent, Santa Clara, CA) into the sample chamber of the spectrometer. The power at the sample was adjusted to 10 mW/cm^2, as described in the literature.[15] An overhead diagram of this bench is shown in Figure 2.22. The 514 nm line is selected and sent to the FTIR bench,

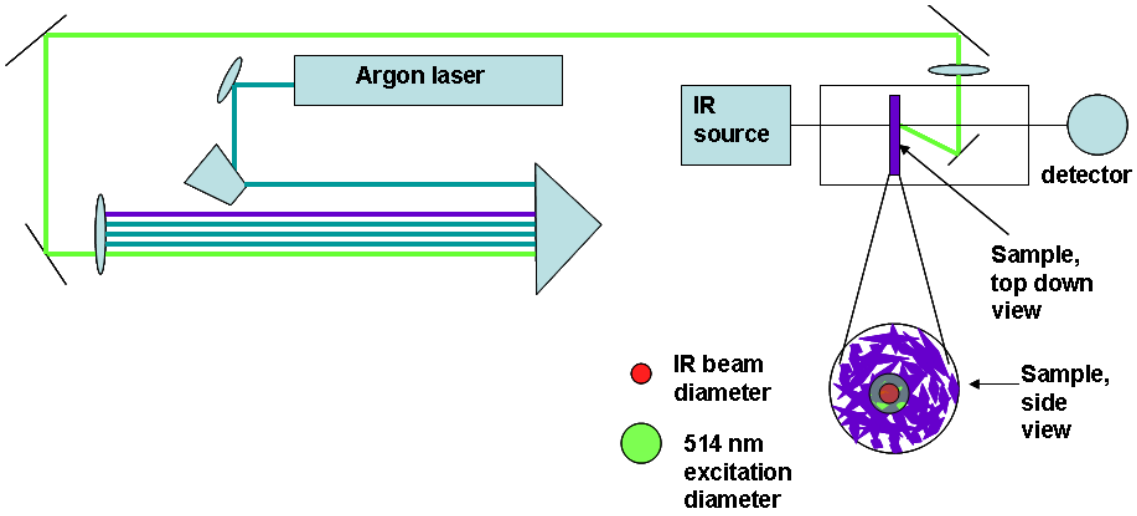

Figure 2.22: Overhead bench setup for FTIR difference spectroscopy

The location of the power meter used to adjust the laser power to 10mw/cm^2 is indicated. The diameter of the 514 nm laser must be kept either equal to or greater than the IR beam sampling area, to ensure that all crystals within the IR sampling area are being excited by the 514 nm line. Initial attempts at taking the difference spectrum of either native membrane or a mass of bcbR crystals were hampered by the presence of a fluctuating water concentration. Figure 2.23 illustrates three different attempts to obtain the difference spectrum of native bR in DDW at 5ºC. Although the positive 1760 cm^{-1} band (protonated Asp_{85}) and the negative 1528 cm^{-1} band (depletion of the C=C stretching of protonated retinal) are present, the large positive 1560 cm^{-1} band that would indicate creation of the C=C of deprotonated retinal (the M state) is not clearly observed. In addition, the shift in the amide I frequency from 1670 to 1650 cm^{-1} observed in the literature[15] is not observed. Large negative bands appear at 1590 and 1645 which are not described in the literature.

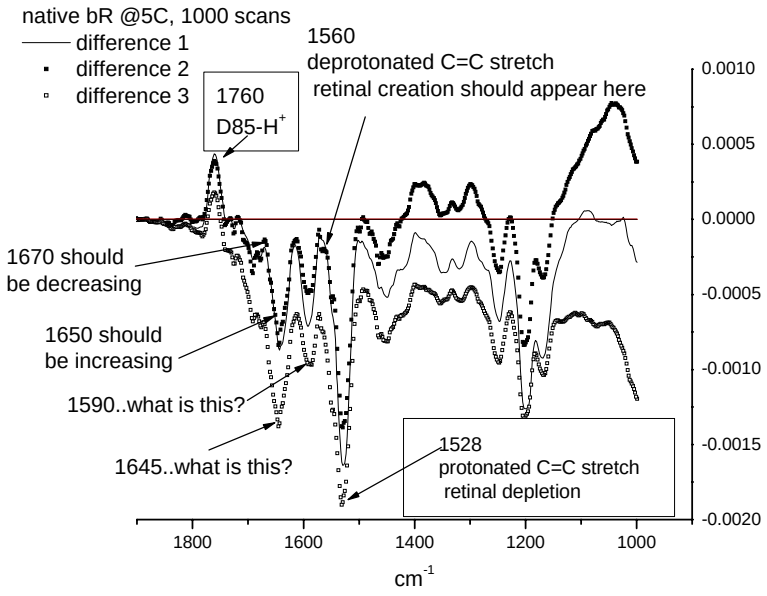

Figure 2.23: Three different attempts to replicate the IR difference spectrum of native bR at 5ºC.

As mentioned earlier in the chapter, water vapor appears in the same region of the IR spectrum as do protein vibrations. The Nicolet Magna 860 bench is purged by a 74-5041 FT-IR Purge Gas Generator (Parker Bolston Analytical Gas Systems, Cleveland, OH). This gas generator compresses surrounding air to 80 psi, and passes the air through filters that remove CO_2 and H_2O before passing the air to the bench via ¼" OD Teflon tubing at a flow rate of approximately 20 SCFH. For the difference experiment to be successful, the water vapor concentration does not need to be 100% absent, as long as the concentration does not fluctuate on a scale larger than differences in the protein upon laser excitation. If the water vapor concentration is constant throughout the data acquisition time, its intensity in the spectrum remains constant and it is subtracted out in difference spectroscopy to only reveal changes in the protein and retinal during

irradiation. However, if the water vapor concentration is fluctuating (due to an inefficient purge, for example), then the difference spectrum of the protein is overlaid with interfering water bands. To confirm that this was the case, a series of spectra were taken of an empty sample chamber of the FTIR bench after the sample chamber was closed and had been purging overnight. Figure 2.24 shows four different 'background' spectra of the empty FTIR sample chamber. Each spectrum is the result of an average of 5 scans and were all taken with in the same one-minute sampling period.

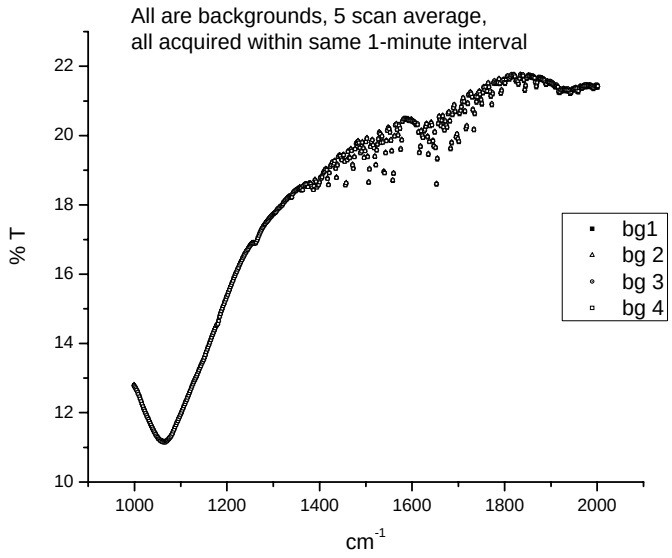

Figure 2.24: Four different 'background' spectra of the empty FTIR sample chamber.

Figure 2.25 shows the difference spectra resulting from subtracting the second background from the first, the third background from the second, and so on. For a steady purge, these difference spectra should be as flat as possible, or at least smaller than the changes expected in the difference experiment with sample in the chamber. The %T

scale indicates that not only is the water vapor background fluctuating, but that it is fluctuating to produce noise on a larger scale than the data would.

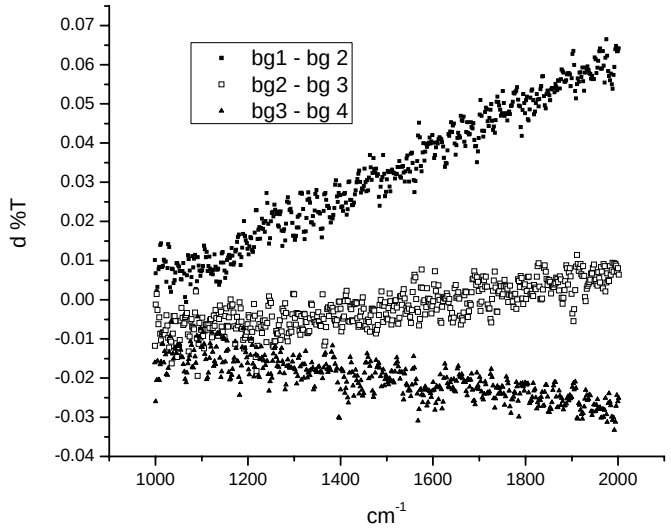

Figure 2.25: Differences between these background spectra.

A Bruker v66 model FTIR spectrometer (Bruker Optics, Billerica, MA) was used by Heberle *et al.*[15] in the difference spectroscopy performed on cbR crystals. This bench features a vacuum sample chamber, which eliminates water completely. In contrast, the sample chamber for the Nicolet Magna 860 bench used for these bcbR difference experiments is not under vacuum purge, but instead uses the Whatman 74-5041 FT-IR Purge gas generator (Parker Hannafin, Cleveland, OH. This purge gas generator uses a Gast 2HAH-11T-M200X compressor (Whatman Inc, Haverhill, MA) that intakes lab air and compresses it to approximately 80 psi. The temperature of this hot compressed air is then lowered by sending it through an aftercooler. After this point it is then sent through

a set of prefilters before it travels through the two regenerative desiccant driers (towers) that alternate between each other to remove residual water and CO_2.

Dr. Bridgette Barry of the Georgia Tech School of Chemistry and Biochemistry was consulted about the issue of insufficient water vapor removal. After this meeting, modification of the present bench was undertaken to include a desiccant column through which the compressed air must pass between the compressor to the instrument. It was anticipated that this additional stage would filter out the residual water vapor getting into the bench. The desiccant column was a LabClear model DGF-250 Disposeable gas filter with ¼" OD fittings and 600 cc volume (Labclear, Oakland, CA). The filter contained both indicating Drierite desiccant and #13x molecular sieve. The Teflon tubing connecting the compressor to the bench was cut and the filter inserted as shown in Figure 2.26.

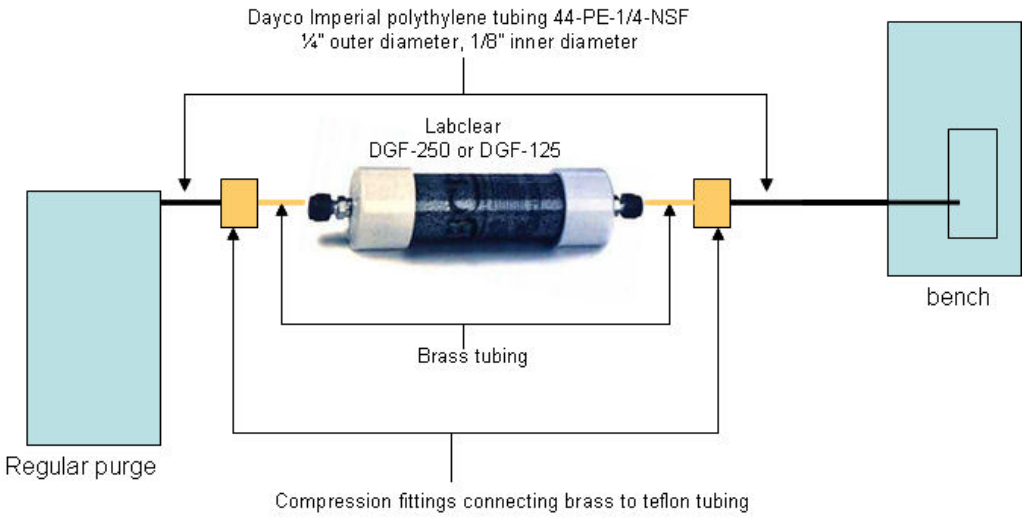

Figure 2.26: Addition of desiccant column to remove residual water vapor in purge air before it enters FTIR sample chamber.

2.13 Sample Preparation and Data Acquisition for FTIR Difference Experiments After Desiccant Column Added

After the desiccant column was added, the change in the spectrum of the empty FTIR chamber was monitored for a period of two days to determine the effectiveness of the new column to maintain a more stable environment days. After purging with the new column for a period of two days the fluctuation was much smaller than before and the difference experiments were conducted again.

The native sample was prepared as described in Section 2.12, except that a temperature control cell was not used for this and all following experiments. The native sample in H_2O was allowed to dry on a CaF_2 window until the level is hydration was satisfactory. A second CaF_2 window was placed on top, and parafilm was used to seal the windows together. The sample was placed in the FTIR chamber, adjusted to give maximum signal, and the chamber door closed. The sample was allowed to purge overnight before any measurements were taken. The following day, thirty scans were taken of the native sample with the laser off, and another thirty scans were taken immediately afterward with the 514 nm laser power at 15 mW/cm^2. The mirror velocity was 0.6329; the aperture was set to 50. The 'laser on' spectrum was subtracted from the 'laser off' spectrum.

Since the spectrum of a sample of crystals gives much lower signal, more sample spectra were needed to observe the small changes. A sample of crystals in H_2O was allowed to dry and was concentrated on a single CaF_2 window as described in Section 6.2. A second CaF2 window was sealed over the first with parafilm and the sample was placed in the chamber to purge overnight before any spectra were taken. The following

day a series of spectra were taken to experiment with the collection time and sample aperture to give the largest difference spectra without damaging the crystals. The optimum difference spectra resulted from exposure of the crystals to 15mW/cm^2 of 514 nm laser for 500 scans (approximately 8 minutes at a mirror velocity of 0.6329) with a sample aperture of 150. The laser was blocked and a 500-scan of the crystals was taken immediately afterward. This process was repeated 47 times to give 47 difference spectra for the crystals. These were averaged to give a single difference spectrum for the crystals. The data from these experiments is presented in Chapter 6.

References

(1) Bowie, J.; Farham, S. *Journal of Molecular Biology* **2002**, *316*, 1.

(2) Oesterhelt, D.; Hess, B. *European Journal of Biochemistry* **1973**, *37*, 316.

(3) Faham, S.; Yang, D.; Bare, E.; Yohannan, S.; Whitelegge, J. P.; Bowie, J. U. *Journal of Molecular Biology* **2003**, *335*, 297.

(4) Sanii, L. S.; Schill, A. W.; Moran, C. E.; El-Sayed, M. A. *Biophysical Journal* **2005**, *89*, 444.

(5) Kriebel, A. N.; Albrecht, A. C. *Journal of Chemical Physics* **1976**, *65*, 4575.

(6) Godfrey, R. E. *Biophysical Journal* **1982**, *38*, 1.

(7) Vogel, H.; Gaertner, W. *Journal of Biological Chemistry* **1987**, *262*, 11464.

(8) Du-Jeon-Jang; El-Sayed, M. A.; Stern, L. J.; Mogi, T.; Khorana, G. *FEBS* **1990**, *262*, 155.

(9) Cassim, J. Y. *Biophysical Journal* **1992**, *63*, 1432.

(10) Wang, J.; Link, S.; Heyes, C. D.; El-Sayed, M. A. *Biophysical Journal* **2002**, *83*, 1557.

(11) Claborn, K.; Puklin-Faucher, E.; Kurimoto, M.; Kaminshy, W.; Kahr, B. *Journal of the American Chemical Society* **2003**, *125*, 14825.

(12) Silvertein, R. M.; Bassler, G. C.; Morrill, T. C. Infrared Spectroscopy. In *Spectrometric Identification of Organic Compounds*; 5th ed.; John Wiley and Sons, Inc.: New York, 1991; pp 91.

(13) Heyes, C. D.; Wang, J.; Sanii, L. S.; El-Sayed, M. A. *Biophysical Journal* **2002**, *82*, 1598.

(14) Heyes, C. D.; El-Sayed, M. A. *Biochemistry* **2001**, *40*, 11819.

(15) Heberle, J.; Buldt, G.; Koglin, E.; Rosenbusch, J. P.; Landau, E. M. *Journal of molecular biology* **1998**, *281*, 587.

CHAPTER 3

LIGHT-DARK ADAPTATION AND TRAPPING OF THE DEPROTONATED SCHIFF BASE IN BICELLE BACTERIORHODOPSIN CRYSTALS STUDIED BY VISIBLE AND RAMAN SPECTROSCOPY[*]

Abstract

In this chapter, visible spectroscopy will be used to examine a mass of bicelle bacteriorhodopsin (bcbR) crystals still embedded within their detergent matrix for their ability to light adapt upon exposure to white light. For single crystals removed from their detergent matrix and dried under ambient temperature and pressure, a new band at 430 nm in the visible and a Raman band at 156 cm^{-1} in the spectrum are observed. The Raman band has been characterized in the literature[1-10] as the deprotonated Schiff base of the retinal chromophore. The absorption of the 430 nm band is close to the 412 nm absorption of the M intermediate of the photocycle, whose protonated Schiff base has been ionized.[11-22] When the bcbR crystals are dried in the dark and examined by the above two techniques it is found that the deprotonation is photochemically induced by the intense observation light of the microspectrometer used.

3.1. UV-visible Spectroscopy of the Native Membrane and the Structure of Retinal

At pH 7, the protein bacteriorhodopsin of *Halobacterium salinarium* exhibits two bands in the wavelength range 200-700 nm, one at 280 nm and another in the 560-568 nm

[*] Manuscript accepted: Sanii, Laurie S., El-Sayed, Mostafa A. "Partial Dehydration of the Retinal Binding Pocket and Proof for Photochemical Deprotonation of the Retinal Schiff base in Bicelle Bacteriorhodopsin Crystals" *Photochemistry and Photobiology*. ASAP. 2005

range, depending upon the light exposure of the sample (Figure 3.1).[23-25] The 280 nm absorption band is due to the π-π* transition of the tryptophan and tyrosine amino acid

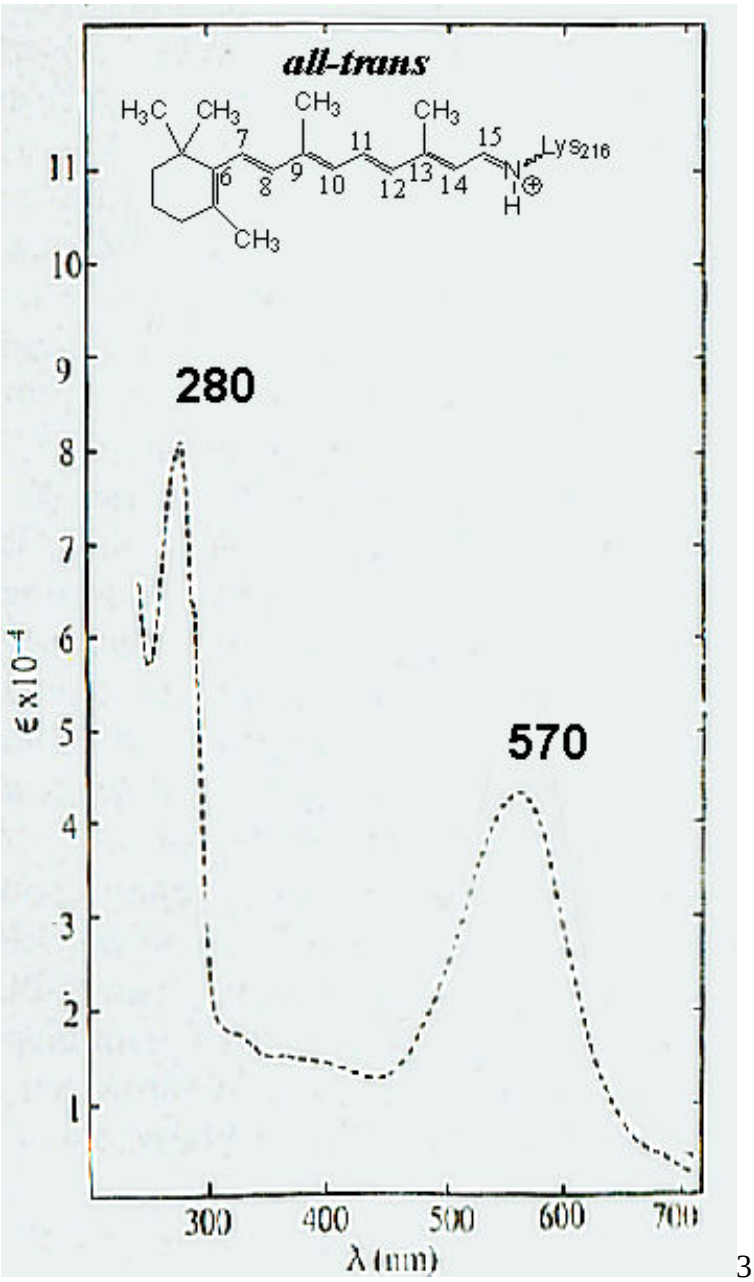

3.

Figure 3.1: Absorption spectrum of the light-adapted purple membrane.

residues of the protein backbone.[21] The second band is due to the absorption of light by the chromophore retinal, housed in the center of the seven α helices of amino acids.[23] The main backbone of the retinal molecule consists of a 2,6,6-trimethylcylohexene group with a 13-carbon conjugated chain, terminating with a protonated Schiff base. This protonated Schiff base connects the molecule to the rest of the protein via residue Lys_{216} on the seventh helix of the protein.[26-29]

3.2. Conversion Between Two Retinal Isomers in Native Form of Bacteriorhodopsin During Light/dark Adaptation

When the transmembrane protein bacteriorhodopsin is kept in the dark for several hours, the retinal molecules are found as a mixture of two isomers, commonly referred to as the "13-*cis*" and the "all-*trans*". More specifically, these two species are 13-*cis*,15-*syn* and the all-*trans*,15-*anti* isomers:[20,30-35]

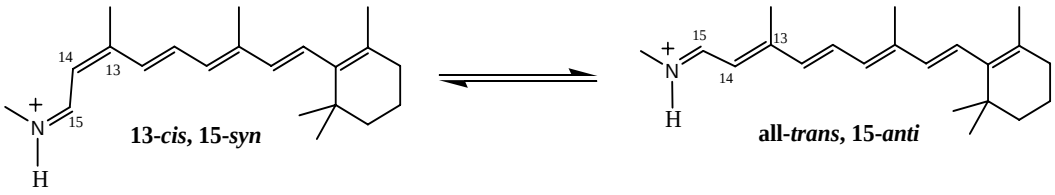

This mixture of isomers gives rise to a retinal absorption band in the visible spectrum centered at 560 nm. Upon exposure to white light, the retinal population converts to nearly all-*trans*,15-*anti* and the absorption band shifts to 568 nm.[20,22,24,35-38] The dark adapted and light adapted states of the protein are often referred to as bR_{560} and bR_{568}, respectively. Absorption of a photon by all-*trans*,15-*anti* retinal results in its isomerization from all-*trans*,15-*anti* to 13-*cis*,15-*anti* configuration:

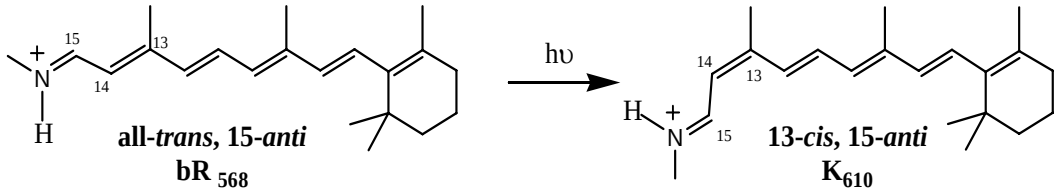

The 13-*cis*,15-*anti* form of the retinal molecule is the high-energy K_{610} intermediate that drives the rest of the photocycle through a thermal relaxation photocycle resulting in the translocation of a proton from the cytoplasmic to extracellular side of the membrane:[24,39-55, 56-61]

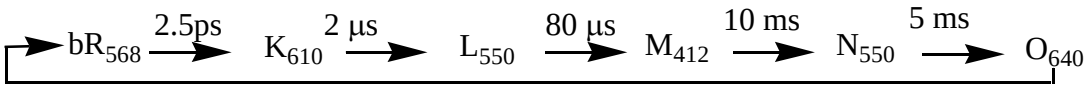

The formation of the 13-*cis*,15-*anti* retinal intermediate initiates changes starting at the Schiff base region and extending to the rest of the protein over the photocycle.[62] From visible spectroscopy, the shift in visible absorption from 560 nm → 568 nm during light adaptation of the protein allows us to follow the isomerization of the chromophore retinal, a necessary precursor for the photocycle to proceed from the all-*trans*,15-*anti* population of retinal.

3.3 Does Retinal Isomerize in Bicelle Bacteriorhodopsin Crystals?

In 2002, Bowie and Farham published a method to crystallize bR by a bicelle crystallization method, creating bicelle bR (bcbR) crystals.[63] The X-ray structure of these crystals revealed that the protein packing structure of the protein contained within these bicelle crystals no longer consists of parallel trimers, as was the case with the native membrane and in the previously-published cbR crystals made by the *in-cubo* crystallization method,[64] but of antiparallel monomers. It is not known how this novel packing structure affects the functionality of this protein. Can the retinal within these bcbR crystals isomerize under exposure to white light? If so, can it also pump protons, characterized by the creation of the deprotonated retinal Schiff base?

If the retinal in the bcbR crystals is unable to light adapt there should be no change in the visible absorption spectrum in the 560-568 nm region upon exposure to white light. If this is the case, we can say that the bcbR crystal is unable to isomerize and continue the photocycle. However, if isomerization between the dark- and light-adapted states is possible, a shift in the visible spectrum in this region should be observed for the bcbR crystals after their exposure to white light and the bcbR crystals may be able to undergo the photocycle. If isomerization is possible, bcbR crystals will be removed from their detergent matrix and examined by both single-crystal visible and Raman spectroscopy to see if the deprotonated Schiff base can be created and trapped by dehydration.

Experimental Methods

3.4 Light Adaptation Experiments on a Mass of Detergent-embedded bcbR Crystals

The bR samples were obtained from a cell line of *Halobacterium salinarium* and were purified by established procedures.[40] The concentration of bR was adjusted to approximately 10 mg/mL by monitoring the absorbance of the light-adapted (20 minutes light exposure using a 40 W bulb) bR sample at 570 nm until the absorbance spectrum was constant. Diamond-shaped bR bicelle crystals were made by the method of Bowie *et al.*[63] with the following modifications: the precipitant well solution was made by mixing 4.0 M NaH_2PO_4, H_2O, and 6.0 M 1,6-hexanediol in a 29:1:1.4 volume ratio, and this precipitant solution was mixed with an 8.0 mg/mL bR/8% bicelles mixture.[63] The samples were monitored periodically for the next two weeks as the fluid suspension slowly gelled during equilibration with the saturated salt solution underneath. The slides were then examined by light microscopy for evidence of crystal growth. Typical bicelle bR crystals, having dimensions of 100 μm x 200 μm, are shown in Figure 3.2 (left). This same sample preparation was repeated for bR samples that had not been crystallized (a film) to see the effect of crystallization on light adaptation. Before acquiring the absorption spectrum of the film, the sample was hydrated with a drop of water, a cover slip sealed over it, and allowed to equilibrate overnight. This film is shown in Figure 3.2 (right).

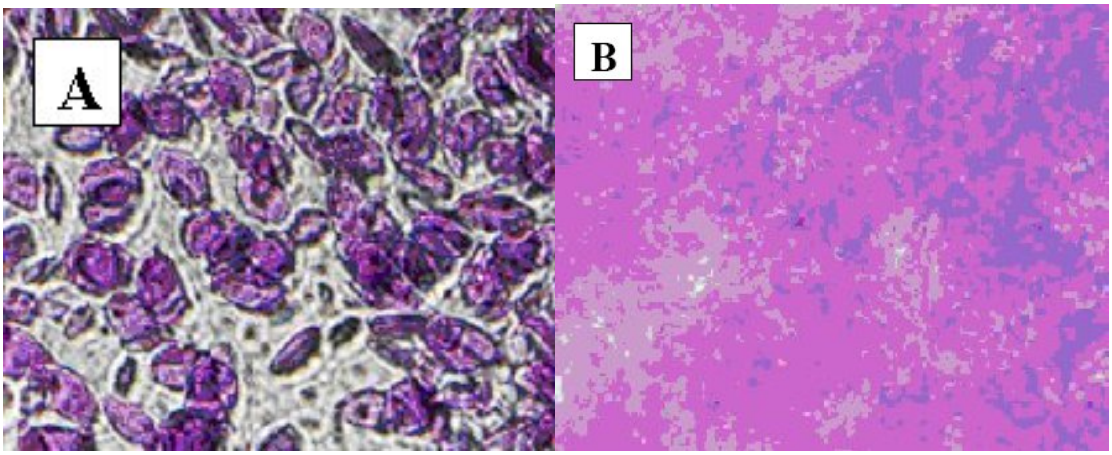

Figure 3.2: Microscope images of a random assembly of multiple bicelle crystals embedded within their detergent matrix (left) and of a hydrated film of native bR (right).

A Shimadzu 3101 PC UV/VIS/NIR double-beam spectrophotometer running the Personal Spectroscopy Software v3.9 software package (Shimadzu, Kyoto, Japan) was used to examine the matrix-embedded bcbR crystals in the range from 400-800 nm for their ability to light adapt under exposure to white light. An ISR-260 integration sphere attachment replaced the solution-phase sample holder in order to increase signal intensity. Because exposure to air dries out the matrix and embedded crystals, the glass cover slip of matrix-embedded bicelle bR crystals to be examined was removed from its crystallization well, a 2 mm thick circular rubber o-ring spacer was placed around the matrix spot, and a second slide was placed above it (Figure 3.3). The o-ring spacer provided a sealed compartment to prevent sample desiccation during the experiment, eliminating spectral changes due to fluctuations in the hydration level of the sample during the experiment. The sample sandwich of either the hydrated native bR film or of several bcbR crystals within their detergent matrix was placed in the integration sphere,

scanned, and adjusted in the beam path until maximum signal was found. Once this position was found, the chamber door closed, and the sample kept in the dark overnight.

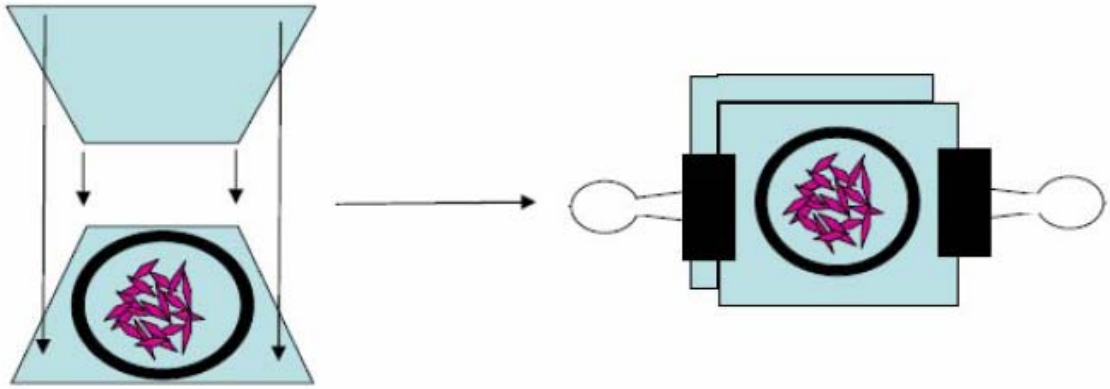

Figure 3.3: Assembly of the bicelle crystal sandwich used to take visible spectra of a sample of multiple crystals embedded within the detergent matrix.

After scanning this dark-adapted sample from 400-800 nm, the chamber door was opened and a white light source (desk lamp with 40W incandescent bulb) was used to focus a spot of light on the sample. Care was taken to distance the light source from the sample to prevent denaturation by the lamp's radiant heat. The sample was scanned periodically until the visible spectrum remained constant. At this point, the chamber door was closed and the spectrum was monitored periodically to see if the light-dark adaptation process was reversible. The X-Y absorption data were plotted and fitted using the OriginPro software package version 7.5 (OriginLab Corporation, Northampton, MA).

3.5 Single-Crystal Visible Spectroscopy

For the single-crystal visible spectroscopy experiments studying the effect of dehydration under bright field exposure on a single bcbR crystal, the bcbR crystals were removed from

their detergent matrix and fixed to a glass slide by the following procedure: crystals were first removed from their detergent matrix by adding a few drops of deionized, distilled water (DDW) to the matrix, gently mixing the matrix gel to loosen the components, and then transferring to a micro-centrifuge tube containing DDW. After vortexing the tube to dislodge the crystals from the matrix, the crystals would settle to the bottom of the tube within a matter of minutes, leaving the matrix components on top, in the supernatant. The supernatant was then removed by pipette, more DDW added, and the process repeated until the milky matrix components were no longer detected by eye. A 5-10 µL drop of crystals in DDW were then removed by pipette and placed on a glass slide. The crystals settled to the bottom of this drop, close to the surface of the glass slide, and the excess DDW was removed by a combination of pipetting and evaporation as the crystals were exposed to ambient lighting and temperature. Once the excess DDW had been removed, the crystals became immobilized on the glass slide and were easily transported to the microscope for single-crystal visible spectroscopy.

A S.E.E. 1000 MSP visible microspectrometer running the SEEScope version 4.0.0 software package (S.E.E. Inc, Middleboro, MA) was used for single-crystal visible absorption experiments to compare the light-adapted spectrum of hydrated single crystals to hydrated native films. The microspectrometer had a wavelength range from 400-800 nm that allows for the examination of the retinal absorption within the protein. The 20X objective used in these experiments has a sampling area of 8 µm squared. Since on average these crystals are 100 x 200 µm in size, several different areas on a single crystal could be examined individually. Spectra were collected from multiple areas of the same crystal, and also from different crystals. The same process was repeated for several

locations on a hydrated native film as well. In all cases, spectra were collected after the sample was exposed to a drop of DDW for a period of one hour under the same intensity bright field of the microscope. All data taken was saved as .spc files and opened again in the ONMIC v 5.2 software package (Nicolet Instrument Corp, Madison WI), where the baseline could be smoothed. After smoothing, the data were saved as .csv files and opened in the OriginPro software package v7.5 for plotting. All the crystal spectra were averaged, and all the native film spectra were averaged. The same microspectrometer was also used for the single crystal visible absorption experiments examining the effect of dehydration of a single crystal by dry nitrogen stream under constant bright field exposure of the microscope.

3.6 Single-Crystal Raman Spectroscopy

For the single-crystal Raman experiments studying the effect of dehydration on a single bcbR crystal under increasing 514 nm laser irradiation, the crystals were removed from their detergent matrix as described above and fixed to a glass slide that was covered by a piece of aluminum foil. The aluminum foil was used to prevent the appearance of interfering phonon Raman bands caused by interaction of the 785 nm Raman incident laser with the glass surface. For the experiments studying the effect of dehydration on a single bcbR crystal dried in the dark, the crystals were removed from their detergent matrix and fixed to an aluminum foil-covered glass slide by the procedure above. The focus was set on a single crystal was set under bright field exposure of the microscope using the 20X objective and a 5-10 µL drop of DDW was added to the crystal surface to

re-hydrate it. The bright field turned off and the crystal was kept on the stage of the Raman microscope in the dark for a period of 4 days at ambient temperature and pressure and allowed to dry. After this period of time, the excess DDW on the surface evaporates, bringing the crystal into focus again without the need for exposing the crystal to the bright field of the microscope to check the focus before acquisition of the dehydrated crystal Raman spectrum.

A Holoprobe Research 785 Raman microscope running the Kaiser Optical Systems' "Holograms" software package (both Kaiser Optical, Ann Arbor, MI) was used for single-crystal Raman experiments to examine the effect of dehydration on the Raman spectrum of single crystals. The crystals were examined under 10x objective. The Raman microscope was housed in a black felt-lined Plexiglass box to prevent the entrance of stray light. The Raman microscope had a spatial (microscope) resolution of approximately 1 μm, a 3 mW 785 nm incident laser with a spot size of approximately 15 μm diameter, and spectrometer spectral resolution of approximately 3 cm^{-1}. Laser excitation was provided by the 514 nm line of an Innova 300 Argon laser (Coherent, Santa Clara, CA). To allow the passage of laser light onto the stage, a hole was drilled into the left side of the box and a series of mirrors and lenses focused the Argon line toward the sample on the stage. The Raman spectrum of the same area of a single crystal was taken in the range from 2000-1000 cm-1, under increasing 514 nm laser power from 0.01W to 0.3 W. The X-Y data were saved as .spc files and opened again using the ONMIC v 5.2 software package, where the baseline could be smoothed. After smoothing, the data were saved as .csv files and opened in the OriginPro software package v7.5 for plotting.

3.7 Visible Spectroscopy of a Mass of bcbR Crystals Dried in the Dark

The bcbR crystals were removed from their detergent matrix by the same procedure used in the visible and Raman experiments above. A mass of crystals in DDW was concentrated to a rectangular sample size of approximately 3 x 7 mm and allowed to dry for a period of 4 days in the dark until the excess DDW had been removed by evaporation. The glass slide with its mass of crystals immobilized to the surface was transferred under red light to the sample chamber of the spectrometer.

A Beckman DU 650 UV-Vis spectrometer (Beckman Instruments, Inc, Arlington Heights, IL) was used for visible spectroscopy experiments studying the effect of dehydration of a mass of bcbR crystals dried in the dark. Unlike the visible microspectrometer, which acquires spectra under bright field illumination and CCD camera, this spectrometer has a scanning monochromator, which allows for the acquisition of a dark-adapted spectrum of the crystals without their exposure to broad band white light. The crystals were removed from their detergent matrix by the same procedure used for the visible absorption experiments described previously, and concentrated to a 3 x 7 mm rectangular area on a glass slide as described above. The wavelength range from 300-800 nm was scanned. The X-Y data was saved in ASCII format and opened again in the OriginPro software package v7.5 for plotting. Scanning within this wavelength range involved the changing of grating that resulted in spikes in the spectrum. These spikes were subtracted out using the OriginPro software package.

Results and Discussion

3.8 Light and Dark Adaptation of the Retinal within the Bicelle Crystals

The changes in the visible absorption spectrum for a sample of bcbR crystals within the detergent matrix upon their exposure to white light are shown in Figure 3.4a. For comparison, the visible absorption spectra for the hydrated native bR film are shown in Figure 3.4b. In Figure 3.4a the retinal absorption for a mass of bcbR crystals within their detergent matrix ranges between 558 nm (after being kept in the dark overnight) to 563 nm (following exposure to light for 45 minutes, after which the spectrum remained constant). In 3.4b the retinal absorption of the native hydrated film of bR ranges between 560 nm after overnight dark adaptation and 568 nm following light exposure for 30 minutes, after which the spectrum remained constant. This red shift in the absorption maximum for a mass of bcbR crystals upon light exposure indicates that the retinal molecules within the bicelle bR crystals are not “locked” into a particular conformation; they have the ability to isomerize.

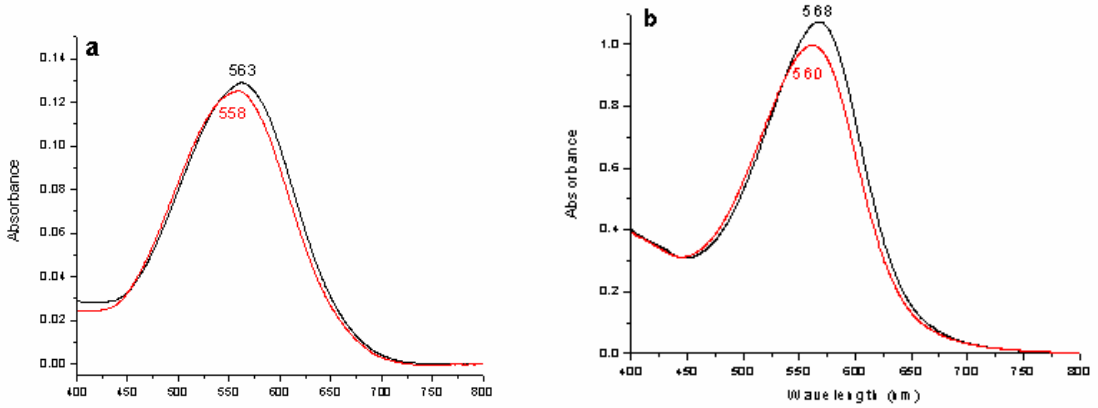

Figure 3.4: Effect of light adaptation on the visible absorption spectrum of several bicelle bR crystals suspended in the detergent matrix

3.9 Comparison of Single-Crystal Visible Absorption to Native

Figure 3.5 compares the average visible spectrum from multiple areas of single hydrated crystals to the average spectrum from multiple areas of a hydrated native film. The data have been normalized to Absorbance of 1 for ease of comparison. In the bcbR crystal spectrum, the absorption maximum is blue-shifted to 560 nm relative to the 568 nm absorption maximum for the hydrated native film. This blue-shifting of the light-adapted spectrum for crystals relative to that of light-adapted native film is similar to what was observed in Figure 3.4. In Figure 3.5 a small absorption at approximately 430 nm is observed in the spectrum for the crystals that is not observed in the native. In addition, the band width of half-height is 30% larger for the crystals than it is for the native. Since the spectrum for the crystals presented represents an average of multiple areas taken of several crystals, the argument of band broadening due to light scattering can be rejected.

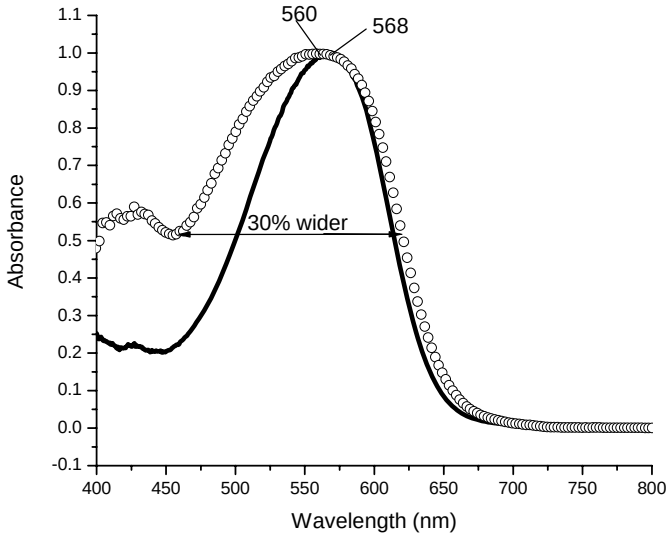

Figure 3.5: Comparison of band widths at half-height between the average light-adapted state of a hydrated native film of bR (solid line) and the average light-adapted state of a single bcbR crystal (circles)

In their work comparing the absorption spectra of single cbR crystals to native membrane, Schelkl *et al.*[65] also noted that single cbR crystals had an absorption band approximately 30% wider than that of a native suspension and a blue-shifting of the absorption spectrum to 560 nm. However, the small 430 nm band observed here for the bcbR crystals was not observed in the cbR crystals. They proposed that the band broadening of the cbR crystals was due to a difference in hydration among the retinal binding pockets in the cbR crystals,[65] a proposal that was confirmed by monitoring the band width of the cbR crystal before and then after exposure of the cbR crystal to a stream of dry nitrogen.

To see if the band broadening and the presence of the 430 nm band in the bcbR crystals is also due to a difference in hydration among the retinal binding pockets, the same experiment was performed for a single bcbR crystal and the results shown in Figure 3.6.

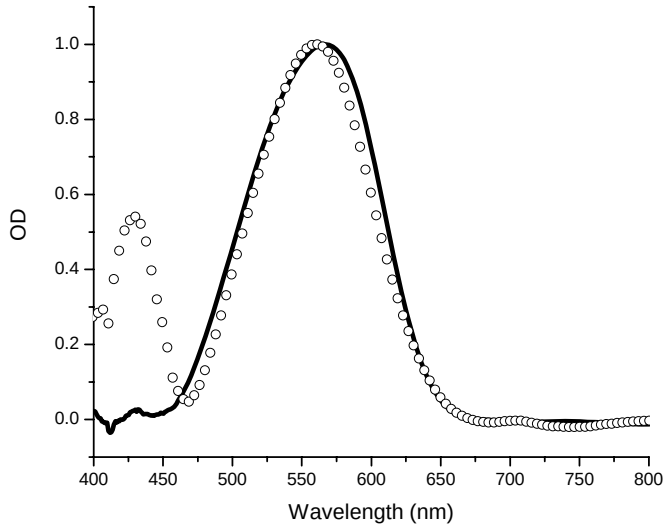

Figure 3.6: Spectrum of a single hydrated bcbR crystal before (solid line) and after (circles) drying with stream of nitrogen under broad band light.

A single bcbR crystal was kept under constant bright field exposure on the microscope stage while being exposed to a stream of dry nitrogen. Drying of the bcbR crystal results in a small blue shift in the retinal absorption spectrum, a slight decrease in band width, and most dramatically, an increase in the 430 nm band. The narrowing of the bcbR crystal's retinal absorption band upon dehydration indicates that the larger band width of hydrated bcbR crystals relative to that of hydrated native films is due to a difference in hydration environments of the retinal binding pocket of the bcbR crystals.

The existence of the 430 nm band in hydrated bcbR crystals and its intensity increase upon dehydration under bright field indicates that in the bcbR crystals the deprotonated Schiff base is formed. Before we can say that we are actually trapping the M intermediate of the photocycle by this dehydration, the experiment needs to be performed on crystals dried in the dark to make sure that the deprotonation is due to the trapping of the M intermediate of the photocycle and is not simply a product of thermal deprotonation of the parent.

3.10 Effect of bcbR Crystal Dehydration in Dark

Because the spectra acquired by the S.E.E. 1000 MSP visible microspectrometer are produced by CCD camera, the sample has to be exposed to the bright field of the microscope during sample acquisition. The experiments examining the visible spectrum of bcbR crystals dried in the dark have to be carried out on a spectrometer with a scanning monochromator, in this case a Beckman DU 650 UV-vis spectrometer. Because this spectrometer is not a micro-scale spectrometer, a single crystal cannot be examined. Instead, a large mass of crystals that were dried in the dark were examined. The absorption spectrum in the 300-800 nm range for this mass of bcbR crystals is shown in Figure 3.7.

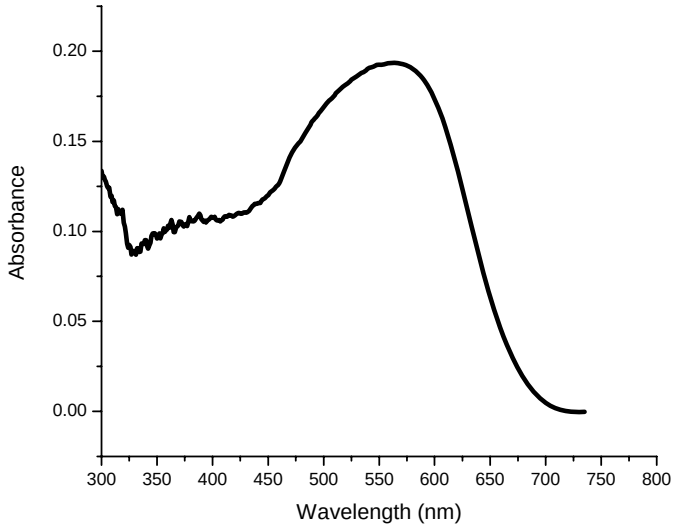

Figure 3.7: Spectrum of a mass of bcbR crystals after drying in the dark for a period of 3-4 days under ambient temperature and pressure.

Unlike bcbR crystals dried under bright field, bcbR crystals dried in the dark lack the strong absorption band at 430 nm. Exposure of this mass of crystals to a stream of dry nitrogen in the dark for a period of several hours produced no changes in the spectrum, indicating that the crystals could not be dried further. This finding provides support for the proposal that the deprotonation of the retinal Schiff base is due to the formation and trapping of the M intermediate of the photocycle, not just dehydration of the parent.

3.11 Effect of Dehydration of Single bcbR Crystal

In Figure 3.8, the Raman spectrum of a single bcbR crystal under 785 incident laser is taken as a second 514 nm excitation laser is focused on the sample as it dries under ambient temperature and pressure.

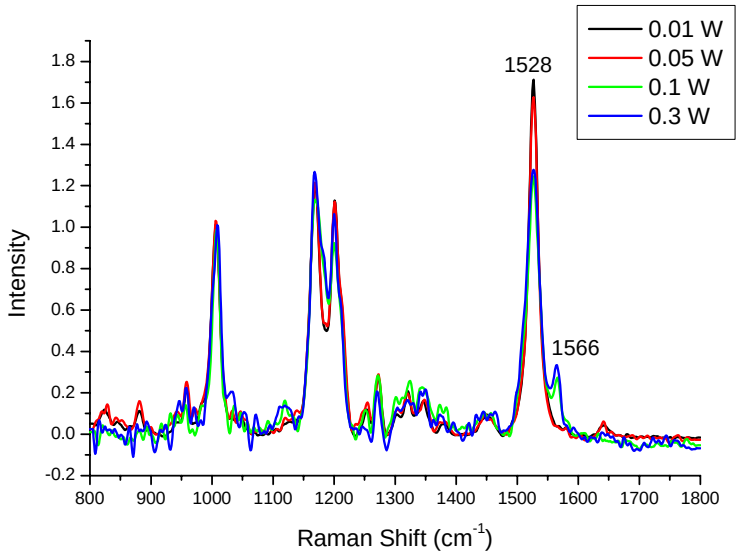

Figure 3.8: Changes in the Raman spectrum of a single air-exposed bcbR crystal during increase of the power of the 488 nm line of an Argon laser.

The power of the 514 nm laser is increased from 0.01 W to 0.3W. As the laser power increases, a new band appears at 1566 cm^{-1}. This band is well-characterized literature[1-10] as the C=C stretching of the deprotonated retinal Schiff base. To affirm that this the appearance of this band is not due to thermal deprotonation of the parent, a single bcbR crystal was allowed to dry in the dark for a period of four days under ambient temperature and pressure, after which time the Raman spectrum in Figure 3.9 was taken with 785 nm laser. The absence of the 1566 cm^{-1} band for the bcbR crystal dried in the dark provides further evidence that the appearance of the 1566 cm^{-1} band in the bcbR crystal exposed to 514 nm excitation is due to the creation and trapping of the M intermediate in the bcbR crystals. Exposure of the crystal to dry nitrogen stream for a period of one hour resulted in no further changes in the spectrum.

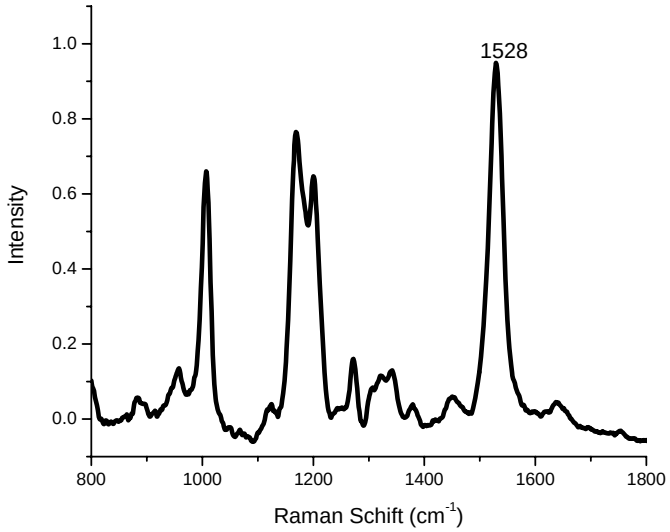

Figure 3.9: The Raman spectrum of a single air-exposed bcbR crystal left in the dark for a period of 3-4 days

In summary, the retinal contained within the novel packing structure of these bcbR crystals is photo-responsive, able to isomerize and not locked into a particular conformation. The average absorption spectrum of well-hydrated, light-adapted single bcbR crystals is broader than native films, a finding that is in agreement with the absorption spectrum of single cbR crystals.[65] In contrast to cbR crystals, there is a small absorption at 430 nm, which is close to the absorption of the M intermediate of the deprotonated retinal Schiff base. Upon dehydration under bright field, the absorption band of a single bcbR crystal narrows and blue-shifts, with a large increase in this 430 nm band. Visible experiments done on a mass of crystals dried in the dark do not show a band at 430 nm, providing evidence that that this Schiff base deprotonation is photochemical and not thermal. A band at 1566 cm^{-1} in the Raman spectrum of a single crystal appears and its intensity increases as the crystal is dried under increasing 514 nm

laser power. This band does not appear for a crystal when it is dried in the dark for a few days. Together with the visible absorption experiments, these experiments provide further evidence that the deprotonated retinal Schiff base is the M intermediate if the photocycle, trapped by dehydration during excitation. They also show that thermal deprotonation of the bcbR crystals does not take place.

References

(1) Lin, S. W.; Fodor, S. P. A.; Miercke, L. J. W.; Shand, R. F.; Betlach, M. C.; Stroud, R. M.; Mathies, R. A. *Photochemistry and Photobiology* **1991**, *53*, 341.

(2) Mathies, R.; Freedman, T. B.; Stryer, L. *Journal of molecular biology* **1977**, *109*, 367.

(3) Oseroff, A. R.; Callender, R. H. *Biochemistry* **1974**, *13*, 4243.

(4) Hildebrandt, P.; Stockburger, M. *Biochemistry* **1984**, *23*, 5539.

(5) Stockburger, M.; Klusmann, W.; Gattermann, H.; Massig, G.; Peters, R. *Biochemistry* **1979**, *18*, 4886.

(6) Braiman, M.; Mathies, R. *Biochemisrtry* **1980**, *19*, 5421.

(7) Henderson, R.; Sulkes, M.; Lewis, A.; Marcus, M. A. *Biochemistry* **1978**, *17*, 4712.

(8) Althaus, T.; Eisfeld, W.; Lohrmann, R.; Stockburger, M. *Israel Journal of Chemistry* **1995**, *35*, 227.

(9) Chronister, E. L.; El-Sayed, M. A. *Photochemistry and Photobiology* **1987**, *45*, 507.

(10) Aton, B.; Doukas, A. G.; Callender, R. H.; Becher, B.; Ebrey, T. G. *Biochemistry* **1977**, *16*, 2995.

(11) Hessling, B.; Souvignier, G.; Gerwert, K. *Biophysical journal* **1993**, *65*, 1929.

(12) Bitting, H. C., Jr.; Jang, D. J.; El-Sayed, M. A. *Photochemistry and Photobiology* **1990**, *51*, 593.

(13) Lin, C. T.; Chyan, Y. G.; Kresheck, G. C.; Bitting, H. C., Jr.; el-Sayed, M. A. *Photochemistry and photobiology* **1989**, *49*, 641.

(14) Hartsel, S. C.; Cassim, J. Y. *Biochemistry* **1988**, *27*, 3720.

(15) Dunach, M.; Seigneuret, M.; Rigaud, J. L.; Padros, E. *Biochemistry* **1987**, *26*, 1179.

(16) Maurer, R.; Vogel, J.; Schneider, S. *Photochemistry and Photobiology* **1987**, *46*, 255.

(17) Sheves, M.; Albeck, A.; Friedman, N.; Ottolenghi, M. *Proceedings of the National Academy of Sciences of the United States of America* **1986**, *83*, 3262.

(18) Chang, C. H.; Chen, J. G.; Govindjee, R.; Ebrey, T. *Proceedings of the National Academy of Sciences of the United States of America* **1985**, *82*, 396.

(19) Takeuchi, Y.; Ohno, K.; Yoshida, M.; Nagano, K. *Photochemistry and Photobiology* **1981**, *33*, 587.

(20) Lazarev, Y. A.; Terpugov, E. L. *Biochimica et biophysica acta* **1980**, *590*, 324.

(21) Becher, B.; Tokunaga, F.; Ebrey, T. G. *Biochemistry* **1978**, *17*, 2293.

(22) Kung, M. C.; DeVault, D.; Hess, B.; Oesterhelt, D. *Biophysical Journal* **1975**, *15*, 907.

(23) Oesterhelt, D.; Stoeckenius, W. *Nature (London), New Biology* **1971**, *233*, 149.

(24) Lozier, R. H.; Bogomolni, R. A.; Stoeckenius, W. *Biophysical Journal* **1975**, *15*, 955.

(25) Oesterhelt, D. *Angewandte Chemie* **1976**, *88*, 16.

(26) Krebs, M. P.; Khorana, H. G. *Journal of Bacteriology* **1993**, *175*, 1555.

(27) Heyn, M. P.; Cherry, R. J.; Mueller, U. *Journal of Molecular Biology* **1977**, *117*, 607.

(28) Lin, S. W.; Mathies, R. A. *Biophysical Journal* **1989**, *56*, 653.

(29) Tang, L.; Ebrey, T. G.; Subramaniam, S. *Israel Journal of Chemistry* **1995**, *35*, 193.

(30) Tanford, C. *Annual review of biochemistry* **1983**, *52*, 379.

(31) Harbison, G. S.; Smith, S. O.; Pardoen, J. A.; Winkel, C.; Lugtenburg, J.; Herzfeld, J.; Mathies, R.; Griffin, R. *Proceedings of the National Academy of Sciences* **1984**, *81*, 1706.

(32) Sperling, W.; Carl, P.; Rafferty, C. N.; Dencher, N. A. *Biophysics of Structure and Mechanism* **1977**, *3*, 79.

(33) Aton, B.; Doukas, A. G.; Callender, R. H.; Becher, B.; Ebrey, T. G. *Biochimica et Biophysica Acta* **1979**, *576*, 424.

(34) Yudd, A. P. Studies of Artificial Visual Pigments. Ph.D.Thesis, Columbia University, 1975.

(35) Korenstein, R.; Hess, B. *FEBS Letters* **1977**, *82*, 7.

(36) Oesterhelt, D.; Meentzen, M.; Schuhmann, L. *European Journal of Biochemistry* **1973**, *40*, 453.

(37) Kropf, A.; Whittenberger, B. P.; Goff, S. P.; Waggoner, A. S. *Experimental Eye Research* **1973**, *17*, 591.

(38) Goldschmidt, C. R.; Ottolenghi, M.; Korenstein, R. *Biophysical journal* **1976**, *16*, 839.

(39) Fodor, S. P.; Ames, J. B.; Gebhard, R.; van den Berg, E. M.; Stoeckenius, W.; Lugtenburg, J.; Mathies, R. A. *Biochemistry* **1988**, *27*, 7097.

(40) Oesterhelt, D.; Hess, B. *European Journal of Biochemistry* **1973**, *37*, 316.

(41) Stoeckenius, W.; Lozier, R. H. *Journal of Supramolecular Structure* **1974**, *2*, 769.

(42) Jan, L. Y. *Vision Research* **1975**, *15*, 1081.

(43) Henderson, R. *Annual Review of Biophysics and Bioengineering* **1977**, *6*, 87.

(44) Stoeckenius, W.; Lozier, R. H.; Bogomolni, R. A. *Biochimica et Biophysica Acta* **1979**, *505*, 215.

(45) Michel, H.; Oesterhelt, D. *FEBS Letters* **1976**, *65*, 175.

(46) Bakker, E. P.; Rottenberg, H.; Caplan, S. R. *Biochimica et biophysica acta* **1976**, *440*, 557.

(47) Belyakova, T. N.; Kadziauskas, J.; Skulachev, V. P.; Smirnova, I. A.; Chekulaeva, L. N.; Jasaitis, A. *Doklady Akademii Nauk SSSR* **1975**, *223*, 483.

(48) Lewis, A.; Spoonhower, J.; Bogomolni, R. A.; Lozier, R. H.; Stoeckenius, W. *Proc. Natl. Acad. Sci. U.S.* **1974**, *71*, 4462.

(49) Braiman, M.; Mathies, R. *Proceedings of the National Academy of Sciences of the United States of America* **1982**, *79*, 403.

(50) Mathies, R. A.; Brito Cruz, C. H.; Pollard, W. T.; Shank, C. V. *Science* **1988**, *240*, 777.

(51) Pollard, W. T.; Cruz, C. H.; Shank, C. V.; Mathies, R. A. *Journal of Chemical Physics* **1989**, *90*, 199.

(52) Ames, J. B.; Mathies, R. A. *Biochemistry* **1990**, *29*, 7181.

(53) Braiman, M. S.; Mogi, T.; Marti, T.; Stern, L. J.; Khorana, H. G.; Rothschild, K. J. *Biochemistry* **1988**, *27*, 8516.

(54) Gerwert, K.; Hess, B.; Soppa, J.; Oesterhelt, D. *Proceedings of the National Academy of Sciences of the United States of America* **1989**, *86*, 4943.

(55) Varo, G.; Lanyi, J. K. *Biochemistry* **1991**, *30*, 5016.

(56) Lozier, R. H.; Niederberger, W.; Bogomolni, R. A.; Hwang, S.-B.; Stoeckenius, W. *Biochimica et Biophysica Acta* **1976**, *440*, 545.

(57) Birge, R. R. *Annual Review of Physical Chemistry* **1990**, *41*, 683.

(58) Ebrey, T. G. *Thermodyn. Membr. Recept. Channels* **1993**, 353.

(59) Lanyi, J. *Biochemica et Biophysica Acta* **1993**, *1183*, 241.

(60) Wang, J.; El-Sayed, M. A. *Journal of Physical Chemistry A* **2000**, *104*, 4333.

(61) Racker, E. *Science* **1987**, *235*, 959.

(62) Lanyi, J. K. *Biochemica et Biophysica Acta* **2000**, *1460*, 1.

(63) Bowie, J.; Farham, S. *Journal of Molecular Biology* **2002**, *316*, 1.

(64) Landau, E. M.; Rosenbusch, J. P. *Proceedings of the National Academy of Sciences of the United States of America* **1996**, *93*, 14532.

(65) Schenkl, S.; Portuondo, E.; Zgrablic, C.; Chergui, M.; Suske, W.; Dolder, M.; Landau, E. M.; Haacke, S. *Journal of Molecular Biology* **2003**, *329*, 711.

CHAPTER 4

EVIDENCE FOR THE CREATION OF THE M_{412} INTERMEDIATE BY RAMAN SPECTROSCOPY*

Abstract

In Chapter 3, a combination of photo-excitation and dehydration of bcbR crystals to 'trap' the M intermediate was performed. In this chapter, resonance Raman spectroscopy of single *hydrated* bcbR crystals is performed to search for evidence of a photocycle, indicated by creation of the M intermediate. An introduction of Resonance Raman spectroscopy is first given and finally applied to bacteriorhodopsin.

4.1. Raman Spectroscopy

A beam of radiation passed through a medium results in the scattering of a fraction of the incident beam in all directions by the species present. C.V. Raman observed in 1928 that a small portion the radiation scattered by certain molecules differs in wavelength from that of the incident beam. The shift in wavelength depend upon the chemical structure of the molecules responsible for the scattering.[1] The difference in energy between the incident and the scattered radiation corresponds to the energy of the vibration causing the scattering. While the requirement to observe an infrared absorption spectrum is that the vibrational mode of the molecule has to change its dipole moment.

---

* Manuscript published: Sanii, Laurie S., Schill, Alex W., Moran, Cristin E., El-Sayed, Mostafa A. "The Protonation-Deprotonation Kinetics of the Protonated Schiff Base in Bicelle Bacteriorhodopsin Crystals" *Biophys J.* (2005) 89, 444-451.

A Raman scattering spectrum is observed for vibrations in which the polarizability of the molecule changes during the vibration.[1] This gives rise to the selection rules.

This difference in the selection rules between IR and Raman spectroscopy suggest that, for a given molecule, its Raman activity may markedly differ from its infrared activity depending on the symmetry of the molecule[1]

For molecules there are different types of vibrations: stretching, bending, and scissoring. Stretching involves movement along the bond axis in which the inter-atomic distance changes during the vibration. On the other hand, the other types of vibrations involve a change in bond angle. In all these atomic motions the whole molecule is not allowed to translate or to rotate.[2] Stretching vibrations can also be symmetric or asymmetric. Only vibrations resulting in a change in the dipole moment of the molecule can undergo infrared absorption and are therefore IR active.[1,2] In general, functional groups that have a strong dipole give rise to strong absorptions on the IR.[2] On the other hand, Raman active vibrations result in a change of the polarizability of the molecule as a whole.

4.2. Resonance Raman spectroscopy

In normal Raman spectroscopy (described above), the incident laser of the instrument is chosen so that its energy is far below the energy of the lowest excited state of the chromphore. Figure 4.1 is a description of the processes involved in of normal Raman scattering spectroscopy adapted from Ferraro *et al*.[3] In normal Raman spectroscopy, the incident laser wavelength υ_o is chosen so it lies below the first excited energy state of the

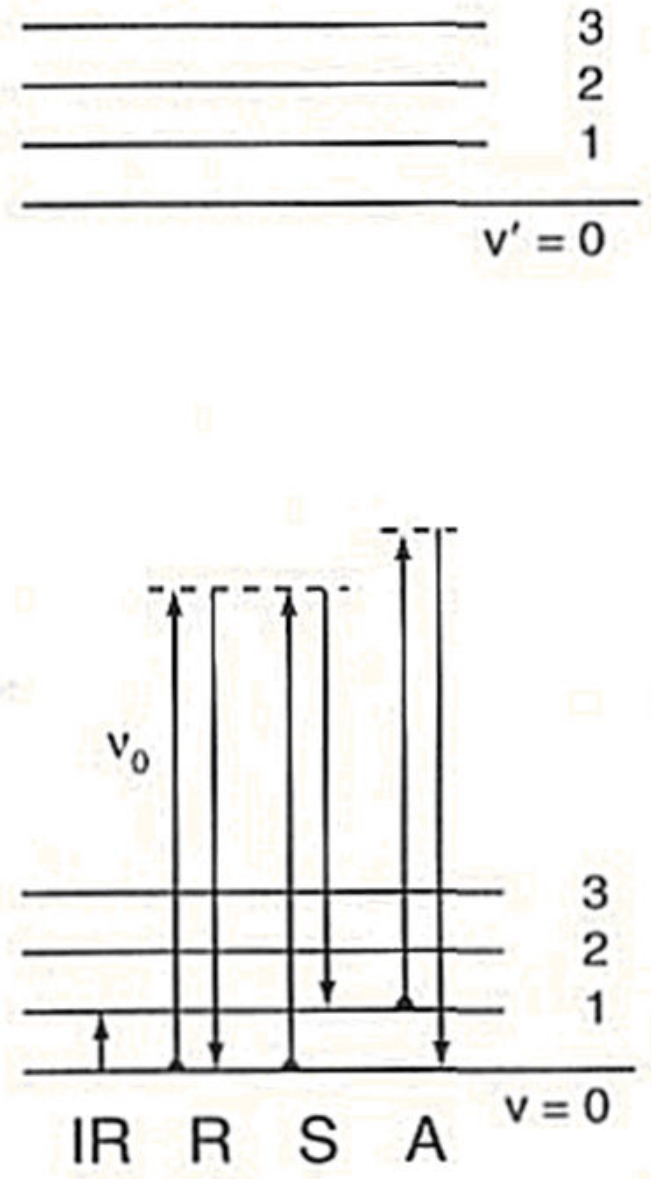

Figure 4.1: Description of the processes involved in of normal Raman scattering spectroscopy.

chromophore. This energy of the laser provides enough energy to the molecule to induce a change in the vibrational energy without providing enough energy to promote an electron to its excited state. In this figure, the processes involved with infrared absorption (IR), the Rayleigh scattering (R), normal Stokes (S) and anti-Stokes (A) Raman scattering are illustrated.

On the other hand, in resonance Raman spectroscopy the energy of the incident laser corresponds to the energy of an electronic transition of a certain chromophore in the molecule. Figure 4.2 shows a sketch of the resonance Rayleigh and Raman scattering processes, adapted from Ferraro *et al*.[3] In resonance Rayleigh and Raman spectroscopy, the incident laser wavelength is chosen so it *corresponds* to the energy of an electronic transition of the chromophore. This energy of the laser provides enough energy to the molecule to provide enough energy to promote an excited state. Raman bands originating from this chromophore are selectively enhanced[3] by a factor of 10^3-10^5. In this figure, the processes involved with Rayleigh scattering (R), Stokes (S) and anti-Stokes (A) Raman scattering are illustrated.

Raman bands originating from the vibration of this chromophore are selectively enhanced by a factor[3] of 10^3-10^5. This important enhancement is vitally important in studying biological systems as one can study changes in the chromophore without the interference of the large number of amino acids present in the protein.

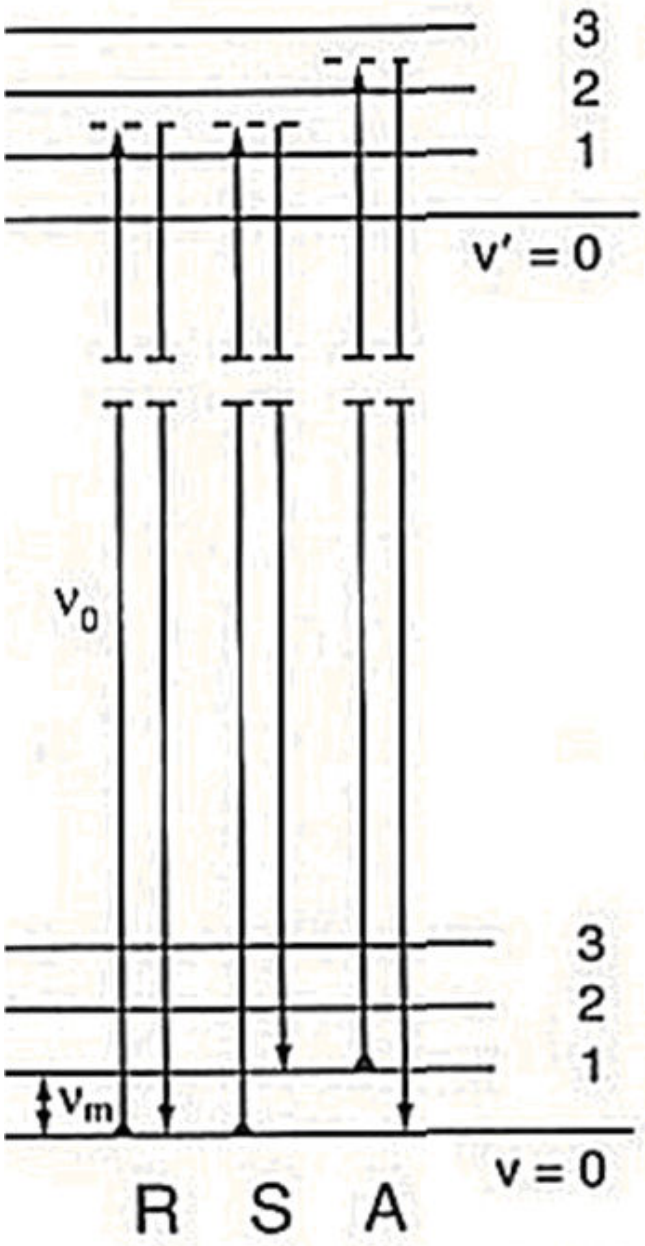

Figure 4.2: Sketch of the resonance Rayleigh and Raman scattering processes.

4.3. Raman Spectroscopy of Bacteriorhodopsin

In these experiments we are dealing with bacteriorhodopsin, a retinal protein that has a visible absorption spectrum with at least two resolved bands in the region between 250-700 nm. The 280 nm absorption is due to the aromatic residues of the protein backbone. The 570 nm absorption is due to the protonated Schiff base of the all-*trans* isomer of the retinal chromophore within its binding pocket of the protein.[4] If kept in the dark for a period of several hours, the retinal population converts[5-8] to a mixture of the 13-*cis* and all-*trans* isomers, and the absorption here blue-shifts about 10 nm from 560 to 568 nm. In Raman spectroscopy, excitation of the protein with laser light of wavelengths larger than the chromophore's 570 nm absorption band should only result in Raman scattering of the species present in solution, without inducing the photocycle. This means that if we are using an 830 nm laser to get the Raman spectrum of the dark-adapted species, we will observe a mixture of bands arising from the 13-*cis* and all-*trans* isomers in principle. If we use the same 830 nm laser to examine a protein that has just been light-adapted, we will only see bands arising from the all-*trans* retinal species (together with the weak protein bands). However, using an incident laser having a wavelength that lies *within* the absorption band of the retinals (as in the case of using the 514 nm laser) we should observe the resonance enhanced retinal spectrum of the parent bR, as well as that in any photoproduct intermediate produced photochemically.

As mentioned in Section 4.2 above, in resonance Raman spectroscopy, the bands arising from the chromophore are selectively enhanced by a factor between 10^3-10^5. In native bR, we know that in its light-adapted state, the protein has approximately a 98%

all-*trans* retinal configuration, with a protonated Schiff base. From the visible spectroscopy in Chapter 3, we know that within the bicelle crystal the retinal is photo-responsive, as evidenced by a shift in the retinal absorption maximum. It may be the case that in the light-adapted state of the crystals, there are two populations of retinal with respect to the Schiff base region – one in which the retinal is deprotonated and the other in which the retinal is protonated. If this is the case and we see the development of new bands switching from the 830 to 514 nm excitation laser which have been characterized in the literature as belonging to the M intermediate of the photocycle (a 13-*cis* isomer with a deprotonated Schiff base) do we know that these new bands appearing under 514 nm laser are actually due to the *creation* of the M intermediate in the crystals, or are just the result of *resonance enhancement* of a 13-*cis*, deprotonated species that already exists in the light-adapted crystal without a photocycle actually taking place? These questions will be addressed in the Experimental Design and Results/Discussion sections.

One of the great advantages Raman spectroscopy has over infrared spectroscopy in the study of hydrated biological systems in general is that in Raman spectroscopy, water is transparent due to its negligible Raman scattering cross-section. Because the molecule is already polarized due to this dipole, its polarizability change is small, giving rise to no Raman bands, in particular, when the wavelength of the laser is very far from its vacuum UV absorption. In contrast, water gives rise to strong bands in the IR spectrum that often overlaps and thus obscures the 2000-1300 cm^{-1} region where many protein vibrations occur.

The Raman spectrum of the native solution-phase bR has been studied and characterized in the literature.[9-15] Althus *et al* .[16] assigned the vibrational bands of the all-

trans, light adapted state of native bR ("bR_{568}"), as shown in Figure 4.3. The most prominent of these bands is centered at 1528 cm^{-1} and is due to the C=C stretching of the parent molecule. The $C=NH^{+}$ of the protonated Schiff base gives rise to a band centered at 1640 cm^{-1}. The single-bond C-C stretches are located in the region between 1167-1215 cm^{-1}. The 828-1008 cm^{-1} region was assigned to the hydrogen out-of-plane (HOOP) wags of the C-H groups, the 1157-1215 cm^{-1} region was assigned to the fingerprint C-C stretches, and the 1255-1378 cm^{-1} region was assigned to the CC-H in-plane rocking motions.[17] The frequency of the stretching vibration is sensitive to the protonation state of the Schiff base. The $C=N-H^{+}$ stretching frequency is observed in the region[10,18-20] between 1637 and 1640 cm^{-1}. From both time-resolved Raman and deuterium exchange experiments with the only ionizable proton of the chromophore, the C=N stretching frequency moves to about 1620 cm^{-1} upon loss of the proton.[10,11,16,20-24]

In the Raman spectrum presented in Figure 4.3 for bR_{568}, three key regions should be addressed: the C=C stretching region, the fingerprint region, and the Schiff base region. The ethylenic C=C stretch region from 1510-1570 cm^{-1} contains a single strong band observed at 1528 cm^{-1}. In the literature this band has been characterized as the C=C stretching of the conjugated retinal chain of $bR_{568,}$ and has been reported in the literature[16,20-22,25-29] to appear between 1525-1530 cm^{-1}. This stretching frequency is due to the C=C vibration of retinal in which the electrons are delocalized over the C=C-C bond of the protonated Schiff base.

The so called "fingerprint region" shown here in the region between 1120–1215 cm^{-1} consists of fairly strong C-C vibrations of the retinal chain and are the most sensitive to geometric changes of the retinal chain.[16] From Figure 4.3, bR_{568} has two main bands

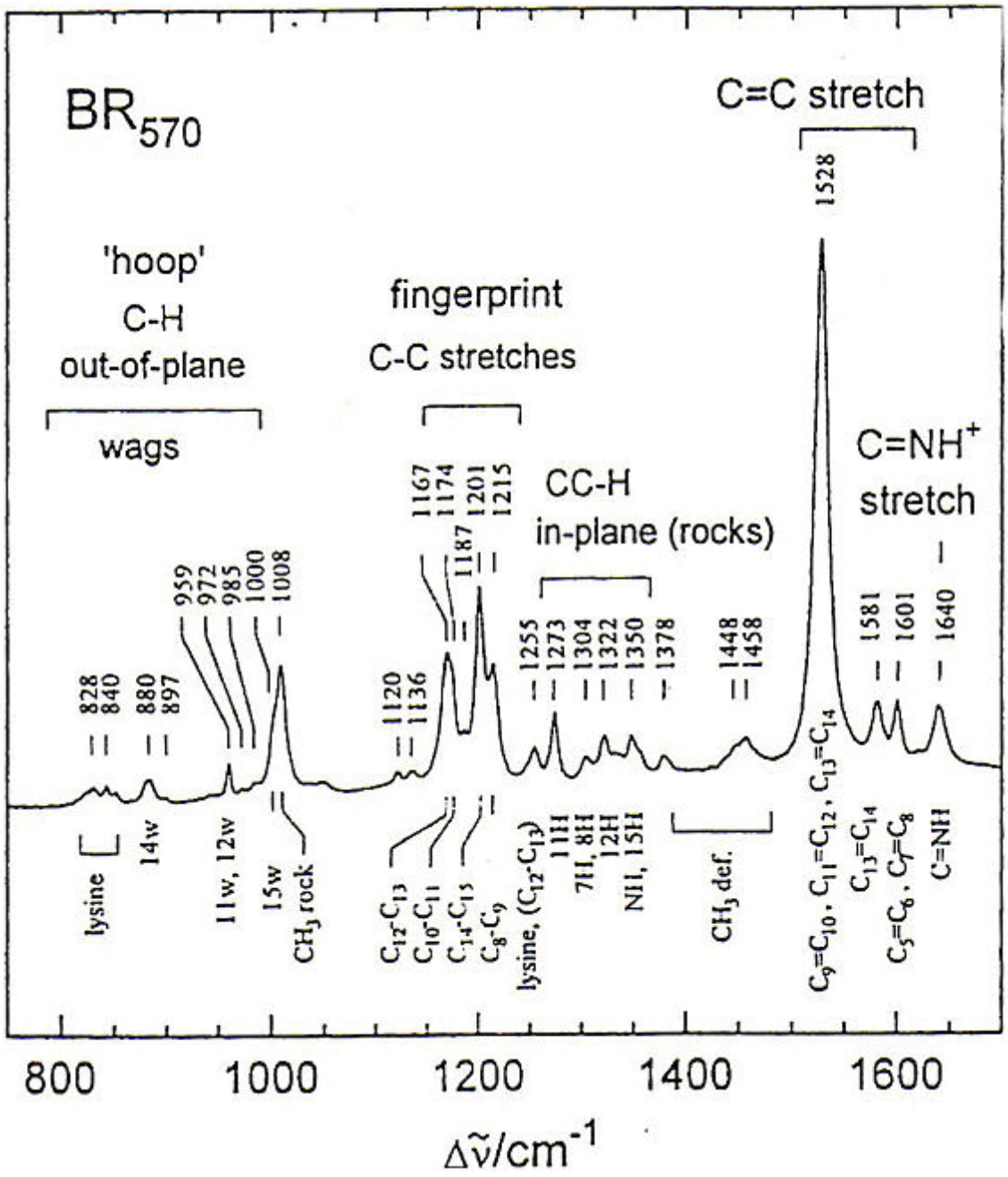

Figure 4.3: Raman spectrum of bR_{568}.

here, observed at 1167 cm^{-1} and 1201 cm^{-1}, and a weaker one that appears as a shoulder at 1215 cm^{-1}.

The Schiff base region is shown here as a single band at 1640 cm^{-1}. This Schiff base of retinal links this chromophore to the rest of the protein as a whole via a covalent bond with Lys_{216} of the protein backbone. The vibration observed here at 1640 cm^{-1} is due to the C=N stretching of the protonated Schiff base and has been observed in the literature from 1635-1655 cm^{-1}.[11,20,22,26,30-32] Time-resolved Raman spectra of the native membrane, and the same membrane with amino acid point-substitutions, have revealed several intermediates with retinal having different structures during the photocycle.[12,15,32-46]

The spectrum of the M_{412} intermediate[31] of native bR_{568} is shown in Figure 4.4. In the ethylenic C=C stretching region, the appearance of a new band at approximately 1566 cm^{-1} corresponds to the C=C stretching of the retinal in the M_{412} intermediate, in which the Schiff base is deprotonated. This deprotonation results in an electron localization in the C=C bonds of the conjugated chain and shifting the band[16,20-22,25-29] by over 30 $cm^{-1.}$ In the Schiff base region, deprotonation of the Schiff base in M_{412} results in a shift in the C=N stretching frequency[10,11,16,20-24] from 1640 to 1620 cm^{-1}.

Figure 4.5 shows the changes in the fingerprint region between the spectrum of the light-adapted, all-trans bR_{568} and of this M_{412} spectrum in more detail, as detailed by Lin *et al.*[31]. In the fingerprint region, the appearance of a new band, shown here at 1191 cm^{-1} between the two bands for the C-C stretching of the ground state has been characterized by time-resolved Raman spectroscopy as belonging to the 13-*cis* concreation of retinal.[16,19,22,27,37,45,46] The chromophore is in the 13-*cis* concreation during

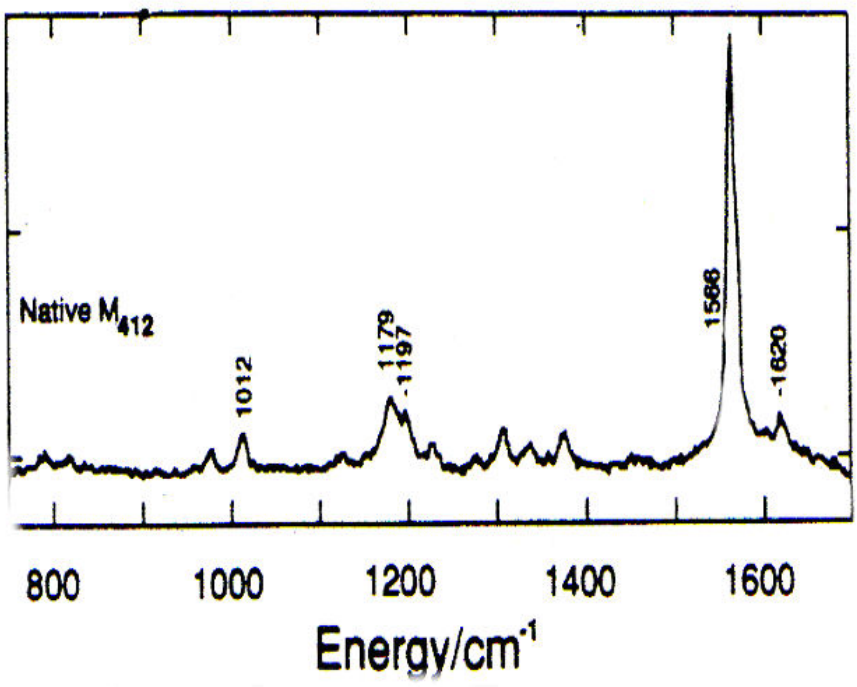

Figure 4.4: Raman spectrum of the M_{412} intermediate in the native parent bR_{568}.

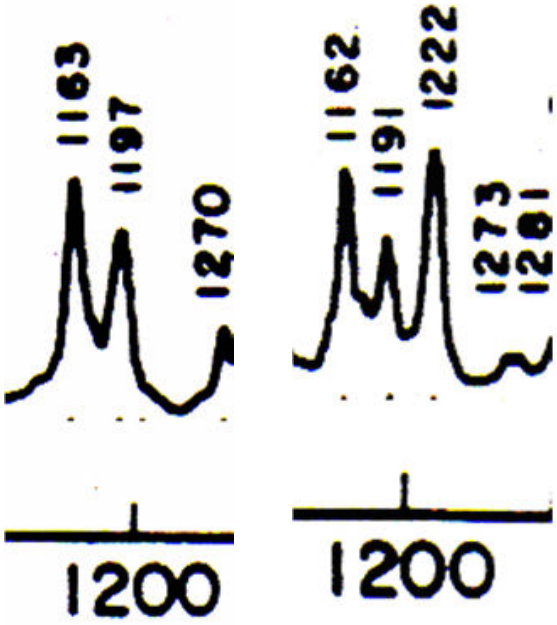

Figure 4.5: Comparison of the fingerprint regions between (left) the light-adapted, all-*trans* bR_{568} and (right) the M_{412} intermediates.

the majority of the photocycle, (K, L, M, N, and O). It should be emphasized that although retinal is in the 13-*cis* configuration for several intermediates of the photocycle, the M intermediate is unique in that it is the only intermediate in which the Schiff base is deprotonated. This, in addition to the appearance of the 1191 cm^{-1} band in the fingerprint region (13-*cis* configuration) the C=C stretching frequency will shift from 1528 to 1566 cm^{-1} (protonated to deprotonated Schiff base).

4.4. Raman Micro-Spectroscopy of bcbR Crystals

The goal of this study is to obtain both the Raman spectra of the bcbR crystal at 830 nm and 514 nm incident wavelengths and compare it to the data obtained for native membrane solutions of bR in water under the same experimental conditions. A Raman laser at 830 nm is used to collect the spectrum of the light-adapted bR. This incident wavelength is far-removed from the 570 nm absorption maximum of the chromphore, and thus should result in scattering from only the unphotolyzed bR species. A Raman incident laser at 514 nm is used to both excite the sample and obtain the spectrum of the mixture of intermediates that may develop. If the crystal undergoes a photocycle, new bands should appear near 1566 cm^{-1} (the C=C stretching of M), and another one between 1167 and 1201 cm^{-1} (13-*cis* retinal). In addition, any deprotonation of the Schiff base during the creation of the M intermediate should result in a shift of the C=N stretch from 1640 to 1620 cm^{-1}.

In order to ensure that any new bands appearing under 514 nm laser excitation are not just a result of resonance enhancement, the ratio of the intensities of most bands of bR are compared to the those characterizing the M state under increasing power of the 514 nm laser. The most prominent bands are 1525 cm^{-1} (for the C=C stretching vibration when the Schiff base is protonated) and the 1566 cm^{-1} band (for the same vibration when the Schiff base is deprotonated). One would expect that changing the incident Raman laser wavelength from 830 to 514 nm would result in an increase in all bands due to resonance enhancement. However, if the 514 nm laser also photolyzes bR which forms the M intermediate as well, then we should see a change in the ratio of these two bands upon an increase in the power of the 514 nm laser. If the 514 nm incident laser is *only* causing resonance enhancement of all bands and is *not* resulting in the production of M, then we would expect the ratio of the two bands to remain constant with increasing 514 nm laser power. If the 514 nm incident laser is also resulting in the production of the M intermediate in the crystals, then we would expect that increasing the power of the 514 nm laser would increase the relative amount of M intermediate, and this would be reflected as an increase in the ratio of the 1566 cm^{-1} to 1525 cm^{-1} intensities.

Experimental Methods

4.5. Growth of bcbR Crystals and Washing from their Detergent Matrix

The bR samples were obtained from a cell line of *Halobacterium salinarium* and were purified by established procedures.[47] Diamond-shaped bR bicelle crystals were made by the method of Bowie *et al*.[48] Using this method, the concentration of bR was adjusted to

approximately 10mg/mL by monitoring the absorbance of the light-adapted (20 minutes light exposure using a 40 W bulb) bR sample at 568 nm until the absorbance spectrum was constant.

The two detergents 1,2-Dimyristoyl-*sn*-glycero-3-phosphocholine ("DMPC", Avanti Polar Lipids) and 3-[(3-Cholamidopropyl)dimethylammonio]-2-hydroxypropanesulfonic acid ("CHAPSO", ICN Biomedicals) were combined in a 2.8:1 molar ratio, and made into a 40% (by weight) bicellular solution in water. The 10 mg/mL bR solution and the bicellular solution were each kept on ice in separate vials. These two vials were then mixed in a 4:1 protein solution:bicellular solution volume ratio by repeated pipetting on ice to yield approximately 8.0 mg/mL bR/8% bicelles mixture. A precipitant well solution was made by mixing 4.0 M NaH_2PO_4, H_2O, and 6.0 M 1,6-hexanediol in a 28.6:1:1.4 volume ratio. A 6 μL aliquot of the protein/bicelle solution, 2.5 μL of the well solution, and 1 μL of 2.5% β-octylglucoside solution were mixed by gentle pipetting on a 22 mm diameter glass cover slip. The cover slips were inverted over 1 mL of the precipitant solution in a crystallization well, sealed with vacuum grease, and placed in a 37 °C incubator. The samples were monitored periodically for the next two weeks as the relatively fluid mixture suspension slowly gelled during equilibration between the suspended solution and the saturated solution underneath. The slides were then examined by light microscopy for evidence of crystal growth. Crystals were collected by repeated washing of the crystal-detergent matrix with deionized distilled water into microcentrifuge tubes. The higher-density crystals settled to the bottom of the solution within a matter of minutes, while the white detergent flakes remained suspended in the supernatant, which was easily removed. Washing the crystals in this manner

removed the bulk detergent while leaving the crystals intact. After washing, a concentrated drop of the crystal suspension was placed on a glass cover slip covered with aluminum foil and the sample was allowed to dry at room temperature under ambient light until the bulk water above the drop had evaporated, immobilizing the crystal on the surface. After the crystals were dried to the glass slide, a drop of water was added to the crystal before the visible or the Raman spectrum was taken.

4.6. Single-Crystal Raman Spectroscopy

Raman spectra of single crystals were acquired using a Renishaw in Via Raman spectrometer running the WiRE 2.0 software package (Renishaw, Gloucestershire, UK). The sampling area was approximately 1 μm^2. In order to ensure that the hydration level of all samples remained uniform, all Raman spectra were taken by submerging the objective underwater to obtain the spectrum of the native film or the single crystal. The intense Raman band at 520 cm^{-1} of a silicon wafer was used for automatic wavelength calibration by the software. All data presented were imported as x-y data first to OMNIC E.S.P. 5.2 (Thermo-Electron, Waltham MA) for baseline correction, and then transferred to OriginPro 7.5 software package (OriginLab, Northampton, MA)

Results and Discussion

The first goal of these experiments was to compare the Raman spectra resulting from irradiation of a native hydrated bR_{568} film under the 830 nm and the 514 nm laser.

If these spectra were different, then the second goal of these experiments was to examine whether the differences in the two spectra were due to production of the M intermediate of the photocycle, or just due to resonance enhancement of the protonated (parent) bR and deprotonated bR present in the unphotolyzed bicelle crystals.

It is already known that a hydrated native bR film undergoes a photocycle. The first experiment was done to compare the spectrum we record of the all-*trans,* light-adapted bR_{568} film with literature using the 830 nm incident laser. Furthermore, we show that the use of the 514 nm incident Raman laser in a separate experiment results in the creation of photointermediates, detected by the observation of the M intermediate Raman spectrum. The creation of M was verified by a power dependence experiment of the 514 nm incident laser in which the ratio of the intensities of the M C=C band to that of the unphotolyzed state (bR_{568}) is examined. No change in the ratio would indicate that use of the 514 nm laser only increases the band intensities due to resonance enhancement, while an increase in the M/bR ratio would indicate that the 514 nm laser also increases the M intermediate population.

4.7. Single-Crystal Raman Spectroscopy of Hydrated Native bR Film at 514 nm and 830 nm

Figure 4.6 presents the Raman spectra resulting from irradiation of a hydrated native film of bR_{568} at two different incident laser wavelengths, 830 nm (black) and 514 nm (red). The 830 nm laser is far-removed from the absorption maximum of the sample, so irradiation of the sample following its exposure to white light with this laser should not induce the photocycle, but only result in the ground state spectrum for the light-adapted,

all-*trans* retinal. In contrast, the 514 nm laser lies within the absorption of the retinal, so in addition to resonance enhancement of bands absorbing at this wavelength, one would expect that this laser has the potential to both inducing the photocycle and simultaneously give this Raman spectra of the resulting intermediates.

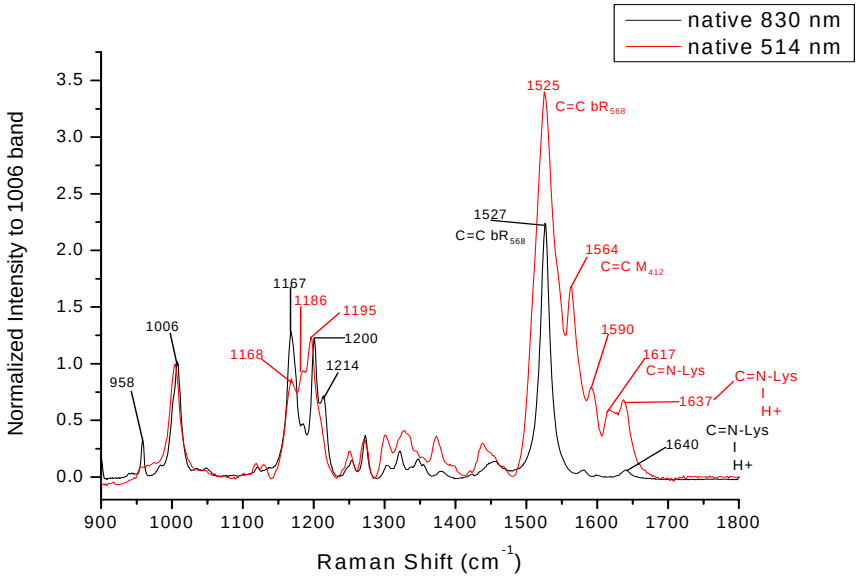

Figure 4.6: The ground state (black) and excited state (red) Raman spectrum on a hydrated native bR_{568} film.

For the hydrated native bR film irradiated at 830 nm (black spectrum) the presence of characteristic ground-state bands are observed in Figure 4.6. The band at 1527 cm^{-1} band is assigned in the literature as belonging to the C=C ethylenic stretching of the conjugated chain of the all-*trans*, retinal of light-adapted[11,16,26,49,50] bR_{568}. The small band at 1640 cm^{-1} has been characterized as the C=N-H^+ stretching vibration of the protonated Schiff base of the chromophore.[10,11,16,20-24] The large valley between the C-C

single bond stretches at 1167 and 1195 cm^{-1} indicates that the population of the 13-*cis* isomer is very low.

For the native bR film irradiated at 514 nm (red spectrum) the presence of new bands may indicate structural changes in the retinal. Most notably, a new band at 1564 cm^{-1} is observed. The C=C stretching arising from the deprotonated Schiff base of the M_{412} intermediate is often observed in the literature[16,20-22,25-29] at 1567 cm^{-1}. This new 1564 cm^{-1} band is in close agreement with this shift. In addition, the C=C stretching of parent bR, observed here at 1525 cm^{-1}, is still observed, and increases in intensity. This increase can be explained by resonance enhancement. Taken together, this data may indicate that under 514 nm laser irradiation, we are observing a mixture of photolysis intermediates.

In the fingerprint region, the valley between the two bands at 1168 cm^{-1} and 1195 cm^{-1} becomes shallower when the incident laser wavelength is changed from 830 nm to 514 nm. Time-resolved Raman spectroscopy has demonstrated that this region is sensitive to the isomeric configuration of the chromophore.[46 12,42,51] The broadening of the bands in this fingerprint region resulting from 514 nm Raman laser irradiation may indicate a change in the isomeric configuration of the retinal to a higher population of 13-*cis* retinal. Retinal changes its concreation from all-*trans* to 13-*cis* approximately four picoseconds after excitation and this 13-*cis* configuration remains during the K, L, M stages of the cycle.[52] The increase of the 1186 cm^{-1} band in this region under illumination by 514 nm light therefore lends more support for the creation of the 13-*cis*-containing photocycle intermediates of retinal. In the Schiff base region, a new band appears at 1617 cm^{-1} under 514 nm incident Raman laser. This is in close agreement to

the 1620 cm^{-1} shift corresponding to the deprotonated C=N stretch. [10,11,16,20-24] Another band at 1637 cm^{-1} may indicate the presence of some remaining protonated Schiff base, $C=N-H^{+}$. The fingerprint region shows the increase in the 1186 cm^{-1} 13-*cis* band between the Raman incident 830nm laser (black) and the 514 nm laser (red).

4.8. Single-Crystal Raman Spectroscopy of Single Hydrated bcbR Crystal at 514 nm and 830 nm

Figure 4.7 presents Raman spectra resulting from irradiation of single hydrated bicelle crystal at two different incident laser wavelengths, 830 nm (black) and 514 nm (red). Again, the 830 nm laser is far-removed from the absorption maximum of the sample, so irradiation of the sample with the 830 nm Raman incident laser following its exposure to white light should only result in the ground state spectrum for the light-adapted, all-*trans* retinal within the bicelle crystal. In contrast, the 514 nm laser lies within the absorption of the retinal, so if the crystal is capable of undergoing a photocycle this laser could potentially induce the photocycle and simultaneously provide the spectrum of a mixture of intermediates. We will verify that this is the case by repeating the power dependence experiment above with the hydrated crystals.

For the bicelle crystal irradiated at 830 nm (black spectrum) the presence of characteristic ground-state bands are observed. The band at 1527 cm^{-1} band is assigned in the literature as belonging to the C=C ethylenic stretching of the conjugated chain of retinal of bR_{568}, the all-*trans*, light-adapted ground state.[11,16,26,49,50] The small band at

1640 cm^{-1} has been characterized as the C=N stretching of the protonated Schiff base of the chromophore.[10,11,26] The large valley between the C-C single bond stretches at 1167

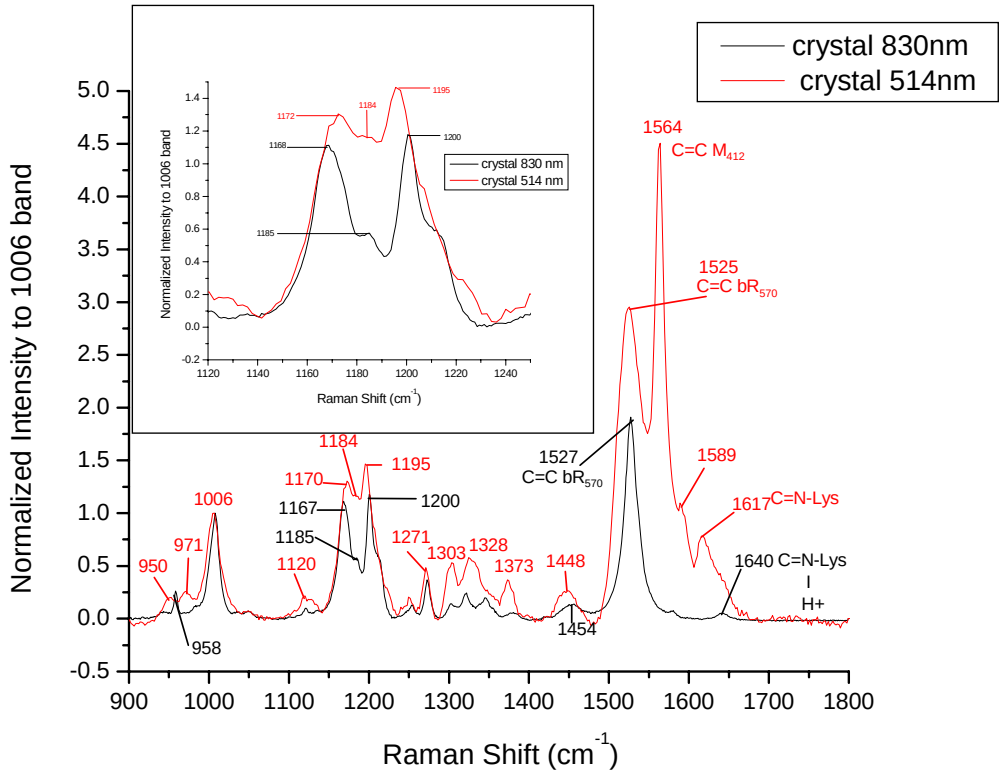

Figure 4.7: The unphotolyzed native bR (black) and photolyzed (red) Raman spectrum on a single hydrated bicelle crystal.

and 1200 cm^{-1} indicates that the population of the 13-*cis* isomer, seen here as a small shoulder at 1185 cm^{-1}, is relatively low. In the same figure, for the bicelle crystal irradiated at 514 nm (red spectrum) the presence of new bands may indicate a change in the structure of the retinal. Most notably, a new 1564 cm^{-1} band is observed, along with the 1525 cm^{-1} band observed for C=C stretching of bR_{568}. This may indicate that in using 514 nm Raman incident laser we are observing a mixture of the ground and excited states. As noted with the native hydrated bR sample above, The C=C stretching of the

M_{412} intermediate is often observed in the literature at 1567 cm^{-1}.[16,20-22,25-29] This new 1564 cm^{-1} band for the hydrated bicelle crystal is in close agreement with this shift.

In the fingerprint region (inset), the valley between the two bands for the hydrated bicelle crystal at 1170 cm^{-1} and 1195 cm^{-1} becomes shallower when the incident laser wavelength is changed from 830 nm to 514 nm. The broadening of the bands in this fingerprint region resulting from 514 nm Raman laser irradiation could very likely indicate a change in the isomeric configuration of the retinal to a higher population of 13-*cis* retinal, the isomer present in the K, L, M states of the photocycle.[52] [16,19,22,27,37,45,46] The appearance of the broad 1184 cm^{-1} band in this region under illumination by 514 nm light therefore lends more support for the creation of the 13-*cis*-containing photocycle intermediates of retinal. In the Schiff base region, a new band appears at 1617 cm^{-1} under 514 nm incident Raman laser. This is in close agreement to the 1620 cm^{-1} shift corresponding to the deprotonated C=N stretch, [10,11,16,20-24] and was also observed for the hydrated native bR film previously in Figure 4.8. A magnified view of the fingerprint region of the hydrated crystal under both 830 nm and 514 nm incident Raman lasers is shown in the inset of Figure 4.7, showing the increase in the 1184 cm^{-1} 13-*cis* band between the Raman incident 830nm laser (black) and the 514 nm laser (red).

As mentioned above, one of the difficulties in using a 514 nm incident laser in these experiments is that since it lies within the absorption band of the retinal chromophore, the development of the new bands may be due to resonance enhancement, not production of the M intermediate of the photocycle.

If the appearance of the new bands under 514 nm laser is due *only* to resonance enhancement of certain bands that are present, but not resonance-enhanced using the 830

nm laser, then we would expect *all* bands of the 514 nm spectrum to increase to the same degree upon increasing the power of the laser. On the other hand, use of the 514 nm laser might simultaneously cause resonance enhancement *and* initiation of the photocycle. If this is the case, then we would expect that increasing the power of the 514 nm laser would increase the production, and thus the population, of the M intermediate. The ratio of the intensity of the M bands relative to the intensity of the ground state bands can be calculated upon increasing 514 nm laser power. If this ratio increases with increasing 514 nm laser power, then we can say we are seeing an increase in the production of M – evidence for a photocycle. If this ratio remains constant with increasing 514 nm laser power then we know we are only seeing resonance enhancement, and that this experiment provides no evidence of a photocycle.

4.9 Effect of Increasing the 514 nm Laser Power on the Raman Spectrum of a Single Hydrated bcbR Crystal

Figure 4.8 shows the effect of increasing the 514 nm laser power on the Raman spectrum of a single hydrated bcbR crystal. The inset of this figure is a plot of the ratio of the intensity 1562 cm^{-1} band to the intensity of the 1525 cm^{-1} band as a function of the power of the 514 nm laser. Increasing the 514 nm laser power results in an increase in the this ratio, indicating an increase in the M population with increasing power of the 514 nm laser.

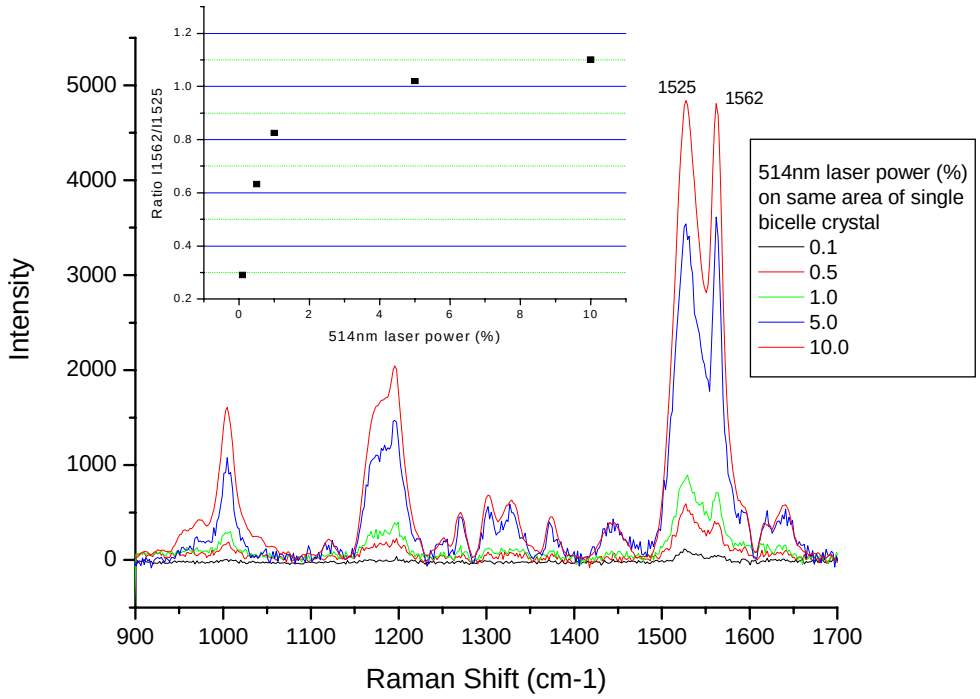

Figure 4.8: Intensity changes in the Raman spectrum of a single hydrated bicelle crystal under increasing power of the incident 514 nm laser.

In summary, this study demonstrates the first evidence for the existence of a photocycle in single hydrated bcbR crystals. This is important because it reveals that this crystal form has retained its ability to undergo the concreational changes associated with proton translocation, and is not locked into some dead-end configuration within these bicelle crystals.

References

(1) Skoog, D. A.; Leary, J. J. Raman Spectroscopy. In *Principles of Instrumental Analysis*; 4th ed.; Saunders College Publishing: Orlando, 1992; pp 296.

(2) Silvertein, R. M.; Bassler, G. C.; Morrill, T. C. Infrared Spectroscopy. In *Spectrometric Identification of Organic Compounds*; 5th ed.; John Wiley and Sons, Inc.: New York, 1991; pp 91.

(3) Ferraro, J. R.; Brown, K. W.; Brown, C. W. *Introductory Raman Spectroscopy*, 2nd ed.; Academic Press: Amsterdam, 2003.

(4) Oesterhelt, D.; Stoeckenius, W. *Nature (London), New Biology* **1971**, *233*, 149.

(5) Tanford, C. *Annual review of biochemistry* **1983**, *52*, 379.

(6) Harbison, G. S.; Smith, S. O.; Pardoen, J. A.; Winkel, C.; Lugtenburg, J.; Herzfeld, J.; Mathies, R.; Griffin, R. *Proceedings of the National Academy of Sciences* **1984**, *81*, 1706.

(7) Sperling, W.; Carl, P.; Rafferty, C. N.; Dencher, N. A. *Biophysics of Structure and Mechanism* **1977**, *3*, 79.

(8) Aton, B.; Doukas, A. G.; Callender, R. H.; Becher, B.; Ebrey, T. G. *Biochimica et Biophysica Acta* **1979**, *576*, 424.

(9) Mendelsohn, R. *Nature (London, United Kingdom)* **1973**, *243*, 22.

(10) Heyde, M. E.; Gill, D.; Kilponen, R. G.; Rimai, L. *Journal of the American Chemical Society* **1971**, *93*, 6776.

(11) Lewis, A.; Spoonhower, J.; Bogomolni, R. A.; Lozier, R. H.; Stoeckenius, W. *Proc. Natl. Acad. Sci. U.S.* **1974**, *71*, 4462.

(12) Terner, J.; Campion, A.; El-Sayed, M. A. *Proceedings of the National Academy of Sciences of the United States of America* **1977**, *74*, 5212.

(13) Eyring, G.; Curry, B.; Mathies, R.; Fransen, R.; Palings, I.; Lugtenburg, J. *Biochemistry* **1980**, *19*, 2410.

(14) Eyring, G.; Curry, B.; Mathies, R.; Broek, A.; Lugtenburg, J. *Journal of the American Chemical Society* **1980**, *102*, 5390.

(15) Braiman, M.; Mathies, R. *Proceedings of the National Academy of Sciences of the United States of America* **1982**, *79*, 403.
(16) Althaus, T.; Eisfeld, W.; Lohrmann, R.; Stockburger, M. *Israel Journal of Chemistry* **1995**, *35*, 227.

(17) Eisfeld, W.; Pusch, C.; Diller, R.; Lohrmann, R.; Stockburger, M. *Biochemistry* **1993**, *32*, 7196.

(18) Smith, S. O.; Braiman, M. S.; Myers, A. B.; Pardoen, J. A.; Courtin, J. M. L.; Winkel, C.; Lugtenburg, J.; Mathies, R. A. *Journal of the American Chemical Society* **1987**, *109*, 3108.

(19) Spiro, T. G.; Editor *Biological Applications of Raman Spectroscopy, Vol. 2: Resonance Raman Spectra of Polyenes and Aromatics*, 1987.

(20) Aton, B.; Doukas, A. G.; Callender, R. H.; Becher, B.; Ebrey, T. G. *Biochemistry* **1977**, *16*, 2995.

(21) Stockburger, M.; Klusmann, W.; Gattermann, H.; Massig, G.; Peters, R. *Biochemistry* **1979**, *18*, 4886.

(22) Hildebrandt, P.; Stockburger, M. *Biochemistry* **1984**, *23*, 5539.

(23) Stern, D.; Mathies, R. *Springer Proceedings in Physics* **1985**, *4*, 250.

(24) Marcus, M. A.; Lewis, A. *Science* **1977**, *195*, 1328.

(25) Mathies, R.; Freedman, T. B.; Stryer, L. *Journal of molecular biology* **1977**, *109*, 367.

(26) Oseroff, A. R.; Callender, R. H. *Biochemistry* **1974**, *13*, 4243.

(27) Braiman, M.; Mathies, R. *Biochemisrtry* **1980**, *19*, 5421.

(28) Henderson, R.; Sulkes, M.; Lewis, A.; Marcus, M. A. *Biochemistry* **1978**, *17*, 4712.

(29) Chronister, E. L.; El-Sayed, M. A. *Photochemistry and Photobiology* **1987**, *45*, 507.

(30) Mathies, R. *Chem. Biochem. Appl. Lasers* **1979**, *4*, 55.

(31) Lin, S. W.; Fodor, S. P. A.; Miercke, L. J. W.; Shand, R. F.; Betlach, M. C.; Stroud, R. M.; Mathies, R. A. *Photochemistry and Photobiology* **1991**, *53*, 341.

(32) El-Sayed, M. A. Time-Resolved Chromophore Resonance Raman and Protein Fluorescence of Intermediates in some photobiological changes. In *Trends in Photobiology*; C. Helene, M. L., Th. Montenay-Garestier, and G. Laustriat, Ed.; Plenum Publishing Co., 1982.

(33) Doig, S. J.; Reid, P. J.; Mathies, R. A. *Proceedings of SPIE-The International Society for Optical Engineering* **1991**, *1432*, 184.

(34) Doig, S. J.; Reid, P. J.; Mathies, R. A. *Journal of Physical Chemistry* **1991**, *95*, 6372.

(35) Doig, S. J.; Reid, P. J.; Mathies, R. A. *Springer Proceedings in Physics* **1992**, *68*, 45.

(36) El-Sayed, M. A.; Hsieh, C.-L.; Nicol, a. M. *Springer Series in Chemical Physics (Picosecond Phenom.)* **1982**, *23*, 302.

(37) El-Sayed, M. A.; Hsieh, C.-L. *Time-Resolved Vibrational Spectroscopy* **1983**.

(38) Ames, J. B.; Fodor, S. P. A.; Gebhard, R.; Raap, J.; Van den Berg, E. M. M.; Lugtenburg, J.; Mathies, R. A. *Biochemistry* **1989**, *28*, 3681.

(39) Ames, J. B.; Mathies, R. A. *Biochemistry* **1990**, *29*, 7181.

(40) Atkinson, G. H.; Ujj, L.; Zhou, Y. *Journal of Physical Chemistry A* **2000**, *104*, 4130.

(41) Atkinson, G. H.; Zhou, Y.; Ujj, L.; Aharoni, A.; Sheves, M.; Ottolenghi, M. *Journal of Physical Chemistry A* **2002**, *106*, 3325.

(42) Campion, A.; Terner, J.; El-Sayed, M. A. *Nature* **1977**, *265*, 659.

(43) Chronister, E. L.; Corcoran, T. C.; Song, L.; El-Sayed, M. A. *Proceedings of the National Academy of Sciences of the United States of America* **1986**, *83*, 8580.

(44) Delaney, J. K.; Subramaniam, S.; Schmidt, P.; Atkinson, G. H. *Journal of Physical Chemistry B* **1997**, *101*, 5619.

(45) Hsieh, C. L.; Nagumo, M.; Nicol, M.; El-Sayed, M. A. *Journal of Physical Chemistry* **1981**, *85*, 2714.

(46) Hsieh, C. L.; El-Sayed, M. A.; Nicol, M.; Nagumo, M.; Lee, J. H. *Photochemistry and Photobiology* **1983**, *38*, 83.

(47) Oesterhelt, D.; Hess, B. *European Journal of Biochemistry* **1973**, *37*, 316.

(48) Faham, S.; Yang, D.; Bare, E.; Yohannan, S.; Whitelegge, J. P.; Bowie, J. U. *Journal of Molecular Biology* **2003**, *335*, 297.

(49) Gill, D.; Heyde, M. E.; Rimai, L. *Journal of the American Chemical Society* **1971**, *93*, 6288.

(50) Rimai, L.; Gill, D.; Parsons, J. L. *Journal of the American Chemical Society* **1971**, *93*, 1353.

(51) Van den Berg, R.; Jang, D. J.; Bitting, H. C.; El-Sayed, M. A. *Biophysical Journal* **1990**, *58*, 135.

(52) Griffiths, J. A.; Masciangioli, T. M.; Roselli, C.; El-Sayed, M. A. *Journal of Physical Chemistry* **1996**, *100*, 6863.

CHAPTER 5

STUDY OF THE PROTON PUMP PROCESS USING FLASH PHOTOLYSIS SPECTROSCOPY*

Abstract

In this chapter, pump-probe flash photolysis spectroscopy is used to study the M rise and decay kinetics of bcbR crystals. As discussed in Chapter 4, the M intermediate forms in hydrated bcbR crystals. However, the ease of photochemical deprotonated of the retinal Schiff base (M rise) and the efficiency of reprotonation of the deprotonated Schiff base (M decay) are not known. In this chapter, we are trying to examine the how packing in bcbR crystals affects the efficiency of its photocycle.

5.1. Detecting Photocycle Intermediates by Pump-Probe Nanosecond Spectroscopy

The photocycle of native bR has been studied in the mid-1970's[1] and is well documented in the literature. Upon the absorption of light by the all-*trans* retinal chromophore of bR, isomerization occurs as the first step in the photocycle that forms different intermediates of lifetimes ranging from ps to ms and the results in the transfer of a proton from the cytoplasmic to the extracellular side of the membrane with intermediates with well-characterized visible absorption spectra.[2-10] At a critical step in the cycle, a proton is transferred from the Schiff base of the retinal to a nearby Asp_{85} residue of the hydrophilic channel, resulting in the only deprotonated retinal intermediate in the cycle, the M

* Manuscript published: Sanii, Laurie S., Schill, Alex W., Moran, Cristin E., El-Sayed, Mostafa A. "The Protonation-Deprotonation Kinetics of the Protonated Schiff Base in Bicelle Bacteriorhodopsin Crystals" *Biophys J.* (2005) 89, 444-451.

intermediate. In the M intermediate the absorption of the retinal is at 412 nm.[11] The retinal is then reprotonated in a subsequent step with a proton that originates from the Asp_{96} residue of the hydrophobic channel. This process results in the ejection of a proton to the extracellular side of the membrane, thus regenerating the protonated Schiff base of retinal present at the beginning of the cycle. The Asp_{96} residue is also reprotonated by the end of the process, both ready for another turn of the cycle. The only light-dependent event in the photocycle is the initial all-*trans* to 13-*cis* isomerization of retinal. All subsequent steps are thermal relaxation steps.[11]

In the native membrane, the bR molecules are arranged as hexagonal sheets of trimers consisting of three monomer units each in a hexagonal unit cell 63-Å in diameter.[6,12,13] Within each monomer, the retinal molecule lies in a plane transverse to the plane surrounding alpha helices, and is attached to the protein via a protonated Schiff base at Lys_{216} of helix G. Retinal separates the hydrophilic extracellular region (containing many polar side-chains and bound water molecules) from the more hydrophobic cytoplasmic region.[14] The key amino acids involved in the proton transport and the direction of proton transport are shown in Figure 5.1.[15]

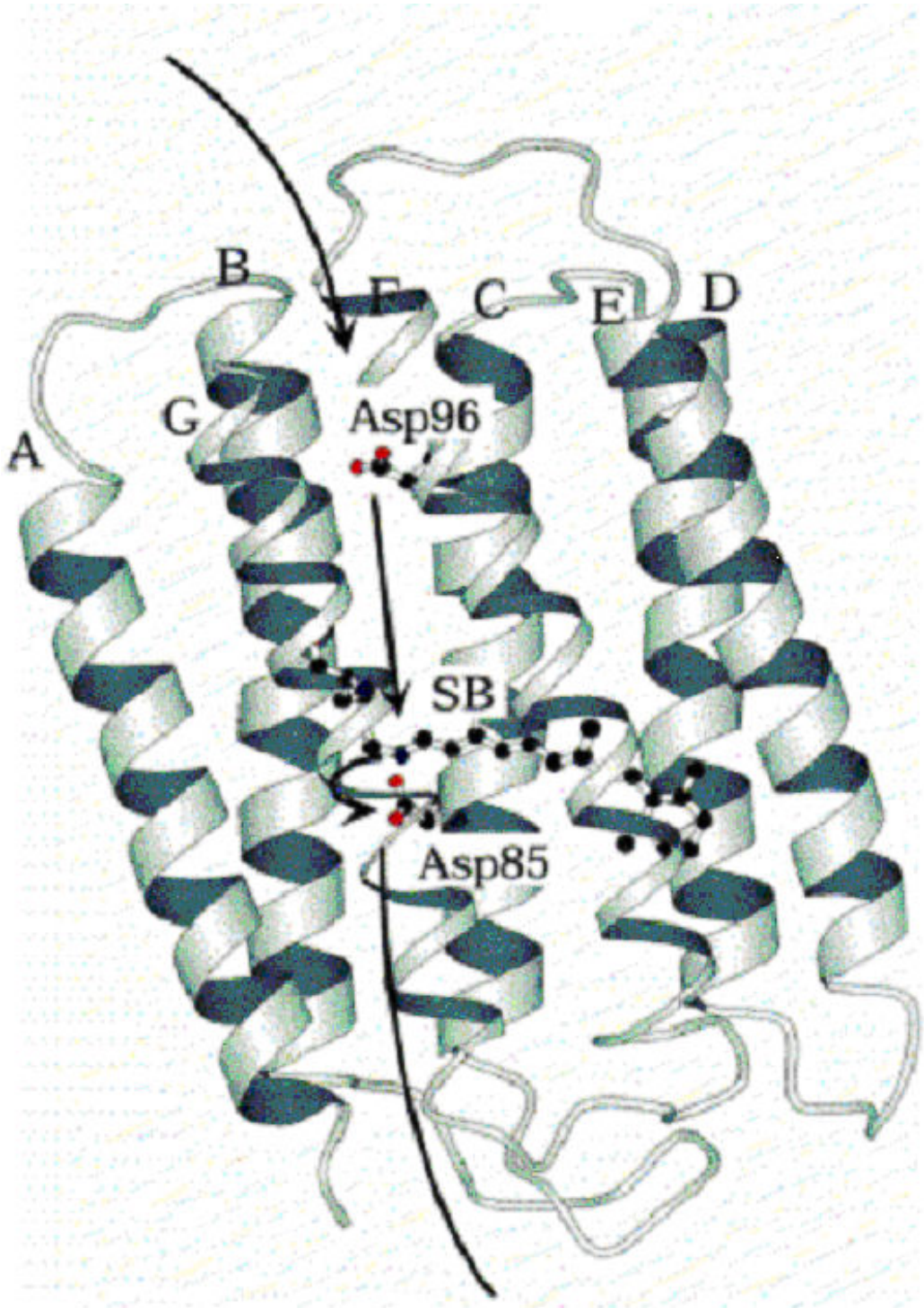

Figure 5.1: Side-view of retinal (shown here as "SB" for Schiff base") within its binding pocket, located at the center of the seven-alpha helices of the protein.

5.2 Characterization of the M Intermediate of the Photocycle

In 1975 Slifkin and Caplan demonstrated that there were at least two species of M intermediate present with different lifetimes,[16] a finding that has been repeatedly confirmed.[17] The rise of the M intermediate in native bR is often characterized as fitting to a biexponential curve.[18-20] Two primary models have been presented to account for this biexponential rise. The first model is of that of parallel photocycles; that there are two different ground state bR species, each going through their own photocycle with the same spectral intermediates.[21-23] The other model assumes that there is only one photocycle but that there is a transition between two M states, M_1 and M_2, that is spectrally silent in the visible region.[19,20,24-26 27] The idea is that during the $M_1 \rightarrow M_2$ transition the Schiff base redirects its orientation from the extracellular to the cytoplasmic half-channel [28] when it accepts the proton from Asp_{96}, the only ionizable residue in the cytoplasmic half-channel.[29]

The overall rise and decay times of the M intermediate have been reported in the literature and can vary with temperature, ionic strength, and pH of the surrounding media.[21,30-34] In addition, the removal of the native lipids from the protein can also affect the kinetics.[35] The rise time for the M intermediate for native bR in unbuffered, distilled, deionized water at room temperature has been characterized as a nearly 60 μs process. Jang and El-Sayed have characterized the rise of the M intermediate as a biexponential process with two rise times contributing to the total rise time, 7.2 μs (15% contribution)

and 57 μs (85% contribution).[35] Later Heyes and El-Sayed[36] reported the values of 8.49 μs (21% contribution) and 75.8 μs (79% contribution).

In the literature, the decay time for the M intermediate has been characterized as either a mono- or biexponential process. Jang and El-Sayed have characterized the M intermediate decay as a monoexponential process with a decay time of 3.8 ms.[35] Later Heyes and El-Sayed[36] reported a decay time of 8.57 ms. This is in close agreement with the value of 7.3 ms reported by Dencher and co-workers[37] for the room-temperature sample in 100 mM (0.1 M) acetate buffer, pH 5.0. However, others have reported the decay as biexponential.[18,19]

One possibility for the range of reported rise and decay values for the M intermediate is the finding by Ohno *et al.*[38] that the ratio of the two species of M intermediate (a faster "M_f" component and a slower "M_s" component) was modulated by the intensity of the actinic flash used to initiate the photocycle. This intensity can produce changes in the shapes of the kinetic curves. At low flash intensities the M_f species was predominant, but with increasing light intensities the fraction of M_f, characterized as M_f /(M_f +M_s), decreased to <0.5,[39] a finding that has also been repeatedly confirmed.[17] The dependence of flash intensity on the shape of the kinetic curves is an important point to keep in mind when comparing experimental to literature values for the M rise and decay timescales, and something to control throughout the experiment.

5.3 Effects of Lipid Removal on Photocycle Kinetics

As mentioned above, the removal of the native lipids of the bilayer surrounding the protein trimers has been demonstrated to alter the M kinetics. The purple membrane is 75% protein and 24% lipid by weight.[40] There are approximately 10 lipid molecules per bR monomer. For each bR monomer there are approximately one squalene (SQ), 2 glycolipid sulfate (GLS), 5-phosphatidyl glycerophosphate (PGP-Me) (methyl ester), 0.5 phosphatidyl glycerol (PG), and 0.5 phosphatidyl glycerosulfate (PGS).[40,41] The structures of these lipid molecules are shown in Figure 5.2. Of these, squalene is the only neutral lipid present in PM.[42]

Later, Heyes and El-Sayed again examined the M rise and decay effects resulting from removal of 75% of the lipid from the protein (via exposure to CHAPSO detergent), and also the effect of monomerization of the membrane (via exposure to Triton-X100 detergent).[36] In the native sample, all native lipids are present and the trimer lattice structure is preserved. In the 75% delipidated sample, the trimer structure is preserved but the removal of 75% lipids results in a decrease in the unit cell dimensions.[43] In contrast, in the monomerized sample the trimer structure is lost and the monomers are free to move away from one another.

As found in the previous study on the kinetics of partially delipidated bR,[35] they found that removal of 75% of the lipids from native bR resulted in a slowing down of the M rise and decay kinetics relative to native (i.e. it increases the M creation and decay times), with an efficiency of M creation only about 30-40% of that of the native bR. than in the native. The rate of M decay was comparable to those of native bR at pH

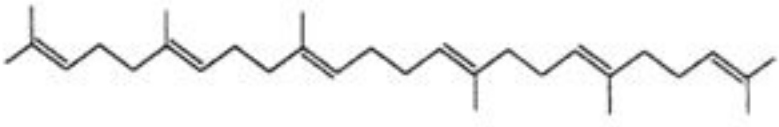

Squaline - (SQ)

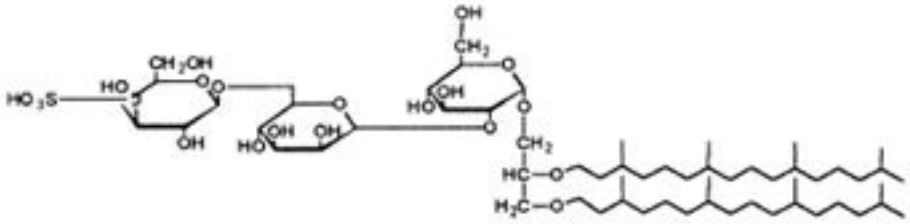

Glycolipid Sulfate - (GLS)

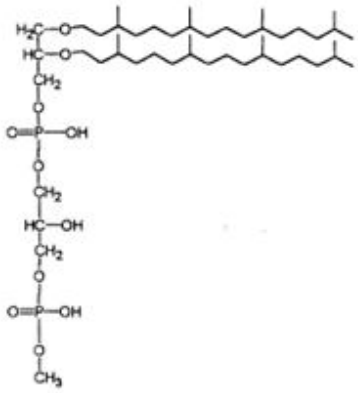

Phosphatidyl glycerophosphate (methyl ester) - (PGP-Me)

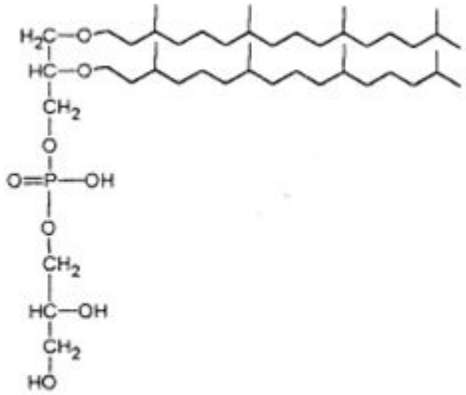

Phosphatidyl glycerol (PG)

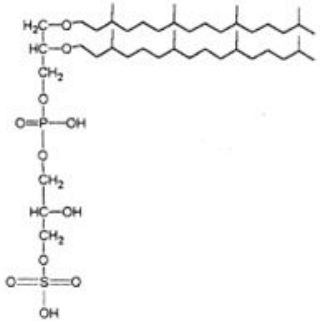

Phosphatidyl glycerosulfate (PGS)

Figure 5.2: Structures of the lipid molecules present in the native PM.

7.[36] In all cases (native, 75% delipidated, and monomerized bR) the M rise fit well to a biexponential and in general the M rise became faster going from native → 75% delipidated → monomerized.

While the M rise kinetics maintained biexponential behavior going from native→ 75% delipidated → monomerized, the trend was more complicated for the M decay. M decay showed monoexponential behavior for the native. For the 75% delipidated sample, the M decay remained monoexponential but the decay rate became slower – the decay time became longer. However, for the monomerized samples, two changes were observed - the decay became biexponential, and the total decay time decreased back to that observed in the native. The M rise and decay times as reported by Heyes and El-Sayed[36] are reported in Figure 5.3.

Kinetic parameters for M rise and decay and relative efficiency of M formation

Sample	M Rise			M Decay			Relative % efficiency of M	Measured pH
	τ_1 (A_1)	τ_2 (A_2)	τ_{avg}	τ_1 (A_1)	τ_2 (A_2)	τ_{avg}		
Native bR in DDW	8.49 μs (0.21)	75.8 μs (0.79)	61.7 μs	8.57 ms	–	8.57 ms	100	7.0
Native + CHAPS in DDW	23.5 μs (0.49)	137 μs (0.51)	81.4 μs	27.7 ms	–	27.7 ms	45	5.0
Native + Trition in DDW	1.76 μs (0.42)	9.71 μs (0.58)	6.71 μs	9.47 ms (0.96)	34.0 ms (0.04)	10.5 ms	145	5.4

τ_{avg} is calculated by $\tau_{avg} = (A_1 \times \tau_1) + (A_2 \times \tau_2)$, where $A_1 + A_2 = 1$.

Figure 5.3: Effect of the structure and type of environment of the protein in bacteriorhodopsin.

5.4 The M Rise Process

The M rise process involves the transfer of a proton from the Schiff base of retinal to the proton acceptor Aps_{85}. In this last study, going from native to 75% delipidated bR via exposure of the native membrane to CHAPS resulted in a slowing down of the M rise kinetics. On the other hand it was also observed that the M rise rate increased going from the native to the monomerized sample.[36] The authors invoked a relationship between the pK_a difference between the Schiff base and Asp_{85} and the distance between bR molecules with the rate of M rise. In the native membrane, all lipids are present and the bR molecules arranged as trimers, each with fixed distances to one another and to other trimers. As mentioned above, removal of 75% of the lipids maintains the trimer structure, but the removal of the lipids results in a tighter unit cell; one in which the bR molecules are closer together. This is the case with treatment by CHAPS, and the M rise rate slows down. Monomerization by removal of all lipids breaks the trimer unit cell apart into individual bR monomers, which are now not forced to be close together. This is the case with treatment by Triton, and the authors observe an increase in the M rise kinetics that is faster than that observed in the native.

5.5 The M Decay Process

During M decay process the Asp_{96} residue re-protonates the Schiff base. In contrast to the constant biexponential behavior of the M rise kinetics with changing lipid composition, the rate of M decay in this report fitted well to a monoexponential in the

native and 75% delipidated samples, but the decay fit better to a biexponential upon monomerization. Again, to explain this trend the authors invoke the relationship between the decreasing unit cell dimensions of the trimer going from native to 75% delipidated. They claim that the tighter unit cell is more resistant to conformational changes necessary in the protein necessary to provide access of the Schiff base to the Asp_{96} proton donor. Of course this means in the monomerized sample, where the trimer unit cell is no longer present and the bR monomers are free to move away from one another, any conformational restraints caused by the trimer structure existing in either the native or the 75% delipidated forms have been removed, thus resulting in an increase in the M decay rate of the monomerized sample relative to both the native and the 75% delipidated.

The effect on M rise and decay kinetics upon detergent treatment of the native membrane has been addressed because the results may give us some indication of what we might expect during the crystallization process. The crystallization of trans-membrane proteins like bR involves the use of detergents to coax the protein out of its native lipid membrane and into a new detergent lipid membrane. As will be addressed in the case of the bicelle crystallization technique, this process removes nearly all the native lipids so that from the X ray crystal structure, only one bound lipid per monomer remains.[44]

5.6 Kinetic Studies on cbR Crystals

In 1998, the first time-resolved functional studies were performed on the hexagonal cbR crystals using time-resolved Fourier transform infrared (FT-IR) difference spectroscopy

and observing the time-resolved vibrational intensities of several marker bands associated with the M intermediate by Heberle *et al*.[45] It is important to note that the time traces for the kinetics of the cbR crystals were essentially the same as those for the native membrane (Figure 5.4). The presence of the trimer structure of the protein units in both the native membrane and within the cbR crystals was the explanation given for these observations, a claim the authors backed up by citing the work of Danshina *et al*.[46] in which monomeric bR dissolved in detergent solution exhibits a long-lived photocycle. It is also important to note that the time-resolved IR difference spectroscopy was the only technique used to monitor the kinetics within the cbR crystals.

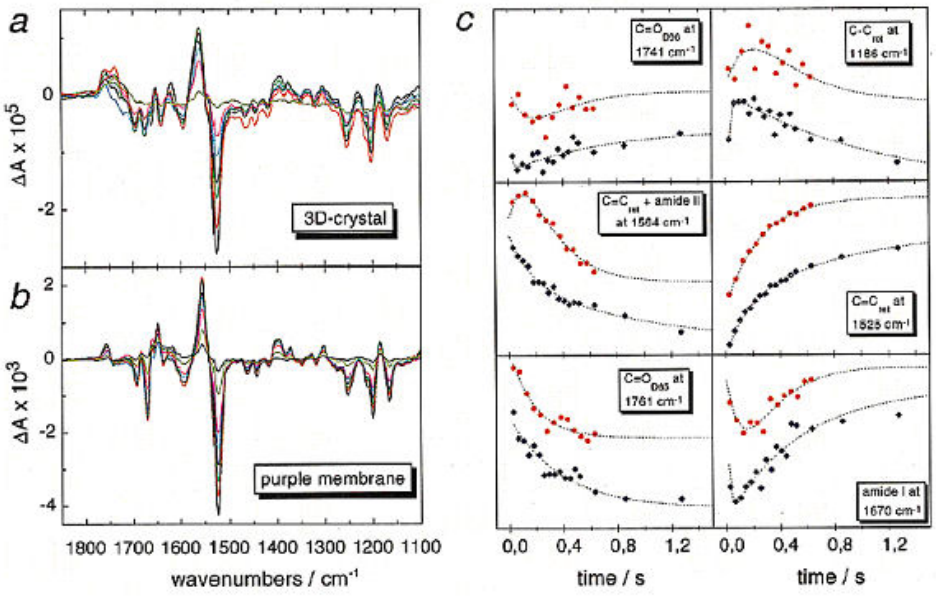

Figure 5.4: Comparison of the photocycle kinetics of cbR crystals to native membrane

5.7 Kinetic Studies on bcbR Crystals

We know from the Raman experiments in Chapter 4 that the bcbR crystals are capable of undergoing a photocycle by the detection of the M intermediate upon illumination with 514 nm light. However, the kinetics of M creation and decay are unknown. In the cbR crystals, which have a parallel trimer structure similar to that of native bR, the M rise and decay kinetics are very similar to that of native. In the bcbR crystals, the trimer structure is no longer intact and instead an antiparallel monomer packing structure exists. We know that in this new packing structure M can form, but what is the efficiency of M creation and its lifetime? These experiments will be performed using pump-probe nanosecond spectroscopy, or 'flash photolysis' technique.

Experimental Methods

5.8 Detecting Photocycle Intermediates by Pump-Probe Nanosecond Spectroscopy

In general, flash photolysis spectroscopy refers to pump-probe methods investigating the fast photochemical reactions arising in samples upon their exposure to very short, intense flashes of light. The rise and decay of the products of these reactions can be in the micro to nanosecond time scale. In these experiments, the intense flashes of light (pump) are provided by an Nd:YAG laser, which provide 1 mJ pulses of 532 nm light at 10 ns pulse width with a 10 Hz repetition rate. The probe light is provided by a 75W Xe Arc lamp running in CW mode. Both the pump and probe light approach the sample at the same

focal point, so that the sampling area spot diameter of the probe light is within the excitation spot size. This assures that all the molecules within the sampling beam are being exposed to the excitation source. The intense laser flashes are coupled to a photomultiplier tube (PMT). The PMT also has a rapid response time (100 ms), and allows for the monitoring of the intensity changes over a time range for a particular wavelength.

5.9 Sample Preparation

Since the crystals were too dense to remain buoyant in water, a sampling system had to be designed in which the crystals could sit at the bottom of a solution well, with the pump and probe light being directed from the top-down through this well and then to the detector. A multi-well sample holder with an optically clear and flat surface was needed in order to examine several different samples quickly. Such a multi-well sampling system was designed by taking a rectangular microscope slide and using spray adhesive to attach a piece of rubber matting approximately 2 mm thick. This rubber matting contained holes punched through it (prior to its attachment to the glass) that were each approximately 3-4 mm in diameter. Figure 5.5 shows both a top-down and a side-view diagram of such a sampling tray. Crystals were collected by repeated washing of the crystal-detergent matrix with deionized distilled water (DDW) into microcentrifuge tubes. The higher-density crystals settled to the bottom of the solution within a matter of minutes, while the white detergent flakes remained suspended in the supernatant, which was easily removed without the need for centrifugation. Washing the crystals in this

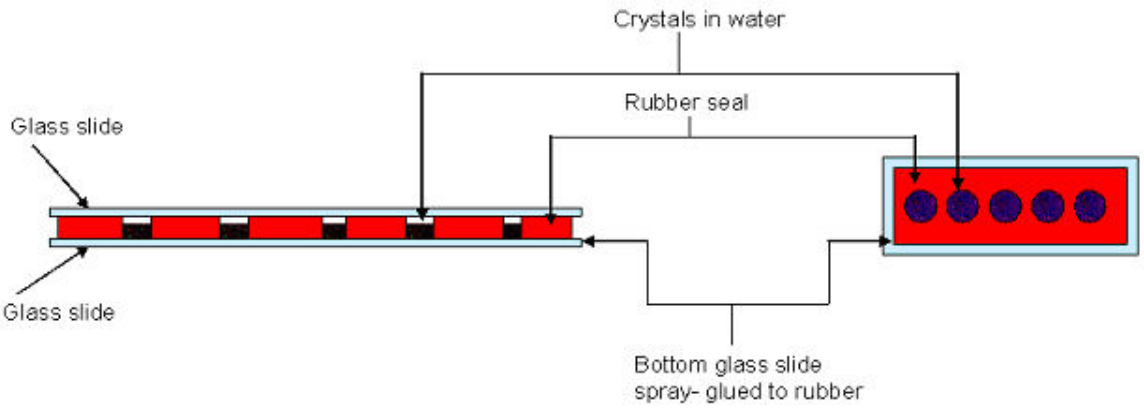

Figure 5.5: The multi-well sample holder used for flash photolysis experiments on solutions of crystals shows from the side (left) and from the top-down (right).

manner removed the bulk detergent while leaving the crystals intact. After washing, a concentrated drop of the crystal suspension in deionized distilled water (DDW) was placed in a well of the sampling tray shown above in Figure 5.5. A glass cover slip was sealed with vacuum grease over the well to prevent evaporation of the water during the experiment.

5.10 Instrumentation

Transient absorption experiments were carried out using the frequency doubled output of a Q-switched nanosecond pulsed Spectra Physics Quanta-Ray Series Nd:YAG laser (Spectra Physics, Mountain View, CA). Monitoring light was provided by a PTI Corporation Xenon arc lamp (PTI Corp, San Jose, CA) running in CW mode. The output of the lamp was focused onto one end of a fiber optic cable and the output from the opposite end of the cable was directed toward the sample, focused to a ~2 mm diameter

spot at the sample, recollected, and focused onto another fiber optic that directed the transmitted light to the entrance slit of the monochromator. The monochromator was adjusted to 412 nm. A filter was placed in front of the entrance slit of the monochromator remove any 532 nm excitation light while allowing passage of the 412 nm light. The filter's transmission profile is shown in Figure 5.6. Single wavelength kinetics monitored at 412 nm were recorded using a Hammamatsu photomultiplier tube (Hammamatsu, Japan) whose response was digitized using a LeCroy 9350 500 MHz oscilloscope (Chestnut Ridge, New York). The excitation at 532 nm had a pulse energy of 1 mJ and was overlapped with the monitoring beam at the ~2 mm focal spot within the sample. The laser Q-switch triggers data acquisition by the LeCroy 9350 oscilloscope at a frequency of 10 Hz. Figure 5.7 shows an overhead view of the bench setup described above. A floppy disk inserted at into the top of the oscilloscope is used to store the kinetic traces. After each experiment, the Winspec 32 software program (Roper Scientific, Trenton, NJ) converts this waveform data into an XY format that can be plotted using the OriginPro v7.5 (OriginLab Corp., Northampton, MA) software package with time on the X axis and intensity at 412 nm on the Y axis.

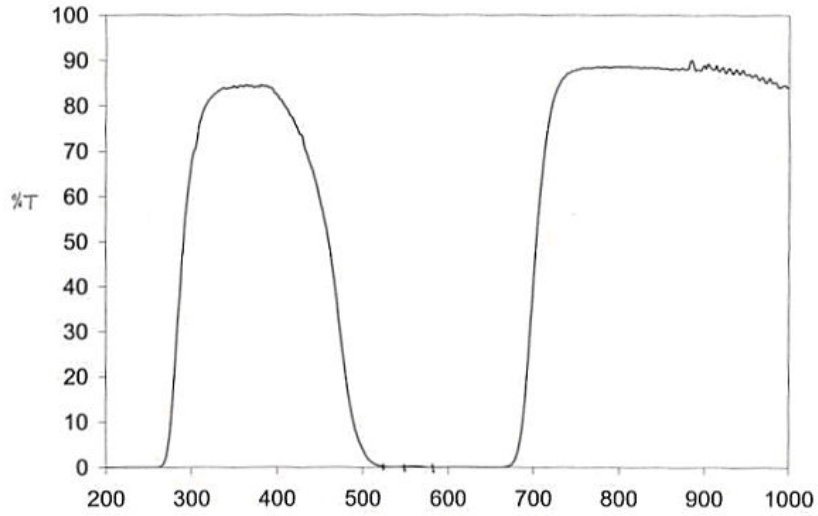

Figure 5.6: Transmission spectrum for the filter used in these experiments

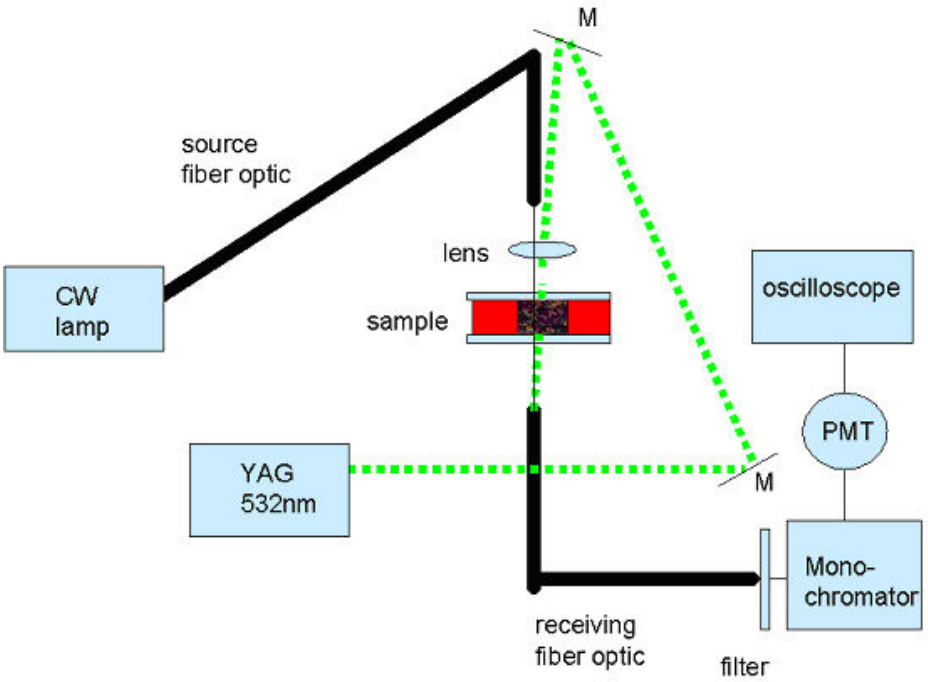

Figure 5.7: bench diagram for using the 532 nm incident pulsed laser as excitation source for M_{412} decay experiments on a crystal sample.

Results and Discussion

5.11. Flash Photolysis of bcbR crystals

Figure 5.8 compares the M rise kinetics as a measure of the intensity of the signal monitored at 412 nm (expressed here as I_{412}) for crystals suspended in deionized, distilled water (DDW) and for a native solution of bR suspended in DDW. Figure 5.9 compares the decay rates of this same process for the same two samples in DDW. In all cases the power of the pulsed laser was kept constant at 1mJ with a 10 ns pulse width at a rep rate of 10 Hz and a laser spot diameter of 4 mm. The data have been normalized for ease of comparison. In all cases attempts were made to fit the rise and decay data for both samples to both a monoexponential and a biexponential decay and the fits with the higher R^2 values and lowest error were chosen. In both the native and the bcbR crystals, the M rise data fit best to a biexponential expression. In the native sample, the M decay fit best to a biexponential expression while the bcbR crystals the M decay data fit best to a monoexponential. The times are reported in Table 5.1.

5.12. M rise of bcbR crystals in H_2O

From Figure 5.8 it is observed that the M rise kinetics for the bcbR crystals is faster than it is for the native sample. The total time for M rise in the crystals in DDW is 18 μs; a two-component rise with $\tau_1 =$ 12 μs (80% contribution) and $\tau_2 =$ 40 μs (20% contribution). For the native the total time for M rise in DDW is 69 μs; a two-component

rise with τ_1 = 16 μs (24% contribution) and τ_2 = 86 μs (76% contribution). These values are reported in Table 5.1. The bcbR crystal's M rise is nearly four times faster in the bcbR crystals. The data for both the native and the bcbR samples fits best to a biexponential M rise. As mentioned in the introduction, the work of both Jang and El-Sayed[35] and of Heyes and El-Sayed[36] demonstrated that while removal of 75% of the native lipids (which reduces the dimensions of the trimer unit cell relative to the native) resulted in a slower M rise relative to the native sample, monomerization of the sample (trimer structure no longer intact) resulted in a faster M rise relative to native. Time-resolved FTIR work of Heberle *et al*.[45] on the kinetics of the M intermediate in the *in cubo* crystals demonstrated that the time traces for the M kinetics were nearly identical to those of the native membrane. Like the native membrane and the 75% delipidated sample described here, the bR molecules within the cbR crystals consist of parallel trimers.

From the crystal structure of the bcbR crystal it is known that the bR molecules are no longer in the parallel trimer packing structure, but are arranged as antiparallel monomers with only one bound lipid per monomer remaining.[44] The parallel trimer packing motif of the bR molecules is observed in native membrane, as well as the native membrane after 75% of the native lipids are removed. The trimer packing motif is also observed in the cbR crystals of Rosenbusch and Landau.[47]

For the parallel trimer packing motif of the cbR crystals, the M kinetics monitored by time-resolved FTIR are about the same as found in the native.[45] In both the monomerized native solution in the literature and in the bcbR crystals examined here,

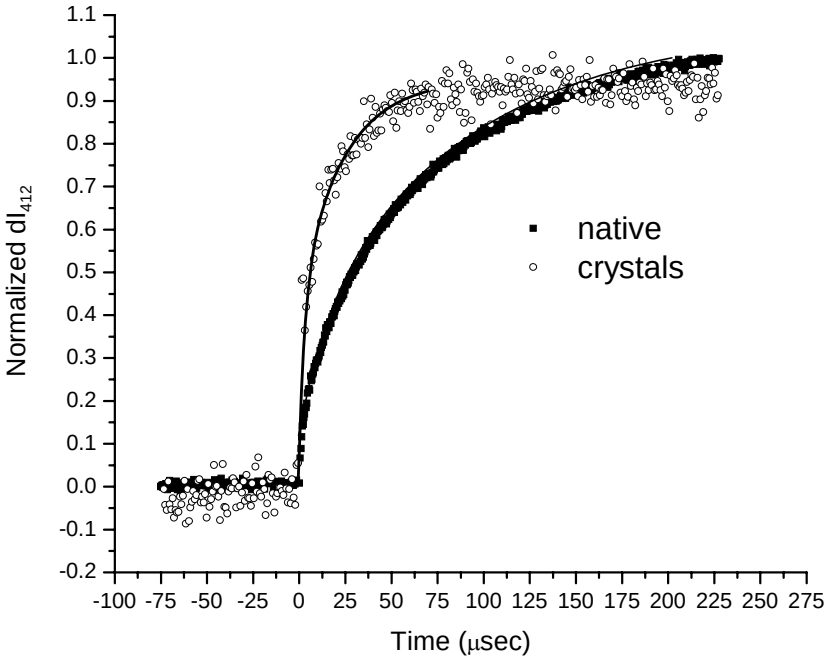

Figure 5.8: Comparison of M rise kinetics in deionized distilled water (DDW), expressed as the intensity of the 412 nm absorption.

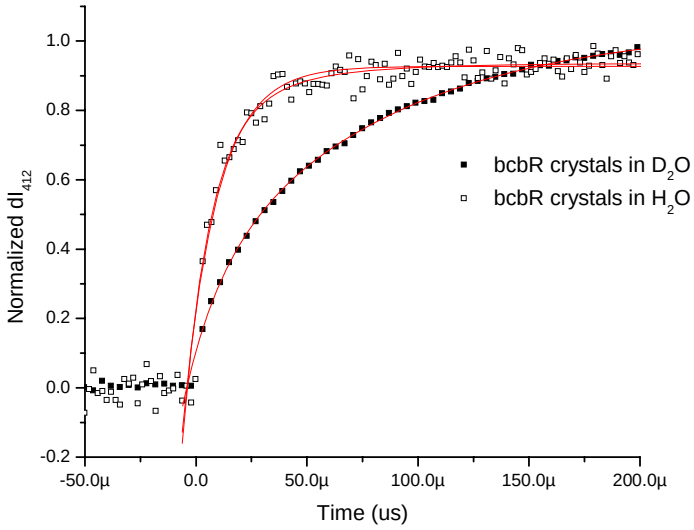

Figure 5.9: Comparison of M rise kinetics in H_2O and D_2O of bcbR crystals, expressed as the change in the 412 nm absorption intensity.

Table 5.1: Summary of the M rise and decay times comparing the photocycle kinetics of the bcbR crystal crystals in deionized, distilled water (H_2O) to that of the native under the same conditions.

	M rise			**M decay**		
Sample	**M rise τ_1 (A1)**	**M rise τ_2 (A2)**	**M rise avg**	**M decay τ_1 (A1)**	**M decay τ_2 (A2)**	**M decay avg**
Native in H_2O[49]	------	------	$\tau_{1/2}$ = 130 μs	------	------	$\tau_{1/2=}$ 6.7 ms
Native in D_2O[49]	------	------	$\tau_{1/2}$ = 730 μs	------	------	$\tau_{1/2=}$ 11.0 ms
Native in H_2O	16 μs (.24)	86 μs (.76)	69 μs	5.9 ms (.71)	19.4 ms (.29)	9.8 ms
Native in D_2O	74 μs (.26)	489 μs (.74)	380 μs	14 ms (.95)	42 ms (.05)	15 ms
Crystals in H_2O	12 μs (.80)	40 μs (.20)	18 μs	73	------	73 ms
Crystals in D_2O	60 μs (.75)	447 μs (.25)	157 μs	148	------	148 ms

τ_{avg} is calculated by $\tau_{avg} = (A_1 \times \tau_1) + (A_2 \times \tau_2)$, where $A_1 + A_2 = 1$

there is a loss of this parallel trimer structure. In both the monomerized native solution and in the bcbR crystals with their antiparallel monomer packing motif, an increase in the M rise rate relative to that of the native trimer sample and the 75% delipidated sample (consisting of smaller unit-cell trimers) is observed. Based on these observations, it might initially be concluded that the loss of the trimer structure results in an increase in the M rise kinetics.

As stated in the introduction, the rise of the M intermediate of the photocycle is due to the transfer of a proton from the Schiff base of retinal to Asp_{85}. In the native membrane, this Asp_{85} residue is located about four to five angstroms below the Schiff base.[19,48] Any environmental or structural difference relative to the native structure that facilitates this transfer would result in an increase in rate of M production. The

authors[35,36] postulated in the introduction that the increase in the M rise kinetics for the native monomerized sample relative to the native sample was due to the increased conformational freedom of the monomers relative to their trimer packing association in the native; the Schiff base could deprotonate more readily because there was more conformational freedom in the protein to do so. They backed up this claim by citing the fact that reducing the unit cell dimensions of the native trimer by removal of 75% of the native lipids resulted in a decrease in the M rise kinetics, while removal of all the lipids, resulting in monomerization (loss of trimer), resulted in a recovery of the M rise kinetics to a rate equal to or surpassing that of the native.[36]

In the bcbR crystals, the parallel trimer packing structure of bR molecules that is present in native bR, 75% delipidated bR, and in the cbR crystals is no longer present; instead the molecules are arranged as monomers packed in an antiparallel fashion. While in the native monomerized bR solution the monomers are no longer packed in the trimer structure and are free to migrate away from one another, in the bcbR crystals the monomers are *not* free to migrate away from one another in this manner. However, perhaps in this new antiparallel packing arrangement within the bcbR crystals the monomers are far *enough* away from each other so that they have more conformational freedom relative to the native solution. It may be that an increase in conformational freedom of the bcbR crystals' antiparallel monomer packing relative to the native trimer packing structure accounts for the increase in the M rise kinetics observed here. A second point to consider is the pK_a for the protonated Schiff base (PSB) in bcbR crystals. It may be the case that in the bcbR crystals the pK_a of the PSB is lower than it is in native or cbR crystals. A lower pK_a could for bcbR crystals could result in a faster proton

donation from the PSB to the proton acceptor in the reaction, which for native and cbR crystals is Asp_{85}. A third consideration is the proton acceptor itself. Perhaps in the bcbR crystals, it is not Asp_{85}, but nearby Asp_{212} that is the proton acceptor during M rise. A change in the proton acceptor might translate into a faster proton transfer between the PSB and the acceptor during M rise.

5.13. M rise of bcbR crystals in D_2O

The kinetic isotope effect after H/D exchange were determined for M rise process. Figure 5.9 compares the M rise process for the bcbR crystals in both H_2O and D_2O. In D_2O, both the bcbR crystals fit to a biexponential rise, with a rise time of 157 μs, compared to the rise time for the crystals in H_2O of 18 μs. Figure 5.10 compares the M rise process for native bR in both H_2O and D_2O.

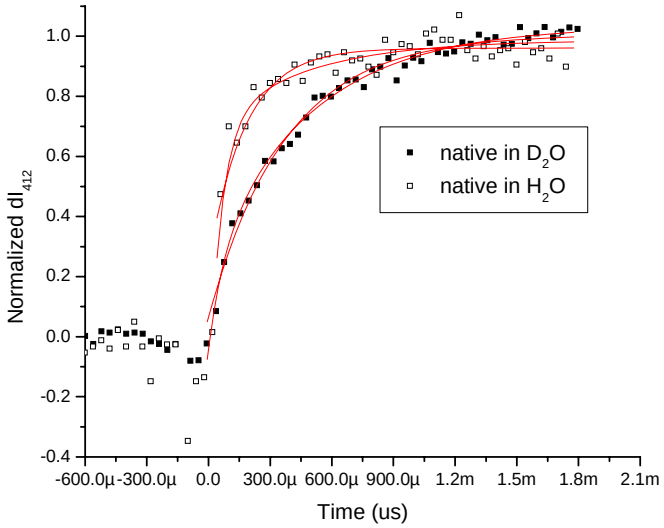

Figure 5.10: Comparison of M rise kinetics in H_2O and D_2O of native bR, expressed as the change in the 412 nm absorption intensity.

In D_2O, the rise time is 380 µs, compared to a rise time of 69 µs in H_2O. Comparing the average M rise time for native in D_2O (380 µs) to the average rise time for native in H_2O (69 µs), kinetic isotope effect (KIE) is 5.5, as reported in Table 5.2. This is in close agreement with the literature[49] for the KIE on the M rise process for native bR, 5.6, also shown in Table 5.2. Comparing the average M rise time for bcbR crystals in D_2O (157 µs) to the average rise time for the crystals in H_2O (18 µs), the KIE is 8.7, as reported in Table 5.2.

Table 5.2: Comparison of kinetic isotope effects (KIE) for both the M rise and M decay processes between native and crystals.

Process Ratio	Time ratio	KIE	Literature KIE[49]
Native M rise avg. D_2O/Native M rise avg. H_2O	380 / 69	5.5	5.6
Crystal M rise avg. D_2O/ Crystal M rise avg. H_2O	157 / 18	8.7	----
Native M decay avg. D_2O/Native M decay avg. H_2O	15 / 9.8	1.6	1.7
Crystal M decay avg. D_2O/ Crystal M decay avg. H_2O	148 / 73	2.0	---

5.14. M decay of bcbR crystals in H_2O

From Figure 5.11 it is observed that the M decay for the bcbR crystals is slower than it is for the native sample. This data for the bcbR crystals fits best to a monoexponential decay, while the decay data for the native sample fits best to a biexponential expression. As mentioned in the introduction, the M decay data for native bR has been characterized in the literature as either a monoexponential[35,36] or a biexponential, with a total decay time in the tens of milliseconds.[18,19] Here for the native samples a biexponential decay is observed with a total decay time of 9.8 ms, given in Table 5.1. For the bcbR crystals, a monoexponential decay with a much longer total decay time of 73 ms is observed. The M decay is over seven times slower for the bcbR crystals than it is in the native.

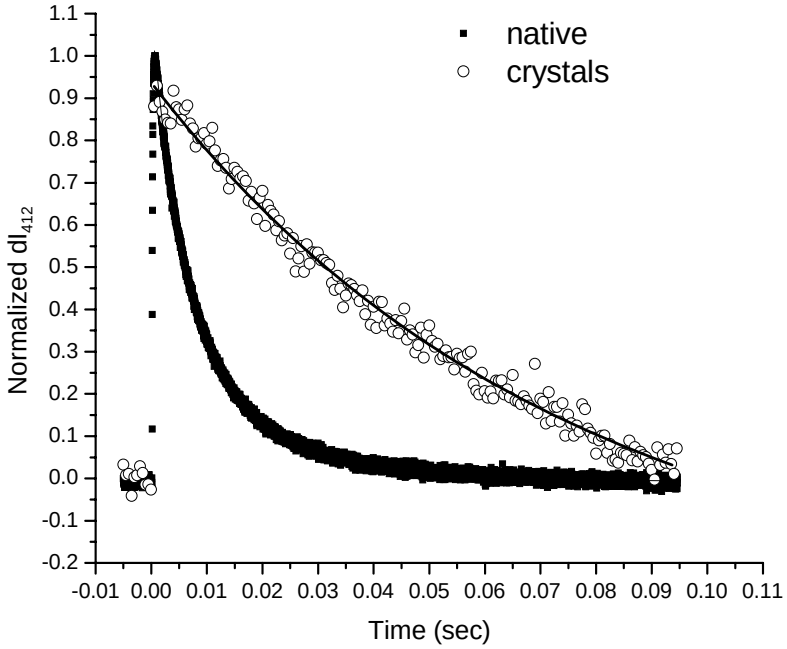

Figure 5.11: Comparison of M decay kinetics in deionized distilled water (DDW), expressed as the intensity of the 412 nm absorption.

As mentioned in the introduction, Heyes and El-Sayed[36] observed that while removal of 75% of the native lipids resulted in a slower M decay relative to the native sample, monomerization of the native sample (trimer structure no longer intact) resulted in a *recovery* of the decay rate such that it was comparable[36] with that of native bR at pH 7. Again, the parallel trimer arrangement of the bR molecules in Rosenbusch and Landau's cbR crystals demonstrated by time-resolved FTIR M kinetics that were essentially identical to that of the native membrane.[45]

From the crystal structure of the bcbR crystal we know that the bR molecules are no longer in the parallel trimer packing structure of the native membrane and the cbR crystals, but are arranged as antiparallel monomers with only one bound lipid per monomer remaining.[44] The trend in the literature is that there is a recovery of M decay kinetics upon monomerization back to a time close to that of the native. In light of this, the fact that the bcbR crystal's M decay rate which is less than seven relative to that in the native sample is surprising.

In both the bcbR crystal and the monomerized native bR solutions, we have a loss of the parallel trimer packing structure found in native bR. However, a key difference between the monomerized native bR solutions and the bcbR crystals is that in the native monomerized samples the monomers are free in solution and so have the ability to tumble and move far away from one another. In the bcbR crystal even though there is a the loss of trimer structure, the monomers are not free to tumble in solution – they are locked in an antiparallel crystal formation. In this packing creation the monomers are not as close together as they are in the parallel trimer structure found in the native, the 75% delipidated, and the cbR crystals, but they are not free to migrate from one another as

they are in the native monomerized solutions. So while the bcbR crystals have a faster M rise rate relative to the native trimer in solution, this does not likewise translate into a faster M decay. The difference in the mobility of the individual bR monomers might account for the longer decay rate relative to the native trimer solution.

Another possible explanation for the slower M decay may be that there is a different H_2O chain structure in the cytoplasmic reprotonation channel of the bcbR crystals that is not organized as well to permit the efficient transfer of H^+ from the Asp_{96} residue to the deprotonated Schiff base. The slower M decay caused by the presence of fewer water molecules in the proton transfer pathway of the bcbR crystals relative to that of the native trimer and native monomer solutions. In native bR and the cbR crystals, M rise is due to the transfer of a proton from retinal's Schiff base to a nearby Asp_{85} residue. However, the M decay is due to the reprotonation of this Schiff base from the Asp_{96} residue in the hydrophobic half-channel. In the native membrane, the Asp_{96} residue is ten to twelve angstroms above the Schiff base; the Asp_{85} residue is closer to the Schiff base, about four angstroms below.[29,48] Henderson *et al*.[50] proposed that there were one to two water molecules in the otherwise hydrophobic reprotonation channel of the native membrane. Perhaps in the bcbR crystal there are fewer water molecules than in the native, or these water molecules are not able to participate as effectively as they do in the native during the reprotonation of retinal's Schiff base, resulting in a slower M decay for the bcbR crystals.

A third possible difference between bcbR crystals and both native and cbR crystals could be a difference in pK_a values for the Asp_{96} residue. If bcbR crystals have

an Asp_{96} residue with a higher pK_a, proton movement from this residue to the deprotonated SB could be hindered, resulting in a slow M decay.

A fourth significant difference between the bcbR and the cbR crystals is the difference in crystal contacts between these two crystal forms. In the cbR crystals, crystal contacts are mediated by organized lipids,[44] with crystal contacts made by lipid-protein interactions within the plane of the membrane, with no protein-protein interactions between trimers.[51] In contrast, in the bcbR crystals the packing involves *extensive* contacts between the protein chains.[44] Each layer of bR crystals grown from bicelles contains two interfaces formed by contacts between two extended hydrophobic surfaces corresponding to the transmembrane region of each monomer .

For the cbR crystals the lipids are holding the bR molecules in the parallel trimer theme. However, the lack of mediating lipids in the bcbR crystal packing means that the bR molecules are now free to arrange themselves as monomers, with their hydrophobic cross sections providing the stabilizing force to hold them in this manner. Perhaps in this antiparallel monomer packing, protons of water molecules are unable to travel as efficiently during the proton transfer from Asp_{96} to the deprotonated Schiff base of retinal as it can in the parallel trimer packing structure.

Finally, a last point to consider in the fast M rise and slow M decay of the bcbR crystals involves the idea of two M states, M_1 and M_2, mentioned in the introduction. In this model, during the $M_1 \rightarrow M_2$ transition the Schiff base redirects its orientation from the extracellular to the cytoplasmic half channel.[19,20,25-28,52] In the case of the bcbR crystals, it may be the case that the M_1 state is in a good proton acceptor configuration such that the rate of M rise process (the donation of a proton to Asp_{85}) is faster relative to the

native membrane and the cbR crystals. In contrast, it may the case that either the M_1-M_2 conversion is slower than usual, or that the M_2 state is not in good proton donor configuration so that the rate of the M decay process (the reprotonation of the Schiff base) is slower relative to the native membrane and cbR crystals.

5.15. M decay of bcbR crystals in D_2O

The kinetic isotope effect after H/D exchange was determined for the M decay processes. Figure 5.12 compares the times for the M decay process for bcbR crystals in both H_2O and D_2O. In D_2O, the decay of the bcbR crystals remains monoexponential and increased to 148 ms, compared to its decay time of 73 ms in H_2O. Figure 5.13 compares the times for the M decay process in native bR in both H_2O and D_2O. In D_2O, the decay of native remains biexponential and increased to 15 ms, compared to its decay time of 9.8 ms in H_2O. These values are all shown in Table 5.1. Comparing the average M decay time for native in D_2O (15 ms) to the average decay time for native in H_2O (9.8 ms), the KIE is 1.6, as given in Table 5.2. This ratio is in close agreement with the literature[49] for the M decay process for native bR (1.7), also shown in Table 5.2. Comparing the average M decay time for crystals in D_2O (148 ms) to the average decay time for crystals in H_2O (73 ms), the KIE is 2.0.

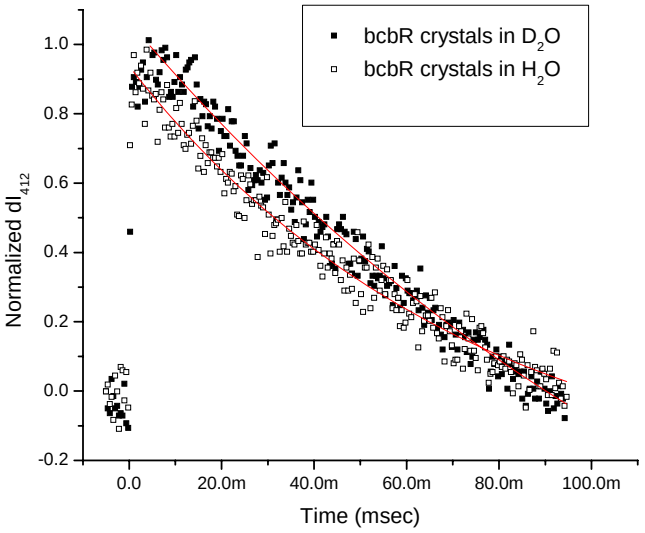

Figure 5.12: Comparison of M decay kinetics in H_2O and D_2O of bcbR, expressed as the change in the 412 nm absorption intensity.

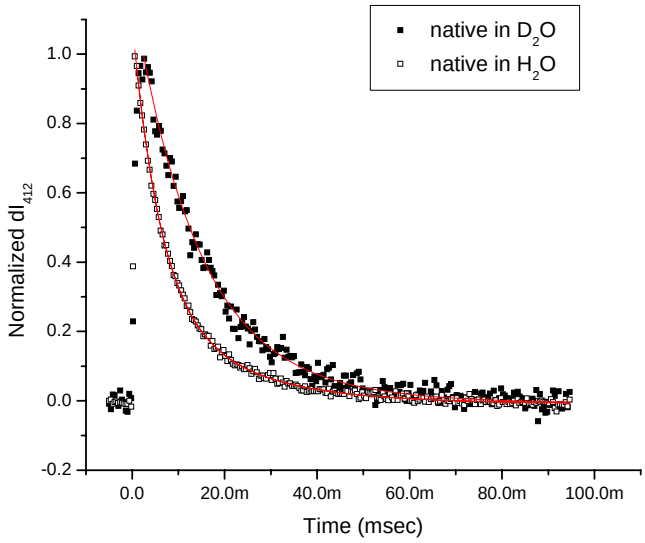

Figure 5.13: Comparison of M decay kinetics in H_2O and D_2O of native bR, expressed as the change in the 412 nm absorption intensity.

5.16. Kinetic Isotope Effect in M Rise and Decay in bcbR Crystals

For the M decay in both the native sample and the crystals, the KIE is about the same (2.0 for the crystals versus 1.6 for native versus). In contrast, for the M rise process, the KIE for the crystals is greater than it is for native (8.7 for crystals versus 5.6 for native). In 1996, le Coutre and Gerwert[49] investigated the kinetic isotope effects after H/D exchange for several reactions in bR and reported a qualitative difference between the intramolecular proton conduction in the proton release and the proton uptake pathways. They noted that a main characteristic of unidirectional proton transfer in a hydrogen bonded network was the presence of two alternating steps: (1) a fast proton displacement within an individual H bond from the donor to acceptor and (2) a slower rearrangement of the H bond to the initial state which involves rotational movements of the respective donor and acceptor groups.[49,53-57] These steps are often referred to as the migration of an ionic and bonding defect ('hop and turn mechanism').[49] In ice the H_2O molecules are highly ordered, forming a hexagonal lattice, where each of the two H donor and acceptor sites are hydrogen bonded to H donor and acceptor sites of adjacent H_2O molecules. The rate limiting step for proton transfer in ice as described as the proton displacement within the H bond.[49,53,54] In contrast, in liquid water the rate limiting step was described to be the rotational movement. The different rate limited steps result in different kinetics isotope effects (KIE's) upon H/D exchange. If the rotational rearrangement is rate limiting, a KIE of $\sqrt{2}$ is observed (1.4), reflecting the mass between proton and deuteron. If the proton displacement within an H bond is rate limiting, much larger KIE's are reported.[49,53,54,57]

In their work on the M rise and decay processes, le Coutre and Gerwert reported that for the L $\rightarrow$ M process (M rise) a KIE of 5.6 was calculated for native bR. In contrast, they reported a KIE of 1.7 for the M$\rightarrow$ N process (M decay).[49] They noted that the strong KIE for M rise indicates proton transfer without rate limiting rotational contributions, and was similar to the one described for ice.[49] They note that the ice-like mechanism during the proton release reaction seems to support an almost irreversible step by increasing the entropy; the proton is expelled from a highly ordered protein environment into the less ordered bulk aqueous phase.[49] In contrast, the lower KIE for M decay suggested to them that the rate-limiting step in the reaction was rotational movement.[49]

From our experiments, we found that the KIE for M rise in the bcbR crystals was much larger than reported for native (8.7 for crystals versus 5.6 for native), while the KIE for M decay in the crystals was about the same as reported for native (2.0 for crystals versus 1.6 for native). The similarity in the KIE for M decay between the native and crystals suggests that in the bcbR crystals, as is the case with native bR, rotational movement (a 'bonding defect') is the rate limiting step in the M decay process. After the retinal Schiff base donates its proton to Asp_{85}, it must rotate itself from the extracellular channel to the cytoplasmic channel to position itself to accept the proton from Asp_{96}.
The similarity in KIE's between native and bcbR crystals for M decay suggests that in both cases rotational motions are necessary for the process to occur.

In contrast, the KIE for M rise in the bcbR crystals was much larger than reported for native. Conservatively, we can say that this means that the rate of the M rise process in the crystals is dictated by only the rate of H transfer, as is the case with native. It is at the

present time unclear why the KIE for M rise in the crystals is larger than that observed in native.

In summary, the rise and decay kinetics of the M intermediate of the photocycle within the bcbR crystals has been characterized as having an M rise that is faster than found in both the native membrane and cbR crystals, and an M decay that is slower than found in both the native membrane and cbR crystals. The faster M rise may be due to an increase in conformational freedom of the monomer units when arranged in this antiparallel manner, or a change in the pK_a of the PSB, while the slower M decay may arise from a variety of possibilities: (1) dehydration of the reprotonation channel, (2) a higher pK_a value for the proton donor Asp_{96}, (3) slower 'switching' of the unprotonated SB from the extracellular to cytoplasmic side, (4) less-than-ideal orientation of the unprotonated SB during reprotonation from Asp_{96}, or some other factor effecting the efficient mobility of protons along the reprotonation pathway between Asp_{96} and the deprotonated retinal. In any case, these results capture the kinetics of the M intermediate of the photocycle. While this and all previous chapters have addressed the motions of the retinal Schiff base within these bcbR crystals, the changes within the protein surrounding this chromophore have not been addressed. In Chapter 6, Fourier Transfer Infrared (FTIR) difference spectroscopy will be used to monitor the protonation/deprotonation of amino acids involved in the creation and decay of the M intermediate in bcbR crystals. Is Asp_{85} still the proton acceptor in the bcbR crystals, or nearby Asp_{212}? Is Asp_{96} still the proton donor during M Decay?

References

(1) Goldschmidt, C. R.; Ottolenghi, M.; Korenstein, R. *Biophysical journal* **1976**, *16*, 839.

(2) Oesterhelt, D.; Hess, B. *European Journal of Biochemistry* **1973**, *37*, 316.

(3) Stoeckenius, W.; Lozier, R. H. *Journal of Supramolecular Structure* **1974**, *2*, 769.

(4) Lozier, R. H.; Bogomolni, R. A.; Stoeckenius, W. *Biophysical Journal* **1975**, *15*, 955.

(5) Jan, L. Y. *Vision Research* **1975**, *15*, 1081.

(6) Henderson, R. *Annual Review of Biophysics and Bioengineering* **1977**, *6*, 87.

(7) Stoeckenius, W.; Lozier, R. H.; Bogomolni, R. A. *Biochimica et Biophysica Acta* **1979**, *505*, 215.

(8) Michel, H.; Oesterhelt, D. *FEBS Letters* **1976**, *65*, 175.

(9) Bakker, E. P.; Rottenberg, H.; Caplan, S. R. *Biochimica et biophysica acta* **1976**, *440*, 557.

(10) Belyakova, T. N.; Kadziauskas, J.; Skulachev, V. P.; Smirnova, I. A.; Chekulaeva, L. N.; Jasaitis, A. *Doklady Akademii Nauk SSSR* **1975**, *223*, 483.

(11) Lanyi, J. *Biochemica et Biophysica Acta* **1993**, *1183*, 241.

(12) Glaeser, R. M.; Jubb, J. S.; Henderson, R. *Biophysical journal FIELD Publication Date:1985 Nov* **1985**, *48*, 775.

(13) Nuss, M. C.; Zinth, W.; Kaiser, W.; Koelling, E.; Oesterhelt, D. *Chemical Physics Letters* **1985**, *117*, 1.

(14) Lanyi, J. K. *Journal of Physical Chemistry B* **2000**, *104*, 11441.

(15) Kataoka, M.; Kamikubo, H. *Biochimica et Biophysica Acta* **2000**, *1460*, 166.

(16) Slifkin, M. A.; Caplan, S. R. *Nature* **1975**, *253*, 56.

(17) Hendler, R. W.; Dancshazy, Z.; Bose, S.; Shrager, R. I.; Tokaji, Z. *Biochemistry* **1994**, *33*, 4604.

(18) Hanamoto, J. H.; Dupuis, P.; El-Sayed, M. A. *Proceedings of the National Academy of Sciences of the United States of America* **1984**, *81*, 7083.

(19) Varo, G.; Lanyi, J. K. *Biochemistry* **1990**, *29*, 2241.

(20) Varo, G.; Lanyi, J. K. *Biochemistry* **1991**, *30*, 5008.

(21) Balashov, S. P.; Govindjee, R.; Ebrey, T. G. *Biophysical Journal* **1991**, *60*, 475.

(22) Eisfeld, W.; Althaus, T.; Stockburger, M. *Biophysical Chemistry* **1995**, *56*, 105.

(23) Hendler, R. W.; Shrager, R. I.; Bose, S. *Journal of Physical Chemistry B* **2001**, *105*, 3319.

(24) Oka, T.; Yagi, N.; Tokunaga, F.; Kataoka, M. *Biophysical journal* **2002**, *82*, 2610.

(25) Perkins, G. A.; Liu, E.; Burkard, F.; Berry, E. A.; Glaeser, R. M. *Journal of structural biology* **1992**, *109*, 142.

(26) Lanyi, J. K. *Acta physiologica Scandinavica. Supplementum* **1992**, *607*, 245.

(27) Varo, G.; Lanyi, J. K. *Biochemistry* **1991**, *30*, 5016.

(28) Schatzler, B.; Dencher, N. A.; Tittor, J.; Oesterhelt, D.; Yaniv-Checover, S.; Nachliel, E.; Gutman, M. *Biophysical Journal* **2003**, *84*, 671.

(29) Gerwert, K.; Hess, B.; Soppa, J.; Oesterhelt, D. *Proceedings of the National Academy of Sciences of the United States of America* **1989**, *86*, 4943.

(30) Logunov, S. L.; Song, L.; El-Sayed, M. A. *Journal of Physical Chemistry* **1994**, *98*, 10674.

(31) Li, Q.; Ebrey, T. G. *Photochemistry and Photobiology* **1986**, *44*, 515.

(32) Lin, G. C.; Awad, E. S.; El-Sayed, M. A. *Journal of Physical Chemistry* **1991**, *95*, 10442.

(33) Takeuchi, Y.; Ohno, K.; Yoshida, M.; Nagano, K. *Photochemistry and Photobiology* **1981**, *33*, 587.

(34) Marinetti, T.; Mauzerall, D. *Proceedings of the National Academy of Sciences of the United States of America* **1983**, *80*, 178.

(35) Jang, D. J.; El-Sayed, M. A. *Proceedings of the National Academy of Sciences of the United States of America* **1988**, *85*, 5918.

(36) Heyes, C. D.; El-Sayed, M. A. *Biophysical Journal* **2003**, *85*, 426.

(37) Dencher, N. A.; Kohl, K. D.; Heyn, M. P. *Biochemistry* **1983**, *22*, 1323.

(38) Ohno, K.; Takeuchi, Y.; Yoshida, M. *Photochemistry and Photobiology* **1981**, *33*, 573.

(39) Shrager, R. I.; Hendler, R. W.; Bose, S. *European journal of biochemistry / FEBS* **1995**, *229*, 589.

(40) Kates, M. *Techniques of Lipidology: Isolation, Analysis, and Identification of Lipids*; American Elsevier Publishing Company, Inc.: New York, NY, 1973.

(41) Dracheva, S.; Bose, S.; Hendler, R. W. *FEBS letters* **1996**, *382*, 209.

(42) Hendler, R. W.; Dracheva, S. *Biochemistry (Moscow, Russian Federation)(Translation of Biokhimiya (Moscow, Russian Federation))* **2001**, *66*, 1311.

(43) Szundi, I.; Stoeckenius, W. *Proceedings of the National Academy of Sciences of the United States of America* **1987**, *84*, 3681.

(44) Bowie, J.; Farham, S. *Journal of Molecular Biology* **2002**, *316*, 1.

(45) Heberle, J.; Buldt, G.; Koglin, E.; Rosenbusch, J. P.; Landau, E. M. *Journal of molecular biology* **1998**, *281*, 587.

(46) Danshina, S. V.; Drachev, L. A.; Kaulen, A. D.; Skulachev, V. P. *Photochemistry and Photobiology* **1992**, *55*, 735.

(47) Landau, E. M.; Rosenbusch, J. P. *Proceedings of the National Academy of Sciences of the United States of America* **1996**, *93*, 14532.

(48) Braiman, M. S.; Mogi, T.; Marti, T.; Stern, L. J.; Khorana, H. G.; Rothschild, K. J. *Biochemistry* **1988**, *27*, 8516.

(49) le Coutre, J.; Gerwert, K. *FEBS letters* **1996**, *398*, 333.

(50) Henderson, R.; Baldwin, J. M.; Ceska, T. A.; Zemlin, F.; Beckmann, E.; Downing, K. H. *Journal of Molecular Biology* **1990**, *213*, 899.

(51) Belrhali, H.; Nollert, P.; Royant, A.; Menzel, C.; Rosenbusch, J. P.; Landau, E. M.; Pebay-Peyroula, E. *Structure (London)* **1999**, *7*, 909.

(52) Oka, T.; Yagi, N.; Tokunaga, F.; Kataoka, M. *Biophysical Journal* **2002**, *82*, 2610.

(53) Eigen, M. *Angewandte Chemie* **1963**, *75*, 589.

(54) Eigen, M.; deMaeyer, L. *Proceedings of the Royal Society of London A* **1958**, *247*, 505.

(55) Nagle, J. F.; Tristram-Nagle, S. *Journal of Membrane Biology* **1983**, *74*, 1.

(56) Nagle, J. F.; Morowitz, H. J. *Proc. Natl. Acad. Sci. U.S.* **1978**, *75*, 298.

(57) Agmon, N. *Chemical Physics Letters* **1995**, *244*, 456.

CHAPTER 6

DETERMINATION OF THE ROLE OF ASPARTATE RESIDUE IN THE FUNCTION OF BCBR CRYSTALS BY FTIR DIFFERENCE SPECTROSCOPY*

Abstract

The primary goal of this chapter is to examine changes in the FTIR spectrum of a mass of deuterated bcbR crystals upon irradiation of the sample with the 514 nm line of an Argon laser. Unlike the previous chapters using Raman and visible spectroscopy, which allow us only to examine changes in the retinal Schiff base chromophore, FTIR spectroscopy allows us to examine the changes in the environment surrounding this chromophore, such as changes in the protonation state of surrounding amino acids. From the work done up to this point, it is understood that the bcbR crystals are capable of undergoing the photocycle (evidenced by formation of the M intermediate) and that the rise time of M in the crystals is faster than that observed for both native bR and cbR crystals in water, with a decay time that is much slower than both. However, one of the questions that still remains that can be answered by FTIR spectroscopy is the fate of the transferred proton. Is the Asp_{85} residue the proton acceptor during the formation of M, (as is the case in both the native membrane and in the cbR crystals), or is the nearby Asp_{212} the proton acceptor in the M rise of bcbR crystals? This chapter examines the pathway of the proton as the protonated Schiff base is deprotonated. In this manner, we examine the difference or similarity of the proton pump mechanism between bcbR crystals and native bR.

* Manuscript in preparation

6.1. Detecting the Changes in Amino Acid Protonation States in bcbR crystals During Their Photocycle by FTIR Difference Spectroscopy

One of the main complications arising in using FTIR spectroscopy to study changes in the IR spectrum upon photoexcitation of bR in general is the interference of water, which has a large absorption in the same 2000-1000 cm^{-1} region where protein vibrations are observed. Since bR needs to be hydrated to pump protons, the water concentration needs to be controlled – it cannot be so great that it swamps out small changes occurring in the protein, but it cannot be so little that the protein is not hydrated enough to function. Since bR crystallized by either the cbR or the bcbR method involves the presence of detergents, an additional complication arises in their absorption in this same wavenumber range as well. However, unlike the bR protein, the detergents used in both methods are not responsive to visible light. This means when a sample of bR crystals and detergent molecules are irradiated with a green laser (514 nm) only the crystals will respond to light. This is what makes FTIR difference spectroscopy the method of choice for examining changes in the IR spectrum of bR protein crystals.

Recently, Heberle *et al.*[1] used FTIR difference spectroscopy to view the protonation and deprotonation of aspartate residues in cbR crystals. The difference spectra for both a hydrated native membrane and for several cbR crystals are shown in Figure 6.1. The creation of the M intermediate upon steady laser photoexcitation is detected by both the presence of the negative band at 1528 cm^{-1}, (the C=C stretch of the decreasing protonated retinal Schiff base population), and the positive band at 1566 cm^{-1}, (the C=C stretch of the deprotonated retinal Schiff base). A change in the protein conformation is detected by the shift in the amide I frequency from 1670 to 1650 cm^{-1},

observed by a negative band at 1670 and a positive band at 1650 cm^{-1}. Protonation of the Asp_{85} residue is confirmed by the positive band at 1755 cm^{-1}. Deprotonation of the Asp_{96} residue is confirmed by the appearance of the negative band at 1743 cm^{-1}. These experiments were used as a guide to performing FTIR difference spectroscopy on bcbR crystals that had been removed from their detergent matrix.

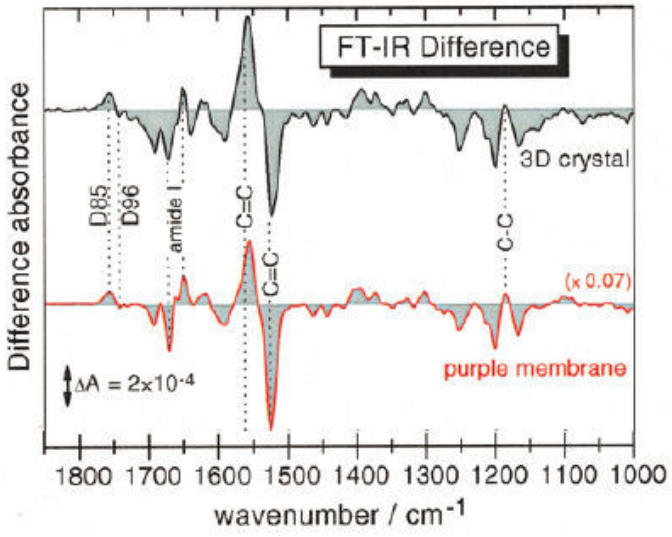

Figure 6.1: Changes in the FTIR spectrum upon excitation with 514 nm laser for several cbR crystals within their detergent matrix (above) and for a native hydrated membrane (below) as detailed by Heberle *et al.*[1]

Experimental

6.2. FTIR Difference Experiments

Bicelle bR (bcbR) crystals were removed from their detergent matrix by the washing method described in Chapter 3. Because the technique is not a micro-scale experiment, a

large volume of crystals needed to be used to achieve maximum signal. A large volume of crystals in either H_2O or D_2O was concentrated on a single 25 mm x 2 mm CaF_2 window (Harrick Scientific Products, Pleasantville, NY) by allowing the water to evaporate under ambient temperature, light, and pressure. During this process, a small pipette was used to blow the edges of the drop toward the center, to prevent the spreading out of crystals over a large area of the window. Once a sample spot of approximately 10 mm was formed and the crystals were fixed to the window, the single window was placed in the sample chamber of a Nicolet Magna 860 FTIR Spectrometer (Thermo Nicolet Instruments, Madison, WI) and the spectrum was checked in the 4000-1000 cm^{-1} range to make sure that either H_2O or D_2O was present but not saturating. A typical spectrum for a mass of bcbR crystals that were soaked in D_2O instead of DDW was taken at this stage is shown in Figure 6.2.

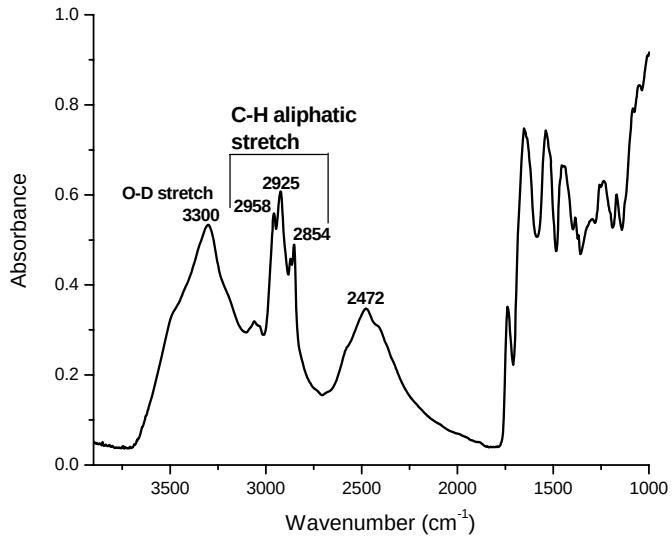

Figure 6.2: Typical FTIR absorption spectrum for a mass of bcbR crystals soaked in D_2O on a single CaF_2 window in the 4000-1000 cm^{-1} region.

This spectrum clearly shows that bulk D_2O is present but not saturating in the 3300 cm^{-1} region. An inset of the protein absorption bands in Figure 6.3 shows that the C=O stretch, N-H bend, and N-D bends of the protein are all clearly observed. The 1741 cm^{-1} band is due to the C=O stretch of the ester group in the DMPC detergent. Here the amide I C=O stretching of the protein is observed at 1660 cm^{-1}, the amide II N-H bending of the protein is observed at 1537 cm^{-1}, and the N-D bending is observed at 1442 cm^{-1}.

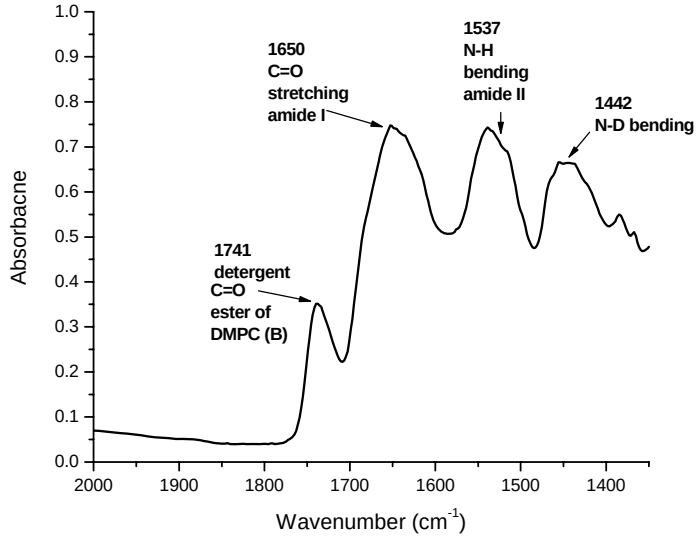

Figure 6.3: Inset of the protein region from above from 2000-1350 cm^{-1}.

Regardless of whether D_2O or H_2O was used, the spectrum was checked in this way to determine if the protein hydration levels were acceptable. Vacuum grease was added to the perimeter of this CaF_2 window, with a second window added. The two windows were additionally sealed held together by parafilm. The vacuum grease served

as an additional barrier to seal in the hydration level of the sample between the windows. The sealed CaF_2 windows were placed in a Harrick temperature control cell and then placed in the sample chamber of the FTIR spectrometer. The temperature was adjusted to 5.0ºC.

A series of optics directed the 514 nm line of an Innova 300 Argon laser (Coherent, Santa Clara, CA) into the sample chamber of the spectrometer. The power at the sample was adjusted to 10 mW/cm^2, as described in the literature.[1] An overhead diagram of this bench is shown in Figure 6.4.

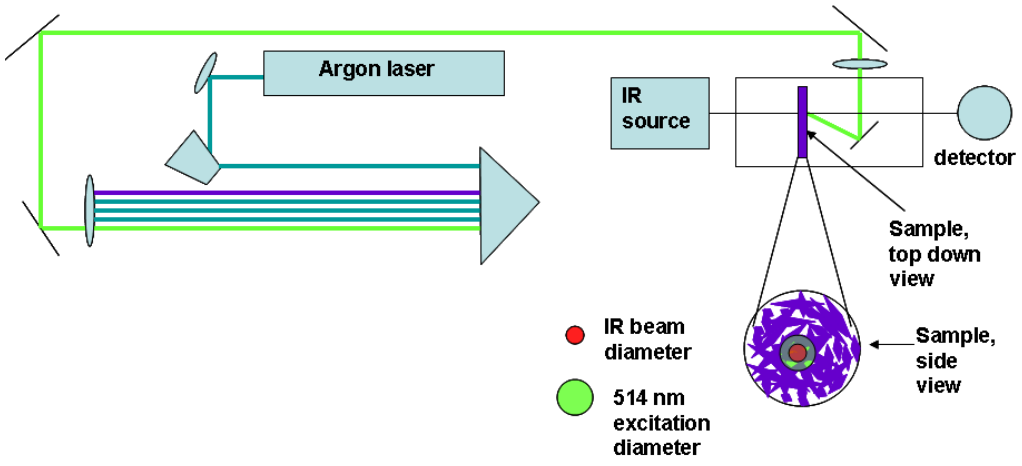

Figure 6.4: Overhead bench setup for FTIR difference spectroscopy experiments.

The 514 nm line is selected and sent to the FTIR bench. The location of the power meter used to adjust the laser power to 10mw/cm^2 is indicated. The diameter of the 514 nm laser must be kept either equal to or greater than the IR beam sampling area, to ensure

that all crystals within the IR sampling area are being excited by the 514 nm line. Initial attempts at taking the difference spectrum of either native membrane or a mass of bcbR crystals were hampered by the presence of a fluctuating water concentration. Figure 6.5 illustrates three different attempts to obtain the difference spectrum of native bR in H_2O at 5ºC. Although the positive 1760 cm^{-1} band (protonated Asp_{85}) and the negative 1528 cm^{-1} band (depletion of the C=C stretching of protonated retinal) are present, the large positive 1560 cm^{-1} band that would indicate creation of the C=C of deprotonated retinal (the M state) is not clearly observed. In addition, the shift in the amide I frequency from 1670 to 1650 cm^{-1} observed in the literature[1] is not observed. Large negative bands appear at 1590 and 1645 which are not described in the literature.

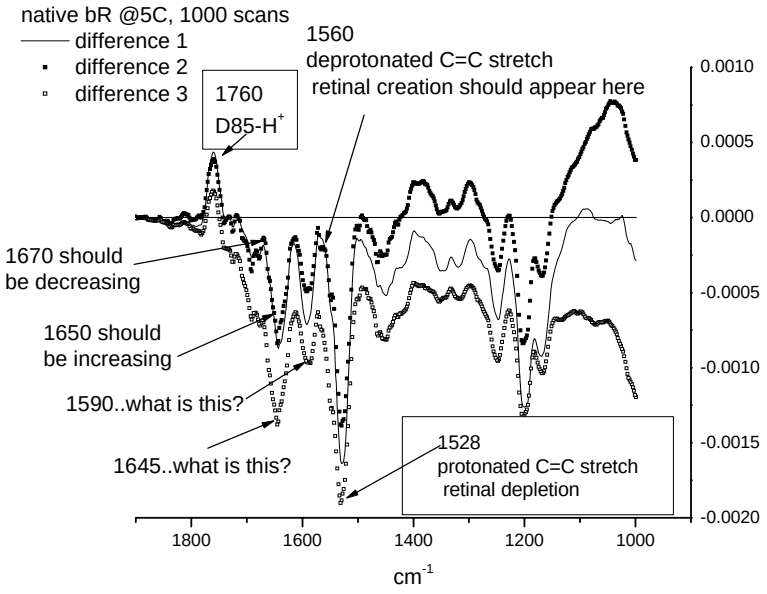

Figure 6.5: Three different attempts to replicate the IR difference spectrum of native bR in H_2O at 5ºC.

As mentioned earlier in the chapter, water vapor appears in the same region of the IR spectrum as do protein vibrations. The Nicolet Magna 860 bench is purged by a 74-5041 FT-IR Purge Gas Generator (Parker Bolston Analytical Gas Systems, Cleveland, OH). This gas generator compresses surrounding air to 80 psi, and passes the air through filters that remove CO_2 and H_2O before passing the air to the bench via ¼" OD Teflon tubing at a flow rate of approximately 20 SCFH. For the difference experiment to be successful, the water vapor concentration does not need to be 100% absent, as long as the concentration does not fluctuate on a scale larger than differences in the protein upon laser excitation. If the water vapor concentration is constant throughout the data acquisition time, its intensity in the spectrum remains constant and it is subtracted out in difference spectroscopy to only reveal changes in the protein and retinal during irradiation. However, if the water vapor concentration is fluctuating (due to an inefficient purge, for example), then the difference spectrum of the protein is overlaid with interfering water bands. To confirm that this was the case, a series of spectra were taken of an empty sample chamber of the FTIR bench after the sample chamber was closed and had been purging overnight. Figure 6.6 shows four different 'background' spectra of the empty FTIR sample chamber. Each spectrum is the result of an average of 5 scans and were all taken with in the same one-minute sampling period. Figure 6.7 shows the difference spectra resulting from subtracting the second background from the first, the third background from the second, and so on. For a steady purge, these difference spectra should be as flat as possible, or at least smaller than the changes expected in the difference experiment with sample in the chamber. The %T scale indicates that not only

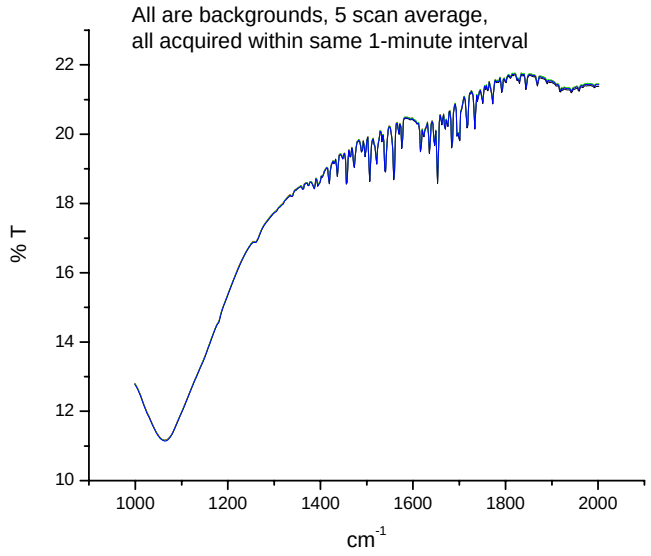

Figure 6.6: Four different 'background' spectra of the empty FTIR sample chamber.

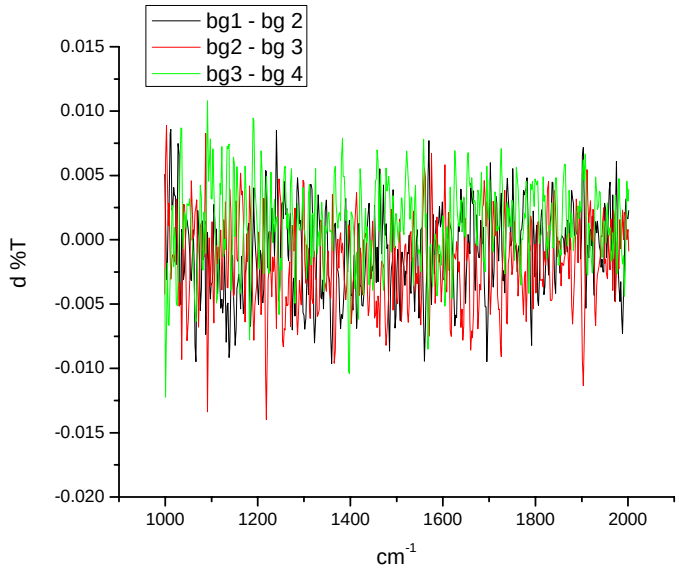

Figure 6.7: Differences between the background spectra of Figure 6.6.

is the water vapor background fluctuating, but that it is fluctuating to produce noise on a larger scale than the data would.

A Bruker v66 model FTIR spectrometer (Bruker Optics, Billerica, MA) was used by Heberle *et al.*[1] in the difference spectroscopy performed on cbR crystals. This bench features a vacuum sample chamber, which eliminates water completely. In contrast, the sample chamber for the Nicolet Magna 860 bench used for these bcbR difference experiments is not under vacuum purge, but instead uses the Whatman 74-5041 FT-IR Purge gas generator (Parker Hannafin, Cleveland, OH. This purge gas generator uses a Gast 2HAH-11T-M200X compressor (Whatman Inc, Haverhill, MA) that intakes lab air and compresses it to approximately 80 psi. The temperature of this hot compressed air is then lowered by sending it through an aftercooler. After this point it is then sent through a set of prefilters before it travels through the two regenerative desiccant driers (towers) that alternate between each other to remove residual water and CO_2.

Dr. Bridgette Barry of the Georgia Tech School of Chemistry and Biochemistry was consulted about the issue of insufficient water vapor removal. After this meeting, modification of the present bench was undertaken to include a desiccant column through which the compressed air must pass between the compressor to the instrument. It was anticipated that this additional stage would filter out the residual water vapor getting into the bench. The desiccant column was a LabClear model DGF-250 Disposeable gas filter with ¼" OD fittings and 600 cc volume (Labclear, Oakland, CA). The filter contained both indicating Drierite desiccant and #13x molecular sieve.

After the desiccant column was added to the inlet to the FTIR spectrometer, the change in the spectrum of the empty FTIR chamber was monitored for a period of two

days to determine the effectiveness of the new column to maintain a more stable environment. Figure 6.8 shows the changes in the difference spectrum of the sample-free chamber before the column was added, taken at 30-minute intervals apart. Here the large fluctuations indicate that the humidity of the sample chamber is fluctuating with time. Figure 6.9 shows the sample-free chamber after it has been purged through the new desiccant column for a period of two days. The much smaller fluctuation indicates that the column is stabilizing the humidity level of the bench. At this point experiments were resumed with native bR first.

The native sample was prepared as described in Section 6.2, except that a temperature control cell was not used for this and all following experiments. The native sample in H_2O was allowed to dry on a CaF_2 window until the level of hydration was satisfactory as described by checking the OH stretch region above. A second CaF_2 window was placed on top, and vacuum grease was used to seal the windows together, with parafilm sealing the windows together as mentioned above. The sample was placed in the FTIR chamber, adjusted to give maximum signal, and the chamber door closed. The sample was allowed to purge overnight before any measurements were taken. The following day, thirty scans were taken of the native sample with the laser off, and another thirty scans were taken immediately afterward with the 514 nm laser power at 15 mW/cm^2. The mirror velocity was 0.6329; the aperture was set to 50. The 'laser on' spectrum was subtracted from the 'laser off' spectrum.

Since the spectrum of a sample of crystals gives much lower signal, more sample spectra were needed to observe the small changes. A sample of crystals in H_2O was concentrated on a single CaF_2 window as described in Section 6.2. This single window

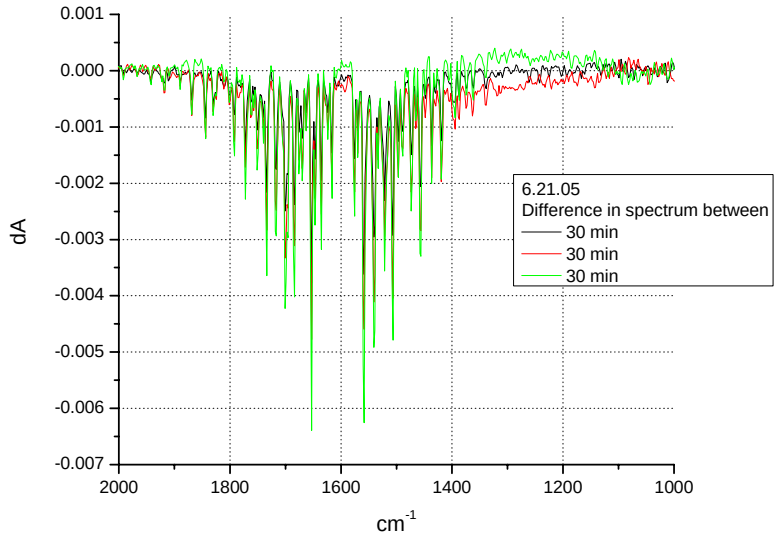

Figure 6.8: Changes in the difference spectrum of the empty sample chamber before the column is added, taken at 30-minute intervals apart.

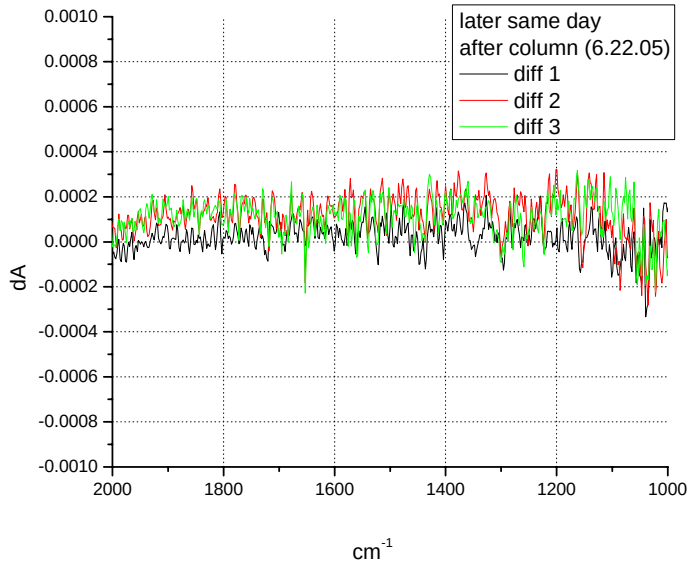

Figure 6.9: Changes in the difference spectrum of the empty sample chamber after the column is added, taken at 30-minute intervals apart.

was inserted into the sample chamber and the intensity of the signal for bulk water at 3300 cm^{-1} was checked to make sure bulk water was present but not saturating. Typical Absorption spectra at this point were similar to that observed in Figure 6.2. After this point a second CaF_2 window was sealed over the first with vacuum grease, and parafilm was also used to keep the two windows together. The sample was placed in the chamber to purge overnight before any spectra were taken.

The following day a series of spectra were taken to experiment with the collection time and sample aperture in order to record the largest difference spectra without damaging the crystals. The optimum difference spectra resulted from exposure of the crystals to 15mW/cm^2 of 514 nm laser for 500 scans (approximately 8 minutes at a mirror velocity of 0.6329) with a sample aperture of 150. The laser was blocked and a 500-scan of the crystals was taken immediately afterward. This process was repeated 47 times to give 47 difference spectra for the crystals. These were averaged to give a single difference spectrum for the crystals. This process was repeated for both the native sample in D_2O and the mass of crystals in D_2O as well.

Results and Discussion

Figure 6.10 is a comparison the FTIR absorbance difference spectrum resulting from subtraction of the 'laser off' spectrum from that of the 'laser on' spectrum for a sample of bcbR crystals in H_2O (A) and a sample of native bR in H_2O (B). The positive band in both spectra at 1760 cm^{-1} has been characterized in the literature[1-4] as the C=O stretch of the protonated Asp_{85} residue. The positive band at 1557 cm^{-1} in the bcbR crystals (A) and

at 1565 cm^{-1} in the native (B) is due to the C=C stretching of the parent deprotonated retinal in the M intermediate.[1,2] The negative band at 1521 cm^{-1} in both spectra is due to the C=C stretching of protonated retinal[1,5-13] (depletion of the parent bR_{568}). The three negative bands at 1248, 1197, and 1162 cm^{-1} in the bcbR crystals (A) and at 1249, 1203, and 1168 cm^{-1} in native bR (B) are due to depletion of the C-C stretches of the parent bR_{568} upon irradiation.[1,11]

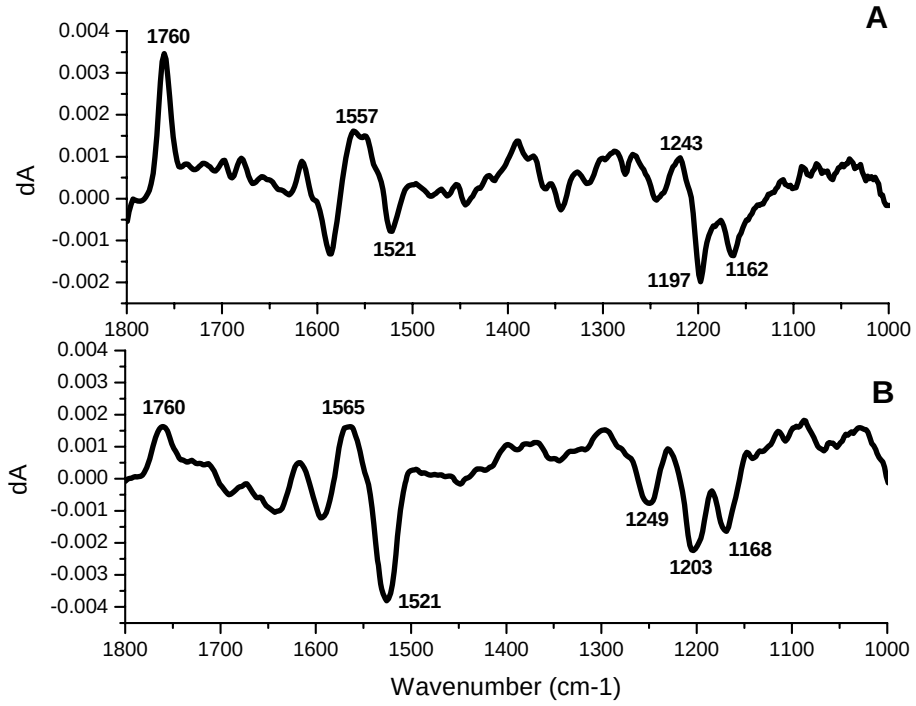

Figure 6.10: Difference spectrum of a mass of bcbR crystals in H_2O (A) and of native bR in H_2O (B).

Figure 6.11 is a comparison the FTIR absorbance difference spectrum resulting from subtraction of the 'laser off' spectrum from that of the 'laser on' spectrum for a sample of bcbR crystals in D_2O (A) and a sample of native bR in D_2O (B). The positive band in

both spectra at 1760 cm^{-1} has been characterized in the literature[1-4] as the C=O stretch of the protonated Asp_{85} residue. The positive band at 1558 cm^{-1} in the bcbR crystals (A) and at 1565 cm^{-1} in the native (B) is due to the C=C stretching of the parent deprotonated retinal in the M intermediate.[1,2] The negative band at 1525 cm^{-1} in both spectra is due to the C=C stretching of protonated retinal[1,5-13] (depletion of the parent bR_{568}). The three negative bands at 1245, 1200, and 1164 cm^{-1} in the bcbR crystals (A) and at 1251, 1200, and 1166 cm^{-1} in native bR (B) are due to depletion of the C-C stretches of the parent bR_{568} upon irradiation.[1,11]

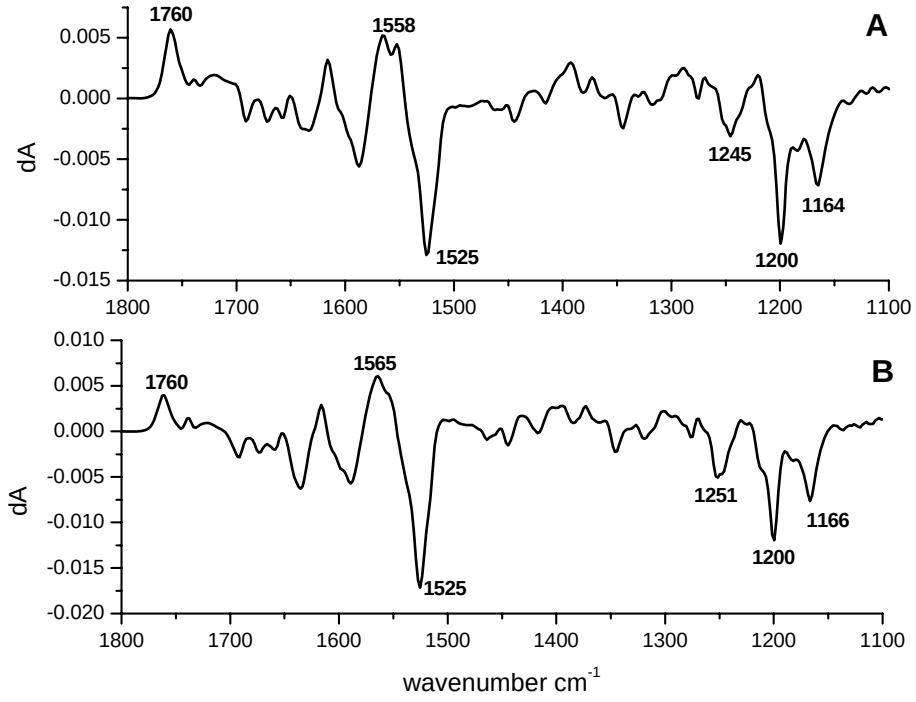

Figure 6.11: Difference spectrum of a mass of bcbR crystals in D_2O (A) and of native bR in D_2O (B).

In summary, FTIR difference spectroscopy on both a hydrated or deuterated mass of bcbR crystals indicates that in the bcbR crystals that deprotonation of the retinal Schiff base results in the transfer of a proton to the Asp_{85} residue. In this respect the bcbR crystals are similar to native bR. In contrast, the deprotonated C=C stretch region of the retinal Schiff base in the bcbR crystals is broader than that of native, which may indicate that in the bcbR crystals there is a heterogeneity in environment surrounding the deprotonated Schiff base relative to that observed for native.

References

(1) Heberle, J.; Buldt, G.; Koglin, E.; Rosenbusch, J. P.; Landau, E. M. *Journal of molecular biology* **1998**, *281*, 587.

(2) Rodig, C.; Siebert, F. *FEBS Letters* **1999**, *445*, 14.

(3) Braiman, M. S.; Mogi, T.; Marti, T.; Stern, L. J.; Khorana, H. G.; Rothschild, K. J. *Biochemistry* **1988**, *27*, 8516.

(4) Fahmy, K.; Weidlich, O.; Engelhard, M.; Tittor, J.; Oesterhelt, D.; Siebert, F. *Photobiochemistry and Photobiology* **1992**, *56*, 1073.

(5) Mathies, R.; Freedman, T. B.; Stryer, L. *Journal of molecular biology* **1977**, *109*, 367.

(6) Oseroff, A. R.; Callender, R. H. *Biochemistry* **1974**, *13*, 4243.

(7) Hildebrandt, P.; Stockburger, M. *Biochemistry* **1984**, *23*, 5539.

(8) Stockburger, M.; Klusmann, W.; Gattermann, H.; Massig, G.; Peters, R. *Biochemistry* **1979**, *18*, 4886.

(9) Braiman, M.; Mathies, R. *Biochemisrtry* **1980**, *19*, 5421.

(10) Henderson, R.; Sulkes, M.; Lewis, A.; Marcus, M. A. *Biochemistry* **1978**, *17*, 4712.

(11) Althaus, T.; Eisfeld, W.; Lohrmann, R.; Stockburger, M. *Israel Journal of Chemistry* **1995**, *35*, 227.

(12) Chronister, E. L.; El-Sayed, M. A. *Photochemistry and Photobiology* **1987**, *45*, 507.

(13) Aton, B.; Doukas, A. G.; Callender, R. H.; Becher, B.; Ebrey, T. G. *Biochemistry* **1977**, *16*, 2995.

CHAPTER 7

MODEL SYSTEM FOR GROWING AND QUANTIFYING *STREPTOCOCCUS PNEUMONIAE* BIOFILMS IN SITU AND IN REAL TIME[*]

Abstract

In this chapter, ATR/FTIR is used to monitor the changing IR spectrum during the attachment and growth of a biofilm created by the organism *Streptococcus pneumoniae.* This organism was chosen because of its clinical relevance; it is one of the organisms suspected in forming biofilms in individuals who develop otitis media, one of the most common causes of ear infections of childhood.[1] In this study, a novel model system was developed for growing and characterizing in time the continuous deposition of a *S. pneumoniae* biofilm on both a Germanium internal reflection element (IRE) and on several Germanium coupons and was monitored by a combination of ATR/FTIR and Epifluorescence microscopy. In contrast to previous ATR/FTIR experiments examining the formation of biofilms on surfaces, this method is unique in that combines two techniques - ATR/FTIR and Epifluorescence microscopy – which used together allow for the simultaneous monitoring of the IR spectrum of the *S. pneumoniae* biofilm as it develops and as provides a method for quantifying total and viable cell counts at various stages during the development. The formation of both the protein and the polysaccharide were followed in time by monitoring their IR bands in the IR spectrum and were

[*] Manuscript published: Donlan, Rodney M., Piede, J.A., Heyes, C.D., Sanii, L.S., Murga, R., Edmonds, P., El-Sayed, I. El-Sayed, M.A. "Model System for Growing and Quantifying Streptococcus Pneumoniae Biofilms In Situ and in Real Time". *Applied and Environmental Microbiology*. 70, 8, 4980-4988.

correlated with the total and viable biofilm cell counts to quantify the biofilm-associated cells.

7.1 - Biofilms: Their Infrastructure and Effects on Surfaces

Microorganisms in both natural and artificial environments attach to solid surfaces and surface films. Both the solute and/or adsorbates can serve as nutrients for these organisms, which excrete extracellular polymers, resulting in biofilms.[2] Biofilms are made up of both cells and extracellular polymeric substances (EPS). The EPS matrix network connects cells with one another and attach then to the surface.[3] These biofilms are vibrant environments capable of changing the chemistry of the surface to which they are attached, as well as both the chemistry of the aqueous and interfacial phase.[4] These changes can have either positive or negative impacts. On the positive side, biofilms are responsible for the removal of pollutants from natural waters[4] and the functioning of sewage treatment plants.[5] On the negative side, biofilms reduce the heat transfer efficiency in heat exchange units,[6] enhance the corrosion of metal structures, are a contamination source of ultrapure water systems, and increase the drag on ships.[7]

7.2 - Problems Biofilms Present to the Medical Field

Life within the biofilm may provide advantages over a solely planktonic existence. Biofilm microorganisms can utilize nutrients from a wide range of sources, including the liquid phase, adsorbed components, metabolites from other attached organisms, and

surface degradation products. In addition, biofilm microbes are less susceptible to antibiotics[8] and biocides.[9]

These last two properties of biofilms are particularly relevant to the medical field. For example, the premature failure of implanted devices, catheters, and transcutaneous devices[10-14] are often caused by the reaction of soft tissues with these synthetic materials, leading to chronic inflammation. Although some degree of inflammation is to be expected with implanted materials, those becoming the locus for bacterial infection must either be replaced, or the resulting infection is alternatively treated like a chronic illness.[15] The body's immune system normally keeps the bacterial population under control. Once bacteria adhere to a surface, however, they may form a biofilm in which the bacterial cells are protected from antagonistic agents (i.e., antibiotics or phagocytic cells) that would otherwise destroy the bacteria. In addition, the components of the EPS of bacteria can also regulate the cellular immune response.[16]

7.3 Biofilm Studies: Background

The earliest biofilm studies (1933) utilized direct light microscopic techniques to qualitatively examine stained cells attached to transparent surfaces.[17] Through the years, several other techniques were used. Phase contrast and transmitted differential interference contrast (DIC) optics were used to examine microscopically unstained preparations in a non-destructive manner.[18] High resolution scanning electron microscopy (SEM) and transmission electron microscopy (TEM) offer additional information on biofilm structure and adhesive structures and matrix materials produced

by microorganisms associated with biofilms.[19] The downside to all the above methods is that they are ultimately destructive in nature, introducing distortions in spatial relationships between structures during sample dehydration. Their labor-intensive sample preparation and non-quantitative nature of the information provided make it generally not amendable to routine biofilm monitoring.[20]

A few on-line monitoring devices have been developed to monitor biofilm attachment based on fluid flow resistance or heat influx.[21] These techniques rely heavily on mathematical models based on system engineering parameters to predict biofilm formation and accumulation. However, by the time these sense that biofilm formation has occurred, the system may have become fouled to the extent that subsequent remedial treatments are not effective.[22] There is a real need for biofilm monitoring equipment that permits remote, sensitive, non-destructive, and more important, a molecular real-time analysis of biofilm formation.[20]

7.4 Nondestructive Biofilm Analysis: Use of ATR/FTIR

The lack of sensitive on-line techniques to effectively monitor the biofilm attachment, development, and chemistry both remotely and non-destructively, and on a molecular level, have limited our insight into the formation mechanism on the surface. Most monitoring techniques to study the growth of microbes have been developed primarily for measurements in the bulk aqueous phase. Unfortunately, since biofilm growth is a phenomenon localized to solid surfaces, conventional monitoring techniques are usually insensitive to most biofilm processes.[20] Often biochemical and microscopic biofilm

studies attempt a quantitative removal of surface films and destructive off-line analysis. Attenuated total reflection/Fourier transform infrared spectroscopy (ATR/FTIR) provides a non-destructive analysis of biofilms, circumventing the need for quantitative film removal by providing real-time FTIR spectrum at specified time intervals during the deposition of the film upon a surface. In ATR/FTIR, infrared (IR) spectroscopy involves multiply reflected IR beams on the inner surface of an internal reflection element (IRE)[23] as shown in Figure 7.1.

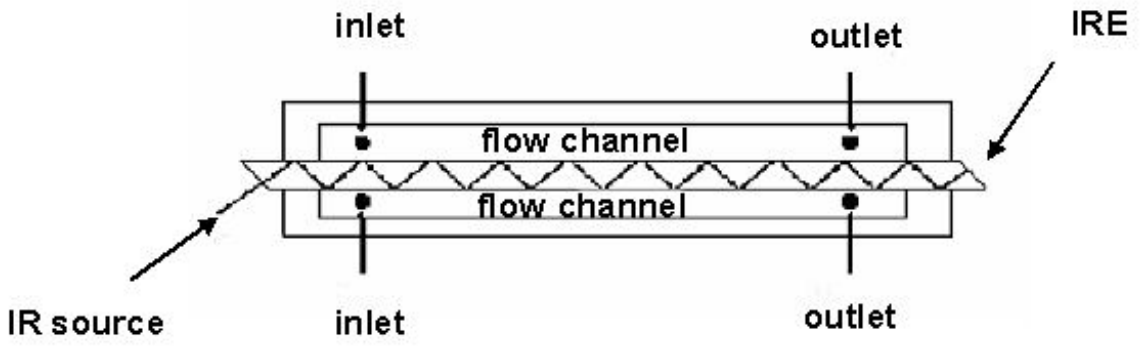

Figure 7.1: Top-down view of ATR/FTIR flow cell.

The IR source beam from the spectrometer is bounced multiple times through the IRE toward the detector. The biofilm deposits on the IRE. At each reflection site a longitudinal wave of radiation penetrates from the IRE to the adjacent environment. The intensity of the IR radiation exponentially decays to zero within about one micrometer of the IRE's surface. This radiation, the "evanescent wave" shown in Figure 7.2, can be

absorbed by compounds near the surface, which produces their IR absorption spectra.[24] This means that only material within 1 μm sampling area of the surface at which the IR beam is reflected will be detected.

Pioneering work in this field of using ATR/FTIR to study biofilm formation was done in 1991 by Bremer and Geesey.[25] In his work, a Germanium internal reflection element (IRE) was used as the solid surface to which an uncharacterized bacterium isolated from a pit in a section of corroded copper tubing could attach. This IRE was interfaced to a Fourier-transform Infrared (FT-IR) spectrometer and the spectral changes were monitored for a period of 188 hours. They found during the course of the experiment that the amount of protein detected at the IRE/medium interface increased throughout the course of the experiment, with extracellular polysaccharides mainly being produced during the initial stages of biofilm development.[25] These results were important because they demonstrated that changes in metabolic activity of surface-associated bacteria during biofilm development on surfaces exposed to a flowing bulk aqueous phase can be evaluated by ATR/FT-IR. Further work in the field was done by David E. Nivens *et al.*[24] In this work, the ATR/FTIR spectra of living *Caulobacter crescentus* cells were studied. Using the amide II band as a marker for biofilm biomass, the detection limit was determined to be approximately $5x10^5$ cells·cm^{-2} and demonstrated that the ATR/FTIR methodology could be used to give chemical information from bacteria and bacterial products located within approximately 1μm of the surface without spectral interferences due to components of the medium. In 1998, Suci *et al*. used the ATR/FTIR technique to follow the time course of the antimicrobial agent ciprofloxacin's appearance at the biofilm/substratum interface for a

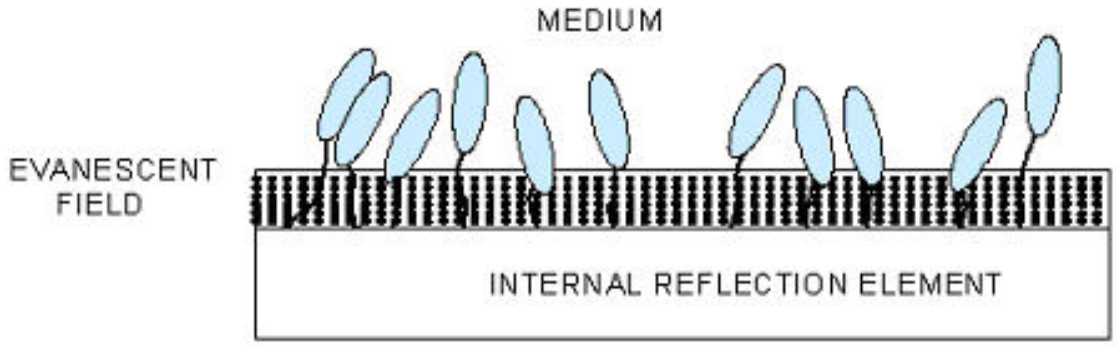

Figure 7.2: Generation of the evanescent field, with an effective penetration depth of 1μm from the surface of the IRE.

biofilm of *Pseudomonas aeruginosa.*[16] After addition of ciprofloxacin to the colonized surface, they observed the appearance of three bands in a 20-minute period. Although the exact nature of these bands was not identified, this study opens the door to modeling the transport kinetics of antimicrobials within a biofilm, which may shed light on structure/function relationships aiding in the development of antimicrobial agents designed to destroy these surface-dwelling microorganisms.

7.5 FTIR Spectra Band Assignments in Biofilms

There are several characteristic bands in the infrared region associated with biofilm formation. Most of the bands due to characteristic group vibrations in the macromolecules produced by all bacteria. Amide linkages produce three types of bands. Amide I bands (1690-1640 μ) are caused by carbonyl stretching modes.[16,20,24,26-28] Amide II (1570-1515 cm^{-1}) and amide III (1300-1200 cm^{-1}) bands result from the interaction between an N-H bending (trans to the carbonyl group) and C-N stretching modes of

secondary amides.[16,20,24,27,28] Free carboxylate ions (1397 cm^{-1}) are probably associated with amino acids, proteins, and acidic polysaccharides.[24,26,27] Carbohydrates and alcohols found in the nucleic acids, the cell envelope, and/or extracellular polymers contributed to the bands in the C-O stretch region (1300-1000 cm^{-1}).[20,24,26] Organic phosphate makes up about 3% of the composition of the microbial cell. The P=O stretching band appears neat 1250 cm^{-1} and P-O absorbs at 1100-1000 cm^{-1}, which overlaps the C-O region.[20,24] The C=O stretch of sugar units [20 16] occurs at 1034 cm^{-1} The phosphodiester linkages of DNA and RNA[16,29] occur in the region between 1300-1000 cm^{-1}.

7.6 Use of ATR/FTIR in Study of *Streptococcus pneumoniae* Biofilms

In this work, ATR/FTIR is used to monitor the changing IR spectrum during the attachment and growth of a film created by the organism *S. pneumoniae*. This organism was chosen because of its clinical relevance; it is one of the organisms suspected in forming biofilms in individuals who develop otitis media, one of the most common infectious diseases of childhood. Otitis media is an inflammation of the middle ear.[1] After acute episodes, fluid may persist in the middle ear for weeks to months, resulting in an average of 2 decibel hearing loss whenever the fluid is present.[30] This condition occurs most frequently in infants and children. Currently the identification of bacteria responsible for acute otitis media requires the invasive procedure of tympanocentesis, puncturing the tympanic membrane with a needle to aspirate fluid from the middle ear.[1] Because so little is known about the particulars of biofilm formation of this clinically relevant organism, it is our model for this ATR/FTIR study.

Only a handful of published studies document biofilm formation by *S. pneumoniae*. In 1997, Budhani and Struthers[31] demonstrated the formation *S. pneumoniae* on cellulose surfaces using a continuous culture biofilm system. However, this did not measure the biofilm EPS nor provide any structural information on the biofilms themselves.

In the present study, a model system was developed for growing and characterizing the continuous deposition of a *Streptococcus pneumoniae* biofilm on both a Germanium IRE and on several Germanium coupons by a combination of ATR/FTIR and Epifluorescence microscopy. The development of both the protein and the polysaccharide bands in the IR spectrum at particular time intervals was then correlated with total and viable biofilm cell counts to quantify biofilm-associated cells.

Experimental Methods

7.7 Bench Setup for ATR/FTIR Experiments

A biofilm reactor containing 1.3 mm-diameter Germanium coupons was connected via silicone tubing to a 10-L carboy containing the medium Brain Heart Infusion (BHI) broth (Difco Laboratories, Detroit, MI) that was supplied to the reactor at a flow rate of 0.5mL/min by a Master Flex peristaltic pump (Cole Parmer, Niles, IL). The coupons were made of Germanium, the same material from which the IRE was constructed. This was done to eliminate discrepancies between the attachment surfaces of the coupons and the IRE. Another set of tubing connected to the same pump above carried the media from the reactor to the ATR cell, where it could flow over both side of

the IRE, then exit the cell and be carried back to the reactor. The reactor was placed in a 34°C water bath stirred at 75 rpm for the duration of the experiment , and the reactor was supplied with a filter-sterile mixture of 85% nitrogen, 10% carbon dioxide, and 5% oxygen. Coupons could be removed from the reactor periodically by pulling the coupon holder through the lid of the reactor. A diagram of the overall bench setup is shown in Figure 7.3.

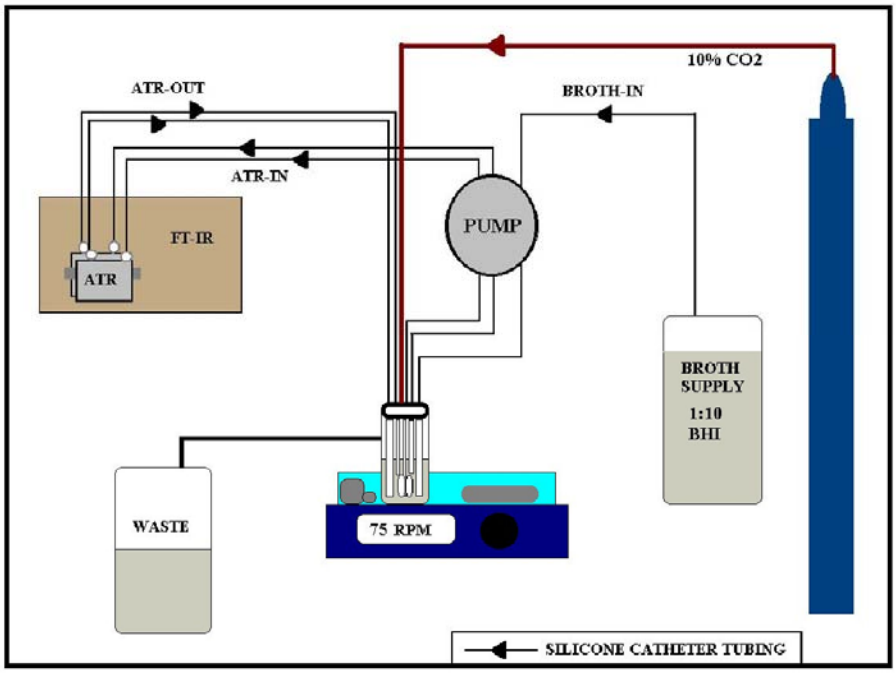

Figure 7.3: Experimental setup for the ATR/FTIR flow cell experiment.

7.8. Preparation of ATR Flow Cell

The ATR flow cell (Harrick Scientific, Ossining, NY) was located in the sample chamber of a Fourier Transform Infrared (FT-IR) Spectrometer (Nicolet Magna 860,

Madison, WI). This cell is shown in Figure 7.4. The two inlet channels carry media from the reactor to both sides of the crystal surface via the flow channels, and the two outlet channels carry the media from the cell back to the reactor. The biofilm reactor, originally designed by Ricardo Murga, Wayne Kirby, and Dr. Rod Donlan of CDC is shown in Figure 7.5. Prior to the experiment all components of the biofilm reactor were sterilized in an autoclave. The ATR cell was sterilized using 2% glutaraldehyde for 10 minutes and then rinsed with 0.6 M filter-sterile sodium metabisulfite for one minute to inactivate any residual glutaraldehyde. The solution was then removed and the cell was rinsed with filter sterilized reverse osmosis water to remove any traces of the sodium metabisulfite solution. The water from the ATR cell was cultured to ensure sterility after this process. The ATR cell was connected to the sterile silicone tubing that was attached to the biofilm reactor immediately after this sterilization process.

The *S. pneumoniae* culture work prior to inoculation of the batch reactor for the ATR/FTIR analysis was performed by Dr. Paul Edmonds and John Piede of the Biology Department, Georgia Tech. The *S. pneumoniae* clinical isolate from the (Boston's Children's Hospital, Boston, MA) was subcultured from a frozen stock on blood agar plates (BD Microbiology Systems, Cockeyville, MD) and incubated at 35°C in a 5% CO_2 incubator overnight. A single colony was then picked and inoculated into a 10-mL tube of BHI broth, which was incubated for 12 hours at 35°C in a 5% CO_2 incubator. A 9 mL volume of this 12 h culture was added to the reactor, providing 2.13×10^7 CFU/mL in the reactor as determined by plating on blood agar incubated at 35°C in a CO_2 incubator.

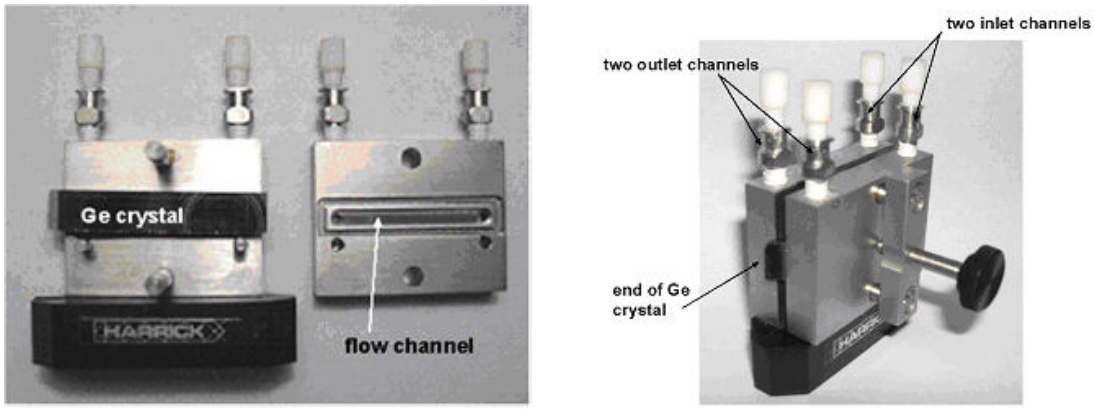

Figure 7.4: The un-assembled (left) and assembled (right) ATR flow cell, manufactured by Harrick Scientific.

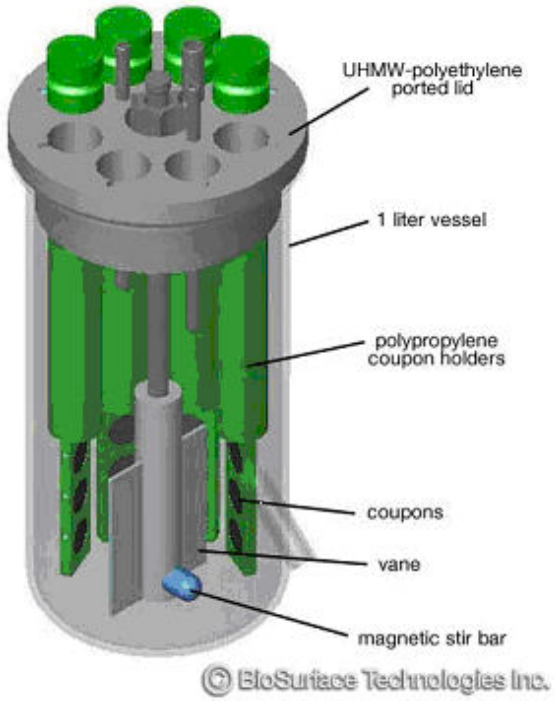

Figure 7.5: The biofilm reactor.

7.9 Preparation of *S. pneumoniae* and Reactor Inoculation

On the first day of the experiment, a 500-mL volume of BHI broth was added to the sterile reactor, followed by the above addition of the 9-mL 12-hour culture. This solution was mixed for a period of 12 hours in 'batch mode', meaning that no additional fresh media was added while the solution was being circulated between the reactor and ATR cell at a rate of 0.5 mL/min. This was done to establish a good *S. pneumoniae* population within the 500-mL volume of the reactor. After 12 hours the system was switched to 'open system', in which fresh media was pumped it at the same rate above while a discharge line was unclamped to allow a constant 500 mL volume in the reactor to be maintained. Biofilm formation was determined in primarily two ways: by observation of the changing IR spectrum resulting from deposition of the biofilm on the Germanium IRE, and by direct microscopic analysis of Germanium coupons removed periodically during the course of the experiment.

7.10. Germanium Coupon Processing and Analysis

Germanium coupons were removed periodically by quickly pulling them through the lid of the reactor as mentioned above. After removal, they were placed in a sterile sample holder holding sterile phosphate-buffered saline (PBS) and transferred to the Biofilm laboratory of Dr. Rod Donlan at the Centers for Disease Control (CDC), who processed the coupons from this point forward. Here, the coupons were subjected to three 30-second cycles of sonication at a frequency of 42 kHz (model 2510; Branson Co.,

Bohemia, NY) and homogenation of the suspension containing the suspended biofilm cells in a tissue homogenizer for 60 seconds (Polyscience Tissue Homogenizer model K-120, Polysciences Co., Niles, IL) at about 16,000 rpm. The resulting suspension was then processed to quantify the number of cells. A 1 mL volume of the sample was diluted and cultured on a Trypticasesoy agar containing 5% sheep's blood (Becton Dickinson Microbiology System, Cockeysville, MD) using the spread plate technique. Colonies were counted after inoculation at 35°C in a CO_2 incubator for 24 hours. A 7 mL portion of the sample was filtered through a 0.2 µm polycarbonate Nucleopore membrane filter (Whatman, Kent, UK) that was fixed in 5% formalin for 5 minutes, stained with a 2 µg/mL 4'6-diamidino-2-phenyl indole (DAPI) solution in filter-sterile reverse osmosis water) for 15 minutes in the dark, mounted on a glass microscope slide, and counted using a Zeiss Axioskop II Epifluorescence Research Microcope containing a DAPI filter set (455/40 excitation, long pass dichroic mirror, 420 nm/long pass emission). Ten fields were counted using a calibrated eyepiece grid.

7.11. IRE Processing and Analysis

In addition to the coupons examined during the course of the experiment, the IRE itself was examined at the end of the experiment by Dr. Rod Donlan. It was rinsed at least twice in filter-sterilized reverse osmosis water, fixed in 5% formalin solution for 5 minutes, stained for 15 minutes in the dark with 2µg/mL DAPI, again rinsed twice in filter-sterile reverse osmosis water, dried, mounted in immersion oil, and examined with

the Zeiss Axioskop II Epifluorescence microscope containing a DAPI filter set (described above) and an oil immersion 100x objective.

7.12. FTIR Spectra Analysis

Biofilm protein and polysaccharide were also quantified spectroscopically using the ATR/FTIR system. The background spectrum of the uninoculated medium was taken over a 12 hour period to insure a consistency in the background. After 12 hours, the system was changed from batch to open mode, allowing the inoculated medium to circulate through the ATR cell. During this period, the FTIR software OMNIC v5.2 (Nicolet, Madison, WI) was set up to record the spectrum obtained every 10 minutes. At each sampling time one hundred scans were averaged. The single-beam spectra were ratioed to the initial background spectrum to produce an absorption change at each sampling time. Two well-characterized regions (protein at 1700-1500 cm^{-1}, polysaccharide at 1200-1000 cm^{-1}) were used to follow the growth of the biofilm over time and under different conditions.

Results and Discussion

The extracted spectra of *S. pneumoniae* biofilms formed in the ATR/FTIR biofilm reactor system are shown in Figure 1.6. In the 1700-1000 cm^{-1} range a number of spectral features are observed. The 1700-1515 cm^{-1} region has been well documented as the region where protein vibrations appear.[24,28,33] The amide I band is caused by the C=O

carbonyl stretch between 1690-1640 cm^{-1}. Water absorbs in this region as well, at 1640 cm^{-1}. Between 1590-1515 cm^{-1} the N-H bend of amides gives rise to the amide II band. The broad band at about 1650 cm^{-1} is likely a hydrated mixture of both amide I and amide II bands in the protein component of the biofilm. The region between 1300-1900 cm^{-1} is broad and complex, and has been characterized in the literature as the region where both DNA/RNA and polysaccharides appear.[16,29,34-36] The C-O-C, C-O, and ring-stretching vibrations, as well as the P=O stretch of phosphodiesters are found in this region.

Figure 7.6 shows the FTIR spectra of *S. pneumoniae* biofilms over the course of 189 hours following inoculation. Note that the band intensities within the polysaccharide region (1300-1900 cm^{-1}) increased at a significantly higher rate than did the band intensity of the amide band region (1515-1590 cm^{-1}) as time progressed. After 141 hours, the intensity of the spectrum as a whole decreased, a trend that continued for the remainder of the experiment. This is likely due to the breaking off of parts of the film from the surface of the IRE after the films achieve a certain critical thickness. The data in Figure 7.6 show that both the polysaccharide and amide bands were detected on the IRE surface within hours after inoculation and continued to increase through 141 hours, then decrease for the remainder of the exposure period. After 141 hours, the intensity of the spectrum as a whole decreased. This is likely due to the breaking off of parts of the film from the surface of the IRE after the films achieve a certain critical thickness. With this *S. pneumoniae* biofilm, the polysaccharide band (1300-1900 cm^{-1}) increased at a significantly higher rate than did the band intensity of the amide band region (1515-

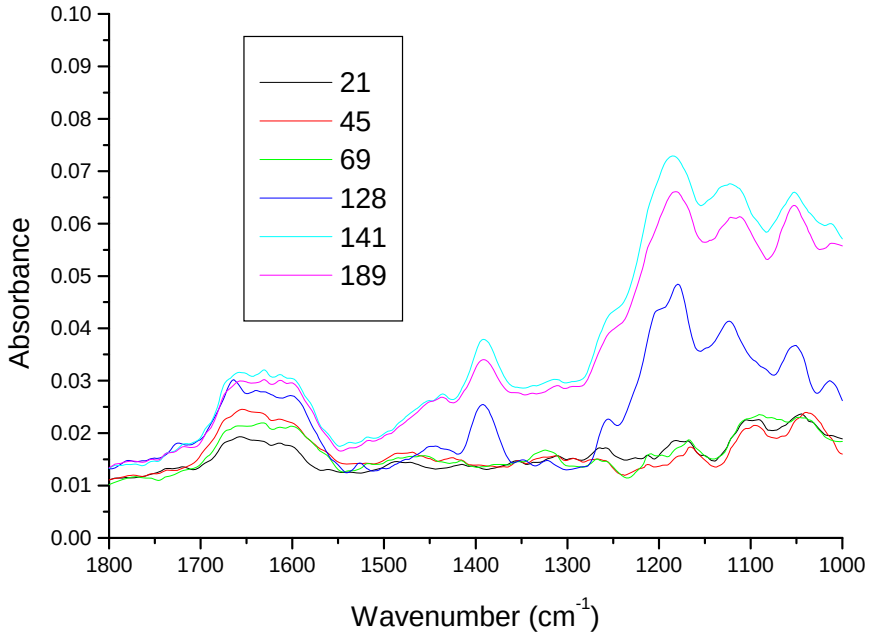

Figure 7.6: FTIR spectra of *S. pneumoniae* biofilms over the course of 189 hours following inoculation.

1590 cm^{-1}) as time progressed. This increase in spectral intensity over time reflects an increase in the coverage of the IRE surface by the biofilm rather than an increase in biofilm thickness.[32] This faster rate of polysaccharide development relative to protein is in contrast to work done by Bremer and Geesey [25] and by Nivens *et al.*[37] In the former, biofilm formation of an unidentified environmental organism ("CP-1") using ATR/FITR observed at over 188 hours demonstrated a continued increase in protein bands, with the protein:polysaccharide ratio increasing with time (Figure 7.7). In the latter, a similar pattern for the organism *Burkholderia (Pseudomonas) cepacia* studied over the course of 76 hours following inoculation is reported (Figure 7.8). The ratio of the intensities of protein bands (Amide I, Amide II) to polysaccharide bands (P-O, C-O) remains relatively constant with time. The *S. pneumoniae* organism in this study produced a greater amount

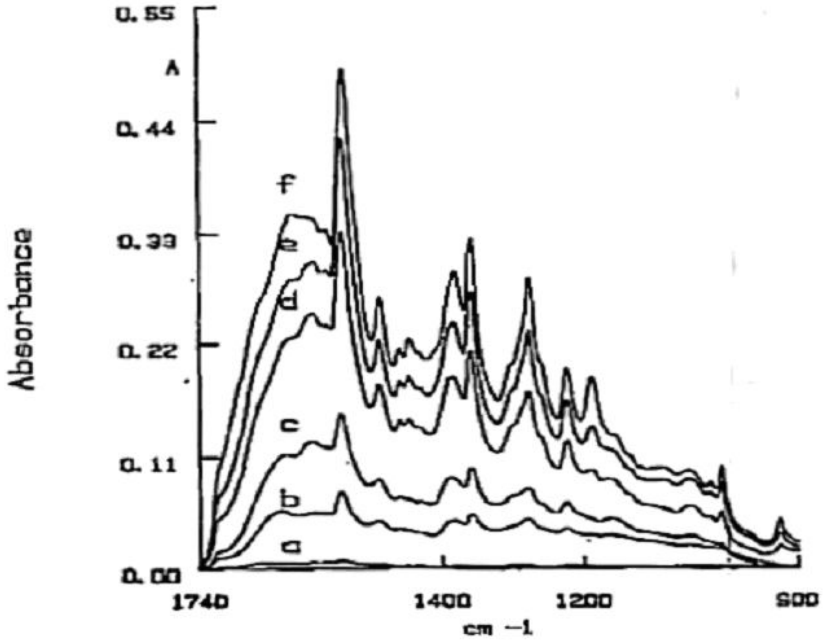

Figure 7.7: The changing FTIR spectrum of CP-1 biofilm over the course of 188 hours following inoculation as reported by Bremer and Geesey Here a=2h, b=26h, c=45h, d=90h, e=118h, f=188h.

of polysaccharides relative to protein, a fact that illustrates that distinct differences in biofilm structure may be exhibited by different organisms. At the conclusion of the experiment, one side of the IRE surface was examined under microscope provided additional evidence for *S. pneumoniae* biofilms (Figures 7.9-1.12). Dense biofilm development several cells in thickness were observed. Figures 7.9 and 1.10 from one area of the IRE, while Figures 7.11 and 7.12 are images from a second area of the IRE. In all four figures the regions are stained with both WGA-AF (wheat germ agglutinin conjugated with Alexa Fluor 488)(Molecular Probes, Eugene, OR) and DAPI (4'6-diamidino-2-phenylindole). WGA-AF will bind *N*-acetylglucosamine, which is a component of the outer peptidoglycan layer of gram positive bacteria.[32,38] WGA-AF

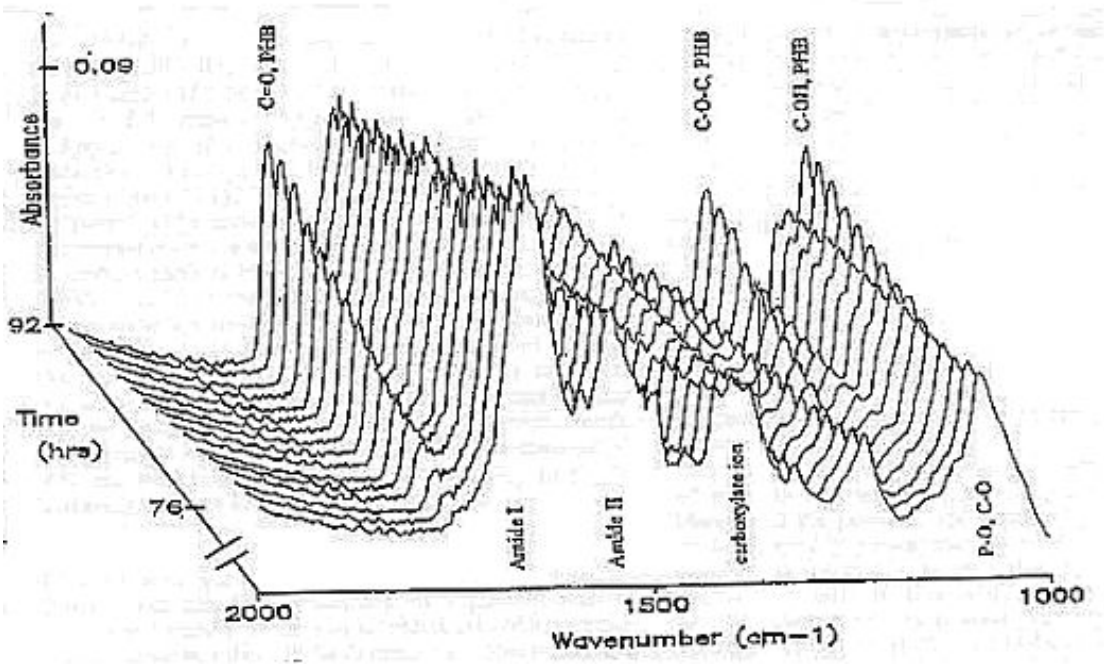

Figure 7.8: The changing FTIR spectrum of *Pseudomonas cepacia* biofilm over the course of 76 hours following inoculation.

will also bind the capsular polysaccharides of *S. pneumoniae*.[32,39] DAPI will stain all nucleic acid-containing cells (but not the extracellular polysaccharide).[32] Figures 7.9 and 7.10 are similar and suggest that most of the cells in this region bound to the WGA-AF either due to the *N*-acetylglucosamine in the cell wall or because they were encapsulated.[32] Figure 7.11 shows another region of the IRE demonstrating a much thicker biofilm with very intense DAPI staining in some areas. This indicates a biofilm structure that is several cells thick in this area.[32] Figure 7.12 shows the same area illuminated to show WGA-AF staining. There is a haze observed, which has been suggested in the literature by Neu and Lawrence[40] to arise from extracellular polysaccharide material (a.k.a. "EPS clouds.") The haze observed following WGA-AF staining and imaging indicates that *N*-acetylglucosamine is one of the components of the

biofilm EPS for this organism.[32] Following IRE surface cleaning and sterilization to remove traces of biofilm and EPS revealed very little fluorescent material was still present. This indicates that the fluorescent signals were not due to nonspecific binding or autofluorescence of the IRE surface.[32]

The numbers of cells attached to the surfaces and in the biofilm were quantified by the collection of coupons at intervals during the course of the experiment. Total cell counts were calculated from staining with DAPI, which stains both viable and nonviable cells. The number of viable cells was calculated from the number of cells forming colonies on blood agar plates.[32] Table 7.1 presents both the viable and total cell counts at six sampling times during the course of the experiment.

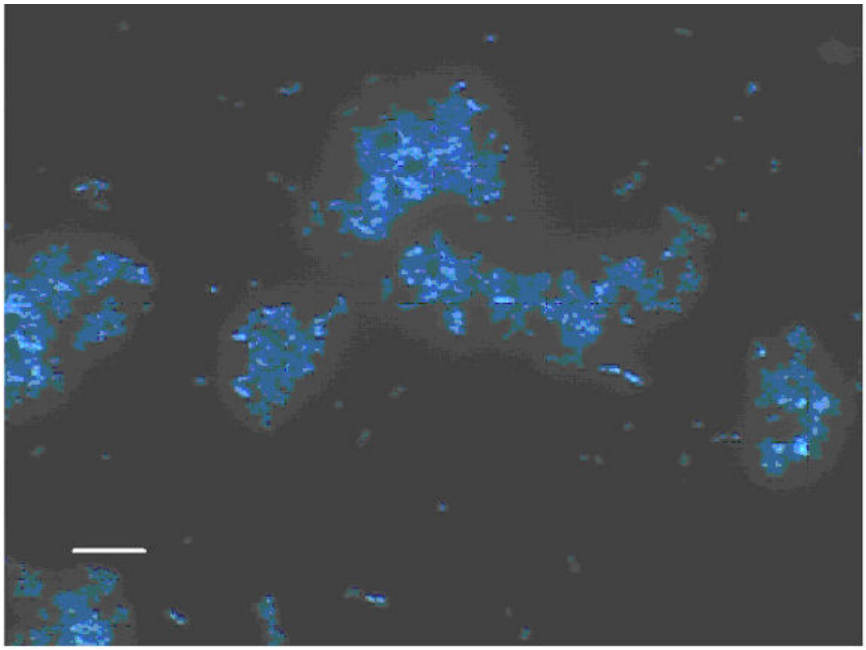

Figure 7.9: *S. pneumoniae* biofilm on IRE surface[32] after staining with WGA-AF and DAPI and imaging with DAPI filter set.

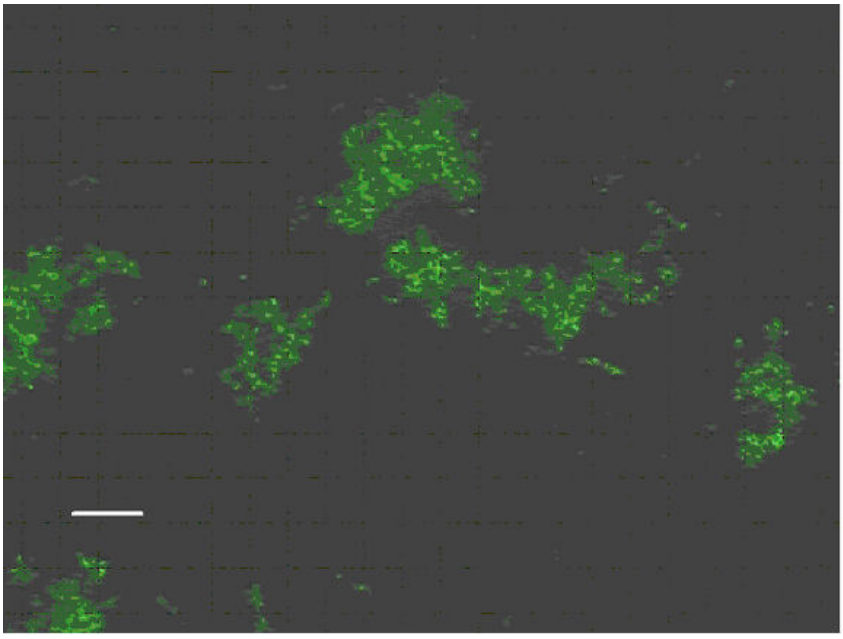

Figure 7.10: *S. pneumoniae* biofilm on IRE surface[32] after staining with WGA-AF and DAPI and imaging with a FITC filter set.

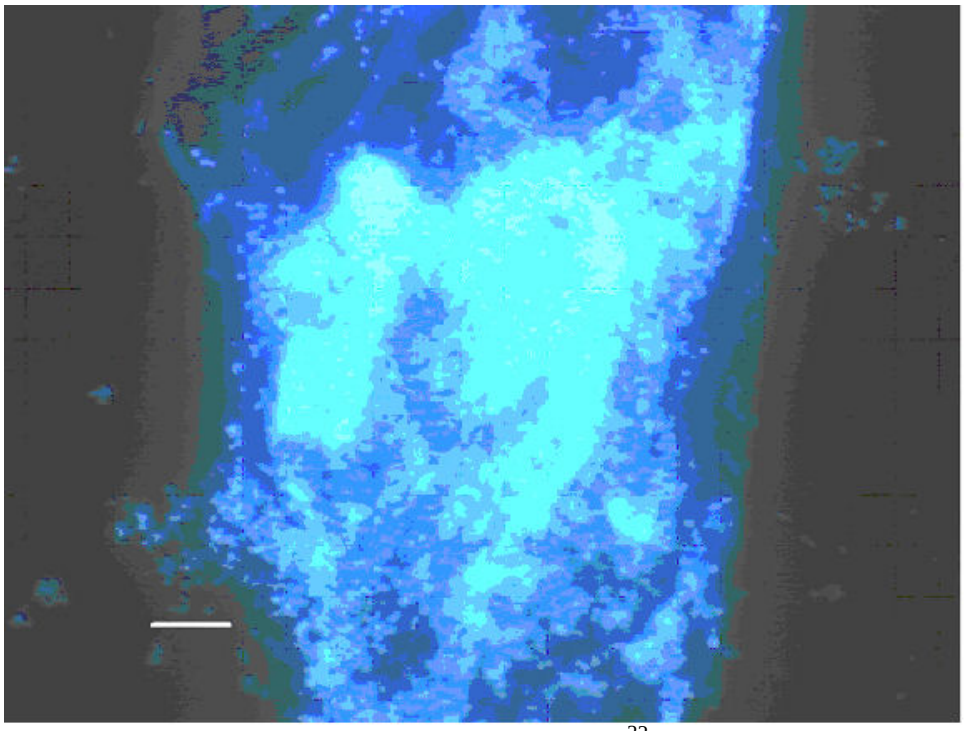

Figure 7.11: *S. pneumoniae* biofilm on IRE surface[32] after staining with WGA-AF and DAPI and imaging with DAPI filter set.

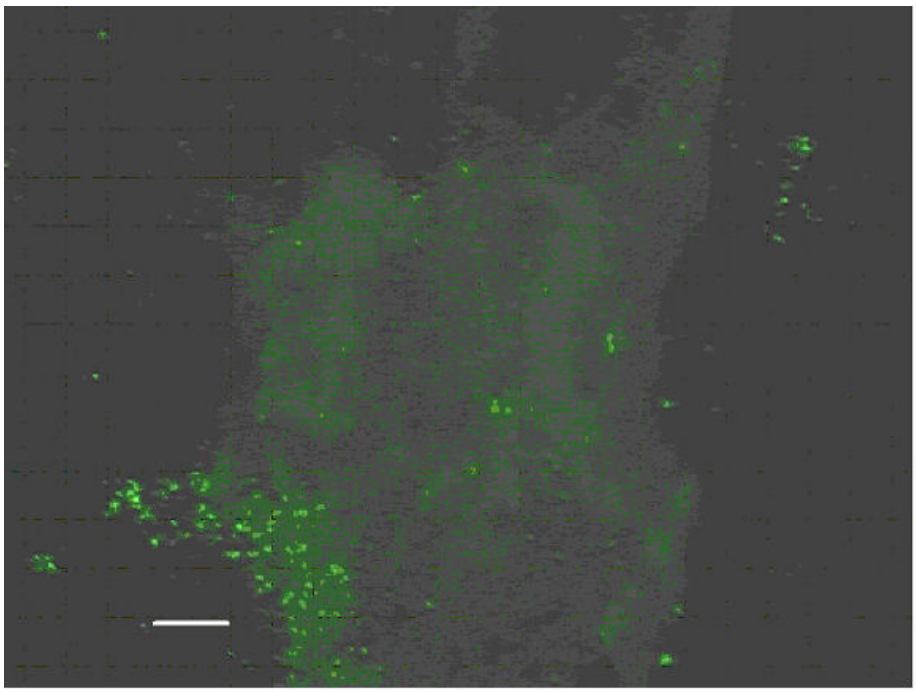

Figure 7.12: Figure 10: *S. pneumoniae* biofilm on IRE surface[32] after staining with WGA-AF and DAPI and imaging with a FITC filter set.

Table 7.1: Total and viable counts of biofilm–associated *S. pneumoniae* collected from germanium coupons exposed in the biofilm reactor.[32]

[a] Data are means +/- standard deviations (*n*-3)

[b] η=2

	Cell count (log_{10} cells/cm^2) per coupon surface[a]	
Time (h) in biofilm reactor	Total	Viable
21	5.23 +/- 0.21	4.99 +/- 0.06
45	5.15 +/- 0.05	4.21 +/- 0.15
69	5.42 +/- 0.14	4.70 +/- 0.13
141	4.95 +/- 0.11	3.08 +/- 0.28[b]
189	5.15 +/- 0.11	3.85 +/- 0.34

The total biofilm count was 6.16 x 10^4 cells/cm^2, which is somewhat lower than counts obtained from the germanium coupons installed in the biofilm reactor.[32] The discrepancy between cell counts is likely due to the difference in fluid flow conditions between the coupon environment relative to that of the IRE surface[32], which has also been documented in the literature.[2] This discrepancy may also be due to the different biofilm recovery methods employed for recovering the biofilms from the IRE and coupon surfaces. In the literature, sonicating and vortexing (used for germanium coupons) removed a larger percentage of biofilm-associated organisms from plastic surfaces than swabbing, which was used for the IRE surface.[32,41]

For *S. pneumoniae*, polysaccharides rapidly accumulated on the IRE surface, with more extensive polysaccharide production relative to protein as time progressed.[32] This is in contrast to the data reported by both Bremer and Gessey[25] and by Nivens *et al*.,[37] in which these ratios remained somewhat constant. This increase in the ratio of polysaccharide to protein with *S. pneumoniae* indicates that there are distinct differences in biofilm structure that may be exhibited by different organisms.[32] Furthermore, the staining results provide evidence that the EPS of *S. pneumoniae* is at least partially comprised of the capsular polysaccharide *N*-acetylglucosamine.[32]

In conclusion, this chapter details the development of a model system for growing and quantifying biofilm formation by *S. pneumoniae*. The ATR cell enabled spectroscopic measurements of biofilm components as they initially formed on the IRE surface. Biofilm protein and polysaccharide components were characterized by a combination of both FTIR spectroscopy and microscopic methods to better understand the biofilm structure of this organism and its EPS. Quantification via total and viable counting methods measured the biofilm-associated cells. Biofilm protein, EPS, and cells were detected within hours of inoculation and continued to grow throughout the course of the experiment.[32]

References

(1) Werkhaven, J. A.; Reinisch, L.; Sorrell, M.; Tribble, J.; Ossoff, R. H. *Laryngoscope* **1994**, *104*, 264.

(2) Donlan Rodney, M. *Emerging infectious diseases* **2002**, *8*, 881.

(3) Donlan, R. M. *Emerging Infectious Diseases* **2002**, *8*, 881.

(4) Phelps, T. J., Niedzielski, J.J., Schram, R.M., Herbes, S.E., and White, D.C. *Appled and Environmental Microbiology* **1990**, *56*, 1702.

(5) Bryers, J. D., and Characklis, W.G. Biofilms in water and waste-water treatment. In *Biofilms*; Characklis, W. G. a. M., K.C., Ed.; Wiley: New York, 1990; pp 671.

(6) Characklis, W. G. Microbial fouling. In *Biofilms*; Characklis, W. G. a. M., K.C., Ed.; Wiley: New York, 1990; pp 523.

(7) Dowling, N. J. E., Mittelman, M.W., and White, D.C. The role of consortia in microbially influenced corrosion. In *Mixed Cultures in Biotechnology*; Zeikus, J. G., Ed.; McGraw-Hill: New York, 1991; pp 341.

(8) Costerton, J. W., Irvin, R.T., and Cheng, K.J. *Annual Review Microbiology* **1981**, *35*, 299.

(9) Franklin, M. J., Nivens, D.E., Vass, A.A., Mittelman, M.W., Jack, R.F., Dowling, N.J.E., and White, D.C. *Corrosion* **1991**, *47*, 128.

(10) Buret, A., Ward, K.H., Olson, M.E., Costerson, J.W. *Journal of Biomedical Material Research* **1991**, *25*, 865.

(11) Ziats N.P., M., K.M., Anderson J.M. *Biomaterials* **1988**, *9*, 5.

(12) Anderson, J. M., Miller, K.M. *Biomaterials* **1984**, *5*, 5.

(13) Gristina, A. *Science* **1987**, *237*, 1588.

(14) Dankert, J., Hogt, A.H., Feijin J. *CRC Critical Reviews* **1986**, *2*, 219.

(15) Dickenson, G. M., Bisno, A.L. *Antimicrobial Agents and Chemotherapy* **1989**, *33*, 602.

(16) Peter A. Suci, J. D. V., Marc W. Mittelman. *Biomaterials* **1998**, *19*, 327.

(17) Henrici, A. T. *Journal of Bacteriology* **1933**, *25*.

(18) Surman, S. B., Walker, J.T., Goddard, D.T., Morton, L.H.G., Keevil C.W., Weaver, W., Skinner, A., Hanson, K., Caldwell, D., Kurtz, J. *Journal of Microbial Methods* **1996**, *25*, 57.

(19) Mack, W. N., Mack, J.P., Ackerson, A.O. *Microbial Ecology* **1975**, *2*, 215.

(20) Geesey, G. G.; Suci, P. A. *Biofilms: Recent Advances in Their Study and Control* **2000**, 253.

(21) Johnson, C., Howells, M. *Power* **1981**, *125*, 90.

(22) Atkinson, D. L. *Industrial Water Engineer* **1979**, *16*, 37.

(23) Harrick, N. J. *Internal Reflection Spectroscopy*; Wiley: New York, 1967.

(24) David E. Nivens, J. Q. C., Tina R. Anderson, Ander Tunlid, John Smit, and David C. White. *Journal of Microbial Methods* **1993**, *17*, 199.

(25) Bremer, P. J.; Geesey, G. G. *Biofouling* **1991**, *3*, 89.

(26) Coimbra, M. A.; Barros, A.; Barros, M.; Rutledge, D. N.; Delgadillo, I. *Carbohydrate Polymers* **1998**, *37*, 241.

(27) Silverstein, R. M.; Bassler, G. C.; Morrill, T. C. *Spectrometric Identification of Organic Compounds. 5th Ed*, 1991.

(28) Geesey, P. A. S. M. W. M. F. P. Y. a. G. G. *Antimicrobial Agents and Chemotherapy* **1994**, *38*, 2125.

(29) P.A. Suci, a. G. G. G. *Journal of Colloid and Interface Science* **1995**, *172*, 347.

(30) Klein, J. O. *Pediatric Infectious Disease Journal* **1989**, *8*, S11.

(31) Budhani, R. K.; Struthers, J. K. *Journal of Antimicrobial Chemotherapy* **1997**, *40*, 601.

(32) Donlan, R. M.; Piede, J. A.; Heyes, C. D.; Sanii, L.; Murga, R.; Edmonds, P.; El-Sayed, I.; El-Sayed, M. A. *Applied and Environmental Microbiology* **2004**, *70*, 4980.

(33) Casal, H. L.; Cameron, D. G.; Smith, I. C. P.; Mantsch, H. H. *Biochemistry* **1980**, *19*, 444.

(34) H.-C. Flemming, G. S., T. Griebe, J. Schmitt, and A. Tamachkiarowa. *Desalination* **1997**, *113*, 215.

(35) P.A. Suci, K. J. S., R.J. Palmer, D.C. White, and G.G. Geesey. *Appled and Environmental Microbiology* **1997**, *63*, 4600.

(36) E. Taillandier, J. L., and J.A. Taboury. Chapter 2- Infrared Spectral Studies of DNA Conformations. In *Advances in Infrared and Raman Spectroscopy*; Hester, R. J. H. C. a. R. E., Ed.; John Wiley and Sons: New York, 1985; Vol. 12; pp 65.

(37) Nivens, D. E.; Palmer, R. J., Jr.; White, D. C. *Journal of Industrial Microbiology* **1995**, *15*, 263.

(38) Sizemore, R. K.; Caldwell, J. J.; Kendrick, A. S. *Applied and environmental microbiology* **1990**, *56*, 2245.

(39) Ebisu, S.; Lonngren, J.; Goldstein, I. J. *Carbohydrate Research* **1977**, *58*, 187.

(40) Neu, T. R.; Lawrence, J. R. *Methods in enzymology* **1999**, *310*, 145.

(41) Donlan, R. M.; Murga, R.; Bell, M.; Toscano, C. M.; Carr, J. H.; Novicki, T. J.; Zuckerman, C.; Corey, L. C.; Miller, J. M. *Journal of clinical microbiology* **2001**, *39*, 750.